INFORMATION TO USERS

This manuscript has been reproduced from the microfilm master. UMI films the text directly from the original or copy submitted. Thus, some thesis and dissertation copies are in typewriter face, while others may be from any type of computer printer.

The quality of this reproduction is dependent upon the quality of the copy submitted. Broken or indistinct print, colored or poor quality illustrations and photographs, print bleedthrough, substandard margins, and improper alignment can adversely affect reproduction.

In the unlikely event that the author did not send UMI a complete manuscript and there are missing pages, these will be noted. Also, if unauthorized copyright material had to be removed, a note will indicate the deletion.

Oversize materials (e.g., maps, drawings, charts) are reproduced by sectioning the original, beginning at the upper left-hand corner and continuing from left to right in equal sections with small overlaps.

Photographs included in the original manuscript have been reproduced xerographically in this copy. Higher quality 6" x 9" black and white photographic prints are available for any photographs or illustrations appearing in this copy for an additional charge. Contact UMI directly to order.

ProQuest Information and Learning
300 North Zeeb Road, Ann Arbor, MI 48106-1346 USA
800-521-0600

UMI®

University of Alberta

ANALYSIS OF SMALL MOLECULES IN BIOLOGICAL SAMPLES USING CAPILLARY ELECTROPHORESIS

by

ZHAOHUI CHEN 

A thesis submitted to the Faculty of Graduate Studies and Research in partial fulfillment of the requirements for the degree of Doctor of Philosophy.

Department of Chemistry

Edmonton, Alberta

Fall, 2001

University of Alberta

Library Release Form

Name of Author: ZHAOHUI CHEN

Title of Thesis: ANALYSIS OF SMALL MOLECULES IN BIOLOGICAL SAMPLES USING CAPILLARY ELECTROPHORESIS

Degree: Doctor of Philosophy

Year this Degree Granted: 2001

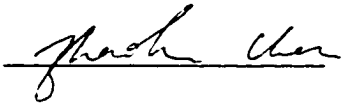

117, 3600 Brenner Drive, N.W.
Calgary, AB T2L 1Y2
Alberta, Canada

Date: JUNE 26, 2001

University of Alberta

Faculty of Graduate Studies and Research

The undersigned certify that they have read, and recommend to the Faculty of Graduate Studies and Research for acceptance, a thesis entitled ANALYSIS OF SMALL MOLECULES IN BIOLOGICAL SAMPLES USING CAPILLARY ELECTROPHORESIS submitted by ZHAOHUI CHEN in partial fulfillment of the requirements for the degree of DOCTOR OF PHILOSOPHY.

Dr. N.J. Dovichi, Supervisor

Dr. F.F. Cantwell

Dr. L. Li

Dr. G. Kotovych

Dr. G.B. Baker

Dr. E.P.C. Lai

June 17, 2001

For my grandma, Wenxiang Zhang

ABSTRACT

The applications of capillary electrophoresis coupled with various detection methods, such as mass spectrometry, laser-induced fluorescence and thermal lens absorbance are demonstrated to study small biological molecules.

On-line electrospray mass spectroscopy is successfully coupled with capillary electrophoresis to rapidly and sensitively determine eight amines normally present in food. Combining both the advantages of CE and MS, this method is used to determine amines which are undetectable with UV or LIF detection system. For the other amines, the dynamic range and the detection limits are comparable to those obtained using conventional UV absorbance.

Fluorescence detection based on a sheath flow cuvette design is successfully applied to the simultaneously determine of 16 neurotransmitters in a single capillary system. Separation methodologies based on micelle electrokinetic chromatography have been developed for the analysis of neurotransmitters in brain microdialysates and homogenate samples with minimum sample pretreatment and sample requirement. The proven feasibility and reliability shows the potential to use the developed CE-LIF method to interpret the mechanism of neurotransmission and pharmacology of the drug therapy.

The design, construction, and performance of a multi-capillary detector based on thermal optical absorbance is demonstrated. This first generation multi-capillary system using a thermal absorbance detector has been developed with a typical theoretical plate number of 10^4. This is the first report of applying a thermal optical detection technique for use with a multiple capillary electrophoresis system.

ACKNOWLEDGEMENT

I would like to thank my research director Dr. Norman J. Dovichi for his guidance, support, and patience throughout this work. He shows me the enthusiasm and the beauty of doing research. The knowledge and expertise of Dr. G. Baker and Dr. Jianzhong Zhang were of invaluable help. I would also like to thank Mr. Eric Carpenter and Mr. Gaya Kariyawasam for their assistance in the hardware and software designs. The support provided by the Machine Shop, Electronic shop in Department of Chemistry at University of Alberta, have been instrumental in this work, and is acknowledged with thanks. I am especially grateful my husband Shijun Sheng and my family back home for their unconditional support and influence. The cooperation of my little baby Grace Ray-Ann Sheng is fondly remembered. It is my daughter and my husband that make my career and life much more meaningful and enjoyable.

TABLE OF CONTENTS

CHAPTER PAGE

LIST OF TABLES

LIST OF FIGURES

Chapter 1

Introduction

1.1 Capillary Electrophoresis (CE)

1.1.1 General Introduction

Capillary electrophoresis (CE) is an analytical technique that employs narrow-bore capillaries (10-200 μm inner diameter) to perform high efficiency separations, which are facilitated by the use of high voltages. It has become a major theme of research and development during the last fifteen years as a powerful separation method for minute quantities of analytes, ranging from small inorganic ions to large biological molecules; and its potential is being increasingly exploited in many areas of the life sciences and biotechnology today in both academia and industry.

Based on the principle of performing electrophoresis in a buffer filled tube and thus separating analytes by differences in their charge-to-size ratio, capillary electrophoresis actually has had a long history, if one considers electrophoresis conducted in columns as its ancestor. Over 30 years ago several workers, especially Hjerten [1] and Catsimpoolas [2], exploited column electrophoresis using high electric field strength and rotating glass tubes of 3-mm inner diameter (i.d.) to demonstrate free-zone electrophoresis. Following Hjerten's seminal work, Everaerts [3-5] explored the separation potential of capillary zone electrophoresis (CZE) performed in 200-μm Teflon capillaries with on-column UV detection and conductivity detection in the 1970s,

reporting the advantages of using glass columns with smaller inner diameter. In a move toward higher separation efficiencies, Mikkers et al. demonstrated separations with plate heights less than 10 μm using Teflon tubes of 200-μm i.d. [5]. In 1981, Jorgenson and co-workers convincingly demonstrated the analytical potential of CZE using 75-μm fused silica capillaries [6-8]. This work is rightly credited with the initiation of capillary electrophoresis because the importance of capillary operation to reduce the joule heating effects caused by the desirable high fields was emphasized. Major breakthroughs in terms of resolution and separation efficiency were realized as well when they performed the separations of amino acids and peptides were performedwith on-column fluorescence detection [9]. Since its introduction in the early to middle 1980s, CE has achieved remarkably rapid development followed by the foregoing pioneering work; noteworthy were the studies of Hjerten [10] on Capillary Zone Electrophoresis (CZE) and Terabe [11] on Micellar Electrokinetic Chromatography (MEKC). By the late 1980s, it was clear to a number of investigators and instrument companies that CE was a major field, especially in the biological sciences. In 1988, Microphoretic Systems (Sunnyvale, CA, USA) introduced the first commercial CE instrument at the conference of the Federation of the Societies for Experimental Biology (FASEB) [12].

From a technique for which only homemade systems were available to fully-automated instrumentation, from a few academic laboratories' anticipations expanded to current worldwide use in routine analysis, from tubes with diameters of 1-3 mm in the early days to currently less than 100 μm fused silica capillary, from the small ion CZE analyses extended to the MEKC applications of neutral species, from single capillary to multi-dimension capillary array, the cumulative experience to date has provided

substantial opportunities for the solution of analytical problems with capillary electrophoresis, and the technique will continue to grow rapidly.

In this chapter, a general introduction of capillary electrophoresis, followed by the combination of CE with some spectrometric techniques, such as ultraviolet and visible radiation (UV/Vis) absorption, laser- induced fluorescence (LIF), and mass spectrometry, will be discussed.

1.1.2 Typical Capillary Electrophoresis System Setup

The basic instrumental configuration for CE is relatively simple. Fig1.1 is a schematic diagram of a typical CE system. The length of the capillary differs in different applications, but is normally 20 to 50 cm. Capillaries are made of fused-silica coated with a thin layer of polymide outside to strengthen the tubes. Usually the separation capillary is placed between two reservoirs filled with the background buffer (typically 10 to 100 mM ionic strength). The solution levels in those vials are always kept the same to avoid unwanted hydrodynamic flow within the capillary. A platinum electrode serves to connect the high voltage power supply, and is put into the reservoir with the injection end of capillary in it. The other buffer vial is grounded. A controllable high voltage power supply (up to 30 kV), either positive or negative, is applied across the capillary and analyte zones are detected as they pass the window at the far end. The high voltage end of the capillary must be enclosed within a nonconductive Plexiglas box equipped with a safety interlock in order to avoid electrical hazards. Detection may take place on- or post- capillary depending the experimental design.

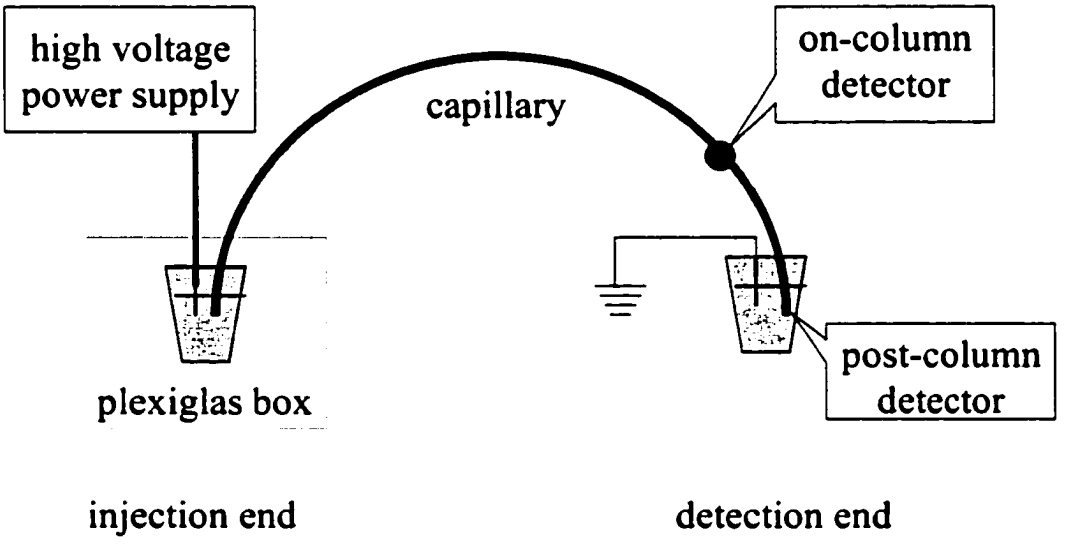

Fig1.1: Schematic diagram of a typical capillary electrophoresis (CE) system.

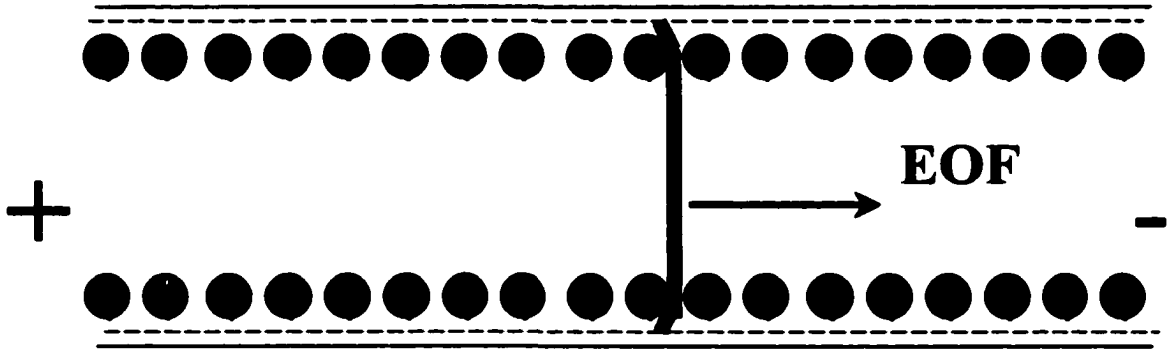

Figure 1.2: Electroosmosis.

1.1.3 Electrophoresis and Electroosmosis

Concerning the basic concepts in CE, early reviews by Jorgenson and Lukacs [9,13-15] provided a simple theory of dispersion in open tubes and discussed the influences of many operational parameters on the quality of separation.

Electrophoresis is the fundamental separation process in CE. When a voltage is applied across the capillary, in the ideal world of absence of any support medium, the mobility of any ion is governed by the propelling forces of the electric field and the retarding effect of the solvent viscosity, which in gross terms is a function of the ion's molecular mass and shape. Thus the ionic components (cations or inions) will move toward the cathode or anode according to their charges. Based on the differences in charge-to-mass ratio, ionic species can be separated into discrete zones through electrophoretic migration. The electrophoretic mobility μ_{ep} (cm^2/sV) of an ion is defined as:

$$\mu_{ep} = v_{ep} / E = (L_{dec}/t_r) / (V/L_{cap}) \qquad (1.1)$$

where v_{ep} is the electrophoretic velocity (cm/s), E is the electric field strength (V/cm), L_{cap} is the length of the entire capillary, L_{dec} is the length of the capillary from the injection end to the detection window, t_r is the migration time, and V is the voltage applied to the capillary.

Another fundamental process in capillary electrophoresis is electroosmosis, which is the primary motive force during separation, shown in Figure 1.4. As introduced in

section 1.1.2, CE is normally carried out in capillaries made from fused silica. The negative charged silanol groups present in this material give rise to a surface negative charge (or zeta ξ potential) which is responsible for the phenomenon of electroosmosis. This surface charge results in a distinctive distribution of cationic species in any ionic solution within the capillary. There is a layer of tightly bound cations immediately adjacent to the capillary wall and a more loosely associated layer that is also largely cationic in nature. The application of an electric field results in the movement of these more loosely bound cations towards the cathode, and since they are hydrated the consequence is a bulk flow of liquid in the same direction. The electroosmotic mobility is defined by

$$\mu_{eo} = v_{eo} / E = \varepsilon \zeta / (4 \pi \eta) \qquad (1.2)$$

where μ_{eo} is the electroosmotic flow velocity (cm/s), E is the electric field strength (V/cm), ε is the dielectric constant of the solution, η is the viscosity, and ζ is the zeta potential at the plane of shear close to the liquid-solid interface.

Because the electroosmotic flow (EOF) is larger in magnitude than the electrophoretic mobility, all sample components, including cations, neutral molecules and even those with a negative charge will be swept along towards the cathode. The order of migration is cations, neutrals, and anions. The overall migration velocity is the sum of the electrophoretic velocity and the electroosmotic velocity:

$$v_{overall} = v_{ep} + v_{eo} \qquad (1.3)$$

Thus the time that it takes a solute to migrate from the injection end of the capillary to the

detection window is defined as the migration time (t_r) of the analyte, which can be given by the following equation:

$$t_r = L_{dec} / (V_{ep} + V_{eo}) \quad (1.4)$$

EOF can be measured readily by injection of a neutral solute such as acetone or DMSO and recording the time taken for it to reach the detector. Its extent and influence has to be under control otherwise reproducibility will be compromised. Electrolyte composition will influence the EOF. High pH will increase the ionization of the silanol groups and therefore increase the effect, while increasing the ionic strength decreases EOF. Addition of organic solvents also affects the EOF, but less predictably.

1.1.4 Sample Introduction

The sample is introduced by dipping the injection end of capillary into the sample solutions and the amount of sample required in CE is on the order of a nanoliter or less. Two injection schemes have been employed in CE: electrokinetic injection by applying low-potential electric field across the capillary for a short time, and hydrodynamic injection via the formation of a small pressure gradient between inlet and outlet of the column. Hydrodynamic injection is not used in this thesis and is not described here.

Electrokinetic injection, also known as electromigration injection, is the most widely used injection form in CE. A computer program can easily control the voltage and time for injection. When a voltage is applied, components with different charges and size will migrate at their specific velocities into the capillary. Analytes with higher electrophoretic mobility travel faster and thus are injected to a greater extent than slower

moving ones. The injection volume of individual compound can be calculated by the following equation [16]:

$$V_{inj} = V_{cap} (t_{inj} / t_r) (V_{inj} / V_{ep}) \quad (1.5)$$

where V_{inj} is the corrected injection volume of a specific component in the sample solution, V_{cap} is the volume of the capillary in use, t_r is the migration time of the component, t_{inj} is the electrokinetic injection time, V_{inj} is the electrokinetic injection voltage, and V_{ep} is the high voltage employed for capillary electrophoresis. This equation assumes the ionic strength of the sample matches the ionic strength of the separation buffer.

1.1.5 Separation Efficiency

The separation efficiency in capillary electrophoresis can be described in terms of theoretical plate count (N), which is given as

$$N = L_{dec}^2 / \sigma^2 \quad (1.6)$$

where σ^2 is the spatial variance of a zone. During migration through the capillary, molecular diffusion occurs leading to peak dispersion σ^2. Unlike a pressure-driven system such as HPLC, CE is an electrically driven system. The driving force for EOF is uniformly distributed along the entire length of the capillary. As a result, the flow velocity is uniform across the entire tubing diameter except very close to the wall where the velocity approaches zero. The cross-sectional flow profile due to EOF is shown as

Figure1.2. Longitudinal diffusion of the molecule contributes the most to band broadening, and is given by:

$$\sigma^2 = 2 D t_m \quad (1.7)$$

where D is the molecular diffusion coefficient of the solute (cm^2/s) in the zone and t_m is migration time. The migration velocity of a particular species is given by

$$v = \mu E = \mu V / L_{cap} \quad (1.8)$$

The time t , required for a zone to migrate the entire length of the tube is

$$t = L_{cap} / v = L_{cap}^2 / \mu V \quad (1.9)$$

Substituting equation (1.9) and the dispersion equation (1.7) into the plate number equation (1.6) yields

$$N = L^2 / \sigma^2 = V \mu / 2 D \quad (1.10)$$

The equation indicates that N is independent of tube length and analysis time. In addition, N is directly proportional to the applied voltage, which suggests the use of highest voltages will provide the greatest efficiency by decreasing the separation time. But Joule heating restrains the application of high field strength in electrophoresis. Joule heat is produced when an electric current is flowing through a solution. Heat is generated uniformly throughout the medium but is only removed at the capillary wall and ends. The temperature in the center of the tube is higher than the area close to the wall and a radial temperature gradient will generate zone broadening. Solute molecules in the warmer center of the capillary will migrate faster while those at the wall will move more slowly. In a well designed system, because of the small dimension of a capillary tube and its large surface-to-volume ratio, heat dissipation is efficient, allowing use of high

separation potentials in CE, and the separation efficiency could reach a few million theoretical plates for low molecular weight analytes.

The plate count can be measured experimentally by the following equation:

$$N = 5.54 (t_m / w_{½})^2 = 16 (t_m / w)^2 \quad (1.11)$$

Where t_m is the migration time of a component in the sample solution, w the full peak-width at the baseline (in units of time), and $w_{½}$ is the full peak-width at one-half peak height (in units of time).

1.1.6 Resolution

Resolution (R) is a measure of the separation between two peaks. The resolution in capillary electrophoresis is given by

$$R = ¼ N^{½} \Delta\upsilon / \upsilon \quad (1.12)$$

where N is the theoretical plate number $\Delta\upsilon$ is the difference in the migration velocity of two components, and υ is the average zone migration velocity [17]. Resolution also can be estimated experimentally by the same equation used in chromatography:

$$R = (t_1 - t_2) / [(w_1 + w_2)½] \quad (1.13)$$

where t_1 and t_2 are the migration times of component 1 and 2 respectively, w_1 and w_2 are the full peak-width at the baseline (in units of time) of peaks 1 and 2.

1.2 CE Operation

1.2.1 CE Separation Modes

Based on different operative and separative characteristics, CE can be classified into the following modes:

1) capillary zone electrophoresis (CZE);

2) micellar electrokinetic chromatography (MEKC);

3) capillary gel electrophoresis (CGE);

4) capillary isoelectric focusing (CIEF);

5) capillary isotachophoresis (CITP);

6) capillary electrochromatography (CEC).

Among them, the first two modes are typically applied to separation of small molecules, which will be covered in the following sections.

1.2.2 Capillary Zone Electrophoresis (CZE)

Capillary zone electrophoresis, also known as free solution open tube capillary electrophoresis, is the simplest and perhaps the most universally useful mode of CE. The separation mechanism is based on difference in electrophoretic mobility, in terms of the charge-to-mass ratio.

Molecular diffusion is a large contributor to zone broadening in capillary zone electrophoresis. Its electric-driven flow profile results in a system with extremely high efficiency. Losses in efficiency, however, can result when column heating, separation time, column geometry, injection and detection volume, sample concentration, and solute adsorption are not optimized.

In order to ensure the reproducibility of the CE operation, EOF should be kept stable. A new capillary must be conditioned before it can be used and between runs to obtain a fully and uniformly charged capillary. Heating can be minimized by providing enough surface area to dissipate the generated heat inside the capillary, either by using small inner-diameter capillaries, long capillaries, or combination of this two. An alternative is cooling the capillary.

The injection volume should be minimized as well to reduce overloading. High solute concentration can lead to asymmetric zones.

Finally, the interaction between the capillary wall and analyte ions, especially cations, can result in significant tailing peaks. One method to prevent this interaction is providing certain electrophoretic conditions that minimize electrostatic interactions, for example, adding salts into the running buffer to compete for the adsorption sites or using high pH buffers. Another solution is dealing with the permanent modification of the capillary wall to produce an inert nonadsorptive surface to minimize the adsorption effect. These efforts have enabled CZE to play a major role in the separations of proteins and other biopolymers.

Buffer selection is the most important issue in capillary electrophoresis. There is a wide variety of buffers with typical concentrations of 5-100 mM that can be employed in CZE. The most common and effective buffer system for an analyte is within one or two pH units of its pKa. Various buffer additives, such as organic modifier, can be applied to change electrophoretic mobility, and thus the selectivity of the separation.

Because all neutral species have zero electrophoretic velocity (υ_{ep} = 0 cm/s), they migrate out of the capillary at the same electroosmotic flow rate (υ_{eo}) without separation. Therefore, CZE is restricted to separation of cationic and anionic analytes.

1.2.3 Micellar Electrokinetic Chromatography (MEKC)

This very important capillary electrophoresis mode not only extends the separation of CE to neutral analytes, but also improves the separation efficiency of ionic analytes [18]. In this system, ionic surfactants are added to the operating buffer at concentrations exceeding the critical micelle concentration (CMC). At these levels, surfactant monomers tend to form roughly spherical aggregates, or micelles, with the hydrophobic tail groups oriented toward the center and the charged head groups along the outer surface. MEKC is mainly based on partition of analytes between micelles (pseudo-stationary phase) and the aqueous buffer solution in addition to electrophoretic migration of charged analytes.

MEKC is most commonly performed with anionic surfactants, especially sodium dodecyl sulfate (SDS); a schematic is shown in Figure 1.3. Micelles form as a consequence of the hydrophobic effect, that is, they form to reduce the free energy of the system. The hydrophobic tails of the surfactant cannot be solvated in aqueous solution and they aggregate. The surfaces of SDS micelles have a large net negative charge, supplying them a large electrophoretic flow toward the anode. However, the magnitude of electroosmotic flow is usually greater than the electrophoretic flow of micelles, resulting in a faster moving aqueous phase and a slower moving micellar phase.

Analytes can partition between those two phases and retention is based on differential solubilization by the micelles. Analytes can diffuse into and move out of the micelles. As a result, when an analyte is associated with a micelle, its overall migration velocity is slowed. When an uncharged analyte resides in the bulk aqueous phase, its migration velocity is that of EOF. Therefore, compounds that have greater affinity for the micelle elute slower compared to those that spend most of their time in the running buffer. With SDS micelles, the general migration order will be anions, neutrals, and cations. Anions spend more of their time in the bulk buffer due to the electrostatic repulsions from the micelles. The greater the anion's charge, the more rapid the migration. Neutral species are separated exclusively based on hydrophobicity. Cations move last due to strong electrostatic attraction (e.g. ion-pairing interaction).

So far, SDS is still the most widely used surfactant in MEKC. Its molecular weight is 288 and the CMC is 8 mM [18]. The aggregation number (number of molecules/micelle) is 62. It is available in highly purified forms and is inexpensive. Naturally occurring compounds such as bile salts (sodium taurochlolate, sodium chlolate, etc) are useful as well. Only hydrophobic mechanisms can influence the order of migration with bile salt micelles [19].

Organic modifiers have been used in free zone CE to overcome solubility problems, while their addition in MEKC is much more profound because of their impact on the partition coefficient of a solute between micelle and the aqueous phase. The organic additives make the bulk solution more hospitable for hydrophobic compounds and generally increase migration velocity of hydrophobic species which spend more time in the aqueous buffer. Methanol and acetonitrile are most commonly employed at

concentrations of 5-25%. Other common organic modifiers are urea, cyclodextrins, and crown ethers.

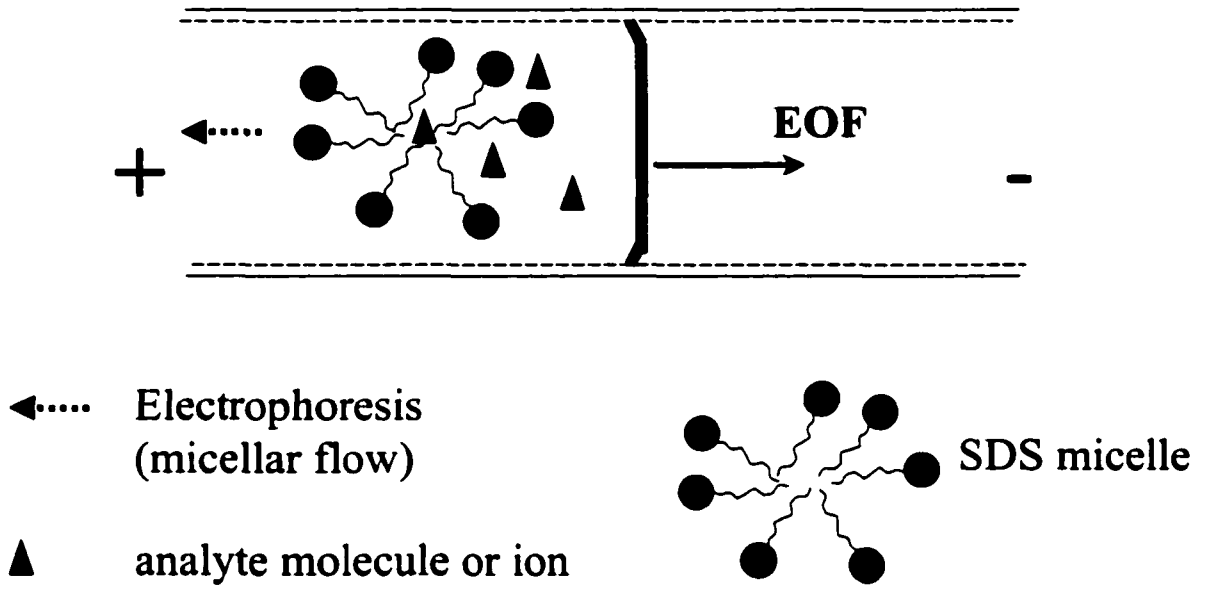

Figure 1.3: Micellar electrokinetic capillary chromatography(MEKC) using sodium dodecyl sulfate (SDS).

1.3 CE Detection

1.3.1 CE Detection Modes

The use of small-volume capillaries provides a great challenge for the detection method applied with CE. Detection sensitivity is always an important issue. In order to produce a high resolution separation, it is necessary to minimize both the sample volume and concentration injected onto the capillary. A variety of detection schemes have been developed for CE, including both on-column and post-column detection.

The polymide coating of a fused-silica capillary can be removed by heating or cutting to provide a small optical window (~ 2mm) for on-column detections, for example, UV/Vis absorbance [5, 11, 20, 21], fluorescence [6, 9, 22-28], refractive index measurements [29-30], Raman [31] and other spectroscopic methods [32].

The analyte molecules eluting out of the detection end of a capillary can also be detected by post-column techniques such as fluorescence [33-35], chemiluminescence [36-38], mass spectrometry [39-41] and electrochemistry [41-43].

1.3.2 Detection Limits

The limit of detection (LOD) is defined as the quantity of an analyte that can produces a signal equal to three times the standard deviation of the blank signal. The background noise can be measured over a certain period of time and the standard deviation can be calculated. In capillary electrophoresis, just like chromatography, it

may be more convenient to calculate detection limits by Knoll's method [44]. The LOD is estimated using the formula

$$C_{LOD} = K_{LOD}\, h_n\, C_s / h_s \qquad (1.14)$$

where C_{LOD} is the LOD quantity, C_s is the concentration of analyte, and h_s is the peak height of the analyte, h_n is the largest noise fluctuation (either positive or negative) observed in the noise measurement interval, and K_{LOD} is a constant, determined for the measurement interval employed. The largest noise fluctuation is measured in a certain interval that is 10-100 times the analyte's peak width at one-half peak height. Values of K_{LOD} are tabulated below in Table 1.1:

Table 1.1: Multiplier constants for LOD of Knoll's method

Peak width multiplier	10	20	50	100
K_{LOD}	1.9718	1.4309	0.9194	0.6536

To calculate detection limit in CE, the electropherogram baseline is inspected over a time period given by a multiple of the full peak-width in terms of time ($w_{1/2}$) at

one-half peak height. Peak height (h_s) and the maximum noise deviation (h_n) are obtained from the electropherogram of a very diluted sample (C_s). The corresponding number of moles of analyte for the limit of detection can be calculated through the following equations:

capillary volume	$V_{cap} = \pi r^2 L_{cap}$	(1.15)
injection volume	$V_{inj} = V_{cap} (t_{inj} / t)$ (injection voltage / CE voltage)	(1.16)
number of moles injected	$n_{inj} = C_s V_{inj}$	(1.17)
detection limit	$n_{LOD} = K_{LOD} n_{inj} (h_n / h_s)$	(1.18)

Detection limits in capillary electrophoresis can often be described using the following units: femtomole (10^{-15} mol), attomole (10^{-18} mole), zeptomole (10^{-21} mole), and yoctomole (10^{-24} mole).

1.3.3 Ultraviolet - Visible (UV/Vis) Absorbance Detection

Ultraviolet (UV)-Visible absorbance, with the fused silica capillary acting as the on-column detector cell, has remained the most popular method of detection applied to CE. Commercially available detectors are single-wavelength, multiple-wavelength, or rapid-scanning spectrometers, and there has been a report of a UV-based diode array detection [45].

One of the main issues with UV/Vis detection is that of insufficient detection limits. Since sensitivity is proportional to path length, therefore its small path length defined by the diameter of capillary limits the concentration sensitivity of absorbance methods. In conventional CZE, the sensitivity of UV detection is about 10^{-5} M, although

the sensitivity in absolute amount is quite high, as much as 10 pg with a molecular mass of 100 and a 10 nL injection volume at this concentration. Investigators have developed many methods to enlarge the path length, such as bubble cell capillaries [46], Z-shaped detection cell [47-48], rectangular glass capillaries[48-49], and multireflection cells [47, 50]. However, they are all fragile and consequently difficult to handle.

1.3.4 Thermal - lens Spectroscopy (TLS)

The photothermal spectroscopic techniques, with special emphasis on the thermal lens spectroscopy (TLS), have been introduced as a detection technique in CE [20, 51-52]. From the analytical viewpoint, it is an extremely sensitive absorptiometric technique with the possibility of reaching very low limits of detection and the capability of making measurements on microsamples.

This technique is based on the optical measurement of the thermal gradient generated by absorption of a laser beam, reviewed by Dovichi [53] and others [54-56]. In the TLS experiment, two laser beams are frequently used. One is the pump laser, which is focused on the sample to provide adequate energy to generate the thermal gradient, also called the thermal lens; another is the probe laser, focused at some distance before or after the sample site. This probe beam reaches the sample with some divergence, and the thermal lens causes the divergence to increase. The decrease in intensity at the center of the probe beam in the far field is related to the concentration of the absorbing species.

The relative change in the probe beam center intensity in the far field $\Delta I_{probe} / I_{probe}$, is given by

$$\Delta I_{probe} / I_{probe} = 1.206\ E_{pump}\ A\ (-dn/dT) / (\lambda k) \quad (1.19)$$

where E_{pump} and λ are the power and the wavelength of the pump laser, and A, dn/dT, k are the absorbance, the temperature coefficient of the refractive index, thermal conductivity of the sample, respectively. By Beer's law, sample absorbance A is proportional to its concentration. Therefore, the sensitivity of thermal lens measurements can be increased by increasing the pump beam energy.

Actually in thermal optical technique, the low detection limit is a consequence of both high sensitivity and low background noise level. There are two main sources for the noise: stability of the lasers and thermal convection. The noise due to the probe beam is reduced by using lock-in detection. Thermal convection should not be the dominant source for noise in a well-designed system. Convective noise can be attributed to changes in temperature, intensity and direction of the stream. When thermal lens signal decreases, the related convection is reduced as well. So reducing the blank signal is a very important way to improve detection limit. Also, the shape of the detection cell can strongly influence the form and the intensity of the convective stream. Especially in the presence of flow, the sensitivity decreases as a consequence of incomplete formation of the gradient, and noise increases owing to flow fluctuations. Finally, the selection of the solvent and the use of additives to modify some background properties should also be considered. The absorbance of water and most common organic solvents in the visible region is not negligible.

In the cross-beam design, the pump and probe beams are crossed at right angles, so the measuring volume is limited to the picoliter region where two beams overlap. This makes the cross-beam configuration attractive for CE, where analytes elute from the 10-

100 μm internal diameter tube. This group has developed a series of thermal optical absorbance detection methods to determine sub-femtomole amounts of (dimethylamino)azobenzene-amino acids and phenylthiohydantoin-amino acids by both CZE and MEKC [20, 51, 57-58]. Recently, the thermal lens detector also has been applied to the analysis of Edman degradation products in protein sequencing [59-60] and the antidepressant drugs in nonaqueous buffer [61]. Bruno reported the on-column separation of various nucleoside and nucleotide mixtures in MEKC buffer and discussed the possibility of extending this technique to native proteins [62]. The mass sensitivity produced by capillary separation, coupled with the high sensitivity of thermo-optical detection, particularly when utilized with a pump laser operated in the ultraviolet portion of the spectrum, suggests a number of compatible applications for the high-sensitivity detection of weak-absorbing substances that are undetectable with conventional CE-UV/Vis technique.

1.3.5 Laser Induced Fluorescence (LIF)

1.3.5.1 General Introduction

Laser-induced fluorescence (LIF) is the most sensitive detection method for capillary electrophoresis. Single molecule detection, which corresponds to the detection in the yoctomolar range (1 yoctomol = 10^{-24} mol), has been demonstrated with LIF detectors [33-35], which is reviewed in [25]. The use of commercial LIF detectors has also been reviewed [63-64]. In contrast with UV absorbance, fluorescence is more selective and potentially more sensitive. Especially for strongly fluorescent substances,

two to six orders of magnitude lower detection limits are typically possible relative to UV absorbance.

On-column LIF detection, by removing the polymide coating outside of the fused silica capillary to provide a on-column transparent window near the exit end of capillary, has an advantage of no extra column bandbroadening, but suffers from a relatively large amount of light scatter, which generates a large amount of background signal due to reflection and refraction at the cylindrical capillary walls. Alternatively, Dovichi's group has reported that stray light can be almost completely eliminated through the use of a sheath-flow cuvette [33-35]. In this post-column LIF system, the end of the capillary is inserted into a square quartz or glass flow chamber (120 μm on a side).

Detection limits in fluorescence measurements are usually determined by shot-noise in the background signal. There are five sources of background signal in fluorescence [65]:

1) Fluorescence from solvent impurities;
2) Fluorescence from detector windows;
3) Raman and Rayleigh scatter from the solvent;
4) Light scatter at the detector-sample interface;
5) Dark current from the photon detector.

To achieve excellent detection limits, each of the sources of background signal must be minimized. For example, solvent impurities are minimized by scrupulous care in sample and buffer preparations. Disposable plastic-ware is used; buffers are kept in dust-free glassware; and bacteria contaminants are avoided by using fresh distilled water and other solvents. Collecting the emitted light at right angles to the excitation source, where

rejection is accomplished by appropriate spectral and spatial filtering, rejects stray light. Water has two Raman bands, one at about 1650 cm^{-1} and the other ranging from 3100 to 3700 cm^{-1}. There are also two minor Raman bands at 1640 and 2200 cm^{-1}. To avoid Raman scatter from water, the excitation wavelength should be chosen so that the analyte emission wavelength occurs where the Raman signal is relatively weak [66].

The excitation source can be a laser beam or an arc lamp, where the excitation wavelength is isolated with a filter [7, 8]. The laser light is most easily focused into small capillaries, leading to the best mass sensitivity. Argon ion lasers have been used extensively as excitation sources. Extremely high laser power is limited in use because optical saturation of the absorbance transition and photodegradation of the analyte molecules occur.

1.3.5.2 Derivatization

The major problem with laser excitation is the paucity of wavelengths available for use. Few chemical species absorb at precisely those wavelengths available, and even fewer have high emission quantum efficiencies. Derivatizations have been used to introduce fluorescent dyes to the analytes of interest and extend the utility of the LIF technique to many compounds. Based on the spectral properties of the chromophors and reactivity between the probe and analyte, the criteria for choosing a fluorescent dye include:

1) The fluorescent dye must be excited easily with an available laser source;
2) The fluorescent dye must have a reasonably high fluorescent quantum yield and low photodistruction rate;

3) The fluorescent dye must have a functional group to react with the analyte;

4) The fluorescent dye must be stable and react quickly with analytes to produce stable derivatives.

One important application of CE is the separation and characterization of amino acids, peptides and proteins. To use high sensitivity laser-induced fluorescence detection, those biomolecules have to be labeled with fluorescent dye molecules. Primary amines can be most easily targeted with fluorescent dye. This modification can also be applied to proteins since almost all proteins have lysine residues, which contain ε - amine groups.

There are pre-, on-, and post-column derivatization strategies available. Precolumn derivatization has a number of advantages:

First, no specialized apparatus or techniques are required. Second, the labeling reactions need not be rapid. Third, side products or excess fluorescent reagents can be separated from the reaction mixture prior to injection or CE separation. On the other hand, it has two disadvantages:

First, the difference in size between similar compounds becomes smaller after labeling, and considerable effort may be required to optimize the separation. Second, multifunctional analyte molecules may produce two or more fluorescent products that are likely to exhibit broader bands or different migration times, which will make the interpretation of the electropherogram more complicated.

For post-column derivatization, the analytes enter a mixing chamber where they react with the fluorescent probe in a short period of time and then the fluorescent derivatives of the analytes are detected. Post-column labeling requires sufficiently fast

devivatization reaction and a well-designed apparatus to carry out the reaction, which are necessary to minimize the degradation of the high efficiency from CE separation and keep the reaction efficiency constant from run to run.

Several on-column designs have also been reported [67], especially for single cell studies [68]. Dovichi et al. described an on-column derivatization procedure that injected different sample zones (probe, analyte or single cell, catalytes) individually into the separation capillary, then waited for a short period of time to allow the solutions inside the capillary to mix together by diffusion and for a labeling reaction to occur before the separation. This approach provides the possibility of extremely high sensitivity and automation.

There is no doubt that the derivatization procedure can improve sensitivity and selectivity. However, there are well-known problems concerning reproducibility and recovery using derivatizations. Furthermore, the yield of some labeling reactions is low and unpredictable byproducts are found.

1.3.5.3 Multiple Capillary Detection

Rapid development of biological and pharmaceutical technology has posed a challenge for high-throughput analytical methods. For one example, current high-sensitivity, high-speed, and high-throughput DNA sequencers based on sheath flow assisted multi-capillary LIF techniques have already been developed for the Human Genome Project and dramatically accelerated the analysis of 3 billion base-pair human genome. Parallel processing permits analysis of multiple samples simultaneously. Our group has many years of experience with CE using multiplex capillaries and sheath flow

cuvette as a fluorescence detector. With attractive features such as rapid analysis time, high separation efficiency, small sample size and low solvent consumption, 16-, 32-, and 96-capillary electrophoresis systems have been successfully used to perform DNA sequencing and other DNA Analysis. Other reports on multiple capillaries started from Mathies in 1992 [69] and Kambara in early 1993 [70]. Also Yeung investigated an optical fiber array to illuminate fluorescence from 10 capillaries [71]. Later more researchers joined the development of multiplex capillary systems [72], and the application extended from fluorescent DNA analysis to absorption detection [73], from conventional capillary arrays to multichannel electrophoretic microchips [74].

1.3.6 Mass Spectroscopy (MS)

The combination of CE with mass spectroscopy is well established and interfaces are commercially available from many MS suppliers. The on-going developments in MS continuously result in improvements in the sensitivity, detection speed, level of structural detail obtainable, and applications of this powerful detector. In one sense, the CE-MS combination is nearly ideal: CE is based on the differential migration of ions, whereas MS analyzes ions by their mass/charge (m/z) ratio. On the other hand, these two highly orthogonal analytical methods exploit ion motions in different environments: conducting liquids for CE and high vacuum for MS. The most important issue in on-line CE-MS is the interface for transfer of substances between the electrophoresis column and the vacuum system of the mass spectrometer. There are some demands on an interface related to a CE-MS combination: the CE flow rates are quite low or negligible, the buffer

is moderately conductive, electrical contact must be maintained with both ends of the capillary and, to maintain the high-separation efficiencies with CE, any "dead volumes" associated with detection need to be avoided or minimized.

Those MS analyzers coupled on-line to CE include inductively coupled plasma (ICP-MS) [75], ion-trap [76], fast-atom bombardment(FAB) [77], sector mass spectrometry [78], and, of course, the most popular electrospray [79]. Smith and co-workers were the first to develop on-line CE-MS under atmospheric conditions using electrospray ionization [40]. The electrospray interface makes electrical contact with the electrophoretic buffer via either a small needle or a thin film of metal deposited on the surface of the capillary or recently, by a sheath flow. In electrospray, a high voltage (3-6 kV) is applied between the electrospray tip and the entrance (skimmer) at the mass spectrometer input. This potential drop provides a cloud of charged droplets, with evaporation assisted by a counterflow of warm drying nitrogen gas. Charged ions are released from very small droplets in the vapor state (ion evaporation) and are then brought directly into the vacuum region of the mass spectrometer through a sampling orifice. Total ion current electropherograms are generated. During the ionization process, the flow rate necessary to sustain a stable ESI source from a capillary of conventional dimensions is generally 1-10 μL/min. CE flow rates are generally much less than desired for ESI, and the CE buffers used are often substantially more conductive than required for ESI. The sheath flow interface introduces a makeup flow of a less conductive and generally more volatile solution (such as pure methanol, methoxyethanol, or acetonitrile, but frequently augmented by as much as 10- 20% formic acid, acetic acid, water, or other reagents), which serves to dilute the CE buffer and assist ESI.

In general, all the concerns in CE relevant to sample injection, buffer composition, and capillary surface interaction efficiency apply to CE-MS. For example, sensitivity can vary significantly with buffer composition and the best sensitivity is usually obtained with the use of volatile buffer components, such as acetic acid at the lowest practical concentration, and by minimizing nonvolatile components. In addition, buffer components that interact strongly with the sample substantially degrade sensitivity. In particular, the use of surfactants, such as sodium dodecyl sulfate (SDS), gives rise to intense signals in either positive- or negative-ion ESI, presenting a major barrier for MECC-ESI application. Also, the use of nonvolatile buffers not only can lead to clogging of vacuum orifices and probe tips, but can form adduct ions that effectively decrease the sensitivity of the instrument by spreading the ion abundances among several masses; such as the formation of $(M+Na)^+$, $(M-H+2Na)^+$ and so on. Therefore, the use of non-aqueous CE electrolytes is particularly attractive for CE-MS since sensitivity can be significantly improved. But the use of MECC buffers requires specific operating procedures, or interfaces, or modified surfactants, to avoid fouling of the MS source with the involatile surfactants.

The major considerations relevant to MS detection are MS sensitivity, resolution, and related scan-speed compromises. The mechanical details of the electrospray interface can influence ESI stability and ease of operation. More important, MS sensitivity is ultimately limited by the ability to efficiently analyze ions produced by electrospray ionization. Only ~0.01% of ions are transported from the ESI source into the MS.

Scan rate is another important factor for a CE-MS instrument. Most current Mass Spectrometers are scanning instruments; that is, a range of masses are scanned over a set time period, which means that the mass spectrometer passes ions of a given mass to the detector for only a very small percentage of the scan time. If the CE peak is sufficiently narrow (only a few seconds or less), the MS may not be passing ions of appropriate mass to the detector when an analyte is eluting, which may lead to missed components. If the MS scans too fast, problems with ion statistics may be encountered; that is, the instrument may be scanning fast enough to pass the appropriate mass when the compound elutes, but too fast to pass sufficient ions to the detector to obtain a reasonable signal/noise ratio (insufficient dwell time). For quadrupole MS, single or multiple ion monitoring, SIM (selected ion monitoring) leads to significantly enhanced detection limits relying on the greater dwell times at specific m/z values.

Several issues remain to be resolved for the use of CE-MS. First, a better understanding of the influence of buffer constituents and pH relative to the electrospray signal is necessary. A second issue is detection levels. Typically, the LODs obtained by CE/MS are similar to those obtained by common UV detection; concentration detection limits of roughly 10^{-5} M have been found, and this is certainly not low enough for trace analysis. Some preconcentration methods, such as coupled column ITP, have been used [79]. In addition, narrow-diameter capillaries of 20 μm or smaller have been applied to reduce the current in the capillary to the nanoampere range, which is similar to that in the electrospray cloud. This permits a more efficient utilization of ions from the capillary. Another limiting factor that is related to electrospray is that only a small fraction of the ions formed in the electrospray are actually collected by the sample orifice and

transported into the mass analyzer. Improvements in ion collection efficiency will also greatly aid in lowering detection limits. Moreover, for effective utilization of a typical few-seconds peak width in CE, rapid-scanning mass spectrometers must be employed.

1.4 Thesis Outline

For a number of years, this laboratory has been developing CE; most of the work has focused on sheath flow assisted laser-induced fluorescent detection. Not all issues are resolved at the present time. The objectives of this research are to further develop the applications of CE coupled with various detectors to small biological molecules, and explore the analytical ability of these techniques with some real samples, such as food products and brain cells/tissues.

Characterizing and optimizing the parameters of both CE-ESI-MS and CE-LIF analysis of biogenic amines in food samples, especially the factors influencing the ESI signals, in order to obtain the best signal characteristics, make up the first part of the thesis. This part of work is limited to standards. Then I expanded the CE-LIF application to real samples: brain microdialysates and tissue homogenates. The remainder of this thesis is the development of multi-capillary thermo-lens absorbance detector for analysis of many samples, followed by the evaluation of this new instrument. The results shown here, although rather preliminary, demonstrate the feasibility of the

multiple capillary system as a separation medium based on the sheath flow cuvette as a thermal optical detector.

References

1. S. Hjerten, *Chromatographic Reviews,* 1967, 9, 122.
2. N. Catsimpoolas, *Separation Science,* 1971, 6, 435.
3. R. Virtanen, *Acta Polytechnology Scandinavian,* 1974, 123, 1.
4. F. E. P. Mikkers, F. M. Everaerts, and T. P. E. M. Verheggen, *Journal of Chromatography,* 1979, 169, 1.
5. F. E. P. Mikkers, F. M. Everaerts, and T. P. E. M. Verheggen, *Journal of Chromatography,* 1979, 169, 11.
6. J. W. Jorgenson, and K. D. Lukacs, *Analytical Chemistry,* 1981, 53, 1298.
7. J. W. Jorgenson, and K. D. Lukacs, *Journal of Chromatography,* 1981, 218, 209.
8. J. W. Jorgenson, and K. D. Lukacs, *Clinical Chemistry,* 1981, 27, 1551.
9. J. W. Jorgenson and K. D. Lukacs, *Science,* 1983, 222, 266.
10. S. Hjerten, *Journal of Chromatography,* 1983, 270, 1.
11. S. Terabe, K. Otsuka, K. Ichikawa, A. Tsuchiya, and T. Ando, *Analytical Chemistry,* 1984, 56, 111.
12. M.J. Eby, *Bio/technology,* 1989, 7, 903.
13. J.W. Jorgenson and K.D. Lukacs, *Journal of Chromatography,* 1985, 30, 121.
14. J.W. Jorgenson, *Analytical Chemistry,* 1986, 58, 743A.
15. J. W. Jorgenson, *ACS Symposium,* 1987, 335, 182.
16. X. Huang, M.J. Gordon, R.N. Zare, *Analytical Chemistry,* 1988, 60, 375.
17. F.F. Cantwell, Course Chem 421 notobook, Section 1.6, *Analytical Separations: Gas Chromatography, Liquid Chromatography, Supercritical Fluid Chromatography and Electrophoresis*, Edmonton,1996.

18. K. Otsuka, S. Terabe, and T. Ando, *Journal of Chromatography,* 1985, 332, 219.

19. H. Nishi, T. Fukuyama, M. Matsuo, S. Terabe, *Journal of Chromatography,* 1990, 498, 313.

20. M. Yu, N.J. Dovichi, *Analytical Chemistry,* 1989, 61, 37.

21. Y. Walbroehl, J.W. Jorgenson, *Journal of Chromatography,* 1984, 315, 135.

22. J.S. Green, J.W. Jorgenson, *Journal of Chromatography,* 1986, 352, 337.

23. W.G. Kuhr, E.S. Yeung, *Analytical Chemistry,* 1988, 60, 2642.

24. M. Albin, R. Weinberger, E. Sapp, S. Moring, *Analytical Chemistry,* 1991, 63, 417.

25. M.A. Cousine, T.B. Jarbawi, H.B. Halshall, W.R. Heineman, *Analytical Chemistry,* 1997, 69, 544A.

26. Q. Xue, E.S. Yeung, *Nature,* 1995, 373, 681.

27. Q. Xue, E.S. Yeung, *Analytical Chemistry,* 1994, 66, 1175.

28. N.M. Schultz, R.T. Kennedy, *Analytical Chemistry,* 1993, 65, 3161.

29. J. Wu, T. Odake, T. Kitamori, T. Sawada, *Analytical Chemistry,* 1991, 63, 2216.

30. A.E. Bruno, B. Krattiger, F. Maystre, H.M. Widmer, *Analytical Chemistry,* 1991, 63, 2689.

31. C.Y. Chen, M.D. Morris, *Applied Spectroscopy,* 1988, 42, 515.

32. W.G. Kuhr, C.A. Monnig, *Analytical Chemistry,* 1992, 64, 389R.

33. D.Y. Chen, N.J. Dovichi, *Journal of Chromatography B,* 1994, 657, 265.

34. D.Y. Chen, N.J. Dovivhi, *Analytical Chemistry,* 1996, 68, 690.

35. D.B. Craig, J.C.Y. Wong, N.J. Dovichi, *Analytical Chemistry,* 1996, 68, 697.

36. R. Dadoo, L.A. Colon, R.N. Zare, *Journal of High Resolution Chromatography,* 1992, 15, 133.

37. M.A. Ruberto, M.L. Grayeski, *Analytical Chemistry,* 1992, 64, 2758.

38. J. Zhao, N.J. Dovichi, *Journal of Microcolumn Separation,* 1993, 5, 331.

39. R.D. Smith, J.A. Olivares, N.T. Nguyen, H.R. Udseth, *Analytical Chemistry,* 1988, 60, 436.

40. J.A. Olivares, N.T. Nguyen, C.R. Yonker, R.D. Smith, *Analytical Chemistry,* 1987, 59, 1230.

41. R.A. Wallinhford, A.G. Ewing, *Analytical Chemistry,* 1987, 59, 1762.

42. R.A. Wallinhford, A.G. Ewing, *Analytical Chemistry,* 1988, 60, 258.

43. A.G. Ewing, R.A. Wallinhford, and T.M. Olefirowicz, *Analytical Chemistry,* 1989, 61, 292A.

44. J.E. Knoll, *Journal of Chromatographic Science,* 1985, 23, 422.

45. K.D. Altria, *Journal of Chromatography A,* 1999, 856, 443.

46. D.N. Heiger, P. Kaltenbach, H-J.P. Sievert, *Electrophoresis,* 1994, 15, 1234.

47. M. Albin, P.D. Grossman, S.E. Moring, *Analytical Chemistry,* 1993, 65, 489A.

48. A. Mainka, K. Bachmann, *Journal of Chromatography A,* 1997, 767, 241.

49. T. Tsuda, J.V. Sweedler, R.N. Zare, *Analytical Chemistry,* 1990, 62, 2149.

50. T. Wang, J.H. Aiken, C.W. Huie, R.A. Hartwick, *Analytical Chemistry,* 1991, 63, 1372.

51. T.G. Nolan and N.J. Dovichi, *Analytical Chemistry,* 1987, 59, 2803.

52. A.E. Bruno, A. Paulus, and D.J. Bornhop, *Applied Spectroscopy,* 1991, 45, 462.

53. N.J. Dovichi, *CRC Critical Review Analytical Chemistry,* 1987, 17, 357.

54. G. Ramis-Ramos, *Anal. Chim. Acta,* 1993, 283, 623.

55. Y. Martin-Biosca, M.C. Garcia-Alvarez-Coque, G. Ramis-Ramos, *Journal of Biochemical & Biophysical Methods,* 1994, 29, 1.

56. J. Georges, *Talanta,* 1999, 48, 501.

57. K.C. Waldron, N.J. Dovichi, *Analytical Chemistry,* 1992, 64, 1396.

58. M. Chen, K.C. Waldron, Y. Zhao, N.J. Dovichi, *Electrophoresis,* 1994, 15, 1290.

59. X-F Li, K.C. Waldron, J. Black, D. Lewis, I. Ireland, N.J. Dovichi, *Talanta,* 1997, 44, 401.

60. K.C. Waldron, X-F Li, M. Chen, I. Ireland, D. Lewis, N.J. Dovichi, *Talanta,* 1997, 44, 383.

61. X-F Li, C-S Liu, P. Roos, N.J. Dovichi, *Electrophoresis,* 1998, 19, 3178.

62. B. Krattiger, A.E. Bruno, H.M. Widmer, and R. Dandliker, *Analytical Chemistry,* 1995, 67, 124.

63. S.R. Rabel, J.F. Stobaugh, *Pharmaceutical Reviews,* 1993, 10, 171.

64. C.E. MacTaylor, A.G. Ewing, *Electrophoresis,* 1997, 18, 2279.

65. C.A. Parker, *Photoluminescence of Solutions, Section 5C,* Elservier, New York, 1968.

66. S. Wu, N.J. Dovichi, *Journal of Chromatography,* 1989, 480, 141.

67. A. Taga, A. Nishino, S. Honda, *Journal of Chromatography A,* 1998, 822, 271.

68. S.N. Krylov, Z. Zhang, N.W.C. Chan, E. Arriaga, M.M. Palcic, and N.J. Dovichi, *Cytometry,* 1999, 37, 15.

69. R.A. Mathies and X.C. Huang, *Nature,* 1992, 359, 167.

70. H. Kambara and S. Takahashi, *Nature,* 1993, 361, 565.

71. J.A. Taylor and E.A. Yeung, *Analytical Chemistry,* 1993, 65, 956.

72. M.A. Quesada, S. Zhang, *Electrophoresis,* 1996, 17, 1841.

73. X. Gong and E.A. Yeung, *Analytical Chemistry,* 1999, 71, 4989.

74. Z. Huang, N. Munro, A.F.R. Huhmer and J.P. Landers, *Analytical Chemistry,* 1999, 71, 5309.

75. K. Sutton, R.M.C. Sutton, J.A. Caruso, *Journal of Chromatography A,* 1997, 789, 85.

76. J.T. Wu, M.G. Qian, M.X. Li, K.F. Zheng, P.Q. Huang, D.M. Lubman, *Journal of Chromatography A,* 1998, 794, 377.

77. R. Caprioli, W. Moore, M.Martin, B. DaGue, K. Wilson, S. Moring, *Journal of Chromatography,* 1989, 480, 247.

78. M.A. Moseley, L. Deterding, K. Tomer, J. Jorgenson, *Journal of Chromatography,* 1989, 480, 197.

79. J.F. Banks, *Electrophoresis,* 1998, 18, 2255

Chapter 2

Detection of Biogenic Amines in Foods with CE-MS Techniques

2.1 Introduction

2.1.1 Occurrence of Biogenic Amines in Foods

Biogenic amines are aliphatic, alicyclic and heterocyclic organic bases of low molecular weight. Because they are very stable compounds which are able to resist heat and survive acidic or alkaline conditions, biogenic amines can interact non-specifically with negatively charged structures to form bridges between them, and therefore connecting them. Hence these substances fulfill essential roles in human cellular metabolism and in the synthesis of DNA, RNA and proteins, such as the control and initiation of the translation of mRNA to form proteins and also the regulation of the fidelity of translation [1]. In general, biogenic amines not only play important physiological roles in living animals and plants; they are the intermediates of decarboxylation and fermentation processes in food. It is believed that dietary biogenic amines at levels normally present in food are nontoxic, while in higher concentrations, biogenic amines exhibit unnatural and toxic effects [2,3]. For example, histamine, formed from bacterial decarboxylation of histadine, has caused food poisoning. Consumption of high levels of histamine can lead to nausea, respiratory distress, oral burning, sweating, and hyper- or hypotension [4,5]. Based on their chemical structure, biogenic amines can be classified as mono-, di-, and polyamines. The compounds that

are of food related interest are the monoamine tyramine, the diamines histamine, tryptamine, putrescine, and cadaverine and the polyamines agmatine, spermidine and spermine, Figure 2.1. During storage, the content of those amines in beef or packaged meat products can be changed due to the action of bacteria involved in the decarboxylation process of free amino acids. Therefore, their presence in high amounts in food is probably associated with food deterioration. Investigating the content of biogenic amines in food to ensure that they are within the tolerated level has been of special interest to the physiologist and biochemist. Some countries, including the US, Sweden, Austria and the Netherlands, have established regulations and legal requirements for the maximum limits of biogenic amines (mainly histamine) in various types of food [6]. These have prompted numerous investigations to determine levels of biogenic amines in food samples.

2.1.2 Determination of Biogenic Amines in Foods

The quantification of biogenic amines has been carried out with different chromatogaphic methods: thin-layer chromatography (TLC) [7-9], gas chromatography (GC) [10-12], high-performance liquid chromatography (HPLC) [13-14] and capillary electrophoresis (CE) [15-27]. Historically, paper chromatography and TLC have been used to separate and identify amines. For most analytical procedures, researchers have turned to GC as a means of separating and identifying complex mixtures. Obviously, with volatile amines, chromatographic volatility is no problem; however, much effort has been spent on making volatile derivatives of normally nonvolatile amines. Current

reference and official analytical methods use HPLC, and most of the reported procedures for biogenic amine analysis in food are time-consuming methods and have limited sensitivity, detection ability and reproducibility. The application of CE for determination of biogenic amine amounts may solve some of these problems.

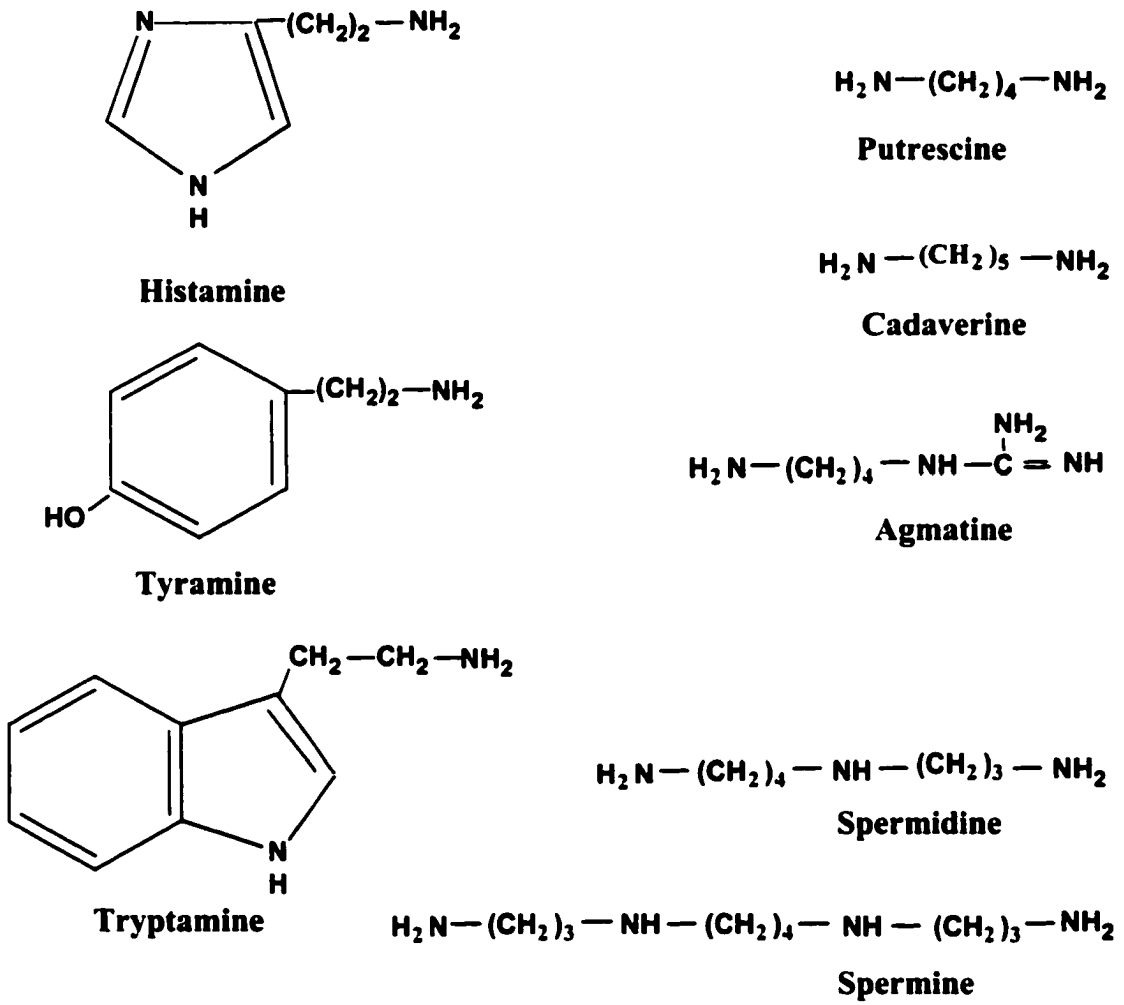

Figure 2.1: Structures of biogenic amines.

CE has become a more popular and powerful separation technique because of its high separation efficiency, high resolution, rapid analysis and small sample consumption [18-19]. Improved separation and determination of biogenic amine mixtures were performed by CE methods with detection based on molecular spectroscopic techniques. W-C Lin and his co-workers [20] separated the amines containing aromatic functional groups by capillary zone electrophoresis with an on-column UV detector. On the other hand, since most amines are UV inactive, Arce *et al.* [21] accomplished the detection of biogenic amines in wine with indirect UV detection. Because of the short path length due to the small inner diameter of capillaries, the concentration sensitivity of UV detection is usually limited. Most advances have been made in using laser-induced fluorescence (LIF) detection [22]. The selectivity of labeling procedures makes it possible to record multiple compounds in a single run. Several fluorescent dyes such as fluorescamine-dioxane [23], fluoresceine isothiocyanate (FITC) [24-26] and 6-aminoquinolyl-N-hydroxysuccinimidyl carbamate (AccQ) [27] were suggested as labeling agents to separate amines in real samples [23-27]. However, since there are not many compounds that possess native fluorescence, fluorescence detection, while highly useful, is limited by the number of available fluorescent tags that will induce fluorescence at wavelengths obtainable with the laser, and the separation may be more complicated due to the derivatization.

The combination of CE with mass spectrometry detectors offers a number of advantages compared to the traditional UV and LIF detectors: the selective and universal detection of mass spectrometry provides helpful structural information, which can greatly

complement CE separation. Peak identification for method validation is much more reliable and simplified, and sometimes possible without reference substances. Moreover, because of the additional information of the mass selective chromatogram, partial resolution is sufficient, e.g., for quantitation. Since Smith and co-workers first developed on-line CE-MS under atmospheric conditions using electrospray ionization in 1987 [28,29], mass spectrometry, especially electrospray ionization mass spectrometry, has emerged as one of the preferred methods to detect biological molecules. The applications of on-line CE-ESI-MS have been primarily for peptide and protein analyses [30-37]. Another important contribution of CE-ESI-MS is the investigation of drug metabolism and structural elucidation of pharmaceutical products [38-40]. Also mass spectrometric detection has been extensively used for the analysis of compounds of environmental concern, such as agrochemicals, pesticides, inorganic compounds and dyes [41-44]. The improvements in CE-MS coupling have made it possible to apply this technique to the detection and quantification of amines.

Few data are available on applications of on-line CE-ESI-MS techniques for determination of biogenic amine molecules in food. The long-term goal of this project is to apply CE-MS to biogenic amine analysis during storage of meat products and to evaluate the undesirable changes that may occur in vacuum or modified atmosphere packaged extended shelf life meat products. In this chapter, I report the applicability of CE-MS as a rapid and sensitive method for determining mixtures of eight amines. The protonated amines were analyzed directly using uncoated fused-silica capillaries (50 μm i.d.) with a sheath flow liquid assisted ESI-MS system. The optimized conditions for

both CE and MS parameters have been examined. The related CE-LIF work also has been investigated.

2.1.3 CE-MS Instrumentation

A schematic diagram of the CE system (Thermo Separation Products, San Jose, CA, USA) followed by a Perkin-Elmer/Sciex API 100 (Thornhill, ON, Canada) mass spectrometer equipped with an ion spray source, which was used to acquire the on-line CE-ESI-MS data in this chapter, is presented in Figure 2.2. The main components of the instrument include the CE (including a fused silica capillary, sample injector, high voltage power supply), an interface system (also called entrance optics), a differentially pumped zone, ion lenses, a single quadrupole mass spectrometer, and a detector.

After the analytes are separated by the electrophoretic flow and appear at the end of the capillary (surrounding by the nebulizing gas and sheath liquid flow), high voltage (3-6 kV) is applied between the electrospray tip and the entrance of a quadrupole mass spectrometer. This potential drop provides a cloud of charged droplets, with evaporation assisted by a counterflow of warm drying nitrogen gas. Charged ions are released from very small droplets in the vapor state (ion evaporation) and are then brought directly into the vacuum region of the mass spectrometer through the entrance optics. The entrance optics consist of the curtain plate, the orifice plates, the skimmer and the focusing ring; details are shown in Figure 2.3. With the exception of the grounded skimmer, voltage potentials applied to these elements help guide the sample ions through the vacuum interface.

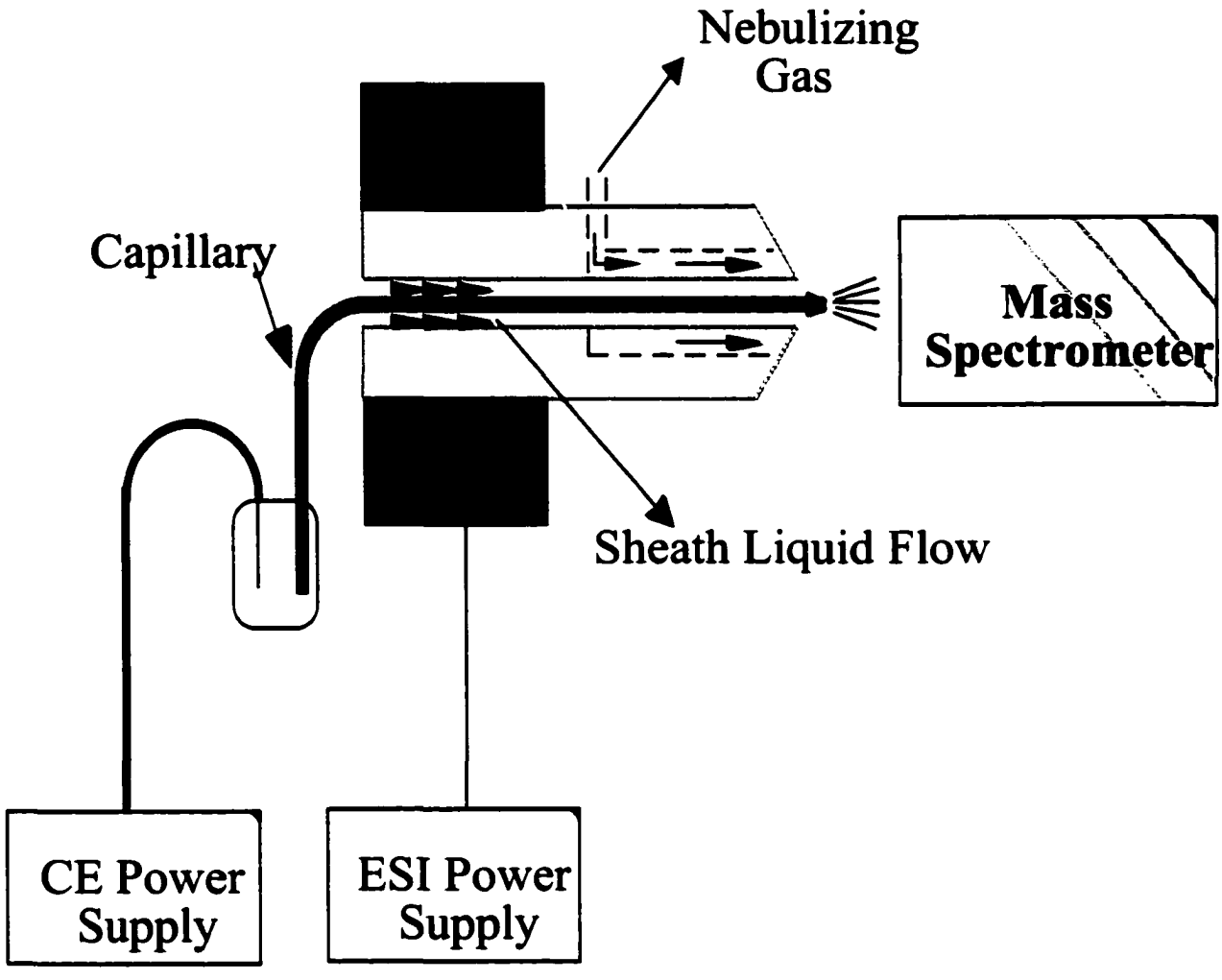

Figure 2.2: Schematic diagram of CE-ESI-MS system.

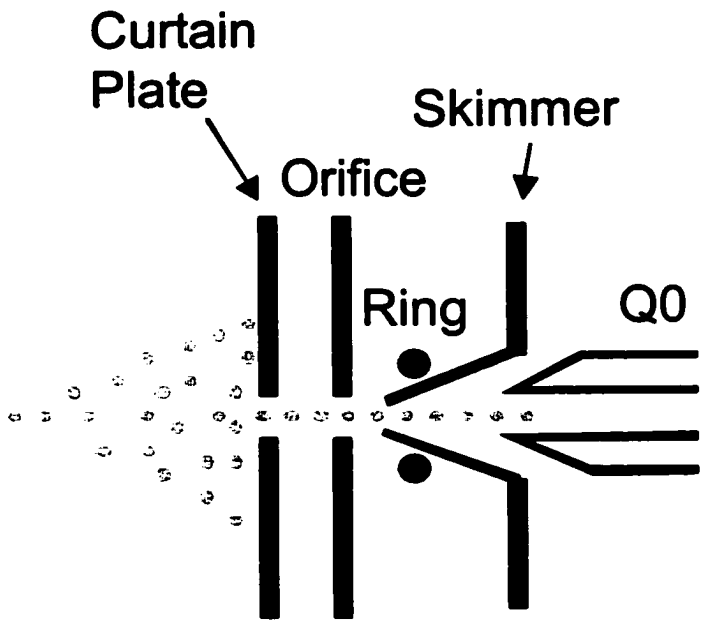

Figure 2.3: Schematic diagram of API 100 entrance optics.

Ions are transferred from the interface to the single quadrupole mass analyzer via the ion optics, which consist of an RF only quadrupole Q0, mass filter quadrupole Q1, the stubbies and an IQ1 interquad lens.

After separation according to mass-to-charge ratio in the mass analyzer, ions are drawn from the Q1 into the ion detector, which is a continuous dynode device called a Channel Electron Multiplier (CEM). The deflector aids the efficiency of collecting the ions. When struck by an ion, the CEM emits an electron pulse, which then is converted to a digital signal, and finally is processed (counted) to provide an absolute ion count.

2.1.4 Operating Parameters for CE-ESI-MS

In order to use CE-ESI-MS efficiently and to take full advantage of its capability, it is necessary to know the effect of the instrument operating parameters on the analytical signals. The physical, electrical and chemical processes involved in CE-ESI-MS are quite complicated and a great number of variables affect the success of coupling a CE separation system to ESI-MS detection. The parameters of both CE and ESI-MS must be considered together to obtain the best performance. These factors include the design and operating parameters of the electrospray interface, the composition and the pH of the CE running buffer, the electrospray buffer composition, and the chemical properties of the analytes. Therefore, the influence of these parameters on the separation efficiency, electrospray stability, detection sensitivity, and charge state distribution will be investigated separately in this chapter.

2.2 Experimental

2.2.1 Chemicals

The compounds studied (Figure 2.1) were as follows: histamine, tyramine, tryptamine, putrescine, cadaverine, agmatine, spermine and spermidine purchased from Sigma (St. Louis, MO, USA). Stock standard solutions of 1 mM were prepared in deionized distilled water and then diluted with CE running buffers or 10-fold diluted running buffer for the further studies. HPLC grade methanol and acetonitrile were from

BDH (Toronto, ON, Canada); ammonium acetate was supplied from Anachemia (Montreal, PQ, Canada).

Generally, acetic acid and organic solvents were added to a certain volume of 100 mM ammonium acetate stock solution, and then a portion of water was used to dilute to a proper concentration of CE running buffer before use. The buffer was degassed for at least 5 minutes before applying high voltage. Water was purified with a Milli-Q deionized water system and all the buffers were filtered with 0.2μm membranes before use.

2.2.2 CE Conditions

CE was carried out using an in-house constructed instrument: 11 or 16 kV high voltage generated from a power supply (CZE 1000, Spellman, USA) was applied to the untreated 56 cm x 50 μm (i.d.) x 140 μm (o.d.) open tube fused-silica capillaries (Polymicro Technologies, Phoenix, AZ) for separations. Before and between runs, fresh running buffers were used to flush the capillary by use of a syringe. Samples were introduced into the capillary by electrokinetic injection at 10 kV for 5 s and the separations were performed with current of 5 to 7 μA. In most CE-MS experiments, the running buffer (pH 3.0) was 30 mM ammonium acetate, 6% acetic acid and 30% methanol. The vial that held the running buffer was discarded after each run to eliminate run to run contamination.

2.2.3 CE-ESI-MS Conditions

The eluents from the capillary of the on-line CE-ESI-MS system were analysed by a single quadrupole mass spectrometer equipped with an ion spray source. The capillary was inserted inside the electrode tube tip; a sheath liquid flowed around the capillary in order to assist the electrospray process. The sheath liquid must be sufficiently conductive to complete the CE separation circuit and to permit ESI, but not so high in ionic strength as to create arcing and discharging in the ESI source. Furthermore, it must be low in surface tension to allow the formation of a Taylor cone while being miscible with the CE buffer. Between the sheath liquid and the inner wall of electrode tube, the coaxial purified nitrogen nebulizing gas was used. All the sheath liquids used were methanol at a flow rate of 2 μL/min for the experiments. During separation, the ion spray voltage (IS) was 4.2 kV and during sample injection, this voltage was set to 0 and the nebulizing gas was adjusted to its lowest setting. The lifetime of the capillary was typically limited to several days of operation before replacement was necessary; failure was usually identified by unstable ion spray signals and this was attributed to loss of electrical contact at the capillary exit. Positive ion mode was used for all the measurements. Both full scan and selected ion monitoring (SIM) were used. For the full scan, the scan range was m/z 50-350 and the step size was 0.5 amu, dwell time was 3 ms, and the scan speed was 1.81 second. For SIM, ions m/z 72, 86, 95, 112, 121, 129, 131, 144 were chosen, and the step size was 0.1 amu, the dwell time was 10 ms, the speed was 89.5 seconds. The data were sent to a Power Macintosh computer and all the CE-MS electropherograms were acquired by LC2 Tune 1.2 software, and then processed by Multiview software from Perkin-Elmer Sciex Instruments.

2.2.4 Real Samples

For the purpose of detecting biogenic amines in real samples, food samples were first ground to a fine powder using a coffee grinder, then added 50 mL 6% perchloric acid (w/w) was added to 25 g of ground food. The mixture was then blended twice for 15 seconds in a glass Virtis jar, and finally the extract was filtered through Whatman #4 filter paper. In order to prepare this sample for derivatization, 25% KOH was added to neutralize and ensure a pH value greater than 7. Furthermore, the sample was stored in a refrigerator for more than one hour until the precipitate settled down. An aliquot was removed for analysis.

2.2.5 Labeling Process

Fluorogenic dye 5-furoylquinoline-3-carboxaldehyde derivatives (FQ-amines) were obtained according to the procedures described as follows:
FQ was prepared by dissolving a certain amount of solid FQ (Sigma, St. Louis, MO, USA) in methanol. Then 100 μmol was distributed in 600-μL centrifuge tubes, where the solvent was evaporated at room temperature (20°C) and stored in the freezer. For the derivatization, the dried FQ was thawed and then mixed with 9 μL samples and 1 μL 25 mM KCN in the dark. After 10 minutes, water was added to quench the reaction and dilute the sample to the required concentration.

Spermine and spermidine cannot be labeled with FQ under the above conditions. Black precipitations were observed during the reaction periods. Only six biogenic amines were examined by CE-LIF.

2.2.6 CE-LIF Experiments

CZE-LIF experiments have been done with an in-house constructed instrument in 25 mM tricine and 4 mM SDS running buffer. The same power supply as in CE-MS was applied to the 40 cm x 50 μm (i.d.) x 140 μm (o.d.) open tube fused-silica capillaries for detection. Biogenic amines 2 μM were electrokinetically introduced at the electric field of 100 V/cm for 5 s, and the separation was carried out with 400 V/cm.

MEKC was performed with 10 μM amine in solution containing 50 mM sodium phosphate, 30 mM sodium cholate, 20 μM γ -cyclodextrine, 4 M urea and 15% acetonitrile at an electric strength of 200 V/cm. The same derivatization procedure was used for the MECC except for a dilution with 10^{-3} M sodium cholate to stop the labeling reaction.

2.2.7 Temperature Effect Experiments

The CZE-LIF experiment has also been used to investigate the effect of temperature. 10 μM amine mixture was injected onto a 73 cm long naked capillary at 100 V/cm for 10 s and separations in 25 mM tricine running buffer have been performed at a voltage of 400 V/cm under different temperature conditions. The capillary was kept

in an isolated heating system and the temperatures were adjusted to 25, 35, 45, 55, 65 °C during the experiments.

2.3 Results and Discussion

2.3.1 MS Parameters

Before performing the on-line CE-MS analysis, micro ion spray experiments were exploited to optimize the electrospray instrument response for the individual amine or amine mixtures. The position of the microspray tip was adjusted for maximum sensitivity while the analytes were infused through the CE column at a flow rate of 2.0 μL/min by a mechanical pump. Positive ion mode was used for all measurements. The other operating parameters, such as ion spray voltage (IS), orifice voltage (OR), ring voltage (RNG), nebulizing gas flow (NEB) and curtain gas flow were optimized every day for maximum total ion spray signals over a mass range of m/z 50-350 using the same flow injection method. A 1.7×10^{-5} Torr working pressure was always kept in the chamber of the analyzer and the ion detector voltage was maintained at 2.3 kV during instrument operation.

1 mM tryptamine was chosen as an example to show how these ion spray parameters were optimized (Figure 2.4, Figure 2.6, and Figure 2.7). Mass spectra of the tryptamine standard in the running buffer solution over the range 50 to 350 amu were acquired at different orifice voltages. This parameter controls the acceleration of the ions in the intermediate pressure region between the atmosphere and the vacuum and thus the

energy of ion-molecule collisions, which are responsible for fragmentation. Even though the proton addition $[M+H]^+$ (m/z 161) is the molecular ion, at the different OR voltages shown in Figure 2.4, the spectrum gave a simple profile in which the dominant peak is always due to the fragment ion $[M+H-17]^+$ (m/z 144) and some small contributions from $[M+H]^+$ (161), $[M+Na]^+$ (183) and $[2M+H]^+$ (321).

There is a significant difference in the intensity of fragmentation signals with different OR. Higher OR voltages discriminate the parent ion (m/z 161) and the major fragment (m/z144), and generate more lower molecular weight fragment ions at the expense of lower total intensity. Moreover, the fragmentation of the protonated parent ion still occurred, even when the voltage was set to the minimum value. In this study, with the lower OR, the fragment ion m/z 144 was quite stable towards the ionization process and did not undergo further fragmentations (Figure 2.5). Therefore, 40 V was chosen to generate less in-source collision-induced dissociation to monitor the most abundant ions (m/z 144). This feature is particularly valuable as the ionizing energy imparted to the ions in atmospheric pressure ionization process is often too low to produce further fragment ions and it is confirmed in the case of other biogenic amines.

Next, the ESI-MS sensitivity for the most abundant ions (m/z = 144) of tryptamine identified in the first experiment was further optimized by changing the ion spray voltage (IS) and ring voltage (RNG) from 2000 to 6500 V at a step size of 200 V and from 0 to 400 V with a step size of 10 V, respectively. It was found that if the IS was higher than 2800 V, the electrospray started to produce signal. With a voltage more than 4800 V, further fragmentations and more dimer species such as $[2M+H]^+$ were generated and the ESI signals started to fluctuate. The effects of the ring voltage offered

similar results. The highest signal was obtained in the middle of the range because more parent ions were found at lower RNG and more fragmentations with higher RNG. Optimum response with regard to signal intensity and stability was obtained with 4200 for IS and 180 for RNG and these settings were maintained for further operation.

The coaxial nitrogen gas flow employed as nebulizing gas, which did not interfere with the electrospray but substantially enhanced the nebulization efficiency, was used to pneumatically assist the ESI process. This nebulization gas at a higher flow rate could induce a pressure difference between inlet and outlet of the capillary column, and therefore generate a significant effect on the CE separation [40]. Usually, the range of nebulizing flow rate was kept within 0.17 to 0.41 L/min (NEB 1 to 3). Furthermore, this setting was reduced to zero (0.03 L/min) during the sample injection procedure in order to avoid siphoning. The curtain gas flow was adjusted with the nebulization gas in order to achieve stable signals. If the NEB was 0, then CUR was 8; if NEB was 2, then CUR was 9.

Unless indicated, the IS was 4.2 kV, OR was 40 V, RNG was 180 V, NEB was 2 (0.26 L/min) or 0 (0.03 L/min), and the curtain gas flow was 9 (1.07 L/min) or 8 (0.95 L/min). The mass spectrometer was calibrated by direct infusion of a solution of a 3-amino acid residue peptide in methanol-water (50:50, v/v) containing 1% acetic acid to give the average molecular masses of the observed signals.

Figure 2.8 gives the ESI mass spectrum of tryptamine, which is representative of typical biogenic amines studied here. The spectrum was obtained by using 1:10 watermethanol buffer solution during continuous flow introduction of tryptamine into the capillary. The spectrum shows a relatively small contribution of the singly charged

molecular ion (m/z 161) and the dominant fragmentation of m/z 144 due to the loss of the NH_3 from the protonated molecular ions.

An additional fragment ion (m/z 117) is also observed in the spectrum from cleavage of the side chain. The contribution of the sodium ion adducts (m/z 183) appear to be related to both the buffer composition and the degree of desolvation during ESI. Under such conditions, most importantly at high analyte concentrations, dimmer and triple species (M_2^+, M_3^+) can become more visible. In general, greater sensitivity and reproducibility could be controlled by using conditions which maximize desolvation and minimize cluster formation.

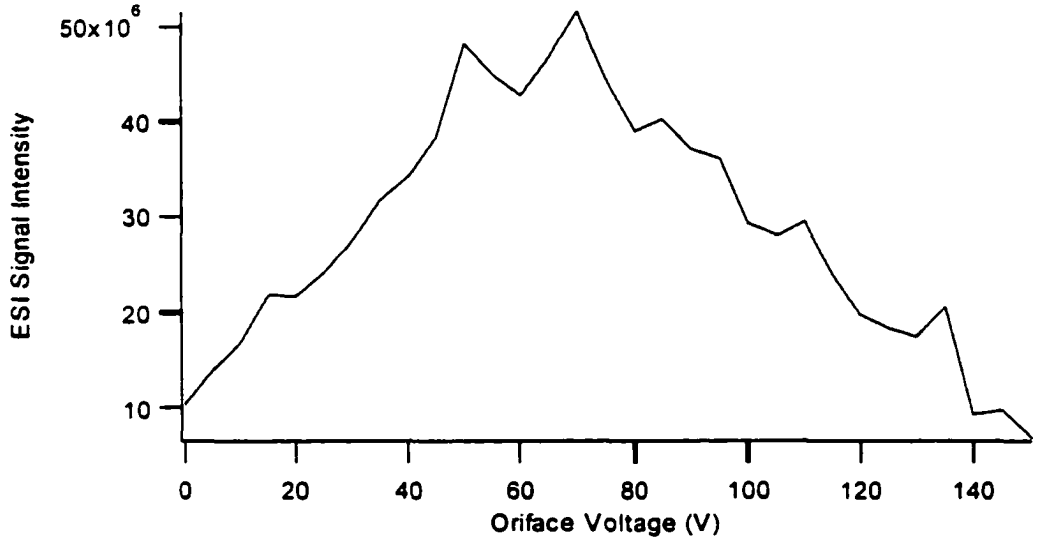

Figure 2.4: Effect of orifice voltage (OR) on the sensitivity of signal for tryptamine. The mass range was 50-350 amu with a step size of 0.5 amu and 3 ms dwell time. The IS was 4200 V and the RNG was 180 V. 1 mM Tryptamine was prepared in water-methanol buffer (1:10).

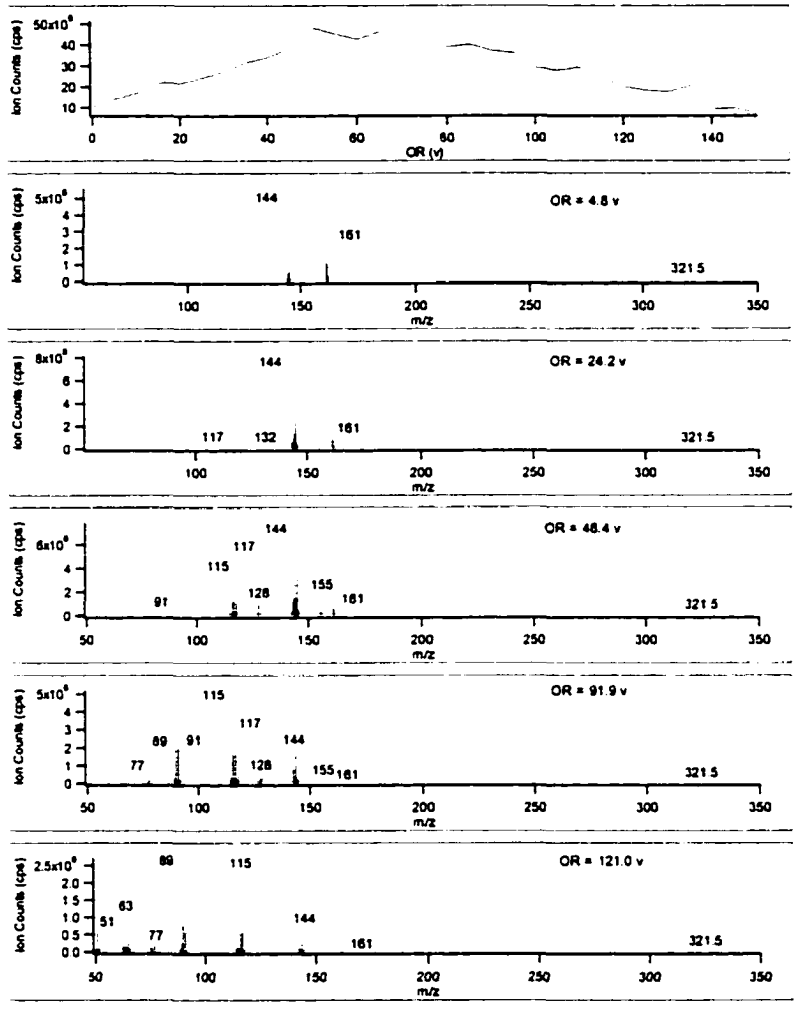

Figure 2.5: ESI-MS spectra of tryptamine at different OR voltages. Lower graphs show the m/z ratios monitored, their relative intensities and the respective OR applied. Other conditions were same as in Figure 2.4.

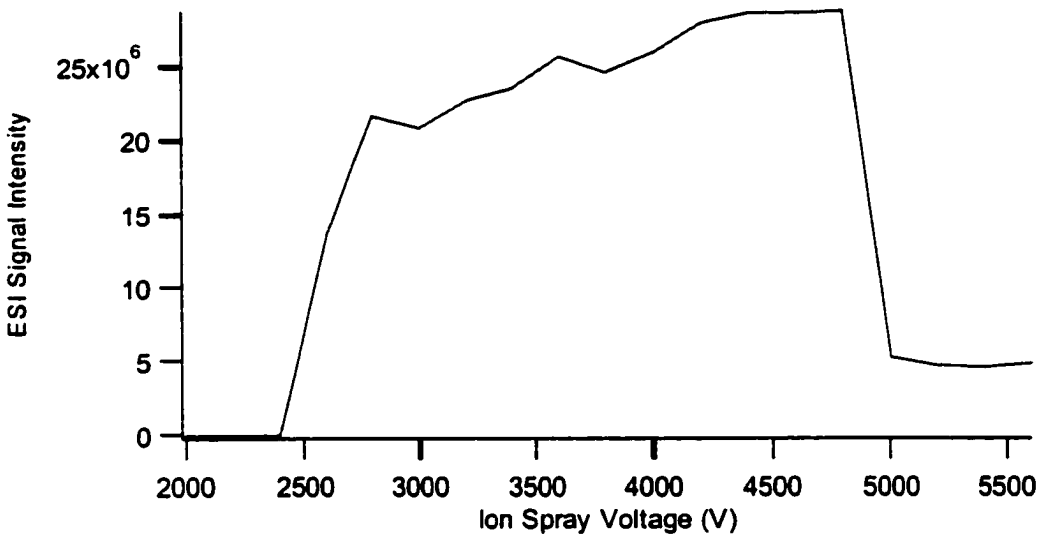

Figure 2.6: Effect of ion spray voltage (IS) on the sensitivity of signal for tryptamine. The mass range was 50-350 amu with a step size of 0.5 amu and 3 ms dwell time. The OR was 40 V and the RNG was 180 V. 1 mM Tryptamine was prepared in water-methanol buffer (1:10).

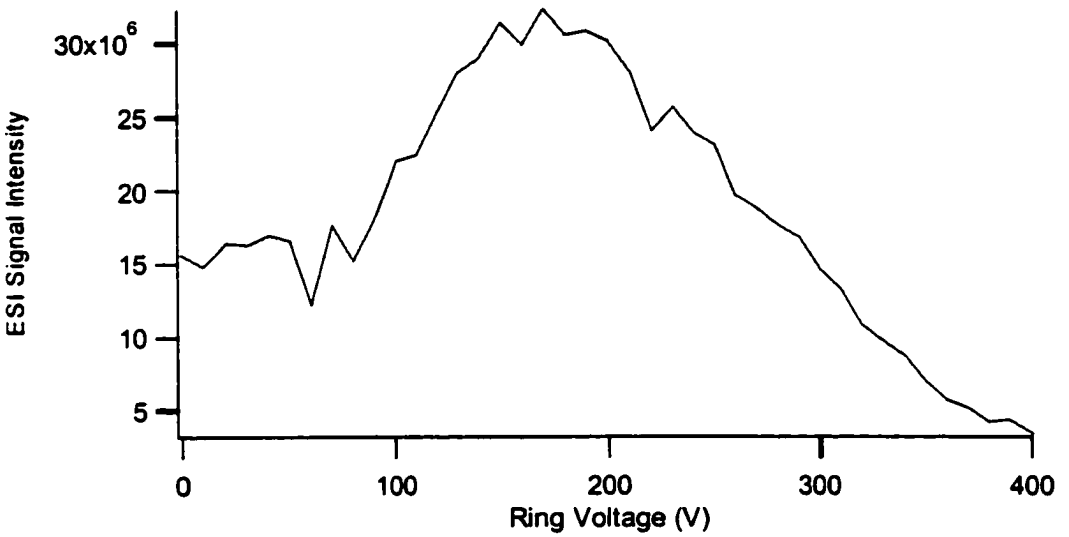

Figure 2.7: Effect of ring voltage (RNG) on the sensitivity of signal for tryptamine at m/z-144. The mass range was 50-350 amu with the step size of 0.5 amu and 3 ms dwell time. The IS was 4200 V and the OR was 40 V. 1 mM Tryptamine was prepared in water-methanol buffer (1:10).

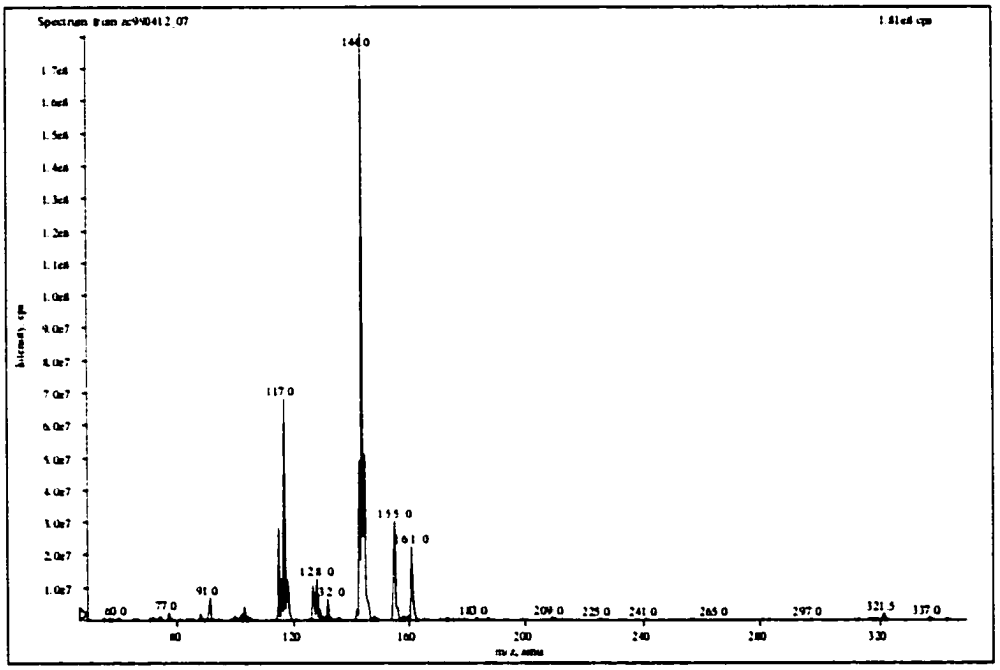

Figure 2.8: Electrospray mass spectrum of tryptamine obtained by continuous flow injection. The solution contained 1mM tryptamine in 1: 10 water-methanol.

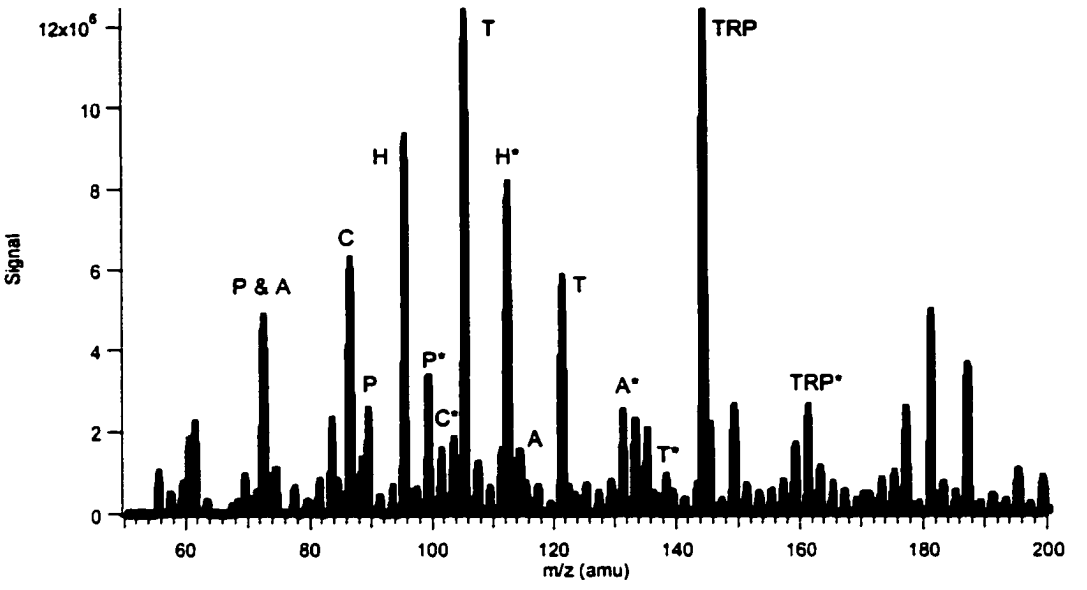

Figure 2.9: Ion spray signal for the mixture of six amines. 80 μM putrescine (P), histamine (H), cadaverine (C), agmatine (A), tyramine (T) and tryptamine (TRP) were continuously injected into the capillary under the optimized conditions.

The mixtures of biogenic amines were prepared in H_2O, methanol, methanol-water (9:1), acetonitrile, mixed methanol-acetic acid solution (90:10), 20% acetic acid, running buffer (30 mM ammonium acetate and 30 % methanol, pH 3.0), or 5x diluted running buffer and then continuously infused at a rate of 1.5 μL/min through the capillary tube to the micro ion spray tip by a syringe pump. Meanwhile the sheath flow liquid was pumped in another capillary at the rate of 1 or 2 μL/min. Except for water and 20% acetic acid, all solvents gave a good ESI signal. Furthermore, the effect of the composition of sheath liquid on the intensity of the electrospray signal was studied. Methanol and the methanol-H_2O-acetic acid solution (50:50:0.2) were investigated and it

was found that better sensitivity was obtained with the methanol sheath liquid. This probably results from the increased chemical noise due to the addition of acetic acid to the sheath. The flow rate of sheath liquid also was chosen to be from 1 to 4 μL/min. The lower the flow rate, the higher the intensity of the signal. The signal became unexpectedly unstable with a sheath flow rate less than 1 μL/min. For most micro ion spray systems and methods development, a pure methanol sheath liquid was used an infusion rate of 1.5 μL/min, and no interference with the separation was observed.

Figure 2.9 shows the ion spray signal of the mixture of six amines under the previously optimized conditions. The similar ion spray properties of the other two amines, spermine and spermidine, have been investigated as well. Several prominent ions can be identified. The most abundant ions in the mass spectra for most amines (except for the protonated molecular ion of agmatine 131) are from the charge-initiated cleavage of the alkyl carbon-nitrogen bond with expulsion of the nitrogen-containing moiety as a neutral species (the loss of NH_3 $[M+H-17]^+$), which corresponds to m/z of 95 (histamine), 121 (tyramine), 144 (tryptamine), 72 (putrescine), 86 (cadaverine). It was also observed that the molecules containing NH_2-$(CH_2)_n$-NH- , such as spermine, spermidine and agmatine are much easier to cleave at the bond of -NH-$(CH_2)_n$ than the NH_2-$(CH_2)_n$, leading to the formation of $[NH_2\text{-}(CH_2)_n]^+$. Figure 2.10 shows the proposed fragmentation and the cleavage of the biogenic amines.

2.3.2 CE Parameters

The CE-ESI-MS separation of an eight-component mixture of biogenic amines was performed using an untreated silica capillary with a capillary zone electrophoretic

system. Generally, the success of coupling a CE separation system to ESI detection depends on many factors, including the design and operating parameters of the electrospray interface mentioned in 2.3.1, the composition and the pH of the electrosprayed solution, and the chemical properties of the analyte, which will be discussed in this section. There were some operating variables responsible for an efficient separation, such as sample treatment and introduction, the composition and pH

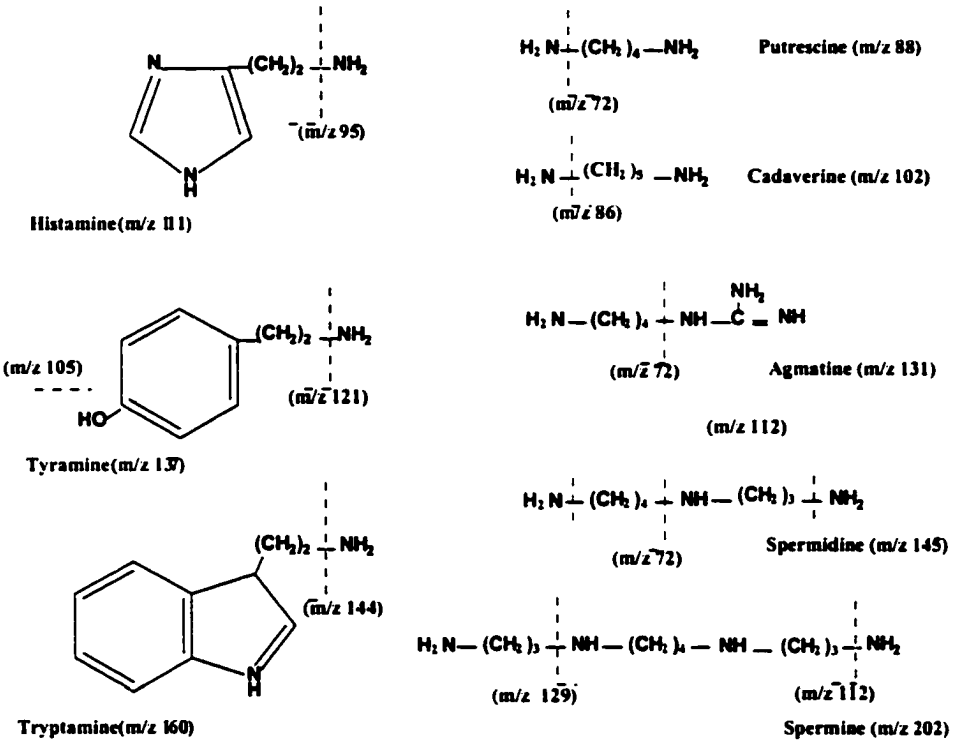

Figure 2.10: Proposed ESI-MS fragmentation signal for eight biogenic amines.

of the running buffer, and the temperature during separation. However, the most important parameter among them is the running buffer composition, because the proper choice of a suitable electrolyte system is essential in achieving both a successful CE

separation and good-quality ESI mass spectra. Therefore, the influence of running buffer components on separation efficiency, electrospray stability, and detection sensitivity was investigated in order to better understand the most important factors that determine the performance of the coupled CE-ESI-MS system. In this study, the CE separation buffer was adjusted by varying the ammonium acetate concentration from 2 to 30 mM, the acetic acid composition from 1 to 8%, and the methanol concentration from 5 to 40%. The increase of the electrolyte concentration improved the resolution, either by helping to minimize analyte adsorption or to reduce the local perturbations of the electric field strength caused by high sample concentrations; with the higher content of ammonium acetate, the level of baseline noise increased and more spikes were observed because it had higher conductivity, which may impede the ability to maintain a stable electrospray. Consequently 30 mM was selected as the optimum concentration (Figure 2.11).

Biogenic amines are weak bases and their ionization, and also electrophoretic mobility, strongly depends on the pH. The relative sensitivities, separation efficiencies, and selectivities, were found to vary dramatically with pH (Figure 2.12). In the lower pH range, biogenic amines are more effectively converted into the protonated species and thus the sensitivity in the electrospray ionization process may be improved. On the other hand, taking into consideration the migration time of the CE separation, the addition of acetic acid reduced the pH of the running buffer and therefore increased the migration time. Therefore, 6% acetic acid was chosen as the proper level. The resolution and selectivity also can be readily optimized by varying the organic modifier content in the running buffer.

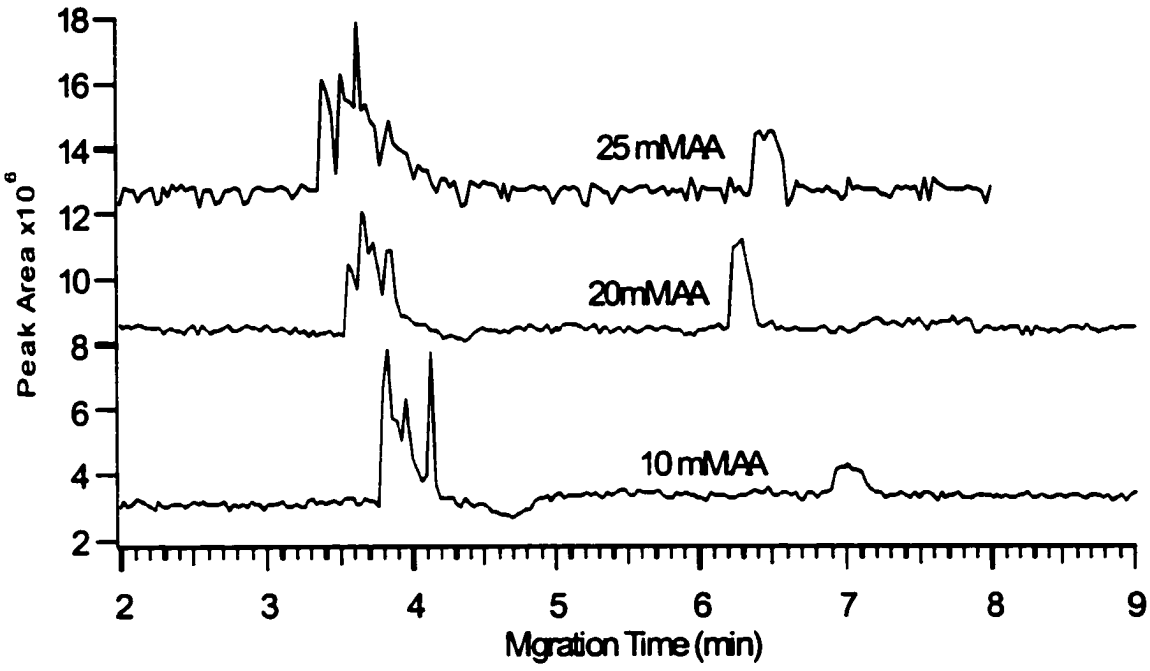

Figure 2.11: Effect of the ionic strength of the running buffer. The TIEs (total ion electrophegram) show the effect of ammonium acetate(AA) concentration on the separation and the migration times of the biogenic amines. The amine mixture was dissolved in water. The separation was performed at 16 kV and current was approximately 7μA. Sheath flow was methanol at the rate of 2 μL/min. Other compounds in running buffer were 1% acetic acid and 10% methanol.

Some organic modifiers such as methanol, or acetonitrile were added to the ammonium acetate - acetic acid buffer. The methanol concentration of 30% proved to be a good choice for solubility, resolution and conductivity (Figure 2.13). Therefore, an electrolyte containing 30 mM ammonium acetate and 30% methanol (pH 3) was regarded as optimum for separation of the biogenic amine mixture with respect to maximum separation efficiency in combination with the highest sensitivity and minimum

analysis time (Figure 2.14). Figure 2.15 gives the mass spectra obtained from a separation of the eight biogenic amines at the 200 μM level within 23 minutes under the established optimum conditions described above (Figure 2.14), in which 8 m/z were

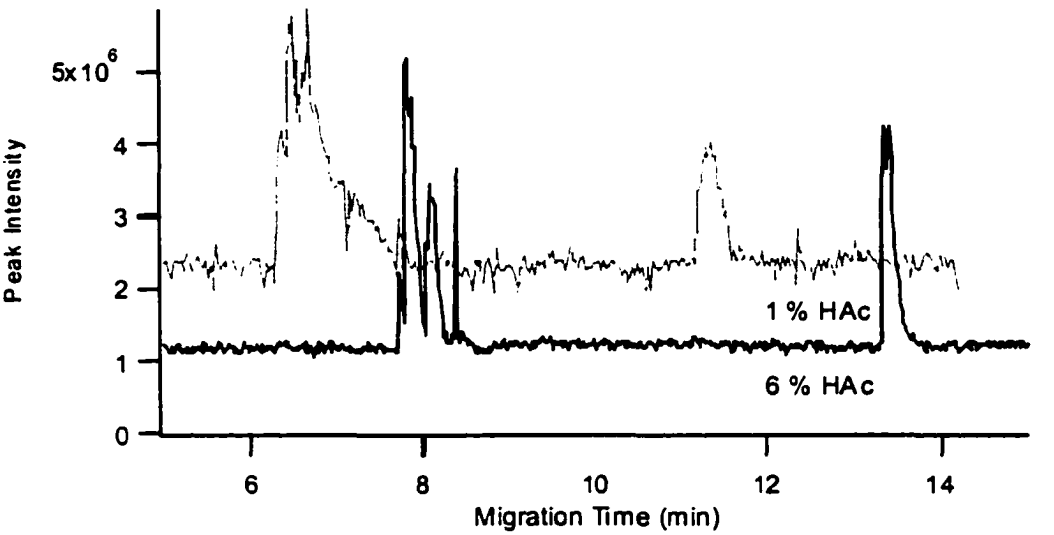

Figure2.12: Effect of acetic acid concentration in the running buffer. The TIEs show the influence of acetic acid concentration on the separation and the migration times of biogenic amines. The amine mixture was dissolved in water and injected at 15 kV for 5 seconds. The separation was performed at 11 kV and the current was approximately 5 μA. Sheath flow was methanol at the rate of 2 μL/min. Other compounds in the running solution were 30 mM ammonium acetate and 10% acetonitrile.

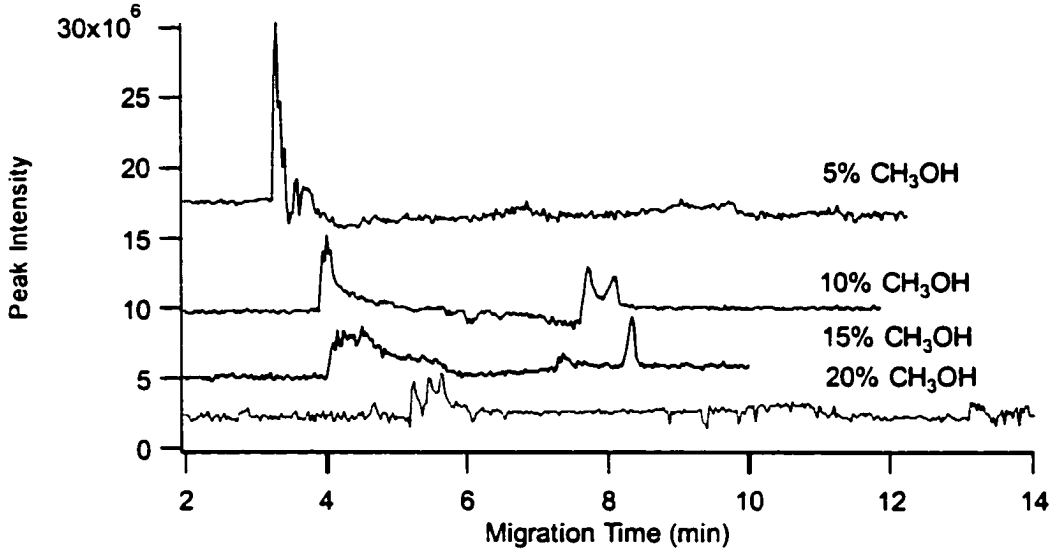

Figure 2.13: Effect of the organic modifier on the CE separation. The TIEs show the influence of methanol on the separation and the migration times of biogenic amines. The amine mixture was dissolved in water and injected at 15 kV for 5 seconds. The separation was performed at 11 kV and the current was approximately 5μA. Sheath flow was methanol at the rate of 2 μL/min. Other compounds in running solution were 2 mM ammonium acetate and 1 % acetic acid.

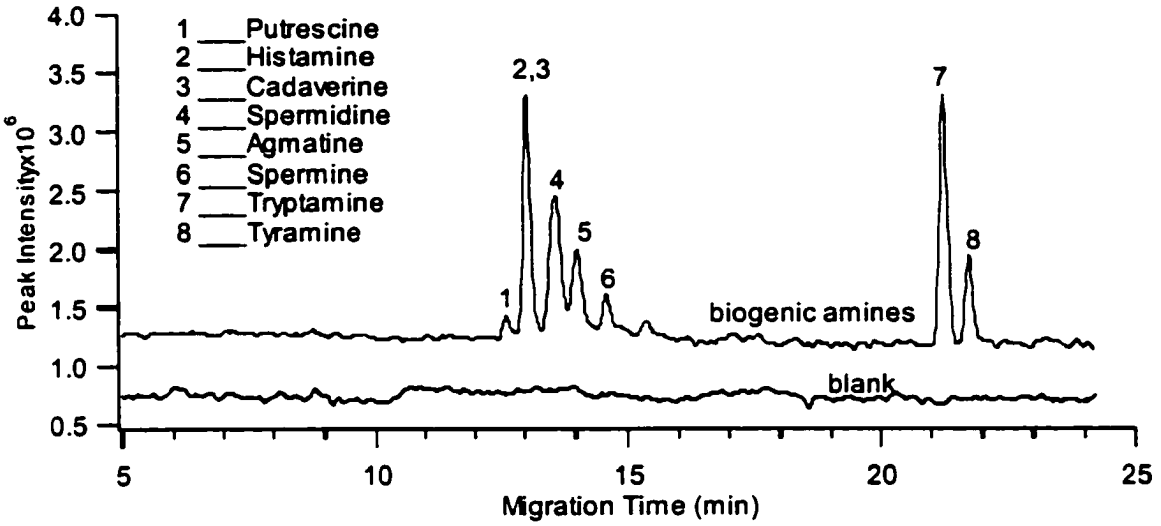

Figure 2.14: Electrophoresis of eight biogenic amines. CE-ESI-MS profile of biogenic amine mixture (200 μM). The separation was performed at the optimized conditions with the current of 5 μA. Sample was prepared with the buffer diluted 5 fold from the running buffer. The peaks were identified by the fragment ions from the continuous injection results.

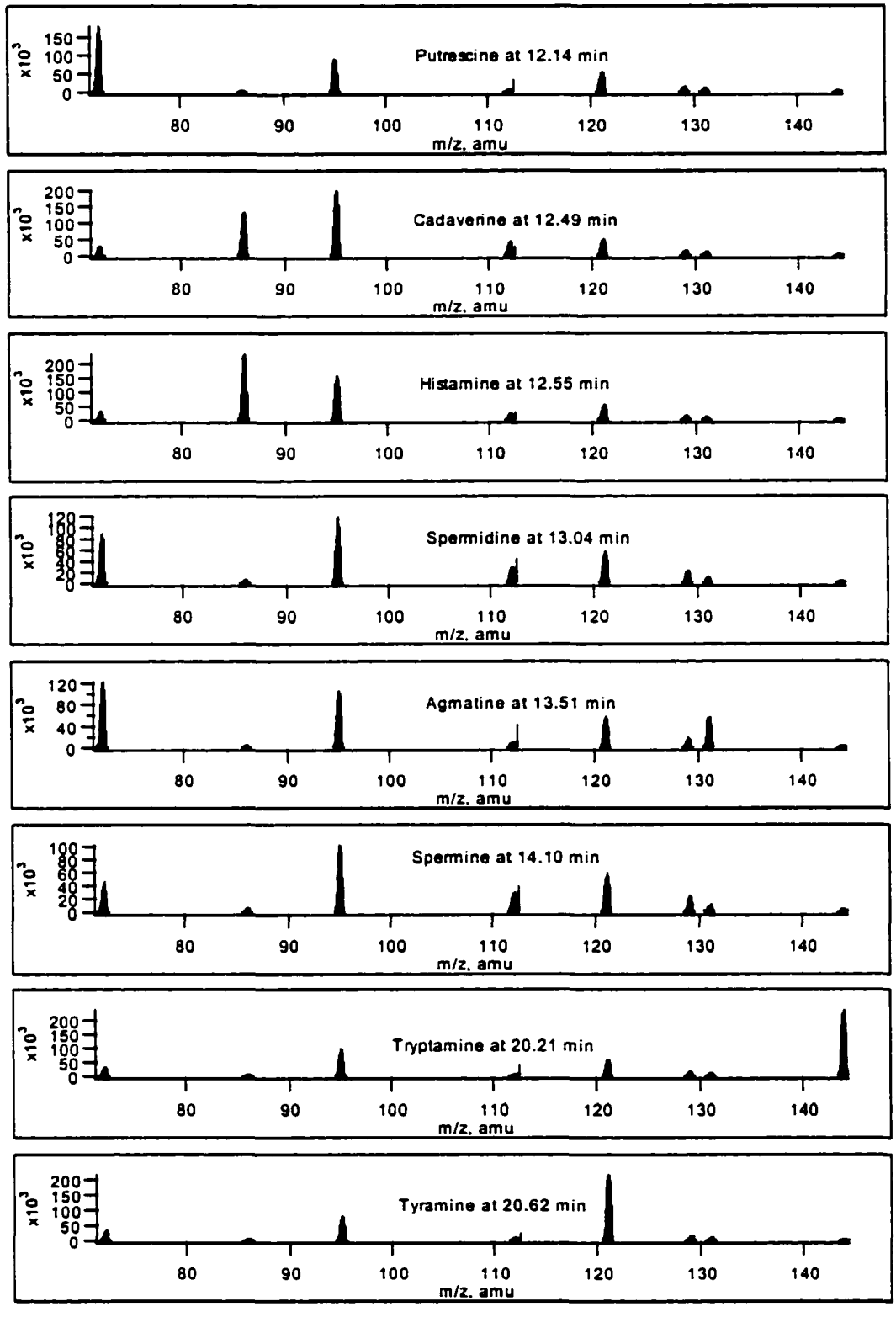

Figure 2.15: Mass spectra for the individual amine components from Figure 2.14.

selected to monitor. Generally aliphatic amines come out first, and then followed by the aromatic ones. With the exception of histamine and cadaverine, all biogenic amines are well separated. Histamine and cadaverine can, however, be differentiated by MS as they possess different molecular masses. The number of theoretical plates ranged from 10^4 m^{-1} for putrescine to 10^6 m^{-1} for tryptamine.

During the study, we have found electroosmotic sample injection to provide a simple, reproducible method for the introduction of a relatively narrow sample band onto the CE column. The separation was monitored for injections at 15, 10, and 5 kV, respectively, for 5 or 3s. As in Figure 2.16, the SIEs shows the influence of electroosmotic injection on the separation and the migration time of biogenic amines. Better peaks can be obtained by lower injection voltages and longer injection times.

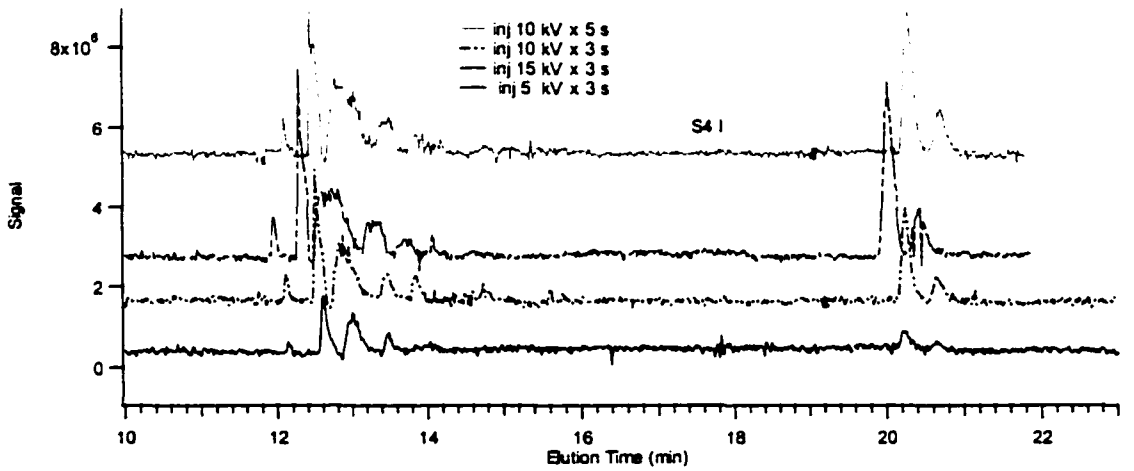

Figure 2.16: Effect of the electroosmotic injection on the CE separation. The amine mixture was dissolved in water and the separation was performed at 11 kV. Other conditions were the same as previously optimized.

2.3.3 Analytical Curve Figures of Merit

CE-ESI-MS calibration curves were prepared for the mixtures of amine standards in 5-fold diluted running buffer, a separation buffer of 30 mM ammonium acetate - 6% acetic acid - 30% methanol, 10 kV electrokinetic injection for 5 s, and using a selective ion scan. The calibration curves were linear over an analyte concentration range of 5 - 240 μM with the correlation efficients being 0.9870 to 0.9995, the linear relationship between peak intensity and concentration of amines are presented in Table 2.1.

Table 2.1 Analytical curve figures of merit.

	Putrescine	Histamine	Cadaverine	Spermidine	Agmatine	Spermine	Tryptamine	Tyramine
Conc (uM)	15 ~ 240	5 ~ 80	15 ~ 120	20 ~ 80	15 ~ 60	40 ~ 320	5 ~ 80	15 ~ 240
r^2	0.9908	0.9870	0.9995	0.9927	0.9934	0.9926	0.9871	0.9969
LOD (uM)	0.15	0.050	0.15	0.20	1.2	0.40	0.020	0.30

2.3.4 Detection Limits

The detection limits in the selected ion monitoring (SIM) mode based on a signal-to-noise ratio of 3:1 were calculated for the eight biogenic amines, and range from 0.020 to 0.40 μM. The results for each compound are given in Table 2.1, where the concentrations of the solution injected are listed. However, when the concentration for an analyte becomes low, the corresponding signal for this compound in mass spectrum

will decrease dramatically due to the suppression caused by background. Therefore, the actual detection limits for biogenic amines under the above CE-MS system are much higher than the theoretical values. Comparison of Table 2.1 with Figure 2.15 shows that there is a wide variation in the ion signal when the range of sample concentrations is considered. In terms of peak height per molar concentration, tryptamine gave a response 120 times greater than agmatine with this buffer.

The detection limits of the biogenic amines using CE and LIF detection are at the level of 10^{-8} M. Tsuda *et al* [23] in the early nineties gave a value of 10^{-5} M for fluorescamine-labeled putrescine, spermine and spermidine, S.F.Y. Li [24] reported values of 10^{-8} M for FITC-labeled amines, and Kovacs and his coworkers [27] obtained data ranging from 1 to 40 μM (S/N=3) for seven AccQ-amines. Using UV detection, the detection limits are 2-3 orders higher than with a LIF detector (0.05 to 0.1 μg/ml) [21]. The sensitivity data obtained in the present study for CE-ESI-MS are comparable to the detection limits using CE with UV detection, which make this technique suitable not only for the determination of aromatic but also aliphatic biogenic amines. These detection limits are sufficient for most applications in the area of food analysis.

However, compared to UV or LIF detection, considerable band broadening is observed with ESI-MS detection which is mainly attributed to column overloading, band spreading in the interface, and scan data acquisition. Efficiencies, measured as numbers of theoretical plates (N), range from as low as 4×10^4 for histamine to 2×10^5 for tyramine.

2.3.5 Real Samples

To demonstrate the feasibility of CE-ESI-MS of real samples, determination of biogenic amines was performed in beef samples. Unfortunately, analysis of biogenic amines identified in samples failed because different amines appeared at the same migration time. This result indicates that the sample preparation was not satisfactory, and that further work will be required to develop a satisfactory method for amines in foods.

2.3.6 Related CE-LIF Work

The determination of fluorescent labeled biogenic amines is another part of this project. Due to its high sensitivity and high resolution, CE-LIF is an important option for the analysis of biogenic amines. It can be useful in reducing the limit of detection because the introducing of laser-induced fluorescence opens up the possibility of detecting in the attomole and subattomole levels [45]. In the CE-LIF study, the mixture of six biogenic amines usually existing in food, including histamine, tyramine, tryptamine, cadaverine, agmatine and putrescine, was pre-column derivatized with the fluorogenic dye 5-furoylquinoline-3-carboxaldehyde (FQ), and then separated with a fused-silica capillary (50 μm i.d.) under different CE buffer conditions.

2.3.6.1 CZE Separation Buffer With Submicellar SDS

An electropherogram resulting from a typical FQ-labeling reaction is shown (Figure 2.17) with the running buffer 25 mM tricine and 4 mM SDS. Changing the concentration of tricine did not have much influence on the separation. However,

compared with running buffer without SDS, the migration times increased dramatically when SDS is added. This indicates that the biogenic amines are spending time in the submicelles. Partitioning of the FQ-amines with the submicellar phase was an essential mechanism for the successful separation. The addition of SDS significantly influenced the migration order and resolution of the FQ-labeling amines. On the other hand, when the concentration of SDS is increased from 4 to 9 mM, the peaks start to elute closely and finally as a big blob. From trying concentrations of SDS from 1 mM to 10 mM, the optimum concentration was found to be 4 mM.

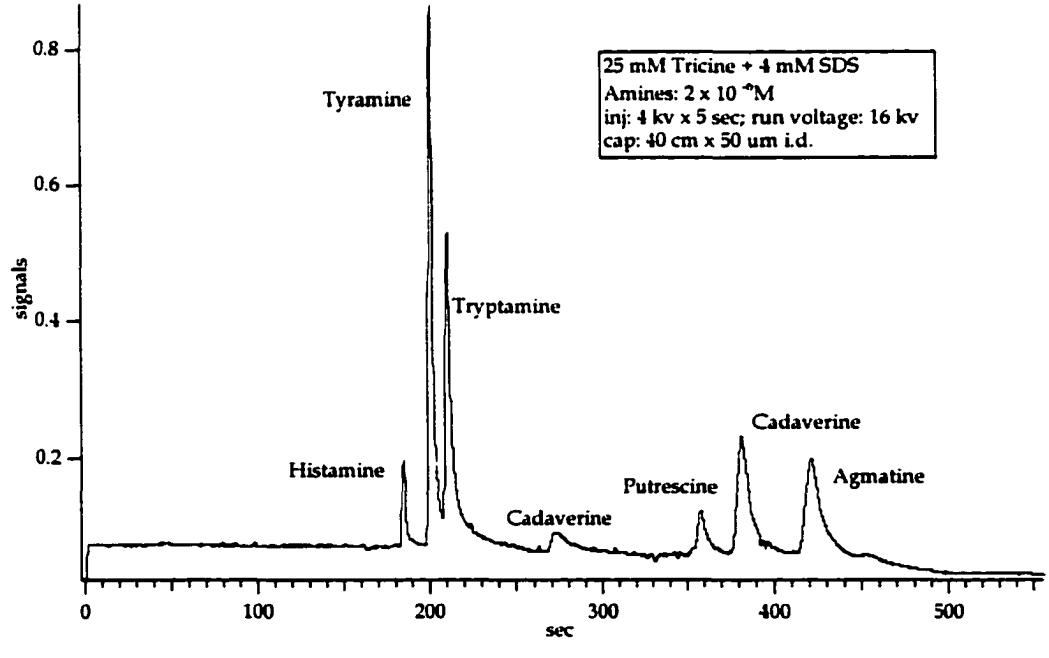

Figure 2.17: CZE separation with submicellar SDS buffer.

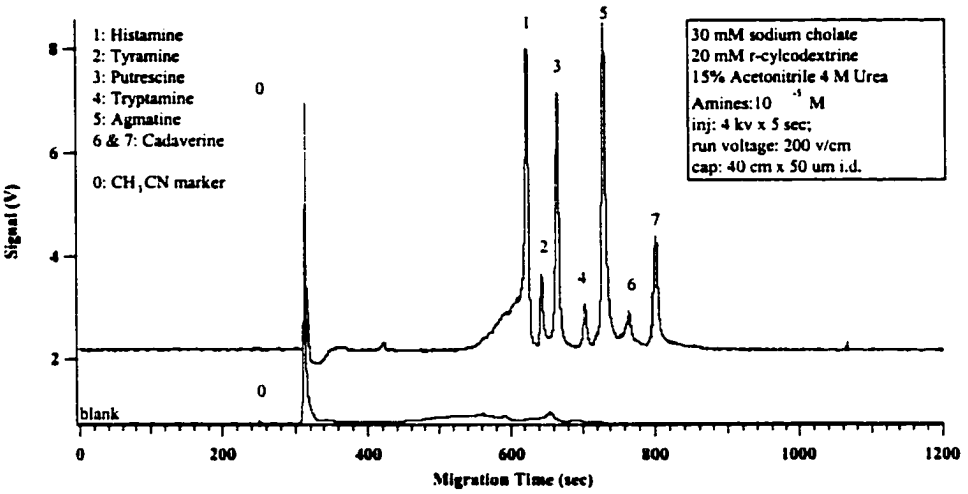

Figure 2.18: MEKC separation with bile salt micelles.

2.3.6.2 MEKC Separation Buffer with Bile Salt Micelles

MEKC was performed with 10 μM amine in solution containing bile salt. The separation of the amines is shown in Figure 2.18. From the migration sequence it is found that aromatic amines always have smaller capacity factor, as in Figure 2.17. The purpose of the urea is to enhance the solubility of cyclodextrin. The other reason is to make the capillary wall more hydrophobic and decrease adsorption. Maybe the reasons given below could explain the difference in efficiency between the bile salt and SDS. First, the size of bile salt micelles is smaller than that of SDS. The aggregation number for bile salt is 20 and SDS is 60, there is stronger interaction between the bile salt micelles and the labeled amines. Secondly, bile salt is less hydrophobic than SDS. Finally, bile salt micelles are more stable in organic solvents.

2.3.6.3 Effects of Temperature

In CE separation systems, adsorption on the capillary wall is a problem for some biological molecules, such as proteins and peptides. In order to clarify whether there is adsorption of amine molecules on the wall of capillary or not, the effects of increasing

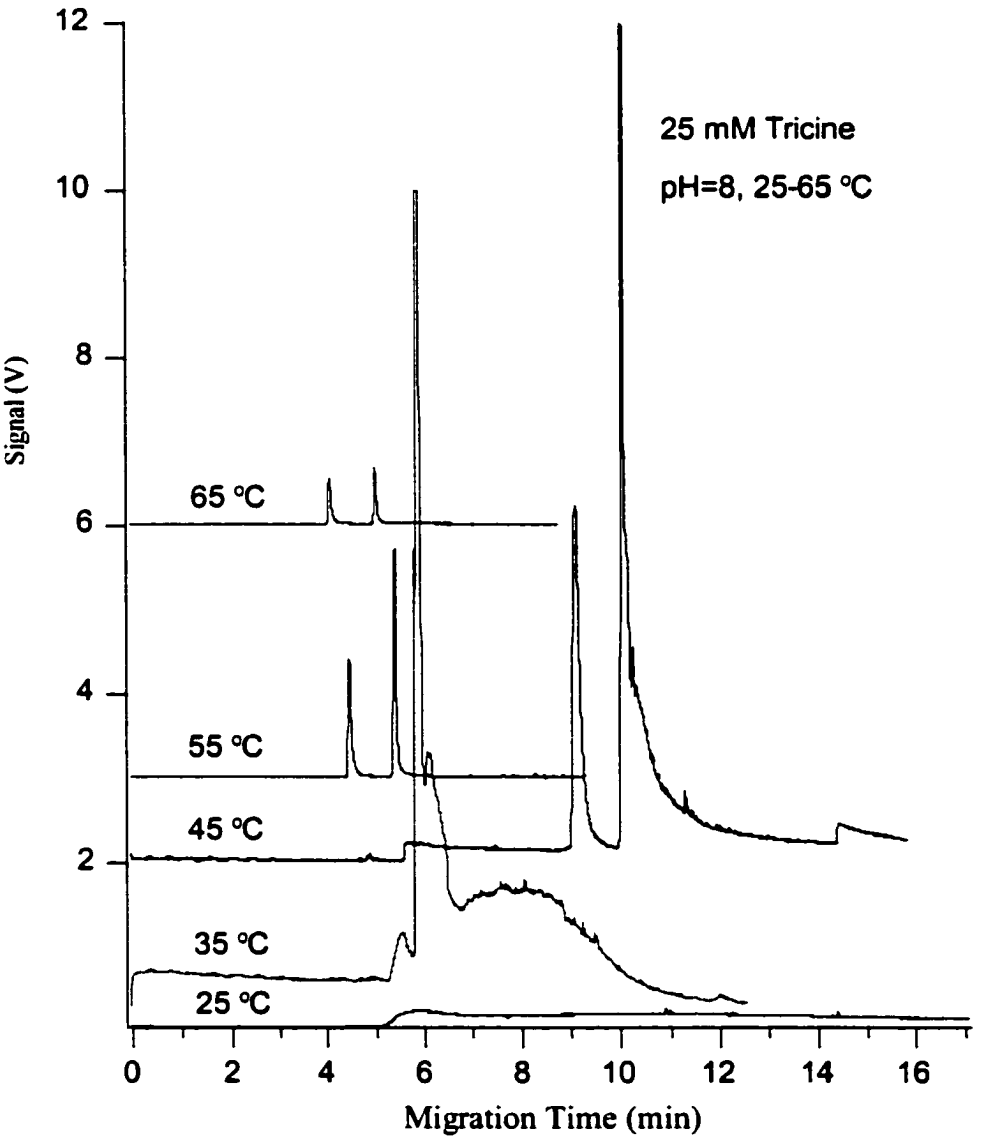

Figure 2.19: Effect of temperature on separations of mixture of biogenic amines.

the temperature were studied. The results in Figure 2.19 show that for low temperatures (near room temperature), the signals are small and all the compounds come out together as a broad peak, which suggests there is some adsorption. If the temperature for separation is increased by 10 °C, the peaks get larger and more than one peak comes out. This result implies that there is adsorption on the capillary wall. But in general these peaks are separated into two groups. This may be because the molecular weight of FQ labeled products are so close that their moving velocities are not different enough to be separated.

2.3.6.4 Limit of Detection for CE-LIF

The detection limits in the above CZE buffer system based on a signal-to-noise ratio of 3:1 were calculated for the six compounds and the results are given below: 8 x 10^{-9} M for histamine, 5 x 10^{-8} M for tyramine, 8 x 10^{-8} M for tryptamine, 2 x 10^{-8} M for agmatine, 8 x 10^{-8} M for putrescine and 2 x 10^{-8} M for cadaverine.

2.4 Conclusion

The CE-ESI-MS and CE-LIF analyses of biogenic amines on uncoated fused silica capillaries are described. The electroosmotic injection process allows extremely small sample volumes (< 20 nL) to be introduced for CZE-ESI-MS with negligible waste. Generally, the best detector response is produced by volatile electrolyte systems at the lowest practical concentration and ionic strength. On the other hand, low electrolyte concentrations cause solute zone broadening during the electrophoretic separation

process due to conductivity differences and adsorption. Consequently, a balance must be achieved between high buffer concentration, which diminishes solute detectability, and low buffer concentration, which degrades the separation efficiency.

The production of positive ions during ESI is enhanced by use of a low pH buffer. However, low pH buffers with a bare capillary could reduce the bulk electroosmotic flow and further influence the CE separation and cause instability in the electrospray. In addition, due to the electrostatic interaction between the positively charged residues of the biogenic amine molecules and the negatively charged silanols of the fused-silica surface, the adsorption of the neutral species or positive ions on the negative capillary inner wall may cause a dramatic loss of separation efficiency in which the undesirable adsorption results in peak dispersion and asymmetry.

Overall, CE-ESI-MS has been used as a universal analytical method since it enables quantification of the amines not detectable with UV or LIF. The lower sample requirement (~ 10 nL) makes it an ideal technique for the measurement of small amounts of samples. Dynamic ranges of linear relationships are achieved from 5 μM to 350 μM and the detection limits obtained are in the range of 1.2 to 0.02 μM, which are required to conduct the measurements of biogenic amines at the levels present in food samples. Nevertheless, compared to LC-MS-MS, CE-ESI-MS can not compete in terms of sensitivity and stability because of the low volume loadability and poorer robustness in CE. Furthermore, the quantitative applications of CZE-MS will ultimately depend upon both the accuracy and precision of the sample injection step and the useful dynamic range of mass spectrometric detection.

Unfortunately, the application of CE-ESI-MS for the separation and quantification of biogenic amines in real food samples was unsatisfactory, possibly due to an incomplete sampling process. More work is required. Solid phase ion-pair extraction may be a good alternative to solve this problem. Another option is operating CE-MS by individual m/z ratio for different amine and separate those biogenic amines in different runs. However, this project was terminated by the relocation of the cooperators for another university.

References

1. S., Bardocz, *Trends in Food Science & Technology,* 1995, 6, 341.
2. J.A. Mega, *CRC Critical Reviews in Food Science and Nutrition,* 1978, 10, 373.
3. D.W.S. Wong, *Mechanism and Theory in Food Chemistry,* Van Nostrand Reinhold, New York, 1989.
4. S.L. Rice, R.R. Eitenmiller and P.E. Koehler *Journal of Milk Food Technoogy,* 1976, 39, 353.
5. L.F. Bjeldanes, D.E. Schutz and M.M. Morris *Food Cosmetic Toxicology,* 1978, 16, 157.
6. O. Busto, J. Guasch and F. Borrull, *Journal of International Science Vigne Vin,* 1996, 2, 1.
7. P. Spettoli, *Industry of Agriculture,* 1971, 9, 1.
8. B. Wortberg and G. Zieprath, *Lebensmittelchemcal Gerichtl Chemistry,* 1981, 35, 89.
9. K.D. Henry Chin and P.E. Koehlev, *Journal of Food Science,* 1983, 48, 1826.
10. P. Capella and E.C. Horning, *Analytical Chemistry,* 1966, 34, 316.
11. W.F. Staruszkiewicz and J.F. Boun, *Journal of Associate Official Analytical Chemistry,* 1981, 64, 584.
12. S. Yamamoto *et al, Journal of Agriculture Food Chemistry,* 1982, 10, 435.
13. W.J. Hurst, *Journal of Liquid Chromatography,* 1990, 13, 1.
14. N. Seiler, *Journal of Chromatography,* 1986, 379, 157.
15. M. Mahendradatta, G. Schwedt, *Dtsch.-Lebensmittel-Rundsch.,* 1995, 2, 117.
16. G. Nouadje, F. Couderc, P. Puig, L. Hernandez, *Journal of Capillary Electrophoresis,* 1995, 2, 117.

17. G. Nouadje, N. Simeon, F. Dedieu, M. Nertz, Ph. Puig, F. Couderc, *Journal of Chromatography A,* 1997, 765, 337.

18. C. Schoneich, A.F.R. Huhmer *et al.*, *Analytical Chemistry,* 1995, 67, 155R.

19. F.T. Chen, A. Sternberg, *Journal of Capillary Electrophoresis,* 1994, 15, 13.

20. W-C Lin *et al.*, *Journal of Chromatography A,* 1996, 755, 142.

21. L. Arce, A. Rios and M. Valcarcel, *Journal of Chromatography A,* 1998, 803, 249.

22. H.E. Schwartz, K.J. Ulfelder, F.A. Chen and S.L. Pentoney, *Journal of Capillary Electrophoresis,* 1994, 1, 36.

23. T. Tsuda and Y. Kobaysshi, *Journal of Microcolumn Separations,* 1990, 2, 1.

24. I. Rodriguez, H.K. Lee, S.F.Y. Li, *Journal of Chromatography A,* 1996, 745, 255.

25. G. Nouadje, H. Rubie, P. Canal, M. Nertz, Ph. Puig, F. Couderc, *Journal of Chromatography A,* 1995, 717, 293.

26. I. Rodriguez, H.K. Lee and S.F.Y. Li, *Electrophoresis,* 1999, 20, 118.

27. A. Kovacs, L. Simon-Sarkadi and K. Ganzler, *Journal of Chromatography A,* 1999, 836, 305.

28. J.A. Olivares, N.T. Nguyen, C.R. Yonker and R.D. Smith, *Analytical Chemistry,* 1987, 59, 1230.

29. R.D. Smith, J.A. Olivares, N.T. Nguyen and H.R. Udseth, *Analytical Chemistry,* 1988, 60, 436.

30. C.G. Huber, A. Premstaller and G. Kleindienst, *Journal of Chromatography A,* 1999, 849, 175.

31. L.J. Deterding, C.E. Parker, J.R. Perkins, M.A. Moseley, J.W. Jorgenson and K.B. Tomer, *Journal of Chromatogaphy,* 1991, 554, 329.

32. R.D. Smith, H.R. Udseth, C.J. Barinaga and C.G. Edmonds, *Journal of Chromatography,* 1991, 559, 197.

33. J.H. Wahl, D.R. Goodlett, H.R. Udseth and R.D. Smith, *Analytical Chemistry,* 1992, 64, 3194.

34. T.J. Thompson, F. Foret, P. Vouros and B.L. Karger, *Analytical Chemistry,* 1993, 65, 900.

35. D. Figeys, I.van Oostveen, A. Ducret and R. Aebersold, *Analytical Chemistry,* 1996, 68, 1822.

36. B. Yeung, T.J. Porter and J.E. Vath, *Analytical Chemistry,* 1997, 69, 2510.

37. K. P. Bateman, R.L. White, M. Yaguchi and P. Thibault, *Journal of Chromatography A,* 1998, 794, 327.

38. A.J. Tomlinson, L.M. Benson, S. Naylor, *Electrophoresis,* 1994, 15, 62.

39. W. Lu, G.K. Poon, P.L. Carmichael, and R.B. Cole, *Analytical Chemistry,* 1996, 68, 668.

40. C.S. Liu, X.F. Li, D. Pinto, E.B. Hansen, C.E. Cerniglia, N.J. Dovichi, *Electrophoresis,* 1998, 19, 3183.

41. S. Pleasance, P. Thibault, J. Kelly, *Journal of Chromatography,* 1992, 591, 325.

42. F. Garcia, J.D. Henion, *Journal of Chromatography,* 1992, 606, 237.

43. T.G. Huggins, J.D. Henion, *Electrophoresis,* 1993, 14, 531.

44. M.H. Lamoree, N.J. Reinhoud, U.R. Tjaden, *Biological Mass Spectrometry,* 1994, 23, 175.

45. D. Pinto, E. Arriaga, D. Craig, N.J. Dovichi, *Analytical Chemistry,* 1997, 69, 3015.

Chapter 3

Analysis of Neurotransmitters in Brain Samples by CE-LIF

3.1 Introduction

3.1.1 Neurotransmitters in Brain

One of the major challenges for modern clinical researchers is to determine the relationship between brain structure and function [1]. Since neurotransmitters play an important role in brain function, a better understanding of the actual chemical processes involved in the brain could lead to improved treatment of neurological and psychiatric disorders, such as Parkinson's disease, Alzheimer's disease, depression and addiction. Such knowledge may also aid in the diagnosis of some brain diseases and the evaluation of new drug therapies.

The term neurotransmitter often refers to small molecules used in communication between neurons in the brain. Specifically, neurotransmitter is defined as a compound synthesized, stored and released from neurons into the synapse and subsequently acting at post- and/or presynaptic receptors. Basically, it includes three groups: (I) amino acid neurotransmitters, (II) biogenic amine neurotransmitters, and (III) neuropeptides [2]. From the quantitative point of view, amino acids are probably the major transmitters in the mammalian central nervous system (CNS), while the better-known ones, such as dopamine, acetylcholine, histamine and serotonin, only account for neurotransmission at a small percentage. Based on the neurophysiological studies, amino acids in brain can be

divided into two classes: inhibitory amino acids, which hyperpolarize mammalian neurons; and excitatory amino acids, which depolarize neurons in the CNS.

γ-Amino-butyric acid (GABA) is one of the inhibitory transmitters. It can induce both hyperpolarizing and depolarizing responses, which are the results of receptor-mediated change in chloride conductance. Recent research implicates the possible involvement of GABA in the pathogenesis of Huntington's disease, Parkinson's disease, depression as well as several other behavior disorders [2].

3.1.2 Microdialysis Technique

3.1.2.1 Principle of Microdialysis

Microdialysis, which was developed by Ungerstedt's group in the 1980s using transcerebral and U-shape probes [3,4], is a powerful tool to monitor extracellular fluid concentrations of several different neurotransmitters. Figure 3.1 is a diagram showing a typical microdialysis sampling apparatus for freely moving awake animals. The principles of the technique are relatively simple: molecules diffuse down their concentration gradient, across the dialysis membrane in either direction, thus permitting molecules to diffuse into the probe from the extracellular environment. Normally, a fine semipermeable dialysis probe (0.2-0.5 mm diameter) is implanted into a living system, such as a discrete brain region, system tissue or fluid of interest. As shown in Figure 3.2, low molecular weight compounds are introduced into or are removed from the extracellular environment to a physiological salt solution that flows through the probe at

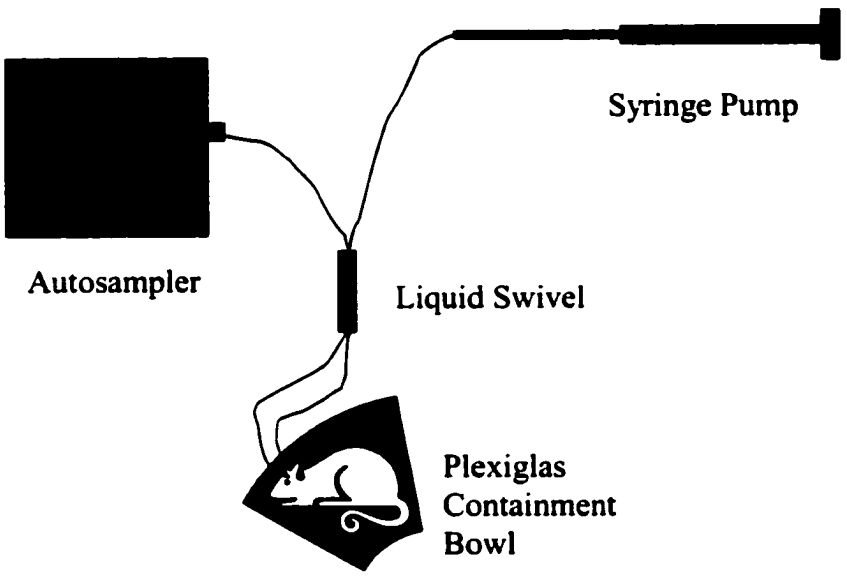

Figure 3.1: Typical microdialysis sampling apparatus for the freely moving awake animal.

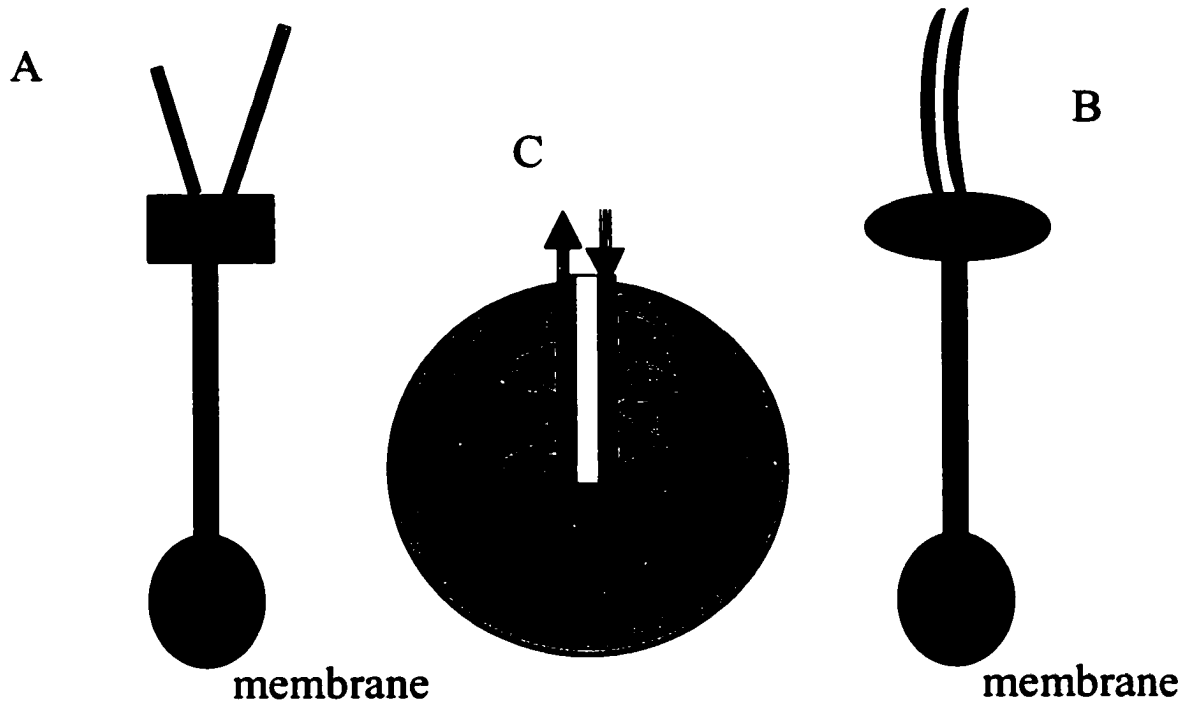

Figure 3.2: Microdialysis probe: (A) & (B) rigid stainless shaft and flexible plastic shaft; (C) illustrates the membrane and the diffusion of molecules into (○) and out (■) of the probe [5].

a constant rate. The perfusate is then collected for further analysis. The conventional flow rate range is usually 0.2-4 μL/min is. With such a low perfusion rate, it is clear that sample volumes are very low and obviously the shorter the sampling time, the lower these volumes become.

3.1.2.2 Advantages and Disadvantages of Microdialysis

Microdialysis sampling is a powerful technique for the study of brain function *in vivo*. Comparing with the conventional techniques such as push-pull perfusion and tissue homogenization, microdialysis provides a number of advantages [6]:
First, molecules can be introduced into or removed from the brain of a conscious or freely moving animal; secondly, extracellular fluid can be sampled incrementally over long periods of time without fluid loss in order to observe chronological changes in chemical composition. Thirdly, the typical commercial probes have a molecular mass cutoff of 30 kDa, allowing collection of low molecular weight compounds [7]. Therefore macromolecules that could interfere with separations are excluded, making sample cleanup unnecessary and drugs can be separated from enzymes that might catalyze their degradation. And lastly, it is possible to monitor multiple analytes by coupling other analytical techniques including HPLC, mass spectrometry, and CE, to the microdialysis system. The main limitation of microdialysis is invasive nature. Insertion of the probe can damage a larger fraction of neurons, which will make the interpretation of data difficult.

3.1.2.3 Microdialysis Applications

Probably some of the most common published microdialysis applications are those dealing with the neurotransmitters from various brain regions. These articles describe a variety of derivatization, separation and detection methodologies to measure many small compounds, such as excitatory amino acids [5], dopamine, serotonin [19], as well as some of the neuropeptides [8].

Pharmacokinetic studies present the largest application of microdialysis next to the measurement of the desired neurochemicals in the dialysate fluid. Pharmacokinetics is the study of the absorption, distribution, metabolism and elimination of any drug introduced into a system. This includes the analysis of both the original administered substances and also subsequent metabolic products. Phenelzine (β-phenylethylhydrazine, PLZ) is the most commonly used of the monoamine oxidase-inhibiting antidepressants. It is also utilized extensively in the treatment of panic disorders [9-11]. There is growing evidence implicating PLZ causes marked increases in brain levels of the neurotransmitter GABA. Also, it is possible that the change in GABA [12] may contribute to the pharmacotherapeutic effects of PLZ. Microdialysis provides a means of sampling free (i.e., non protein bound) drug from any given system with the minimum of disturbance. Administering a known dose and withdrawing samples at timed intervals typically is used to determine the pharmacokinetics of a drug. These samples are then analyzed to derive a concentration-time curve. CE has now been combined with microdialysis technique to study the time course of the effects of PLZ on extracellular GABA levels [13].

3.1.3 Applications of CE in Brain-related Fields

3.1.3.1 Combination of Microdialysis with CE

Of the many analytical techniques currently in use, high performance liquid chromatography (HPLC) has been widely applied with electrochemical (ECD) or fluorescence detection [14-16]. However, the use of HPLC for analysis of neurochemicals in brain samples suffers from some disadvantages. The fluorescence methodology usually involves tedious derivatization processes; on the other hand, electrochemical detection has relatively restricted concentration limits and not every compound is electrochemically sensitive. Furthermore, because many samples of interest come directly from living animals, the sample volumes are quite small and the concentrations of analytes are often low. Microbore liquid chromatography has been compared with conventional HPLC (250 x 4.6 mm i.d.) for analysis of neurotransmitters [17], but no resolution advantage was gained by the use of narrow bore columns compared to conventional columns [17, 18].

Capillary electrophoresis (CE) with laser-induced fluorescence (LIF) is another choice for neurotransmitter measurement. LIF provides extremely high sensitivity, with detection limits approaching the single-molecule level [19, 20]. This exquisite sensitivity makes CE-LIF an ideal technique for the analysis of biological samples, such as microdialysates from discrete brain areas, whose absolute amounts are very small. Also, the theoretical plate number of CE (10^5-10^6) is usually much higher than that of HPLC (10^3-10^4) [21]; this higher column efficiency allows for better resolution, which in some cases can result in shorter analysis times. This higher resolving power is also quite suitable for analysis of multiple compounds in biological samples. Last, the CE

technique requires very low sample volumes, typically less than 10 nL, thereby minimizing the dilution of each analyte prior to detection and also allowing faster sampling rate to facilitate acquisition of dynamic pharmacological information.

CE has been applied increasingly to neuroscience measurements in recent years. Such research started with determination of the catecholamine dopamine [22-23] and several excitatory amino acids [24] with electrochemical detection. However, the ECD detector combined with CE is difficult to handle technically and not many compounds have electrochemical responses.

Recently, several CE-LIF studies have been reported. Guzman and coworkers first analyzed glutamic acid and glutamine in brain microdialysis by CE-LIF [25-27]. The results showed that it was possible to label nanomolar solutions of several amino acids with the fluorescent dye fluorescein isothiocyanate (FITC) and detect them with CE-LIF. Later, eight naphthalene-2,3-dicarboxaldehyde (NDA)-tagged amino acids [28] and 3-(4-carboxybenzoyl)quinoline-2-carboxaldehyde (CBQCA) derivatized amino acids in microdialysate samples [29] were separated and determined. In the past four years, *in vivo* monitoring of amino acids by microdialysis on-line coupled to CE-LIF has been developed [30, 31]. Those results have shown high resolving power, good detection limits, and low sample volume requirements. However, the application of CE-LIF in neuroscience still needs further improvement. A major challenge is to increase the sensitivity and resolution of the analytical technique. Many compounds are not resolved and some of them are not detectable in brain samples with current analytical methods [31].

3.1.3.2 CE Applications in Homogenates

Analysis of compounds in tissue samples from the nervous system is an important area of application for CE. While the studies of single neuron represent the ultimate attainable level for small-scale tissue analysis, many neurochemicals may be present at levels too low to be detected effectively at this scale by current CE technology. Additionally, it may be desirable in some cases to monitor a compound in whole sections of brain tissue rather than at the single molecular level. Because CE uses low sample volume and offers low mass detection limit, smaller tissue samples can be used with CE to analyze trace amounts of neurotransmitters found at very low levels from complicated matrices. Especially with the sensitive LIF detection, it might be possible to decrease the amount of tissue necessary for analysis, and also simplify the purification procedures. Derivatization of analytes in homogenized brain tissue samples has been used to enhance sensitivity for CE analysis with visible absorbance [24], electrochemical [33] and LIF detections [28] as well. These reports illustrate the variety of detection and separation methods available with CE for the determination of a variety of classes of neurochemicals in the brain tissue homogenate.

3.1.3.3 In-house Constructed CE-LIF Instrumentation

One of the most extensively used detection methods is laser-induced fluorescence (LIF) because it provides the greatest degree of sensitivity of any detector currently available for CE. As introduced in Chapter One, CE-LIF contains four elements: a

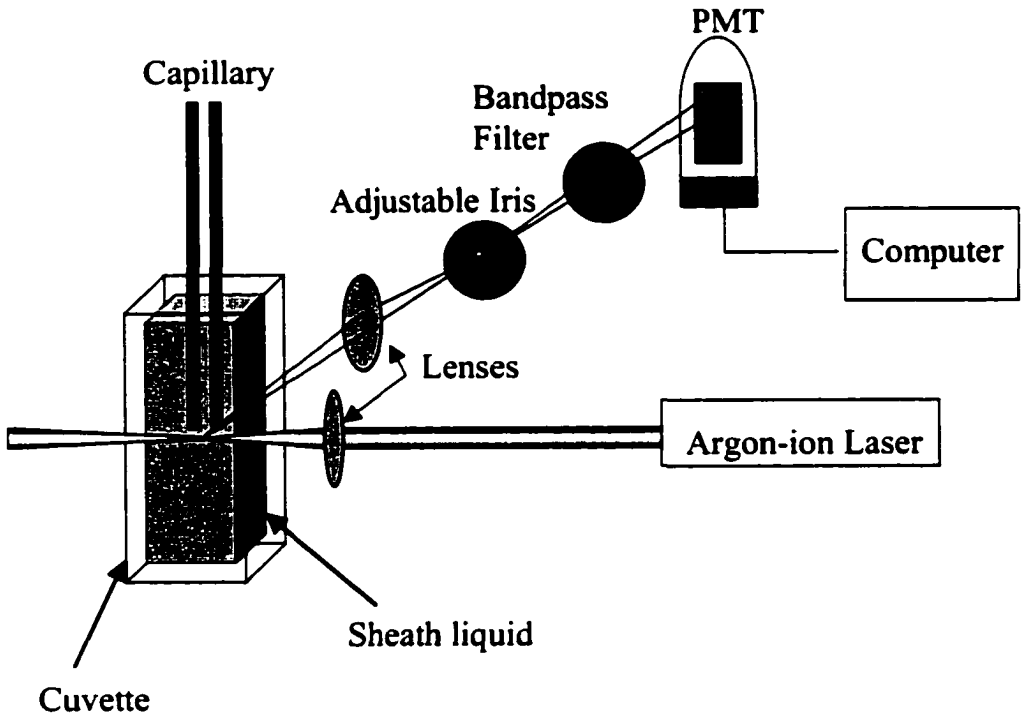

Figure 3.3: Schematic diagram of in-house high-sensitivity sheath flow LIF detector.

separation capillary, a high-voltage power supply, an injector and LIF detector. Figure 3.3 is a schematic diagram of the in-house constructed post-column sheath flow assisted LIF detector, which has been described in detail elsewhere [19, 20, 33].

Post-column LIF detection requires careful design to minimize undesirable extra column band broadening. An ideal way to reduce the background noise from light scattering is to measure fluorescence in a post-column flow chamber with flat windows providing good optical quality. Unlike the conventional on-column detection, in which the change in refractive index at the capillary/buffer interface produces a large amount of light scattering, the post-capillary detector uses a sheath flow cuvette to eliminate the source of scattered light by surrounding the capillary with a sheath liquid of the same refractive index. Also the scattered light from the cuvette/sheath buffer interface can be easily discriminated from the fluorescence using optics and a bandpass filter. The combination of lenses is designed to collect as much fluorescence as possible and remove as much background light (light scattering from solvent) as possible. Furthermore, the bandpass filter only allows light over a small range of wavelengths to pass through and blocks other wavelengths.

3.1.4 Outline of the Project

The goal of the work in this chapter was to develop a high-sensitivity analytical method for important biogenic amines and amino acids in brain samples, including brain microdialysates and tissue homogenate supernatants. After pre-column labeling with the fluorogenic reagent 5-furoylquinoline-3-carboxaldehyde (FQ), 16 neurochemicals

containing a primary amino group were separated with CE-LIF in different sample matrices. The separation was based on a micellar electrokinetic chromatography (MEKC) buffer system. Biogenic amines and amino acids were resolved and detected in a single run and identified by co-migration with standards. Furthermore, we report the accuracy, precision and linearity of the technique. The technique was then used to determine changes in the concentration of GABA, the major inhibitory neurotransmitter in the brain, in rat brain samples after administration of the antidepressant/antipanic drug phenelzine (PLZ). The findings on GABA in the brain samples after drug treatment were similar to those found previously using HPLC with fluorescence detection (after reaction with *o*-phthaldehyde). Minimal workup procedures were involved and as little as 1 μL of sample was required for analysis.

3.2 Experimental

3.2.1 Reagents

All aqueous solutions were made with deionized water obtained from a Milli-Q system equipped with a 0.2 μm filter. Artificial cerebrospinal fluid (CSF) was made as 145.0 mM NaCl (Fisher, Edmonton, Canada), 3.0 mM KCl (Sigma, St. Louis, MO, USA), 1.5 mM $CaCl_2$ (BDH, Toronto, ON, Canada), 1.0 mM $MgCl_2$ (Fisher), 2.0 mM Na_2HPO_4 (BDH), 2.0 mM NaH_2PO_4 (Fisher), and 2 mM dextrose (Fisher). The pH was adjusted to 7.1-7.2 using hydrochloric acid (Fisher). (This recipe was provided by Dr.

Glen Baker from the Neurochemical Research Unit, Department of Psychiatry, University of Alberta.)

Sodium tetraborate (borax) and sodium dodecyl sulfate (SDS) were purchased from BDH. The amino acids, biogenic amines, N-acetyl-l-lysine (FW 188.2) and internal standard (*o*-methyl-L-threonine) were obtained from Sigma. β-cyclodextrin hydrate (β-CD) was provided by Aldrich (Milwaukee, WI, USA). Aqueous stock solutions of amino acids, biogenic amines and internal standard were prepared at a concentration of 1 mg/mL in deionized distilled water; these solutions were diluted daily to the working concentrations with artificial CSF buffer before labeling. The final concentrations of amino acids and biogenic amines before injection varied from 10^{-6} to 10^{-4} g/L (about 10^{-8} ~ 10^{-6} M).

FQ and potassium cyanide were from Molecular Probes (Eugene, OR, USA). The 200 mM stock solution of potassium cyanide was made in deionized distilled water and diluted to 25 mM in 10 mM borate buffer (pH=9.2) before derivatization. FQ solutions needed to be dried before storage. A stock solution of 10 mM FQ was prepared in methanol, and then 10 μL aliquots were placed into 500 μL microcentrifuge tubes. The solvent was removed under vacuum at room temperature using a Speed Vac (Savant Instruments Inc., Farmingdale, NY, USA). The dried FQ was stored at -20°C in a freezer, and was used without further treatment on the day of the experiment.

3.2.2 Instrumentation

The homemade LIF detector and CE system have been developed in this group for more than ten years [33]. Briefly, the samples and standards were injected into a 40 cm long, 50 μm inner diameter, 140 μm outer diameter fused-silica capillary column. Light at 488 nm from an argon ion laser (Omnichrome, CA, USA) was focused to a spot after the column in the sheath flow cuvette and excited the FQ-labeled amines. The fluorescence was filtered by a bandpass interference filter centered at 630 nm and detected by a photomultiplier tube (PMT) operated at 900 V by a high-voltage supply (Spellman, NY, USA). A Macintosh computer was used for instrument control, data acquisition and data processing. The signal from the PMT was conditioned with a laboratory-made current-to-voltage converter before digitization by the computer and all data were analyzed with Igor Pro (WaveMetrics, Oregon, USA).

3.2.3 Surgical and Sampling Procedure for Microdialysates

The microdialysis procedures were performed in the laboratory of Professor Glen Baker (34). Experiments were performed with male rats (Sprague-Dawley, 200-250 g). Briefly, a permanent intracerebral guide cannula was implanted into the region immediately dorsal to the caudate nucleus. The cannula was secured to the skull with four jeweler's screws and cranioplastic cement. In addition, a wire loop was embedded in the cement to attach the rat to the tether during the microdialysis procedures. A dummy cannula was inserted into the guide cannula to keep it free of debris. The skin was sutured rostral and caudal to the cemented area and the incision was sealed with an

adhesive (Vetbond; 3M Animal Care Products). Following surgery, the rats were kept in a warm temperature-controlled environment until recovery from anesthesia.

Each rat was allowed to recover from surgery for at least 4 days and handled for 3 minutes on two separate occasions before microdialysis. Each experiment was conducted during the midlight phase. On the day of microdialysis, the rat was placed in a round Plexiglas bowl (BAS) that contained a mixture of clean bedding from the rat's cage. After 5 min, the rat was attached to the tether. Following a 1-h habituation period, a microdialysis probe (3 mm membrane) was inserted into the guide cannula. The probe was perfused at the rate of 1 μL/min with artificial cerebrospinal fluid. After a 2-h stabilization period, three 25-minute baseline samples were collected. Then, the physiological saline vehicle or the agent of interest was administered intraperitionally (i.p.) into the probe. Following the injection, eleven 25-minute samples were collected. The samples were kept on dry ice during the experiment and then transferred to an -80°C freezer for long-term storage.

3.2.4 Sampling Procedure for Brain Tissue Supernatant

In the time of study, rats (male, Sprague-Dawley, 200-250 g) were injected with PLZ (15 mg/kg i.p.) or physiological saline vehicle. Groups of five animals were killed by cervical dislocation and immediate decapitation at 4 h after injection. The brains were rapidly removed and homogenized in 5 volumes of ice-cold methanol, followed by centrifugation (10000 x g for 20 min) to remove the protein precipitate.

3.2.5 FQ Derivatization Procedure

Four experiments were conducted as described below. The amount of dye FQ was always in large excess.

In the first experiment, microdialysates were labeled to determine which amino acids and biogenic amines were present. A 4 μL microdialysate sample or biogenic amine standard (10^{-6} ~ 10^{-4} M) spiked with 1 μL of the internal standard (1 mg/mL, equivalent to 7.5 mM) *o*-methyl-L-threonine was mixed with 100 nmol dry FQ and 2 μL 25 mM KCN (pH = 9.2). The mixture was reacted in the dark in a 65°C bath incubator (11-718, Fisher Scientific, Edmonton, AB, Canada) for 16 minutes and then was diluted 200-fold before injecting in the capillary for analysis. A blank solution of the same volume was derivatized using the same protocol.

In the second experiment, N-acetyl-L-lysine was labeled to study the mechanism of the labeling process of a typical amino acid. A 10-μL aliquot of a 10^{-4} M solution of N-acetyl-L-lysine was mixed with 100 nmol FQ and 2 μL of a 25 mM KCN solution, prepared in a 10 mM borate buffer, pH 9.2. Reactions were performed in the dark either at room temperature or at 65°C. Aliquots were periodically withdrawn from the reaction vial and diluted 1000-fold (10^{-7} M) in a 2.5 mM disodium tetraborate, 5 mM SDS buffer.

In the third experiment to determine the linearity of the method, different volumes of standards (0, 0.6, 0.9, 1.2, 1.5 μL) and 1 μL internal standard (1 mg/mL, equal to 7.5 mM *O*-methyl-L-threonine) were mixed with artificial CSF buffer to a volume of 5 μL, and derivatized to yield 10^{-8} ~ 10^{-6} M FQ-tagged amino acids and biogenic amines solutions.

In the fourth experiment, the concentrations of GABA in rat whole brain tissue homogenate supernatant samples and in striatal microdialysates were measured by comparing the migration time and the peak intensity with *O*-methyl-L-threonine as an internal standard. The samples were analyzed by HPLC at the same time [34].

3.2.6 Capillary Electrophoresis

The running buffer for electrophoresis was 10 mM borate and 5 mM SDS or 20 mM borate and 60 mM SDS at pH = 9.2. The samples, blanks and standards were injected electrokinetically at 50 V/cm for 2 s or 100 V/cm for 5 s; then the separation was performed at 400 or 200 V/cm. This voltage generated about 10 μA current. After each run, the capillary was flushed with 0.1 M NaOH followed by water and running buffer. The peaks for the analytes were identified by matching the migration time with those in the spiked sample and quantitated by comparing their height-ratios with the internal standard. Data were analyzed using MatLab and a two-point method was used to correct for variations in migration time [35].

3.3 Results and discussion

3.3.1 CE analysis of microdialysates

Brain microdialysis is valuable for collecting small amounts of samples from different tissues in freely moving animals [36]. Electropherograms of a brain

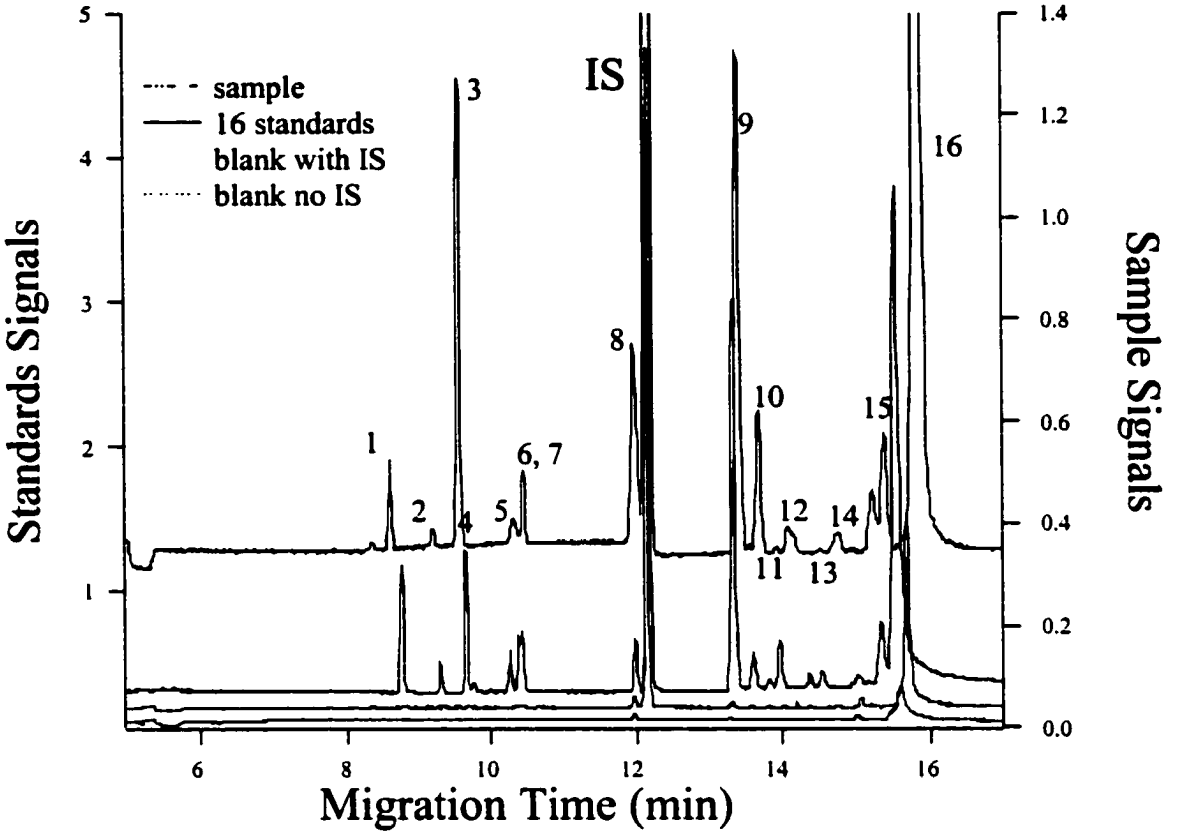

Figure 3.4: Typical CE separations of neurotransmitters: (A) 16 biogenic amine or amino acid standards with internal standard (IS); (B) microdialysate sample spiked with internal standard. Experimental conditions: 16 min reaction time; 5 s x 4 kV injection, 40 cm x 50 μm (i.d.) capillary, E = 205 V/cm; PMT voltage = 900 V; running buffer 20 mM borate and 60 mM SDS. Peaks: 1: serine; 2: threonine; 3: glutamine; 4: glutamate; 5: dopamine (DA); 6: histidine; 7: asparagine; 8: alanine; 9: taurine (Tar); 10: aspartic acid; 11: γ-amino-butyric acid (GABA); 12: glycine; 13: serotonin (5-hydroxytryptamine, 5-HT); 14: norepinephrine (NE); 15: methionine; 16: β-alanine. Variation in migration time was corrected using a two-point method based on the migration of components 1 and 16 (35).

microdialysate sample and a standard mixture spiked with internal standard (*O* -methyl-L-threonine) are shown in Figure 3.4. A little difference of migration time between the microdialysate and the standards indicates the effect of matrix. However it is difficult to mimic exactly the same matrix as the microdialysate sample. A similar solution, artificial CSF buffer (pH 7.1-7.2), was used as buffer for the standard mixture. Variation in migration time was also corrected using a two-point method based on the migration of components [35].

The blank shows the peaks due to the reaction of impurities, and the same peaks are observed for the standard and real sample solutions. There are more than 20 peaks in the dialysate electropherogram; 16 co-migrated with standard FQ-labeled primary amines. This system is suitable not only for the detection of amino acids, but also for important neurotransmitter amines, such as dopamine (DA), 5-hydroxytryptamine (5-HT), and norepinephrine (NE), which are present at considerably lower concentrations than most amino acids.

The separation efficiency was high for this analysis. The number of theoretical plates was typically 120,000 for all peaks, except for peak 16 (β-alanine), which tailed in the electropherogram of the biogenic amine standards.

3.3.2 Derivatization Reaction

To optimize further the labeling reaction, we wished to obtain the kinetics data to determine the reaction rate and activation energy of the derivatization of FQ with a typical amino acid. The reaction between FQ and N-acetyl-lysine was studied by CE and

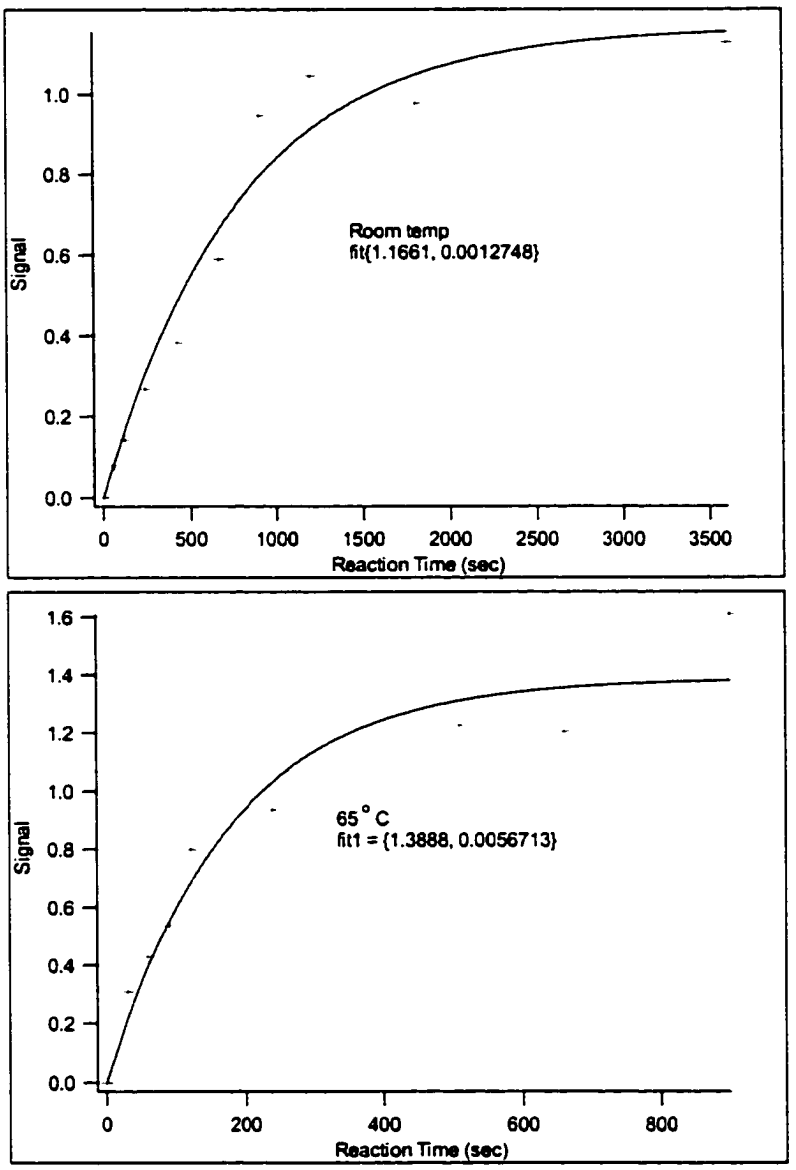

Fig 3.5: The reaction rate of labeling process. The smooth curve is the least-squares fit of first order kinetics to the data. (upper): Room temperature reaction; (bottom): 65°C.

LIF (Figure 3.5). This modified amino acid has its α-amino blocked, so that FQ could only react with one amine: the ε-amine. The data were described by first-order reaction kinetics at room temperature, with a rate constant of 0.0013 s^{-1}. The reaction was five-times faster at 65°C, where the reaction constant was 0.0057 s^{-1}. According to the Arrhenius equation

$k = A \exp(-\Delta G / RT)$

where A is the pre-exponential term, Ea is the activation energy in $KJmol^{-1}$, R is the gas constant, and T is the absolute temperature in K, another equation can be derived as

$\Delta G = R T_1 T_2 \ln(k_2/k_1) / \Delta T$

This increase in reaction rate with temperature was caused by apparent activation energy of 27 kJ/mol. Both the reaction rate and activation energy for the reaction of FQ with N-acetyl-lysine are similar to those measured for the reaction with a number of neurotransmitters found in cerebrospinal fluid [37].

Four experiments were conducted to perform the labeling procedures based on the experimental purpose and sample characteristics, such as concentrations of analytes and pH of the sample matrix. The amount of dye FQ was always kept in large excess to ensure it was a first-order reaction.

3.3.3 Choice of Internal Standard

The observed variation in the migration time and peak intensity of the same sample injected consecutively implied different injection volumes between different CE runs. The analyte taurine was randomly chosen to compare the linearity with or without

internal standard. It was found that the correlation coefficient of the calibration curve increased from 0.93 to 0.99 with internal standard. Therefore, an internal standard was needed in these experiments. There are several requirements for the internal standard.

Table 3.1: Linearity of calibration curves for amino acids and biogenic amines

Compound	Peak # in Figure 3.4	R^2	Slope(arbitrary)	Interceptor	LOD (10-9 M)
Ser	1	0.99	1.6	-0.0024	7
Thr	2	0.97	0.2	0.98	70
Gln	3	0.98	3	-0.0010	4
Glu	4	0.99	0.9	0.0015	10
DA	5	0.97	0.15	0.00080	80
His	6	0.99	10	-0.0027	1
Asn	7	0.98	7	0.00070	2
Ala	8	1.00	1.4	0.0013	8
Tar	9	0.99	100	0.015	0.1
Asp	10	0.96	2	0.0056	6
GABA	11	0.98	8	0.0025	2
Gly	12	0.97	10	0.0065	1
5-HT	13	0.96	9	0.0030	1
NE	14	0.96	0.6	0.0013	20
Met	15	0.98	0.4	0.017	30
β-Ala	16	0.99	11	0.38	1

Detection limit (LOD) is defined as that amount of analyte that generates a peak that is three times larger than the noise in the background signal. Standard three letter abbreviations for amino acids are shown; other abbreviations are listed in the caption for Figure 3.4.

First, it should appear near the middle of the run without overlapping with any analyte. Secondly, because of the uncertainty in the derivatization process, the internal standard must be labeled at the beginning of the procedure. Thirdly, the internal standard should have a similar molecular weight and structure as other analytes.

3.3.4 Calibration Curve

To correct for variations in the injection volume, a modified amino acid, *o*-methyl-L-threonine (7.5 mM), was chosen to be the internal standard (Figure 3.4). This compound is not observed in the brain microdialysates, undergoes the same derivatization reaction as the biogenic amines and amino acids, migrates near the middle of the electropherogram, and does not co-elute with any components in thee brain microdialysates.

Linearity and detection limits (LOD) are summarized in Table 3.1. The calibration ranges were selected according to the predicted concentrations in the dialysate samples to be determined. After normalization to the signal from the internal standard, there is a linear relationship between the concentration of analytes and the peak intensity, with correlation coefficients ranging from 0.96 to 1.00. The intercepts of the calibration curves did not significantly differ from zero, except for β-alanine, whose area was difficult to determine because of tailing. Detection limits were typically at the nanomolar concentration levels, and was found as low as 100 picomolar for taurine. Variations in sensitivity appear to be due to differences in reaction rate [37], injection volume and spectral properties (such as molar absorptivity, emission spectrum and fluorescence

quantum yield) for each component. The final reason could be the variation in the adsorption of analytes on the capillary wall during separation. Taurine has high detection sensitivity; the reason for this sensitivity is not clear.

3.3.5 Brain microdialysates and tissue homogenates

This CE-LIF method has been used for determination of neurotransmitters in the real brain samples, including microdialysates in Figure 3.4 and tissue homogenate supernatants in Figure 3.6.

The influence of the antidepressant/antipanic drug phenelzine (PLZ) on the profile of GABA in rat whole brain homogenates was studied, and the results are shown in Figure 3.6. The concentration of GABA in the brain supernatants increased 3 –fold after drug treatment, which agrees with previous gas chromatography and HPLC (with fluorescence detection after reaction with *o*-phthaldehyde) results [34].

With internal standard *o*-methyl-L-threonine, it was found that the trend of HPLC and CE results are similar but the precision of CE data are much poorer than the HPLC's for analysis of brain supernatant, Figure 3.7. This probably is due to the different reaction rate of *o*-methyl-L-threonine from other amino acids, and its use did not improve precision in this experiment. In order to avoid the variation of reaction for the

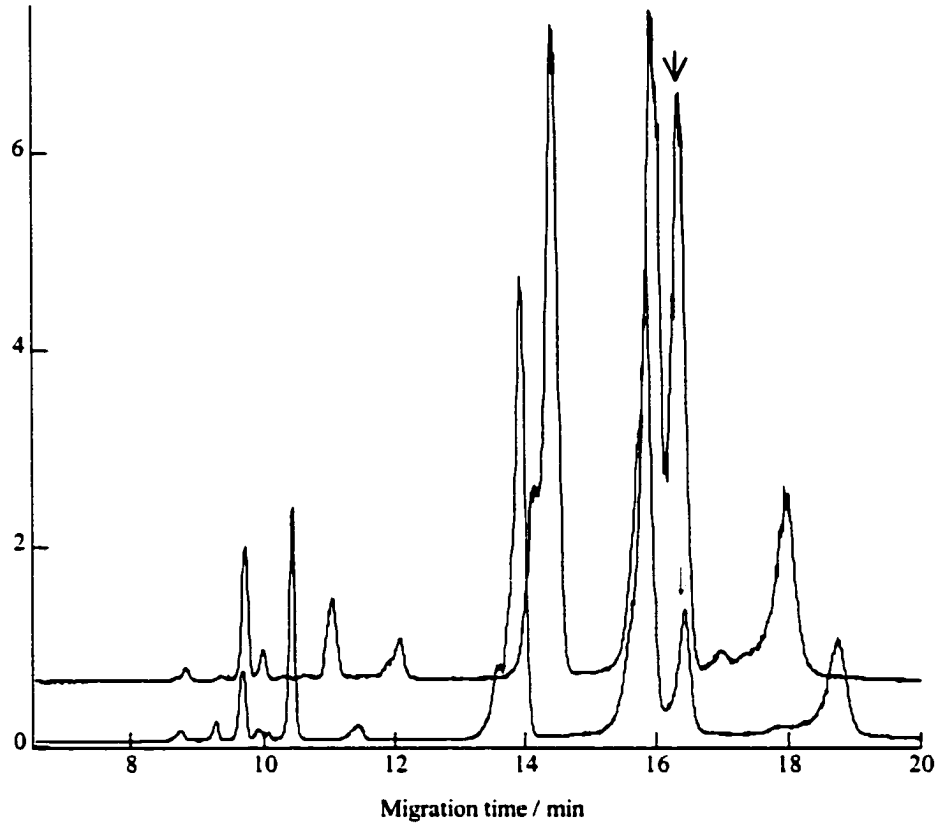

Figure 3.6: Analysis of whole rat brain tissue homogenate supernatants for GABA (the peaks pointed with arrow): (upper) sample from rat treated with PLZ; (bottom) sample from physiological saline vehicle-treated rat with the same protocols as the upper one. 4 μL of 0.1 NaOH was added to the samples, which were reacted for 30 min at 65°C. A slightly longer capillary was used to generate this data compared with Figure 3.4.

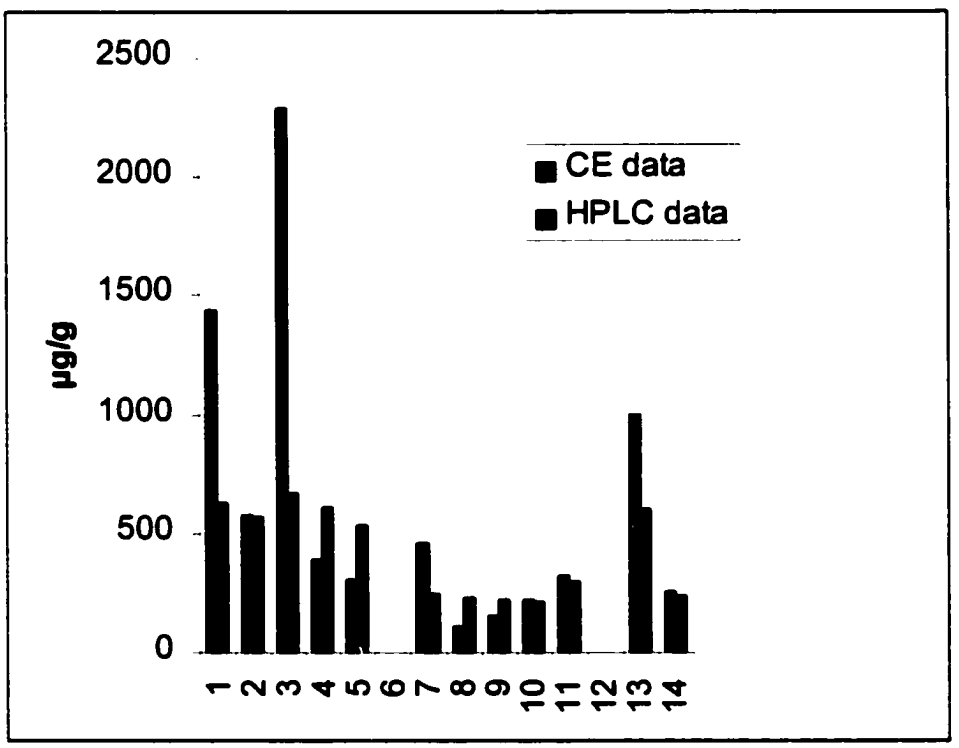

Figure 3.7: Comparison of HPLC and CE data for GABA concentration from brain tissue supernatants with (No.1 ~ No.5, No.13) or without (No.7 ~ No.11, No.14) drug PLZ administration. No.13 and 14 are the average value for No. 1-5 and No. 7-11, respectively.

internal standard, a fluorescent dye Rhodamine 6G was added to the sample as an internal standard after finishing the labeling reaction. Better experimental precision was obtained by a factor of 2 compared to the use of *O*-methyl-L-threonine [37]. The HPLC and CE results were identical for the initial and final GABA levels, but the CE data were systematically slightly higher for intermediate times.

3.4 Conclusions

Unlike the method developed in Chapter 2, the whole process in this chapter started with the separation of real samples directly, and then came back to standards for identification and quantitation. The main advantage of this procedure is to minimize the effect of matrix and find a relatively universal method. The results showed the feasibility and reliability of using CE-LIF to examine these neurotransmitters in real samples. A rapid CE-LIF method has been developed for the simultaneous determination of several important brain biogenic amines and amino acids in a short time. Minimal work-up procedures and only small quantities of samples were required for analysis. The method generated a linear relationship between the concentration of 16 compounds of interest and the peak intensity. The assay was used for the analysis of *ex vivo* brain samples, including both microdialysates and homogenate supernatants. Results were similar to those obtained by HPLC analysis. The number of theoretical plates is typically 120,000.

However, the concentrations of each analyte in the sample vary significantly which influences the efficiency of the labeling reaction. More importantly, the reaction

kinetic data (37) of neurotransmitters with FQ dye shows the reaction temperature and reaction time are critical factors among the labeling conditions. There are no standard pretreatment procedures and optimum derivatization conditions for different types of sample. For example, the FQ labeling requires a basic environment to approach a higher derivatization yield, so that ice-cold methanol, instead of perchloric acid, was used as a solvent to remove the protein precipitate from supernatant samples, and furthermore 4 μL NaOH (0.1M) was used to ensure the alkaline condition for efficient labeling reaction.

The running buffer used in the experiments is a typical MEKC buffer: Borate and SDS. But the last peak in the electrophoregram seems to contain more than one compound, and this is probably because the analytes comigrate with the micelle itself. More patience is required to improve the separation of the solution of analytes.

Coupling CE with microdialysis on-line is of increasing interest for CE application in the microdialysis technique, and in the future, the interface combining CE and microdialysis equipment and the on-column labeling technique will be applied.

Mass spectrometry coupling to CE is a relatively recent development for the analysis of neurotransmitters, but already its application to microdialysis has become apparent with the report that GABA from rat brain can be measured using the electrospray interface [38]. This suggests CE-MS may be useful for the real time monitoring of many neurotransmitters or drugs which can be measured by the microdialysis technique.

References

1. G.I. Stevenson and R. Baker, *Education in Chemistry,* 1996, 9, 124.
2. J.R. Cooper, F.E. Bloom, and R.H. Roth, *The Biomedical Basis of Neuropharmacology,* 7th edition, Oxford University Press, New York, 1996.
3. T. Zetterstrom, T. Sharp, C. Marsden and U. Ungerstedt, *Journal of Neurochemistry,* 1983, 41, 1769.
4. U. Ungerstedt and A. Hallstrom, *Life Science,* 1987, 41, 861.
5. L.A. Dawson, *Journal of Chromatography B,* 1997, 697, 89.
6. A. Adell, F. Artigas, in: A.A. Boulton, G.B. Baker, and A.N. Bateson, (Eds.), *Neuromethods,* In Vivo Neuromethods, Humana Press Inc, Totowa, New Jersey, Volume 32, pp.1.
7. C. Humpel, T. Ebendal, and L. Olson, *Journal of Molecular Medicine,* 1996, 74, 523.
8. M. Takita, T. Tsuruta, Y. Oh-hashi and T. Kato, *Neuroscience Letters,* 1989, 100, 249.
9. J.C. Ballenger, *Journal of Clinical Psychiatry,* 1986, 47(supplement), 27.
10. M.R. Johnson, R.B. Lydiard, and J.C. Ballenger, in: S.H. Kennedy (Ed.), *Progress in Psychiatry,* American Psychiatric Press, Washington, DC, 1994, Vol. 43, pp.205.
11. L. Martin, D. Bakish, and R. Joffe, in: S.H. Kennedy (Ed.), *Progress in Psychiatry,* American Psychiatric Press, Washington, DC, 1994, Vol. 43, pp.147.
12. F. Petty, G.L. Kramer, and W. Hendrickse, in: J.J. Mann and D.J. Kupfer (Eds.), *Biology of Depressive Disorders, Part A,* Plenum Press, New York, 1993, pp.79.

13. Z. Chen, J. Wu, G. Baker, M. Parent, and N.J. Dovichi, *Journal of Chromatography A*, 2001, 914, 293.

14. K.F. McKenna, G.B. Baker, and R.T. Coutts, *Naunyn-Schmiedeberg's Archives of Pharmacology*, 1991, 343, 478.

15. B.D. Sloley, O. Kah, V.L. Trudeau, J.G. Dulka and R.E. Peter, *Journal of Neurochemistry*, 1992, 58, 2254.

16. M.E. Bovingdon, R.A. Webster, *Journal of Chromatography B*, 1994, 695, 157.

17. F.C. Cheng, J.S. Kuo, *Journal of Chromatography B*, 1995, 665, 1.

18. M.I. Davies, C.E. Lunte, *Chemical Society Reviews*, 1997, 26, 215.

19. Y.F. Cheng, N.J. Dovichi, *Science*, 1988, 242, 562.

20. D.M. Pinto, E.A. Arriaga, D. Craig, J. Angelova, N. Sharma, H. Ahmadzadeh and N.J. Dovichi, *Analytical Chemistry*, 1997, 69, 3015.

21. S.D. Gilman and A.G. Ewing, *Journal of Capillary Electrophoresis*, 1995, 2, 1.

22. T.M. Olefirowicz and A.G. Ewing, *Journal of Neuroscience Methods*, 1990, 34,11.

23. J.B. Chien, R.A Wallingford and A.G. Ewing, *Journal of Neurochemistry*, 1990, 54, 633.

24. T.J. O'shea, P.C. Weber, B.P. Bammel, C.E. Lunte, S.M. Lunte and M.R. Smyth, *Journal of Chromatography*, 1992, 608, 189.

25. L. Hernandez, S. Tucci, N. Guzman and X. Paez, *Journal of Chromatography A*, 1993, 652, 393.

26. L. Hernandez, N. Joshi, E. Murzi, P. Verdeguer, J. C. Mifsud and N. Guzman, *Journal of Chromatography A*, 1993, 652, 399.

27. L. Hernandez, J. Escalona, P. Verdeguer and N.A. Guzman, *Journal of Liquid Chromatography,* 1993, 16, 2149.

28. P.L. Weber, T.J. O'shea, S.M. Lunte, *Journal of Pharmaceutical & Biomedical Analysis,* 1994, 12, 319.

29. J. Bergquist, M.J. Vona, C.O. Stiller, W.T.O. Connor, T. Falkenberg, R. Eknan, *Journal of Neuroscience Methods,* 1996, 65, 33.

30. S.Y. Zhou, H. Zuo, J.F. Stobaugh, C.E. Lunte and S.M. Lunte, *Analytical Chemistry,* 1995, 67, 594.

31. M.W. Lada and R.T. Kennedy, *Analytical Chemistry,* 1996, 68, 2790.

32. T.J. O'shea, R.D. Greenhagen, S.M. Lunte, et al, *Journal of Chromatography,* 1992, 593, 305.

33. S. Wu and N.J. Dovichi, *Journal of Chromatography,* 1989, 480,141.

34. M. Parent, D. Bush, G. Rauw, S. Master, F. Vaccarino, G. Baker, *Methods,* in press.

35. X.F. Li, H. Ren, X. Le, M. Qi, I.D. Ireland and N.J. Dovichi, *Journal of Chromatography,* 2000, 869, 375.

36. C.E. Lunte and D.O. Scott, *Analytical Chemistry,* 1991, 63, 773A.

37. J. Wu, Z. Chen and N.J. Dovichi, *Journal of Chromatography B,* 2000, 741, 85.

38. Y. Takada, M. Yoshida, M. Sakairi, and H. Koizumi, *Rapid Communications Mass Spectrometry,* 1995, 9, 895

Chapter 4

Multicapillary Thermo-optical Absorbance Detector

4.1 Introduction

4.1.1 Thermo-optical Absorbance Technique

In the last two decades, our group has developed a set of laser-based absorbance detectors based on the photothermal (or thermal-lens) effect [1-9]. The thermal lens effect described by Leite *et al* [10] in 1964 is a classical example of a thermo-optical technique where a laser beam becomes defocused passing through a refractive index gradient. Although there are many variations in the experiments, in each case a pulsed pump laser beam is directed into the sample that absorbs the laser energy, which causes localized heating in the sample and produces a temperature increase that is highest in the beam center and falls to the ambient temperature in the bulk solution. The temperature rise is proportional to both the sample absorbance and the pump laser power; therefore, the use of a high power laser permits the detection of weakly absorbing compounds. Since the refractive index changes with temperature, this laser-induced heating range forms a refractive index gradient, which acts as a thermal-lens that defocuses either the pump laser beam or another probe beam. The defocusing is usually detected as a decrease in the beam center intensity; the photothermal signal is proportional to the sample absorbance.

In my experiments, the crossed-beam thermal lens technique has been used. As shown in the experimental diagram, the effect is based upon the interaction of a modulated pump beam and a coplanar probe beam crossed at right angles, shown in Figure 4.1. The pump and probe beams interact only at their intersection, producing a cylindrical thermal lens that has a volume as small as a few picoliters. A typical pump laser is an argon ion laser (λ = 488 nm) and a typical probe laser is a low power helium-neon laser (λ = 632.8 nm). While the thermal lens signal is proportional to the sample's absorbance of pump laser photons, it is not dependent on the sample path length. The sample can be a bulk solution [1], a sample eluting from a chromatographic column [3], a sample contained within an electrophoresis capillary [7-9], or a sample flowing in a sheath flow cuvette [4].

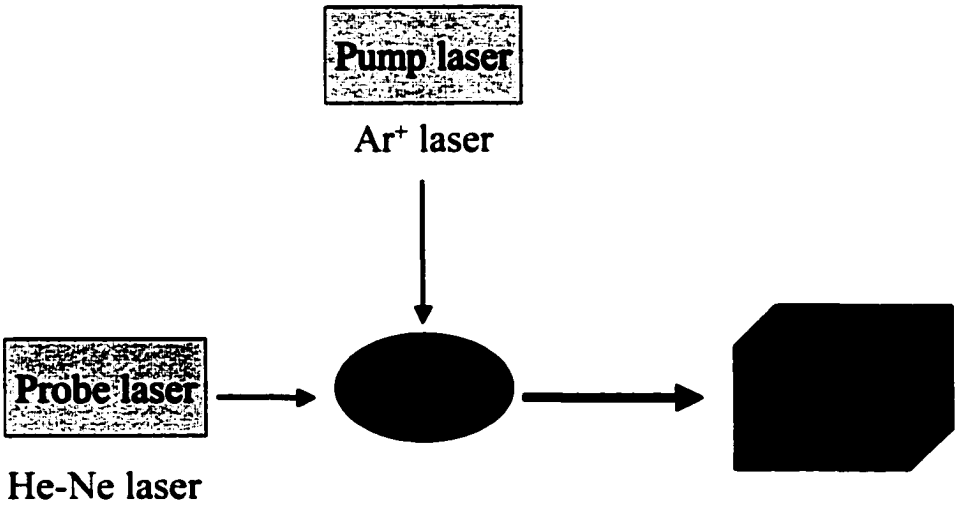

Figure 4.1: Cross-beam thermal-lens experiment.

In this chapter, I will start by presenting several preliminary experiments during the development of the multi-capillary thermo-lens absorbance detector (MCTAD), followed by the design and evaluation of the MCTAD instrument, and finally presenting applications and future work.

4.1.2 Single-capillary Thermo-optical Absorbance

As previous mentioned in 4.1.1, the single capillary thermo-optical technique has been applied to the development of an on-column, thermal-optical absorbance detector for capillary chromatography and capillary electrophoresis [7-9, 11-15]. The experimental design follows the scheme in Figure 4.1. What makes this instrument unique is the refractive index detector. Figure 4.2 shows the configuration of the pump and probe beams with respect to the capillary tube. Sample absorption of the energy from the pump laser followed by the nonradiative relaxation of excited states produces localized heating. The induced temperature rise results in a refractive index gradient. While the probe laser beam is focused on both the capillary tube and the pump beam at right angles, simultaneous diffraction, refraction and deflection of the probe beam are observed since the probe beam passes through several media with different refractive indexes: first air, then fused silica, the sample solution, fused silica again, and finally air. However, because of the crossed-beam configuration of the experiment, photothermal refraction and deflection occur in conjunction with diffraction of the probe beam, and the flow inside the capillary distorts the thermal lens by continuous removal of the heat. The

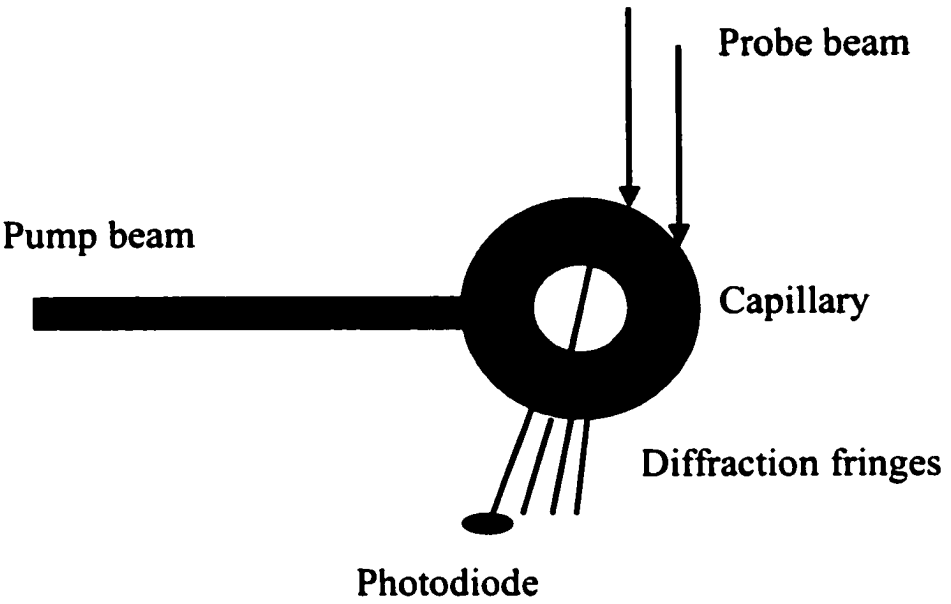

Figure 4.2: On-column thermo-optical absorbance detection. Movement of the diffraction fringes is monitored by the photodiode as a change in the probe beam intensity.

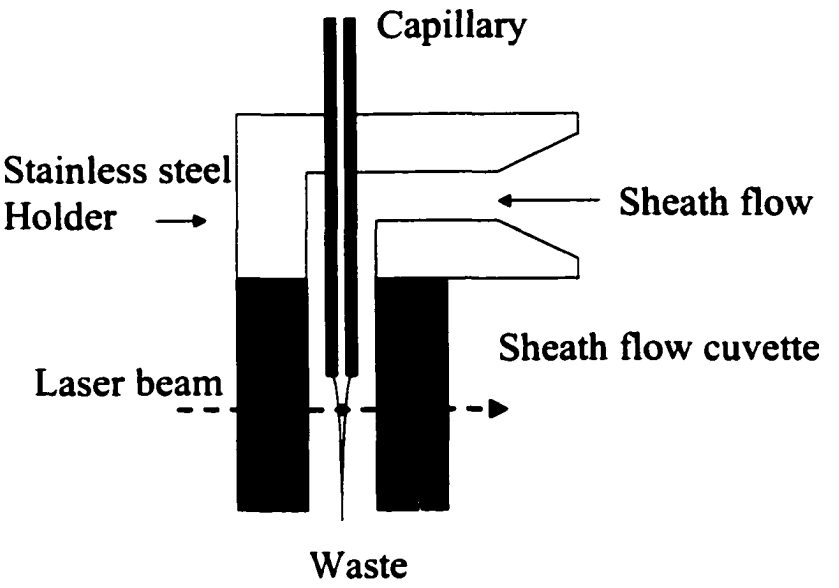

Figure 4.3: A schematic of the sheath flow cuvette as a post column detector. The sheath flow focus the sample stream down the capillary and the laser beam excites the sample beneath the exit of the capillary.

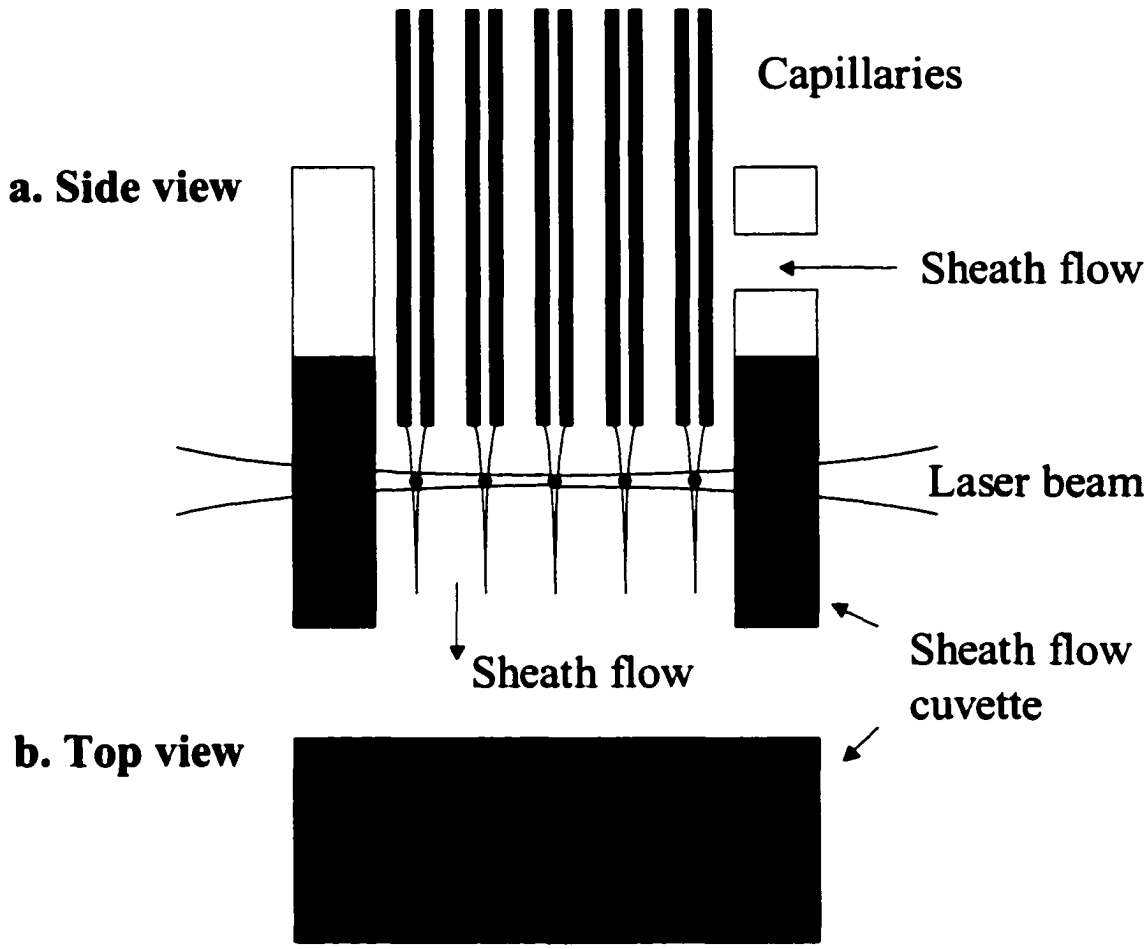

Figure 4.4: A schematic of the multiple capillary sheath flow cuvette chamber for an array of five capillaries. The sheath flow focus the sample stream from each capillary and the laser beam excites all the sample streams simultaneously.

small detector photodiode is positioned beside the first main fringe, which is observed to move when the refractive index of the solution changes.

Concentration detection limits as low as $5x10^{-8}$ M for a DABSYL (4,4 - dimethylaminoazobenzene-4'-sulfonyl) derivatized amino acid [13] and adenosine monophosphate [15] were reported, corresponding to mass detection limits of 37 attomoles and 0.4 femtomoles.

4.1.3 Single-capillary Sheath-flow Cuvette Technique

I used a sheath-flow cuvette as a detection chamber for use with capillary electrophoresis. A schematic of the sheath flow cuvette for single capillary post-column detector is shown in Figure 4.3. Conventionally, the cuvette is made of quartz, has a 200-μm-square in cross section, is 2 cm in length and has 2 mm thick windows. A capillary with an outer diameter (o.d.) of about 150 μm is mounted in the center of the square hole. As the analytes elute from the end of the capillary, the sheath flow sweeps them downstream. Either a high-precision syringe pump or gravity siphoning can drive the sheath liquid at a rate of 0.15 mL/h or so.

This laboratory has over one decade of experience in the development of the sheath flow cuvette in fluorescence experiments, in which a laser beam illuminates the sample stream immediately beneath the capillary tip [16]. Since the sheath flow has the same components as the sample buffer, there is no refractive index boundary between the sample and the sheath stream and there is very little light scattering generated in the cuvette chamber. Meanwhile the analyte forms a narrow stream in the center of the

chamber, far from the cuvette walls; thus the interference due to light scatter from the interface of the cuvette window and sheath stream is minimized. Extremely sensitive fluorescence detection, including single molecular detection, has been reported by this group [19].

In those experiments, the fluorescence is collected at a right angle to the cuvette and transfered to a PMT for detection. As described below, the cuvette can also be used as a high sensitivity absorbance detector based on the cross-beam photothermal effect. In this case, the cuvette allows a single pump beam to illuminate the sample stream and the thermal lens effect can be detected by viewing the image of a probe laser beam using a photodiode or photodiode array.

4.1.4 Multi-capillary Sheath-flow Cuvette Technique

Large-scale DNA sequencing requires instruments that generate high throughput and high accuracy at low cost [20]. The success of a high performance multicapillary DNA sequencer based on the multiple capillary sheath flow cuvette developed in our group has proved to be a good example [17]. This cuvette, which is similar to that used in a single capillary fluorescence detector, consists of a rectangular flow chamber (Figure 4.4). In this system, a linear array of capillaries is held by a set of alignment features etched into the walls that distribute the capillaries with a uniform spacing. A sheath buffer is pumped through the space between the capillaries, and draws the sample from the capillary tips, forming a set of thin sample streams, with one sample stream per

capillary. One laser beam can pass through all of the sample streams, exciting fluorescence from all the samples simultaneously.

In this chapter, I demonstrate that the cuvette design for the multiple capillary fluorescence detector can also be applied as a multiple-capillary absorbance detector based on the photothermal effect.

4.1.5 Advantages of Multi-capillary Photothermal Absorbance Detector

Modern drug discovery requires highly sensitive and universal analytical techniques with high throughput to deal with the large libraries of compounds and relatively low sample concentrations used in combinatorial chemistry. For example, current combinatorial chemistry techniques make it possible to synthesize hundreds or even thousands of compounds per day. This trend challenges the analytical chemists to develop parallel analytical methods to characterize and identify such huge numbers of compounds. Capillary electrophoresis (CE) is an excellent technique for this application due to its high efficiency and low mass detection limit [16]. However, conventional CE suffers from two limitations. First, it is a serial procedure, wherein samples are analyzed sequentially. Secondly, the small dimensions of the capillary provide a significant detection challenge. Especially in absorbance spectroscopy, the inner diameter of a capillary typically is about 50 μm, which provides a very short optical pathlength and makes problematic the detection of trace components. In photothermal experiments, the signal is proportional to both the sample absorbance and the pump laser power; the use of a high power laser allows detection of weakly absorbing compounds. This advantage

makes CE detection based on the thermal-lens effect a complementary technique for use in high sensitivity absorbance determination.

CE run in parallel generates high throughput [17]. 5-, 16-, 32-, and 96-capillary array electrophoresis systems have been successfully used in our group to perform DNA sequencing and other analysis. In these multiplexed CE systems, laser-induced fluorescence had been exclusively employed as the detection method. While fluorescence detection is suitable for DNA sequencing applications due to its labeling features and high sensitivity, absorption detection has remained as a very useful tool because of its ease of implementation and wide applicability. Therefore, our laser based multicapillary absorbance detector could combine the advantages of both multiplex CE and photothermal absorbance techniques.

4.2 Instrumental

4.2.1 Design Consideration

4.2.1.1 General

In the design of the detector, a one-dimensional array of capillaries is used as a separation system. A linear array of capillaries is placed in a rectangular sheath flow cuvette. Sheath fluid is pumped through the space between the capillaries and draws the sample as a discrete stream from each capillary. A modulated pump laser beam is simultaneously passed through all sample streams. Absorbance of the pump laser beam creates a modulated temperature and refractive index perturbation in each stream. This

perturbation defocuses the probe laser beam, which passes at right angles through all of the sample streams. A photodiode array monitors the change in probe-beam intensity in-phase with the pump-laser modulation frequency at the image location for each sample stream.

4.2.1.2 Pump Laser

As introduced in 4.1.1, a pump laser beam is needed to excite the sample molecules to induce the localized heating and to produce a temperature increase. The use of a high power laser allows the detection of weakly absorbing compounds because the temperature rise is proportional to the pump laser power. I used an Argon ion laser, (λ = 488 nm) with a power of over 30 mW. When the concentration of sample is low enough, a single pump laser beam can pass through all of the sample streams, generating photothermal signals from all of the samples simultaneously.

The photothermal heating decays with a characteristic time constant that depends on the solvent thermal conductivity and the laser beam spot size [5]. The pump laser beam is modulated to periodically heat the sample and computer software is used to demodulate the photothermal signal.

4.2.1.3 Probe Laser

The probe laser should be highly stable and of low cost. We typically use a 1-mW helium-neon laser (λ = 633 nm) in our laboratory. The heating induced by the pump laser produces a refractive index gradient, which acts as a lens and defocuses the probe beam. The defocusing is detected as a decrease in the beam center intensity. Rather than

using individual probe beams to monitor the photothermal signal at each sample stream, an elliptically shaped probe beam is used to illuminate all sample streams simultaneously [6]. An array of defocused spots is formed in the probe beam profile, with one spot per sample stream. The extent of defocusing at each spot is proportional to the absorbance of the corresponding sample stream. A cylindrical lens is used to direct the beam to match the dimensions of the array of heated sample spots.

4.2.1.4 Photodiode Array (PDA)

A simple, low cost photodiode array is used to detect the beam defocusing generated by each sample stream. The difference between thermal lens signals due to the pump laser being on and off is recorded across the linear array to determine the sample absorbance. Different elements in the array are used to image different axial locations in the cuvette chamber. Because a PDA has a much larger electron well capacity (tens of million electrons), it is superior to a CCD detector for absorption detection.

4.3 Preliminary Investigations

4.3.1 Thermo-optical Detection with a Conventional Fluorescent Cuvette

4.3.1.1 Experimental

Experimental Set-up

A block diagram of the thermal-lens system using a conventional fluorescent cuvette is shown in Figure 4.5. The system was constructed on a 4 ft by 8 ft optical table.

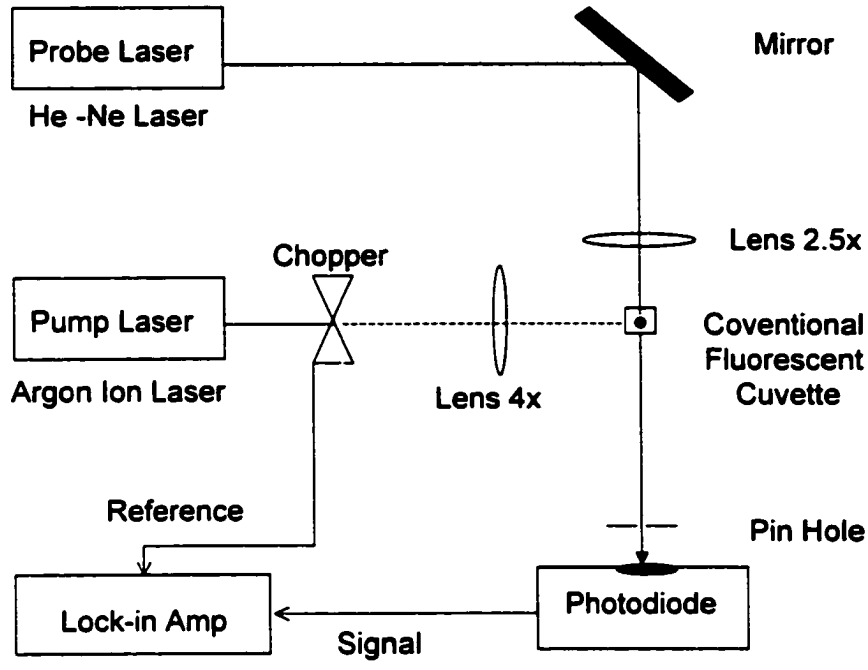

Figure 4.5: A block diagram of the experimental setup using conventional 1cm x 1cm x 3cm fluorescent cuvette. Rose Bengal is used to generate the thermal-lens signal which is then processed by a lock-in amplifier after recording with a photodiode.

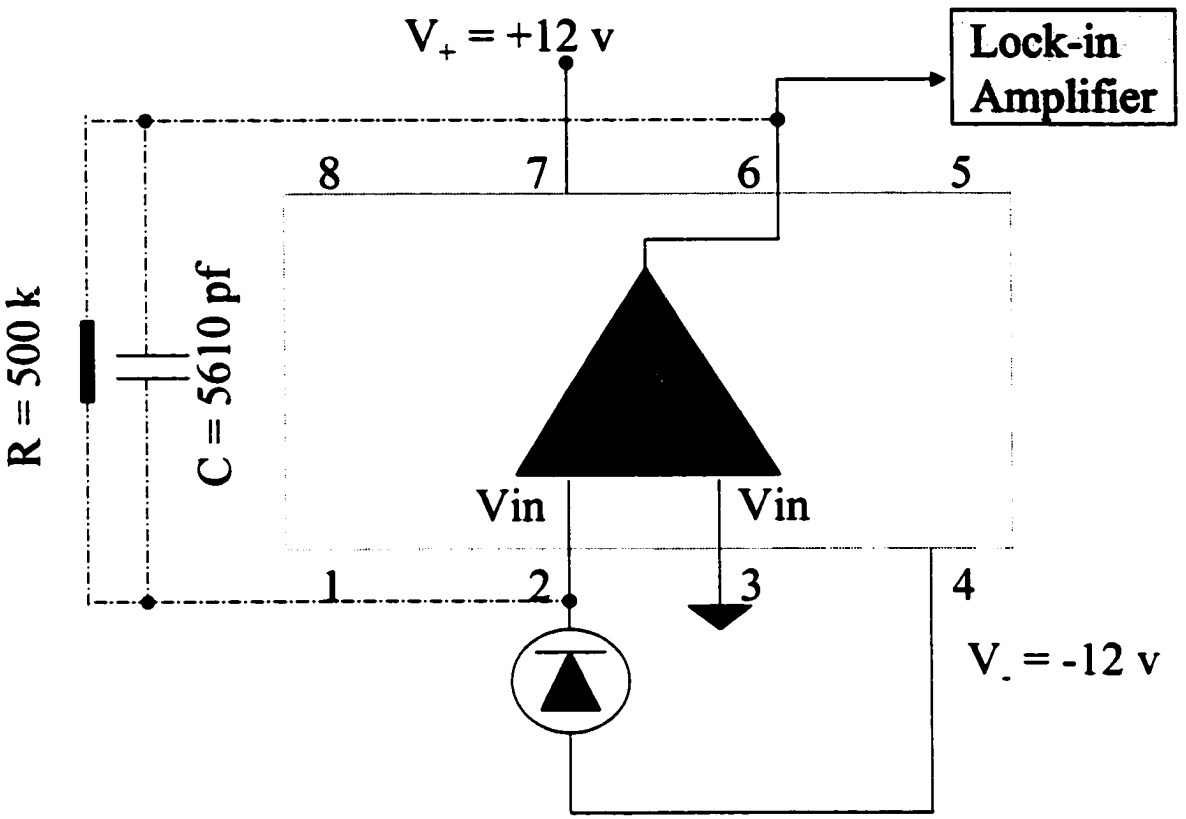

Figure 4.6: An electronic circuit for conditioning the output from the photodiode. The current-to-voltage converter is constructed from an operational amplifier Linear Devices OP07D, wired with a 500 kΩ feedback resistor in parallel with a 5610-pF capacitor. The signal was sent to a lock-in amplifier. Typically a 1 s or 300 ms lock-in time constant was used. The signal was maximized by adjusting the phase of amplifier.

A helium-neon laser produced a 1-mW, linearly polarized probe beam with a wavelength of 632.8 nm. A 2.5x microscope objective focused the probe beam to a waist before the sample. The probe beam spot size in the sample was about 1-2 mm. The 488 nm pump laser beam was modulated periodically in a symmetric square wave with a variable speed chopper and focused at a point near the center of the 1 cm x 1 cm x 3 cm conventional fluorescence cuvette. Perturbation of the refractive index in the heated region changed the intensity of the probe beam at right angle. The change in the probe beam after it had passed through at a right angle was detected 25 cm after the quartz cuvette with a 1-mm^2-silicon photodiode. The photodiode output was conditioned with an electronic circuit (Figure 4.6) and sent to a lock-in amplifier (PAR Model HR-8). The chopper wheel also provided the reference signal.

Reagents

All chemicals were reagent grade or better. A stock solution of 0.13 mM was prepared from rose bengal (4,5,6,7-tetrachloro-2',4',5',7'-tetraiodo-fluorescein, MW = 1017.6) in methanol. A series of rose bengal solutions in methanol was diluted from the stock solution before measurement. Solid sodium iodide (0.03 g/mL) was added to quench the fluorescence.

Alignment

A 10^{-4} M rose bengal solution was placed in the cuvette. The positions for the lens and mirror were adjusted independently by the translation stages. First, without turning on the pump laser, the mirror and the 2.5x lens were used to center the probe beam through the pinhole by maximizing the DC output of the signal detector. Then with the pump laser at 20 mW; the position of 4x lens and the reference frequency were

adjusted to maximize the lock-in signal. If the lenses were at the same height, only a small adjustment was necessary to get the optimized signals.

4.3.1.2 Results and Discussion

A photothermal absorbance signal is sensitive to the alignment of the pump and probe beams. The probe beam lens was moved along the beam path, which produced a corresponding change in the location of the probe beam waist. The photothermal signal was measured as a function of the lens position (Figure 4.7). It is found that the signal changed sign as the probe beam waist passed through the pump beam.

The nature of the calibration curve is an important property of any analytical technique. Under optimized alignment, a sequence of rose bengal solutions were studied in the methanol solvent with sodium iodide at concentration of 0.03 g/mL. As predicted, there was a linear relationship between the sample concentration and the thermal-lens signals (Figure 4.8), with a correlation coefficient of 0.9959.

Since the signal is produced in the localized volume defined by the cross region of the pump and probe beams, the path length is given by the pump laser beam spot size. For methanol as solvent, the measured detection limit is 1.3×10^{-7} M. The concentration detection limit for rose bengal reported here is comparable to the UV-VIS absorbance measurement by a conventional spectrometer. The result is of great interest because a low-power pump laser was used (about 20 mW) and it should be possible to improve the detection limit with higher power pump laser.

The photothermal absorbance signal is generated only in the intersection region of the pump and probe laser beams; refraction and fluorescence by other optical elements do

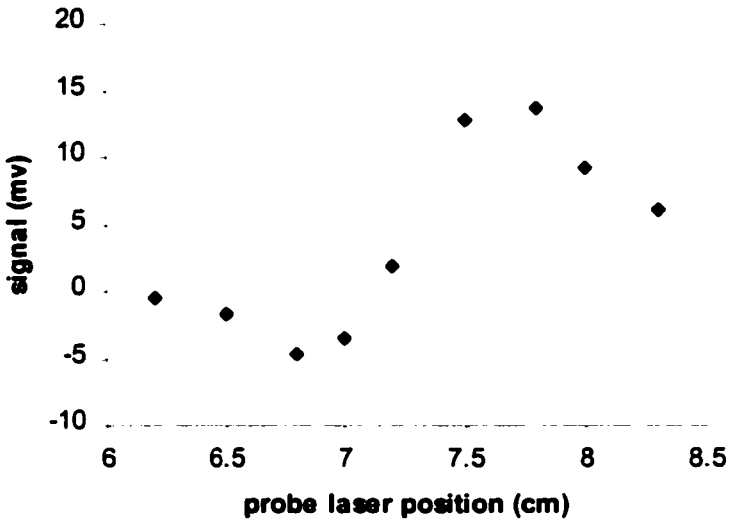

Figure 4.7: Position dependence of the probe laser-focusing lens. The abscissa is the distance of the cuvette to the 2.5x lens for probe beam. The power of pump laser was 20 mW. Chopper frequency was 35 Hz. Time constant for lock-in detection was 300 ms. The concentration of rose bengal was about 1 mM.

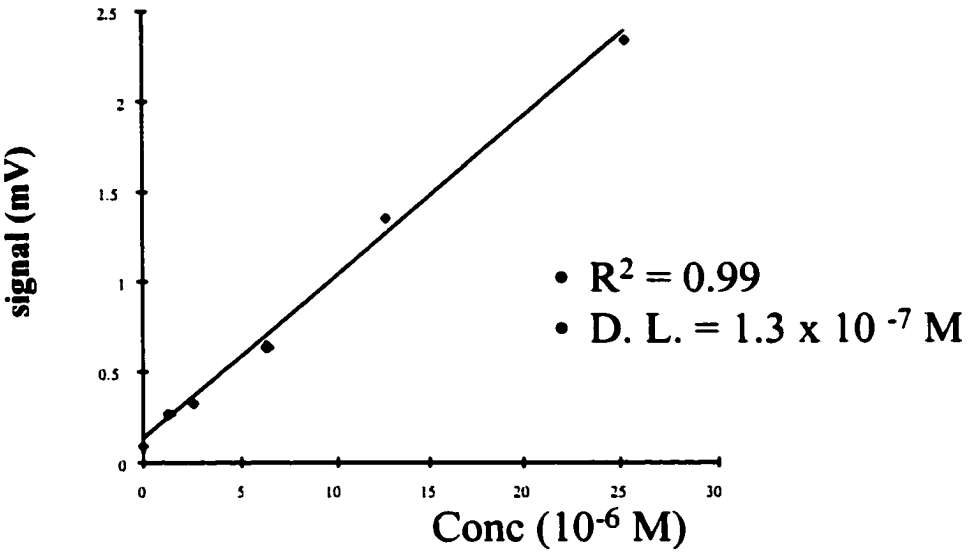

Figure 4.8: The linear relationship between rose bengal concentration and photothermal signal, with a correlation coefficient of 0.99 under optimized alignment. The chopper frequency was 29 Hz, and the power for pump laser was 20 mW. The detection limit for rose bengal under this condition is 1.3 x 10^{-7} M. All samples were prepared in methanol with sodium iodide at concentration of 0.03 g/mL

not contribute to the background signal. At low analyte concentrations, the background signal due to the solvent absorbance would produce a significant amount of noise.

In conclusion, this preliminary experiment provides the results of temperature rise produced by a chopped, Gaussian pump beam within a homogeneous and stationary sample. Water was replaced by methanol as solvent to generate stronger thermal-lens signals and sodium iodide was added to quence fluorescence.

4.3.2 Thermo-optical Detection with a Single-capillary Sheath-flow Cuvette in a Pressure-driven Flow Injection Experiment

4.3.2.1 Experimental

This investigation was studied using a single-capillary sheath-flow cuvette. A capillary with inner diameter of 50 μm (o.d. 184 μm) replaced the 1cm x 1 cm x 3 cm cuvette and rose bengal sample was pumped by a syringe at different flow rates. Epoxy was used in the connection between capillary and syringe. Methanol was used as the sheath flow.

Three axis translation stages were used to align the cuvette. First, with the probe beam blocked, the pump laser was focused on the capillary. Then the cuvette was translated to move the laser spot roughly 50 μm down the capillary tip. Secondly, with the probe laser on and the pump beam blocked, the detector was centered on the probe beam image. And after images of both the cuvette and the capillary were focused by moving the 2.5x lens back and forth along the beam, then the probe beam was adjusted down to cover the downstream area below the capillary. Finally, both the pump and

probe laser beams were turned on, and the positions for those two lasers were optimized by observing the signal from the lock-in amplifier.

4.3.2.2 Results and Discussion

A solution of 1.3 x 10^{-4} M rose bengal in methanol was used first, but I observed small particles, indicating that rose bengal precipitated at this concentration. Thus a 10 or 100-fold diluted sample with 3 or 0.3 mg/mL sodium iodide was used for most of the experiments.

In this experiment, the analyte moved downstream, absorbed the pump laser beam and produced localized heating. The flow of the sample can change the signal intensity dramatically [18]. The signal magnitude decreases with flow rates. Figure 4.9 is a plot of photothermal signal vs. the flow rate of sample passing through the capillary. The flow rate range was 0.001mL/min to 0.01mL/min, which corresponds to the flow rate of analytes during CE. The optimum lock-in amplifier phase shift was changed with sample flow rate; and the signals at certain flow rates were maximized by adjusting the phase with lock-in amplifier. There is a linear relationship between the thermal optical signal and the flow rate of samples, with a correlation coefficient of 0.98.

The flow rate of the sheath liquid also influences the thermal-lens signal. The dependence of signal on the relative height between the sheath flow buffer resevior and the waste resevior is shown in Figure 4.10. With the liquid level in waste bottle kept at the same height as the sample buffer, the position of the sheath flow bottle was changed. When the relative height between the sheath liquid source and the waste became greater,

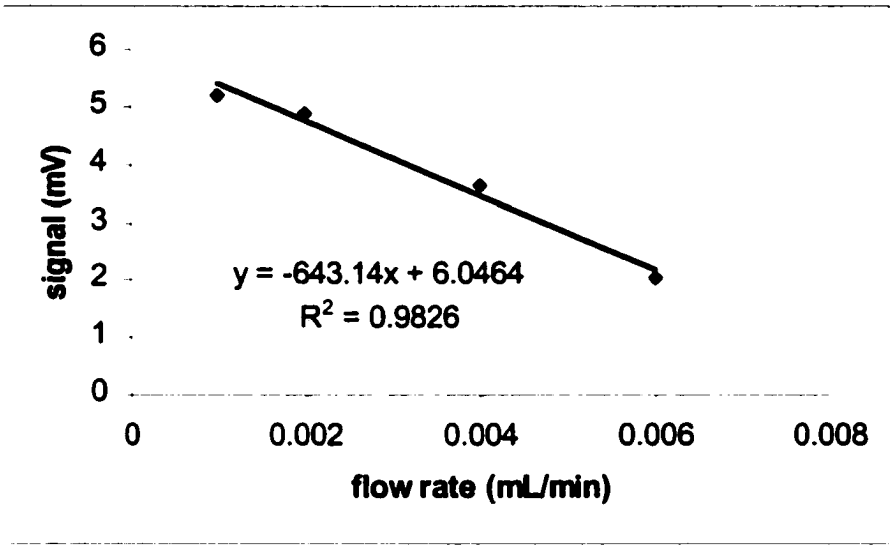

Figure 4.9: Plot of photothermal signal vs. the flow rate of sample passing through the capillary. 1.3 μM rose bengal was used and the chopper frequency was 22.8 Hz. The height for sheath liquid and waste were 15 cm and 4 cm respectively.

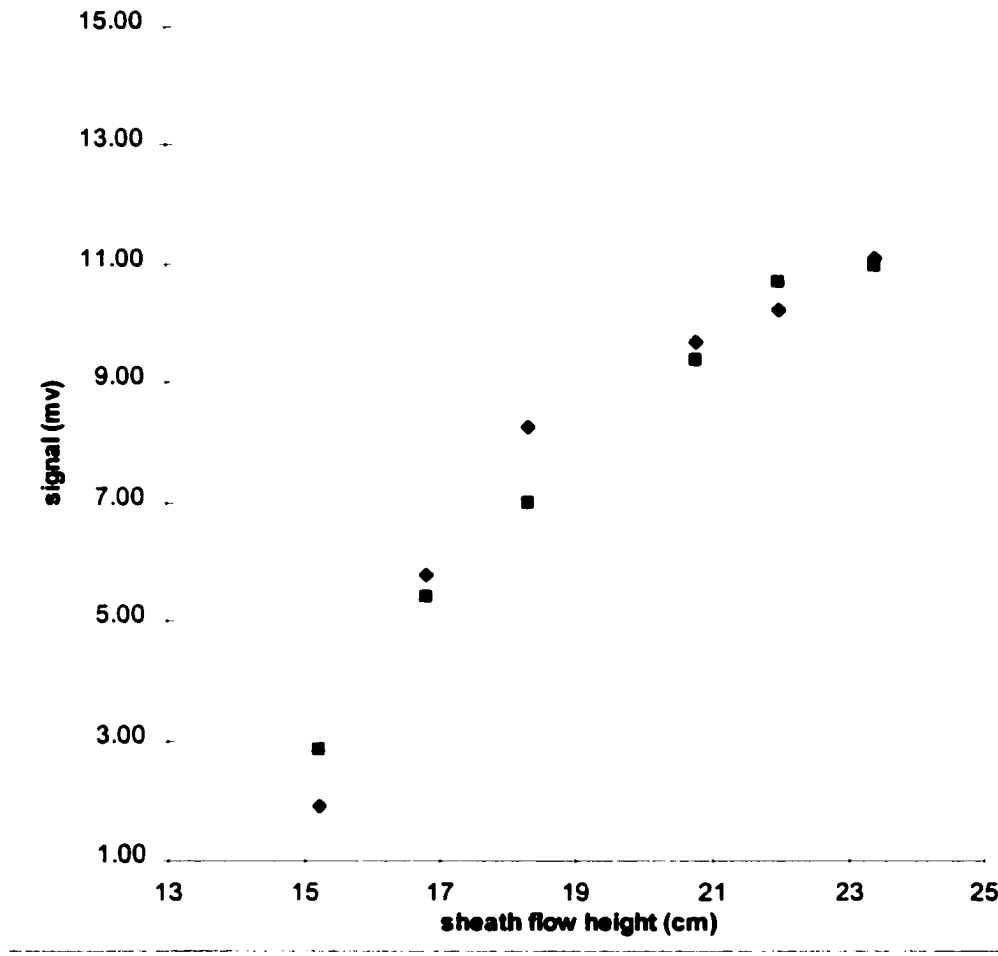

Figure 4.10: The dependence of signal on the height difference between the sheath liquid and the waste. The thermal optical signals were obtained with flushing 1.3 μM rose bengal (in methanol) at 0.002 mL/min. A 20 mW argon ion laser was modulated with the chopper wheel at 26 Hz frequency. Diamond series is the average signals at phase 0° and 90°, and square are the signals after adjusting the lock-in amplifier phase. The liquid level of waste was kept at 13 cm.

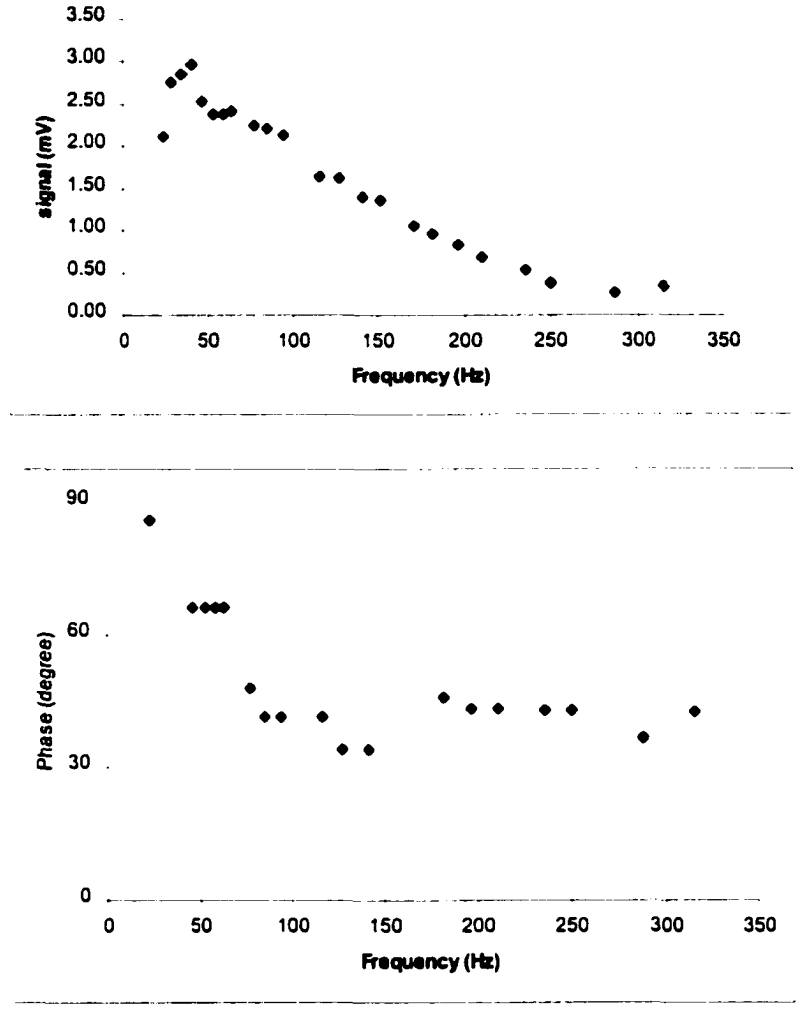

Figure 4.11: The frequency behavior of the photothermal absorbance signal. The top is frequency dependence and the bottom is the phase dependence. The signals intensity and phases were optimized every time after changing the frequency. A solution of 12.68 μM rose bengal in methanol was pumped through the capillary at the flow rate of 0.005 mL/min. The height difference between sheath liquid and waste was 1.5 cm.

in other words, when the sheath flow rate was increased, the thermal-lens signal increased. This was probably because more analyte migrated from the capillary with the faster sheath liquid, and therefore more molecules were excited by the pump laser to generate stronger signals.

The frequency behavior of the photothermal absorbance signal was observed by measuring the signal at a number of chopper wheel frequencies for a solution of 13 μM rose bengal in the methanol solvent pumped through the capillary at the flow rate of 0.005 mL/min (see Figure 4.11). At low modulation frequencies, the thermal lens approaches a steady state. At very high modulation frequencies, the thermal lens does not have a chance to form and the signal magnitude approaches zero. Therefore, in the following experiments, in order to obtain higher sensitivity, the frequency for the chopper wheel was always kept at a lower value, from 7 to 35 Hz.

4.3.3 Thermo-optical Detection with a Single-capillary Sheath-flow Cuvette in a Electrokinetic Flow Injection Experiment

4.3.3.1 Experimental

In contrast to section 4.3.2, this experiment was performed by applying high voltage across the length of a capillary instead of mechanically infusing the sample. A capillary with inner diameter of 50 μm (o. d. 140 μm) was used and 4-dimethylaminoazobenzene-4'-sulfonyl labeled glycine (DABSYL-Gly) was pumped by EOF under different electrical fields. The sheath fluid was always the same as the sample buffer. The aligning procedures were similar to the ones described in 4.3.2.

Reagents

100 mL stock solution of 6.0 mM DABSYL chloride (Sigma, St. Louse, USA) were prepared in acetone. Glycine was dissolved in 12.5 mM borate solution (pH = 9.0) to a concentration of about 60 mM. Both stock solutions were stored at 4°C in the refrigerator.

Methods

The derivatization of the glycine was performed with a standard procedure [22-23]. A 1 mL aliquot of DABSYL chloride was mixed with 0.5 mL glycine at 75°C in a water bath under gentle stirring until the solution turned from red to yellow-orange in color. Then the solution was evaporated to dryness and reconstituted with methanol. The derivatized DABSYL-GLY was stored at -10°C in a freezer and diluted in methanol before use.

4.3.3.2 Results and Discussion

Previously this group introduced a simple and sensitive method to determine dabsyl-amino acids with capillary zone electrophoresis with photothermal detection [12-14]. In the following part of this chapter, I used similar procedures to compare the new multi-capillary thermal-lens detector with the old technique. Therefore, the simplest amino acid, glycine, was chosen to start the experiment.

First of all, the frequency dependence of the photothermal absorbance signal was investigated by measuring the signal at a number of chopper wheel frequencies for a solution of 1 mM dabsylated glycine in methanol with a 400 V/cm electric field, see Figure 4.12 . It was observed that at lower modulation frequencies, the thermal lens

signal was maximized. This result is quite similar to the one in Figure 4.11; a lower modulation frequency results in higher sensitivity.

There is a linear relationship between the signal and the applied electrical potential in Figure 4.13, r = 0.994. At a high infusing rate, more sample elutes to form the thermal lens.

The sensitivity for thermo-optical techniques increases linearly with pump laser power, shown as Figure 4.14. The photothermal absorbance signal increased with laser power until the signal reached a plateau, which suggested photo bleaching occurred at higher pump powers.

With the optimized conditions, a calibration curve was constructed by running a series of DABSYL-glycine solutions of different concentrations under an electrical field of 400 V/cm, Figure 4.15. The detection limit was estimated by Knoll's method. For DABSYL labeled glycine, the detection limit (3σ) was 5.7×10^{-7} M, which is very close to the one this research group obtained with on-column detection and many orders of magnitude superior to those of conventional absorbance techniques for amino acid analysis in capillary electrophoresis [14, 25]. At the detection limit, within the roughly 1 pL intersection volume of the two laser beams, only 5.7×10^{-19} mole or 340,000 molecules of sample were present. At the pump laser wavelength of 488 nm, the molar absorptivity is 7560 L mol^{-1} cm^{-1} molar, and the pathlength can be assumed to be the capillary inner diameter (50 μm), therefore an absorbance detection limit of 2.1×10^{-5} was obtained.

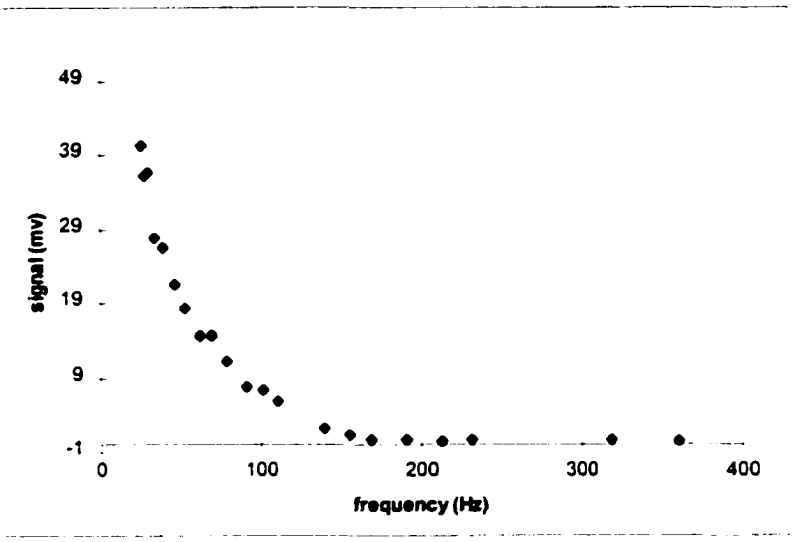

Figure 4.12: The frequency behavior of the photothermal absorbance signal. A solution of 1 mM DABSYL-glycine in methanol was running through a 65.5 cm length capillary at a 400 V/cm electric field. Sheath flow level was 16.5 cm, and waste was 15.0 cm.

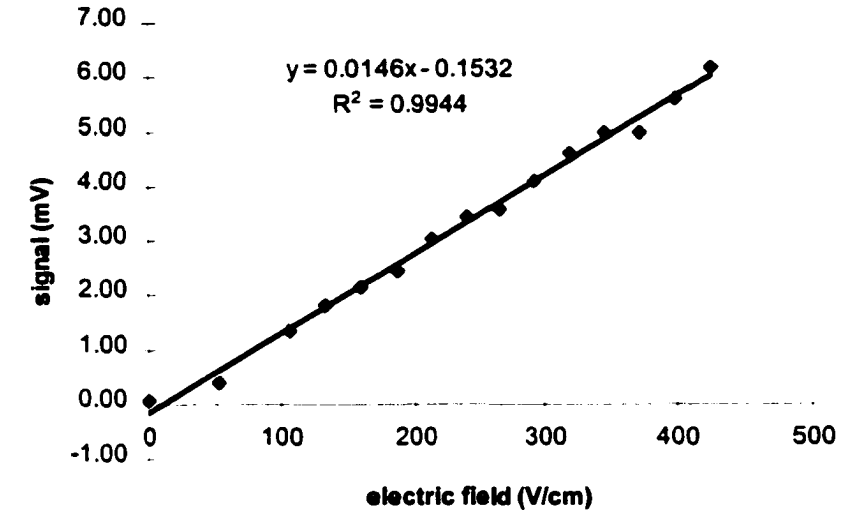

Figure 4.13: The effect of the running voltage on the photothermal absorbance signal (with phase adjustment). A solution of 1 mM DABSYL-glycine in methanol was running through a 68.0 cm length capillary at 0-425 v/cm voltages with the current of 0.0-29.0 μA. Chopper frequency was 26 Hz. Sheath flow level was 19.8 cm, and waste was 12.7 cm.

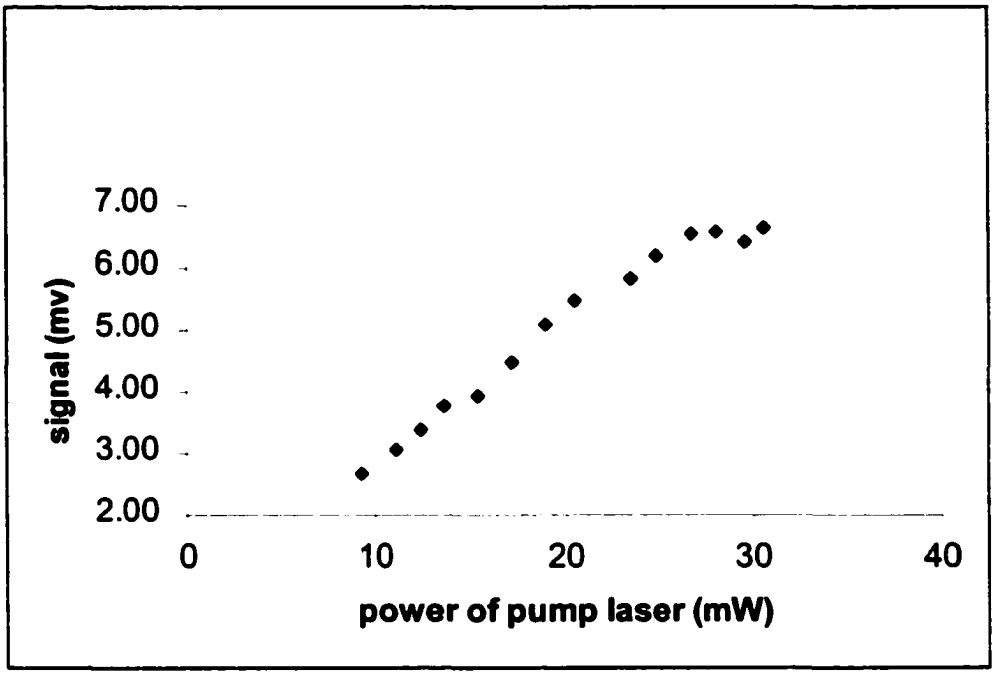

Figure 4.14: The effect of pump laser power on the photothermal absorbance signal (Signal = 0.2259 x + 0.6203, R^2 = 0.9901). A solution of 1 mM DABSYL-glycine in methanol was running through a 64.0 cm length capillary at 450 v/cm voltages with the current of 14.6 μA. Chopper frequency was 26 Hz. Sheath flow level was 17.2 cm, and waste was 12.3 cm.

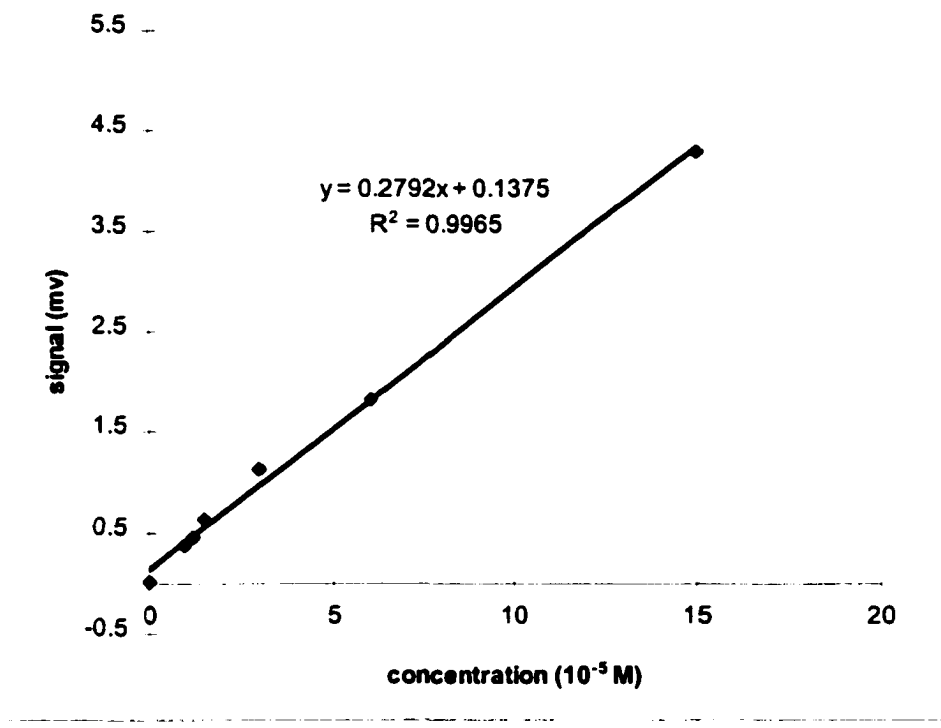

Figure 4.15: The linear relationship between sample concentration and photothermal signal with correlation coefficient of 0.9965. The chopper frequency was 36 Hz, and the power for pump laser was 40 mW. The detection limit under this condition was 5.7 x 10^{-7} M. A series of DABSYL-glycine solutions were continuously injected through a 68.0 cm length capillary at an electric field of 400 v/cm with 15.7 cm sheath flow level and 12.6 cm waste.

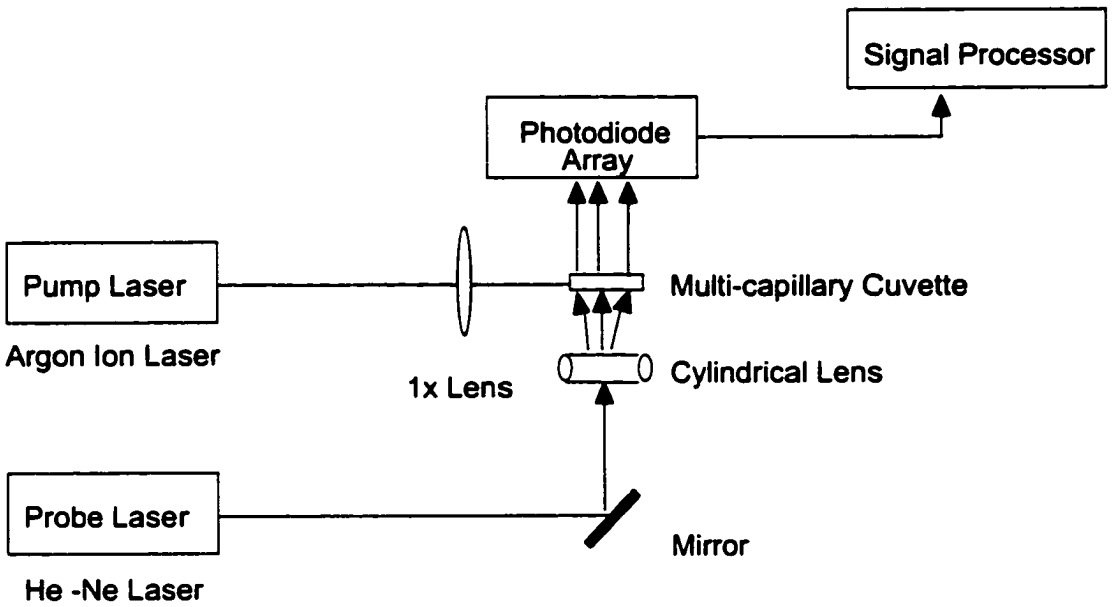

Figure 4.16: A block diagram of the experimental setup for multi-capillary thermal-optical absorbance detector. A computer processes the thermal-lens signal generated in the sheath flow cuvette after recording with a photodiode array.

4.4 Design of Multi-capillary Thermal-optical Absorbance Detector

4.4.1 Optical System

A block diagram for the instrument is shown in Figure 4.16. Instead of utilizing many probe beams and detectors, a single probe beam and detector were employed. The elliptically shaped probe beam intersects the pump beam within the cuvette. The probe beam passes through the heated regions and is imaged on a photodiode array, where each PDA element probes a different region within the cuvette. It was also noted that a 1 x microscope objective ($f = 73.5$ mm) could be used to focus the pump laser before the cuvette, as the beam spot size can then be kept to about 50 μm with a bit divergence.

4.4.2 Photographs of the Probe Beam Profile

The probe beam profile was imaged by placing a sheet of paper at the location of the photodiode array. Photographs were taken of the image using a 35-mm camera.

4.4.2.1 Experimental

Instrumentation

The lasers, sheath flow cuvette, and optical lenses were all attached to an optical table, and their positions could be finely adjusted by the 3-dimensional translation stages. Capillaries of 50-μm i.d. and 140-μm o.d. from Polymicro Technologies (Phoenix, AZ, USA) cut to a 45 cm length were mounted in the channels of the 16-capillary sheath flow

cuvette. At the injection end, the capillaries were bundled together to allow simultaneous sample and buffer introduction. In addition, a platinum wire used as an electrode was inserted in the same vial as the capillaries. A high-voltage dc power supply from Spellman (CA, USA) provided power for electrophoresis or a syringe pump provided pressure to infuse the sample through the capillaries. Sheath flow buffer, which was identical to the sample buffer in the capillaries, was provided by siphoning created by a height between the sheath reservoir and the waste container. A 20 mW argon ion laser beam (Uniphase, CA, USA) with 488 nm wavelength was directed through a 1x microscope objective (f = 73.5 mm, Melles Griot, CA, USA) at right angle to the probe beam, along the cuvette's long axis about 200 μm below the exit end of the capillaries. A He-Ne red laser beam (632.8 nm, 1 mW), expanded through a cylindrical lens, was used as the probe laser beam to cover the 4.8 mm cuvette window; and then recorded using a standard Nikon camera with a 2.5x microscope objective (Melles Griot, CA, USA) mounted in front of it.

Reagents

Fluorescein, DABSYL chloride and glycine were obtained from Sigma (St. Louis, MO, USA). DABSYL was dissolved in acetone to a concentration of about 10 mM and stored at 4 °C. The separation buffers consisted of a 1:1 mix of borate buffer and methanol. The concentration of borate buffer (BDH, Toronto, Canada) was 2 mM, with pH 9.2. 10^{-7} M fluorescein was prepared in the same borate buffer.

Methods

DABSYL-labeled glycine was prepared as described in Section 4.3.3.1. Briefly, 10 mM glycine stock solution was reacted with DABSYL chloride at 75 °C in a water bath until the solution turned from red to yellow-orange. Then the DABSYL-glycine was diluted to 5 mM with the running buffer before loading into the capillaries.

For the capillary electrophoresis experiments, the capillaries were first flushed with water and then 50% methanol/water for cleanup; later the separation buffer (1:1 borate buffer and methanol) was pumped into the capillaries electrokinetically. The injection end was immersed in a sample vial and the analyte was continuously infused at an electric field of 100 V/cm.

Alignment

With the probe laser beam blocked, 10^{-7} M fluorescein was electrokinetically pumped into the capillaries with an electrical field of 100 V/cm. Aided by a microscope, the position of the 1 x lens was finely adjusted to focus the pump laser about 200 μm underneath the capillaries and brightest fluorescent spots were achieved by moving the same lens. Then 5 mM DABSYL-glycine was introduced into the capillaries by the same running voltage. After the fluorescence disappeared, the 2.5 x objective for the probe beam was moved finely up and down or back and forth towards the cuvette to visually optimize the thermal lens signal projected onto a white background.

Data processing

The photographs were scanned by a scanner from Umax company with the software PhotoDeluxe (Adobe) after they were developed and saved as JPEG compressed files. These saved JEPG files were then processed with Igor Pro V 3.12 by summing intensities along the axis perpendicular to that of the spots. After the photograph was processed by the software, each spot on the image was measured by the relative extent of brightness over the background and the photo was transferred into a two dimensional plot, in which the y-axis stands for the relative intensity and the x-axis corresponds to the pixel position on the photodiode array.

4.4.2.2 Results and Discussion

Figure 4.17 is a photograph of the probe beam profile for the 16-capillary thermal-optical absorbance detector obtained with a 20 mW pump beam. All the capillaries were filled with DABSYL-glycine sample. 16 thermal lens spots can be seen in the image, each of which is produced by the sample coming from one capillary.

Figure 4.17 also shows the corresponding change in intensity measured by a 128-element photodiode array generated by software. The average number of pixels covered by one thermal lens is 7.9 (RSD = 13.9%), with a minimum of 6.2 pixels and a maximum of 10.6. From the image, there is no interference between the adjacent capillaries, and the background photothermal signal approaches zero between capillaries.

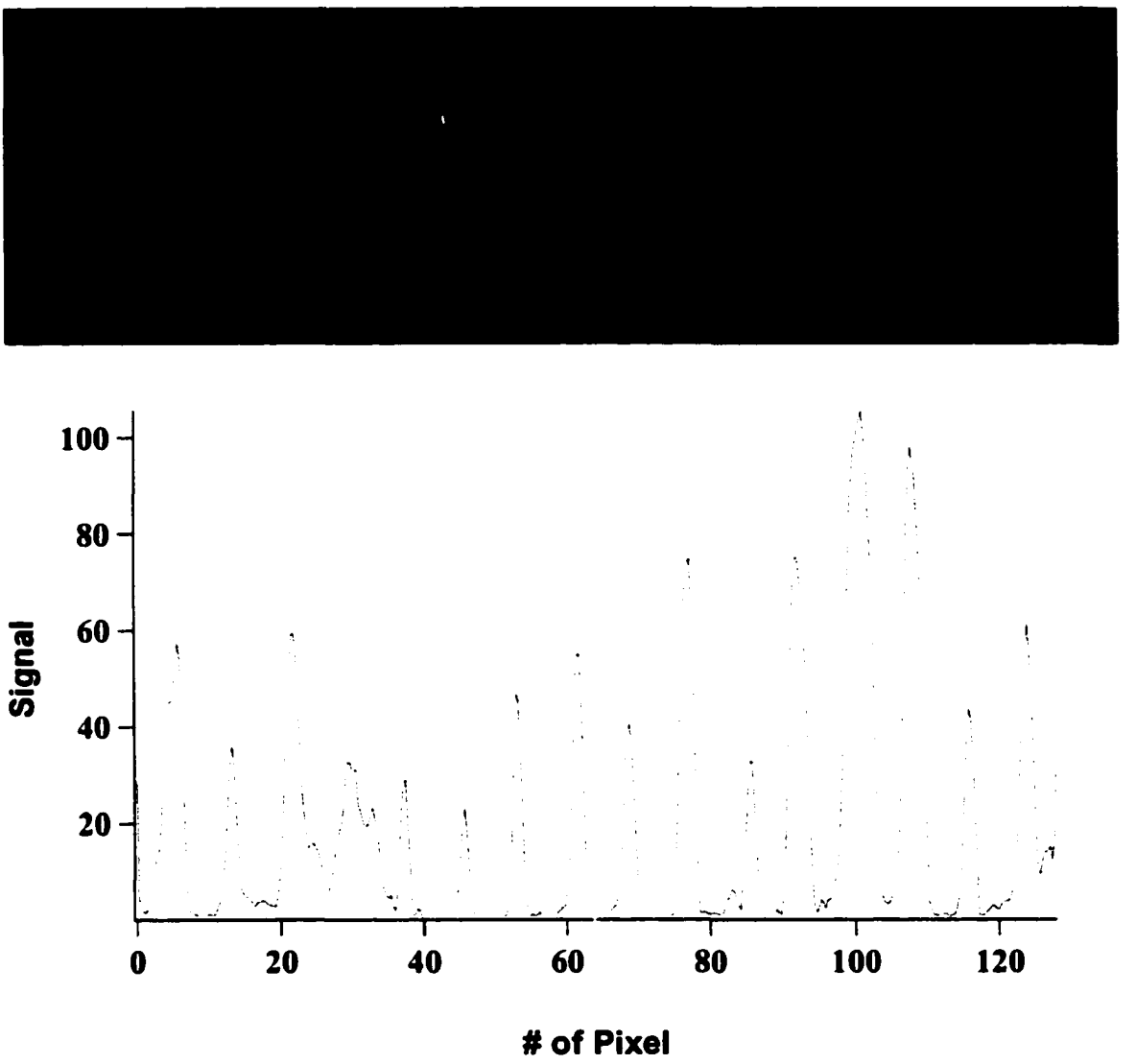

Figure 4.17: Images of thermal-lens signal from 16 capillaries. Top: Photograph of the probe beam profile for the 16-capillary thermal-optical absorbance detector obtained with a 20 mW pump beam. The shadows above the thermal lens are formed by capillaries. Bottom: the corresponding photodiode array profile. The pump laser beam was directed from the right to the left. All the capillaries were filled with DABSYL-glycine sample (1:1 water -methanol). The concentrations in the two capillaries on the right were 0.1 mM and the others were 0.75 mM. The sample flow rate was 10 μL/h.

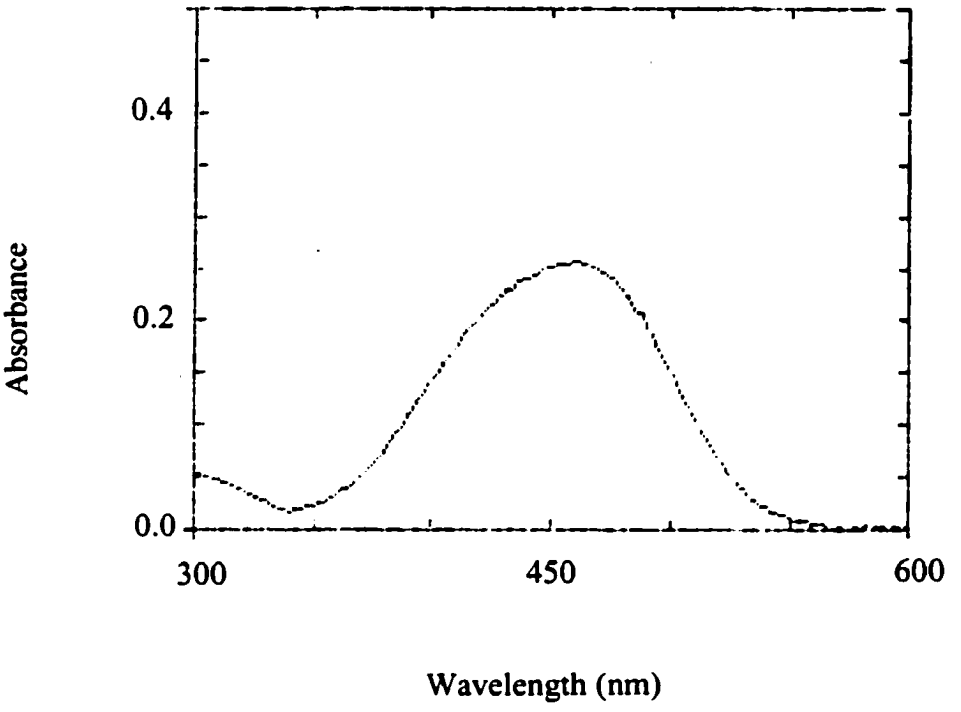

Figure 4.18: Absorbance spectrum of DABSYL-glycine (27.78 μM sample in 1:1 methanol/water in a 1-cm cell) in the range of 300-600 nm.

4.4.3 Attenuation of the Signals

In the design of a multi-capillary thermal-optical detector, the pump laser is directed beneath the array of capillaries, intersecting the sample streams. As shown in Figure 4.4, the pump laser beam passes through each of the sample streams. The geometry is particularly efficient because one pump laser beam is used to excite all of the sample streams simultaneously. This experimental geometry has proved to be very successful in fluorescence detectors based on a linear capillary array because usually in fluorescence detection, sample concentrations are quite low.

In the absorbance experiments, the concentration of analyte will be much higher compared to fluorescence. In Figure 4.17, each time the pump laser passes a sample stream, the sample absorbs energy from the pump laser. According to Beer's law, the intensity of pump laser decreases, which decreases the photothermal signal for the next sample stream.

4.4.3.1 Experimental

The experiment was investigated with a UV-Vis spectrophotometer (8451A, Diode Array Spectrophotometer, Hewlett Packard). 27.78 μM DABSYL-glycine (in 50:50 methanol water) was put in a 1-cm cell and absorbance spectrum was obtained from the range of 300-600 nm, Figure 4.18.

4.4.3.2 Results and Discussion

The molar absorptivity of DABSYL-glycine at 488 nm was measured to be 7560 $cm^{-1} M^{-1}$. Assuming the pathlength for a single sample stream is the inner diameter of a capillary, the absorbance of the pump beam passing through the 16 sample streams is given by

$$A = \log (I_0/ I) = (7560\ cm^{-1} M^{-1}) \times 16 \times (50 \times 10^{-4}\ cm) \times C_{sample} = (604.8)\ M^{-1} C_{sample}$$

The following lists the ratios of the transmitted to the original intensity of the pump laser beam for different concentrations:

$c = 5.0$ mM $\quad I / I_0 = 10^{-3}$;

$c = 1.0$ mM $\quad I / I_0 = 0.25$;

$c = 0.75$ mM $\quad I / I_0 = 0.35$;

$c = 0.50$ mM $\quad I / I_0 = 0.50$;

$c = 0.10$ mM $\quad I / I_0 = 0.87$.

Therefore, for lower concentration samples, the thermal lens signals from the first and the 16^{th} capillary are similar and the attenuation of the pump beam in passing through the 16 sample streams is less significant.

4.4.4 Array Detection System

A photodiode array (PDA) was used as a spatial imaging absorption detector, where light transmitted through the entire width of the flow stream within the cuvette was recorded simultaneously across the linear array. The probe beam was first expanded through a cylindrical lens to cover the sheath flow cuvette and then a 2.5x microscope objective was employed to image the beam onto a photodiode array that had a width of

6.4 mm. The PDA detector (model S 3901) combined with a driver/amplifier circuit (C4070) and a timing pulse generator (C4091, all Hamamatsu, NJ, USA) were mounted in a light-tight metal box fixed on the optical table. The photodiode array contains 128 detector diodes, each of which is 50 μm in width and 2.5 mm in height. Different elements in the array are used to image different axial locations in the cuvette during the CE experiment. The PDA driver/amplifier circuit was interfaced to a PC computer via an analog to digital sampling card.

4.4.5 Data Acquisition

A 12-bit data acquisition board (NI-DAQ 6023E) from National Instruments (TX, USA) was used to interface the PDA circuits and a PC computer (433-MHz Intel Celeron CPU). This multifunction E-series board can acquire analog inputs at a maximum rate of 200 kilosamples per second. The computer operating system was Windows NT Workstation 4.0, all of our codes used to operate the PDA and to acquire the data were written using LabWindows CVI Version 5.0 software written by Mr. Gaya Kariyamasam (Appendix).

LabWindows/CVI, is a powerful interactive development environment based on the C programming language to create virtual instrumentation applications. It contains an editor for creating user interfaces, tools for automatic code generation, and a C language environment for building test, measurement, and automation applications.

The timing signals for the DAQ board can be generated by on board timing circuitry, software control or externally provided to connector pins on the board called

programmable function inputs (PFIs) on the multi-purpose board. A connection called PFI0/TRIG1 can be used to provide a signal from an external device to begin a data sampling scan. This scan is a series of samples, in this case 128, one for each PDA pixel. Alternatively, this pin can be used as an output, to monitor the start of a scan initiated under on-board timing or software control. A second pin, PFI2/CONVERT*, is used to input a signal to initiate each individual A/D conversion within a scan, or to monitor when these samplings have taken place. Some trials with the PFI2/CONVERT* outputting a timing signal to the PDA circuitry to clock the readout of each pixel were performed; however the external timing generator was usually used to produce this signal, and the result was input to both the PDA driver master clock and the PFI2/CONVERT* pin on the DAQ board.

From the results of preliminary experiments, in order to receive high sensitivity, the chopper wheel had to modulate the pump beam within the range of 6-50 Hz. The PDA can be scanned at a speed of 200 kilo-samples per second, so all 128 elements can be scanned within one millisecond.

Two different approaches were used to acquire and process the data. For initial data acquisition, the PDA scanning was synchronized with chopper wheel. The data was sampled once after the chopper wheel changed state, thus the chopper speed determined the sampling rate. The data acquisition system read one scan of 128 pixels when the chopper changed the "ON" or "OFF" state of the pump laser beam. A set of "ON" and a set of "OFF" signals obtained at roughly the same time were paired. The "OFF" was then subtracted from the "ON" to get the set of 128 "photo-thermal" signals. Noise was then suppressed by an exponentially decaying average:

avg (t) = C * data (t) + (1-c) * avg (t-1),

where c determined the decay rate (c=1 is no averaging, c=0 is no decay). The above design allows the PDA to have an integration time controlled by a fixed rate oscillator, insuring uniform integration times for the PDA to acquire a valid readout after the transition of the chopper wheel. However, the signal was obtained with too much noise, therefore an alternative method was applied (Figure 4.19).

The hardware and the software for this project has been developed with the invaluable assistance of Eric Carpenter and Gaya Kariyawasam of this group. The most important part of the data acquisition process is the interface of the computer with the PDA and the extraction of the change in the PDA signals with changes in the pump beam state (on/off).

As shown in Figure 4.19, the C4091 pulse generator provides an output pulse (master start) to tell the photodiode array to start each scan, and also sends a signal to the PFI0/TRIG1 pin on the DAQ board to indicate that the scan from the PDA is to be acquired. The C4091 also generates a master clock signal input to both the PDA and PFI2/CONVERT* pin on the DAQ board, allowing them to begin the transfer of the next pixel on the PDA through the A/D conversion. Since a master start pulse starts a new scan and reset of all 128 pixels, the charge accumulation due to light is proportional to the master start interval. Hence its frequency should be set as low as possible to get the maximum range without saturating the signal and to obtain the minimum noise. Since the signal recorded by PDA and computer inherits changes of the chopper wheel status, a discrete Fourier transform was then performed later to extract the signal.

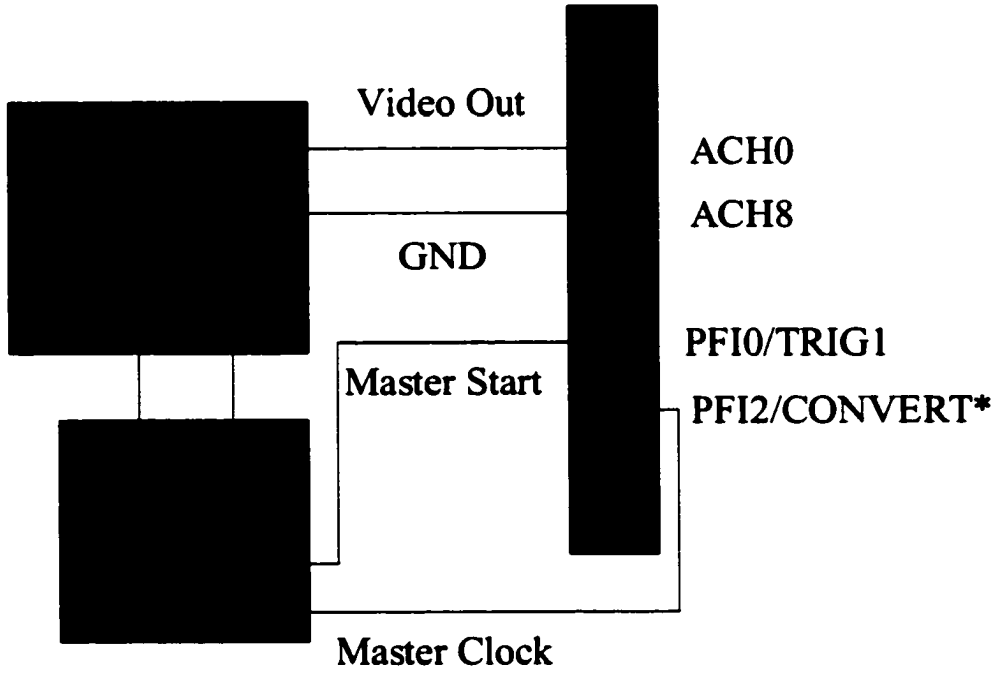

Figure 4.19: Wiring schematic for data acquisition.

4.4.6 Data Processing

Photographs of the thermal lens optical signal from the 16-capillary system were recorded before the detector was connected to a computer.

4.4.6.1 Experimental

Instrumentation

The lasers, sheath flow cuvette and lenses were all attached to an optical table, so that the optical paths could be finely adjusted. Two capillaries already mounted in the cuvette of 50 μm ID and 140 μm OD with a 40 cm length from Polymicro Technologies (Phoenix, AZ, USA) were chosen to perform the experiment. To one capillary (position #6) was applied a 25 kV high voltage; another capillary (position #9) was continuously pumped by a syringe at the rate of 10 μL/h. The sample in each was 5 mM DABSYL-labeled glycine in 50% H_2O-MeOH solution (0.2 mM borate). Siphoning with a height difference of 1 to 2 cm between the sheath fluid reservoir and the waste container provided a sheath flow, which had a content that was the same as the sample buffer in the capillaries. The pump laser power was 139.7 mW, and the chopper frequency was 7.5 Hz.

Data Acquisition and Analysis

Initially data were generated with a rate of approximately 7.5 Hz, which was identical to the pump beam frequency (the chopper wheel frequency). Signals for the

corresponding pixels of PDA were displayed on the user interface through the Lab Windows program. Microsoft Excel and Igor Pro V 3.12 were used to perform data analysis. Graphs produced in Igor Pro show intensities against the position on the photo diode array. The root-mean-squared (rms) noise in all of the images was obtained from a section of baseline of the same width near the peaks of interest.

The thermal lens signal is the difference between the two kinds of PDA signals, when the pump beam is "ON" and when it is "OFF". The sampled signals of two consecutive scans from PDA for pump laser "ON" and "OFF" were observed to almost overlap. In order to enhance the difference seen previously due to thermal-optical absorbance, the cumulative value of the difference between the "ON" and "OFF" signals over one hundred scans was averaged by computer processing. A discrete Fourier transform was made at the expected pump beam modulation frequency during the data processing (Figure 4.20). Figure 4.20 shows raw signals captured by photodiode array for one hundred consecutive scans. The thermal lens signals were generated by the DABSYL-glycine flowing within the two capillaries # 6 and # 9. From the display, we can see that there are two localized heated ranges centered at pixels # 31 and # 78 producing thermal-lens signals, one due to Capillary # 6, and the other from # 9. During 100 successive samples, some fluctuations are visible in the image data. Figure 4.20a shows some photodiode signals changed at approximately scans # 10, # 30, # 50, # 70 and # 90. Figure 4.20b shows that the thermal lens signals were observed at pixels # 31 and # 32; while pixels # 20 and # 40 provided the background signals. This effect was even more clearly demonstrated in 4.20c where the intensities and the differential intensities are shown against time on the photo diode array.

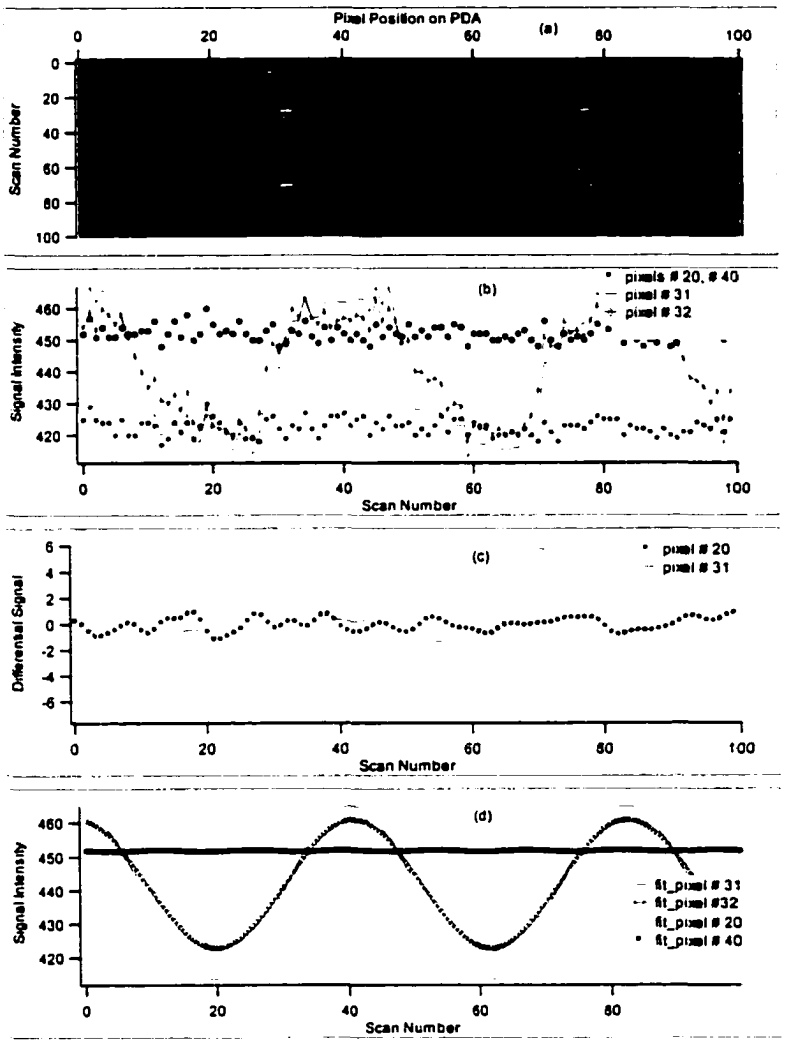

Figure 4.20: A discrete Fourier transform is used to process 100 consecutive scans of data. (a) Images captured by PDA for one hundred consecutive scans. (b) Signals recorded on pixels # 20, # 31, # 32 and # 40. The constant signals of background pixels # 20 and # 40 contrast strongly with the oscillation of pixels #31 and # 32 which image thermal lens spots. (c) Plot of columns from (a) for pixels #20 and 31. (d) Plots of sinusoidal functions fit against the curves plotted in (b). The strong amplitude of the signal from the thermal lens against those of the background pixels led to the decision for Fourier processing.

Then a Fourier transform is applied to the data processing at the corresponding frequency. To filter to a frequency of $f_{\_filter}$ (the chopper wheel frequency) while sampling at a scan frequency $f_{\_scan}$ with a data set scan(i) of 100 points (i = 0 to 99), we define:

$$A = \sum_{i=0}^{99} \text{scan}(i) \sin(\pi i /99) \sin(2\pi i f_{filter});$$

$$B = \sum_{i=0}^{99} \text{scan}(i) \sin(\pi i /99) \cos(2\pi i f_{filter});$$

The sin (π i /99) part is a windowing function that helps to suppress artifacts of the finite Fourier transform, and we chose it because it was simple to implement. Then a measure of the intensity of the oscillation of the signal at $f_{\_filter}$ is

$$S = \text{sqrt}\,(A^2 + B^2)$$

By the above formulas, this process was repeated 128 times, once for each pixel. When the Fourier processing was used, a sequence of 100 consecutive scans from the PDA were recorded once a second. These were then processed to produce 128 photo-thermal signals (one per pixel) that were taken to be the signal strength for that second. The results of the Fourier processing are analogous to fitting a sinusoidal curve against the 100 scans and taking its amplitude as the signal. The transforming effect is shown in detail with Figure 4.20d demonstrating the result of signals after treatment by the Fourier processing on pixels #20, #31, #32 and #40. A software program based on the Fourier processing was designed to manipulate the signals from one hundred consecutive

samplings before being saved to disk or displayed for the operator and was used for thefollowing experiments.

4.4.7 Effect of Frequency

The frequency behavior of the photothermal absorbance in the multiplexed capillary system has been explored with similar experimental protocols to those developed in section 4.4.6. A solution of 1 mM DABSYL labeled glycine was infused at the rate of 40 μL/h while the height difference between the sheath liquid and the waste solution was 4 cm. Three pixels (pixel # 119, # 120 and # 121) out of the 128 elements on the PDA were used to measure a single thermal lens signal, and the dependence of this thermo-optical signal on the frequency of the pump beam strobing within the multi-capillary system is plotted in Figure 4.21. The experimental results are similar to the ones in Section 4.3.2.2 and 4.3.3.2; all of them demonstrate that the thermal lens signal is highest at a lower frequency (about 10 Hz) and falls to lower levels with higher frequencies. It was also noted that the signal-to-noise ratios have the same response as the signals at each pixel. Thus the frequency was always set to about 10 Hz during the following experiments.

4.4.8 Images of Thermal Lens Signal on PDA

4.4.8.1 Experimental

Instrumentation

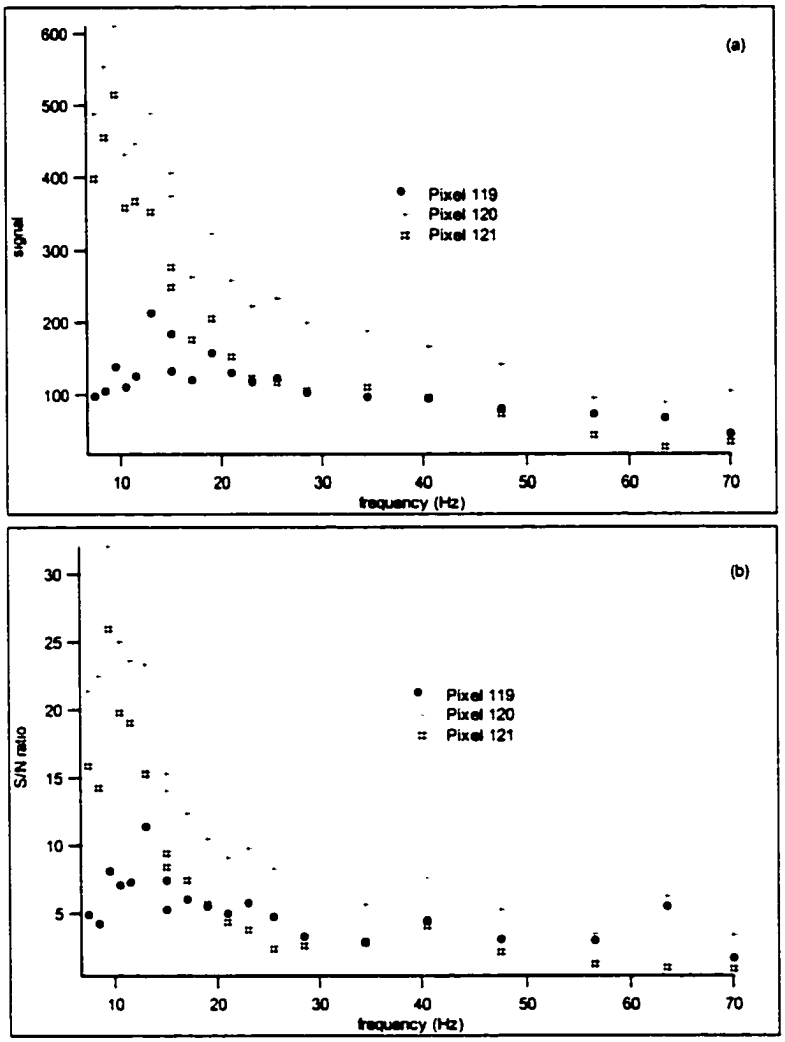

Figure 4.21: The dependence of thermal optical signal on frequency. Three pixels were used to represent one thermal lens. (a) signal behavior. (b) S/N behavior. 1 mM DABSY-glycine was pumped at the rate of 40 μL/h. The height difference between sheath liquid and waste was 4 cm.

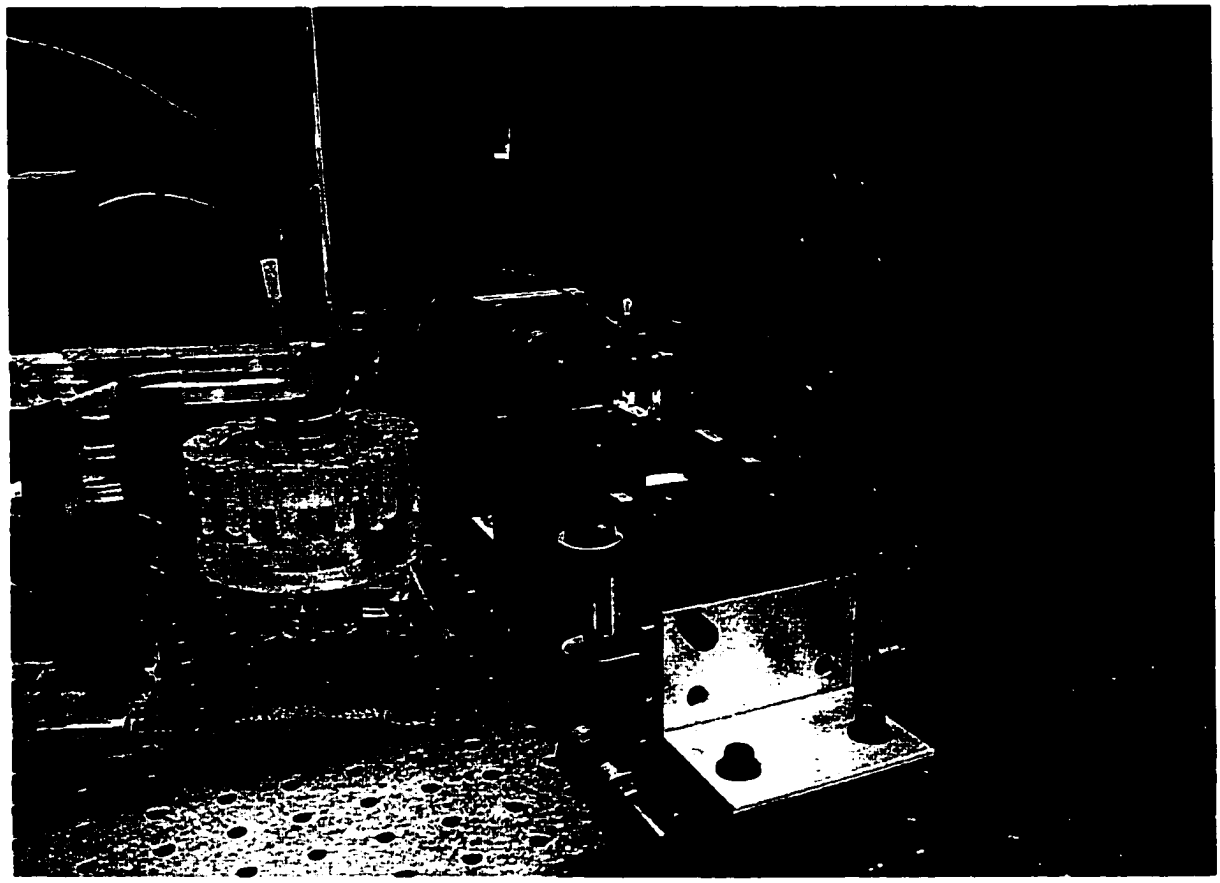

Figure 4.22: Photograph of the experimental setup. Center: 16-capillary sheath flow cuvette; left: injection stand; extreme left: probe laser beam; back: pump laser; right: photodiode array detector with interfaced circuit.

Figure 4.22 shows the experimental setup. Compared with the experiments in 4.4.2, the optical camera was replaced by a Hamamatsu photodiode array. The PDA detector was used with a built-in driver/amplifier circuit interfaced to a PC computer via a data acquisition board. Along with the lasers, sheath flow cuvette and optical lenses, a box with the PDA and related circuitry mounted inside were all attached to an optical table and can be independently adjusted by 3-dimensional translation stages to vary the photothermal signal. Eight capillaries, 50-μm i.d. and 150-μm o.d. with 37.5-cm length were evenly mounted in the every other channel of 16-capillary sheath flow cuvette. At the injection end, the capillaries were bundled together for simultaneous introduction of sample. In addition, a platinum wire was inserted in the same vial as the capillaries to serve as electrode. Electric power was provided by a high-voltage dc power supply to infuse the sample through the capillaries. The power for argon ion laser was 140 mW and this beam was modulated in a symmetric square wave by a chopper wheel (Scitec Model 300) at speed of 9.5 Hz.

Reagents

200 μM DABSYL-glycine was prepared in a 1 mM borate buffer (50% methanol). The sheath flow had the same content as the sample buffer, and the height difference between the surfaces of sheath flow fluid and the waste liquid was 1 cm.

Methods

Two, four and five capillaries were first treated with water and then 50% methanol/water for cleanup; later the capillaries were filled with the separation buffer

(1:1 borate buffer and methanol) by electrical power. Finally the injection ends were immersed in a sample vial and the 200 μM analyte was electrokinetically flushed onto the capillaries at running voltages of 15, 20, and 25 kV, respectively.

Data Acquisition and Analysis

A very large amount of data was generated using the 128-pixel PDA detector with a data acquisition rate of 9.5 Hz. All the data were processed first to reduce their size, and the Fourier processing was therefore done before the data were written to the hard disk. Signals from up to 3 diodes of the PDA could be displayed in the Lab Windows program. Microsoft Excel and Igor Pro V 3.12 were used to perform data treatment and analysis. Many of the graphs produced in Igor Pro show intensities against the position in the photo diode array. The root-mean-squared (rms) noise in all of the images was obtained using a section of the same width of baseline near the peaks of interest.

4.4.8.2 Results and Discussion

The photograph of a single thermo-lens signal from 5 mM DABSYL-glycine (Figure 4.23) was obtained by the same procedure described in section 4.4.2 except sample was flushed under an electric potential of 550 V/cm into a single capillary whose length was 50 cm. From this typical picture, we can see the intensities across the whole active spot are not uniform. There is a dark round spot in the center with a thin bright ring around it. The dark spot area demonstrates circular symmetry and a Gaussian intensity profile. Therefore, the signal imaged on the PDA for a thermal lens after the

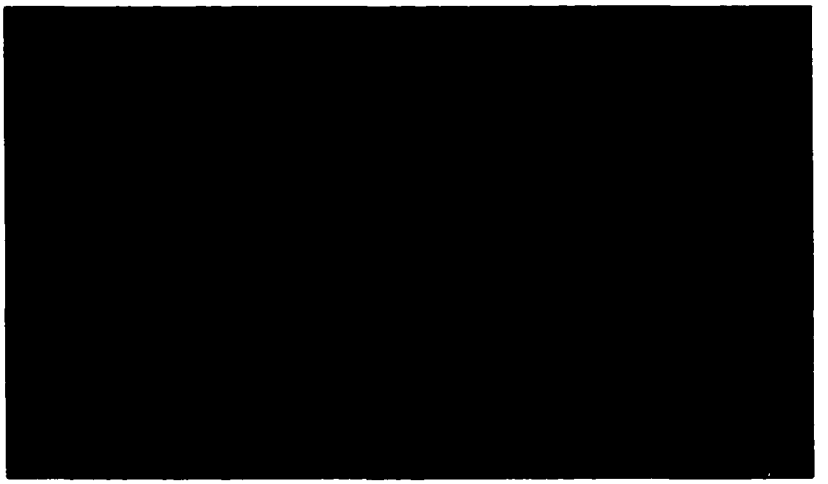

Figure 4.23: Image of single thermo-lens spot. The signal from 5 mM DABSYL-glycine was obtained by the same procedure described in Figure 4.17 except sample was continuously flushed under an electric field of 550 V into a single capillary whose length was 50 cm. The power of pump laser was 100 mW and the chopper frequency was 25 Hz.

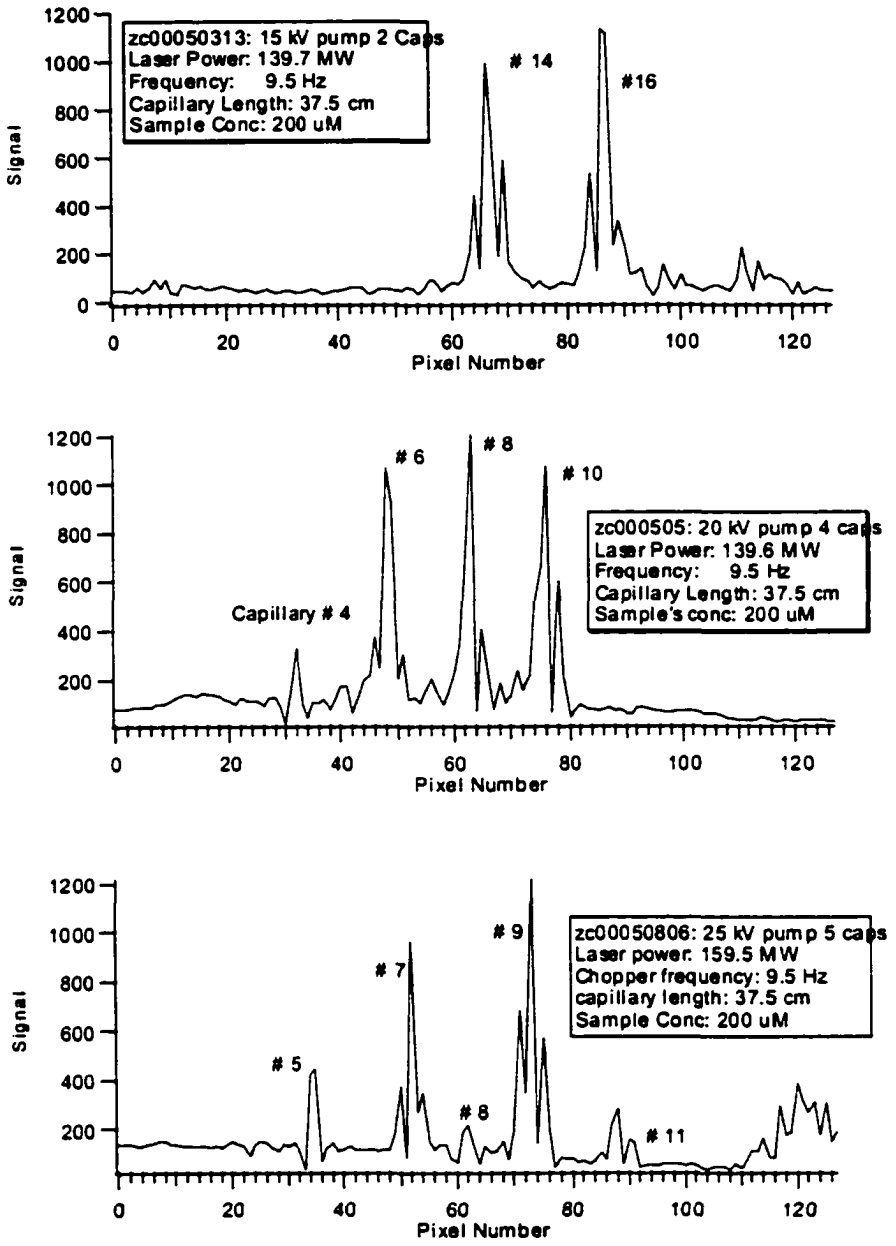

Figure 4.24: Signals from multiple capillaries on photodiode array. Two, four and five capillaries (37.5 cm long) were immersed in 200 μM DABSYL-glycine sample vial and the analyte was electrokinetically flushed onto the capillaries at running voltages of 15, 20, 25 kV, respectively. The power for pump laser was 139 mW and the chopper frequency was 9.5 Hz.

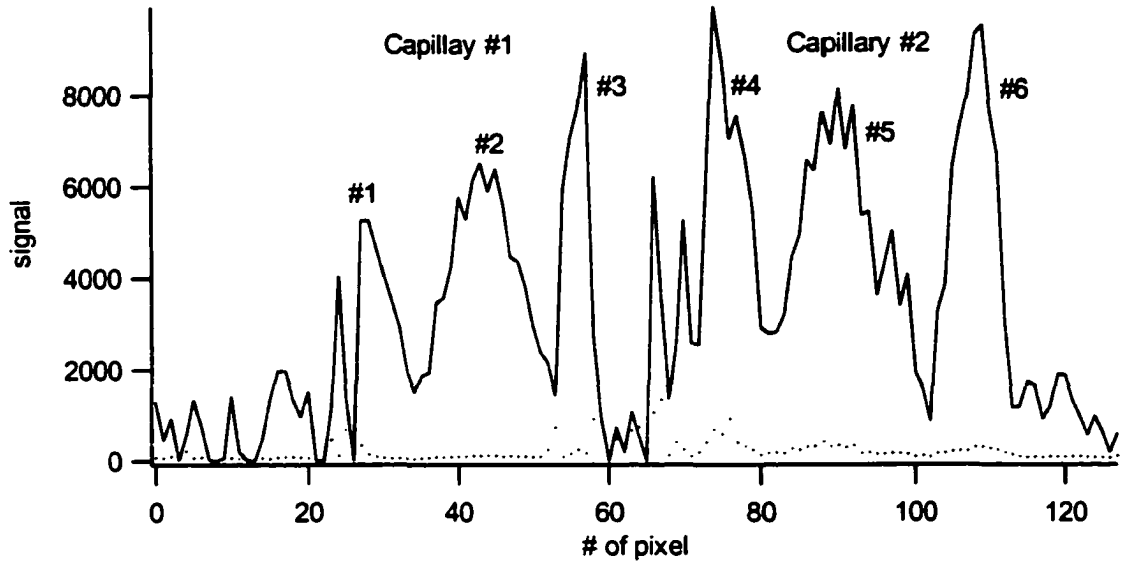

Figure 4.25 (a): Thermal lens signals from two capillaries. A cylindrical lens was placed between the cuvette and PDA to image two thermo-lens spots across the 128 elements of PDA detector. 500 μM DABSYL-glycine solutions in 1:1 (v/v) water:methanol solvent were pumped into capillary #1 and #2 at the rate of 20 μL/h with the sheath flow height of 13.8 cm and the waste liquid level of 11.0 cm. The chopper frequency was 8.5 Hz and the pump laser power was 139.7 MW. Peak #1, #2 and #3 are due to the capillary #1 while peak #4, #5 and #6 belong to capillary #2. The center peak #2 and #5 are the dominant peaks, and the diodes that represent those peaks can be used as the absorption detectors for the corresponding capillaries.

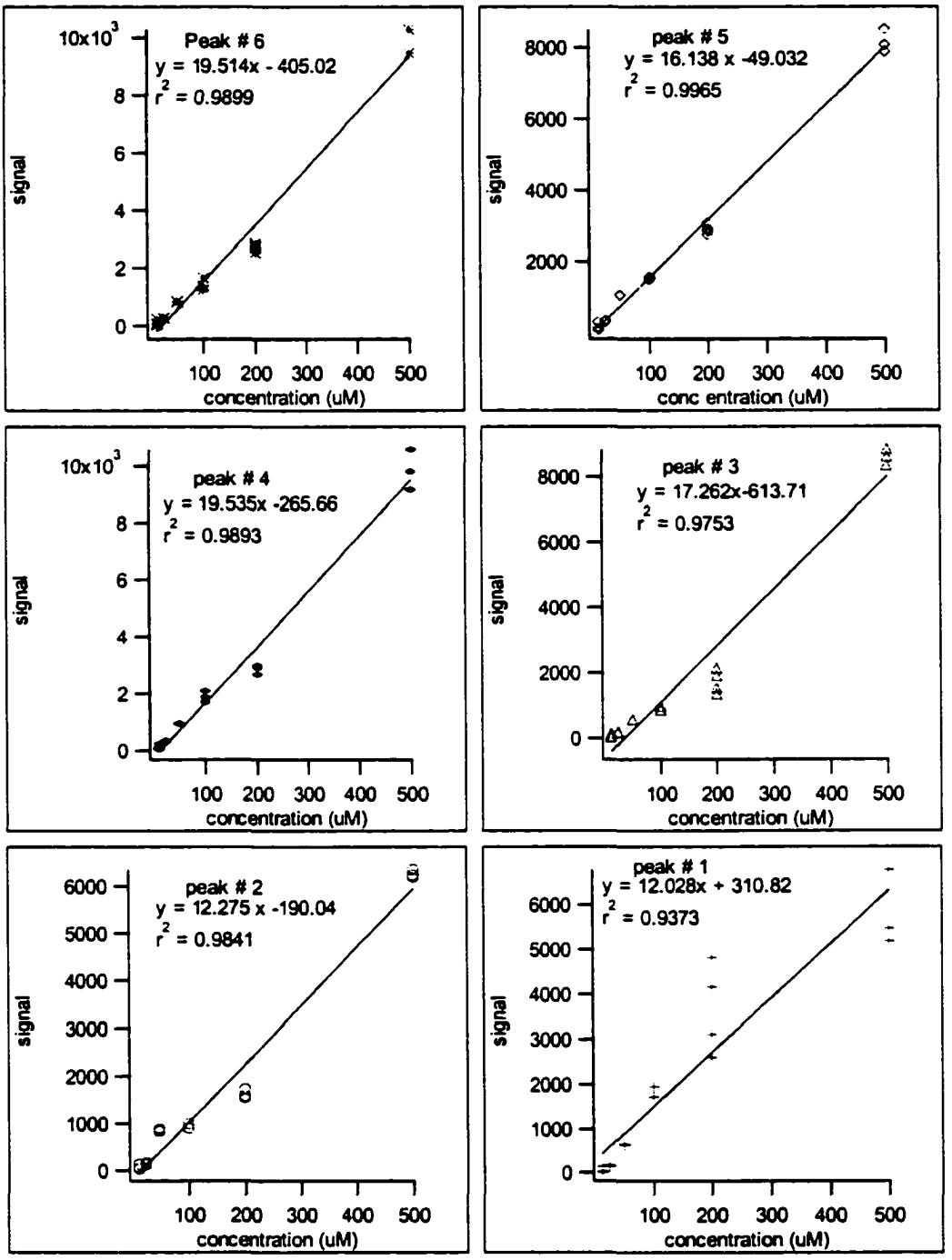

Figure 4.25 (b): Calibration curves for the peaks in Figure 4.25a. A series of DABSYL-glycine solution of concentrations of 12.5, 25.0, 50.0, 100, 200, 500 μM were used. Other conditions were the same as in Figure 4.25a.

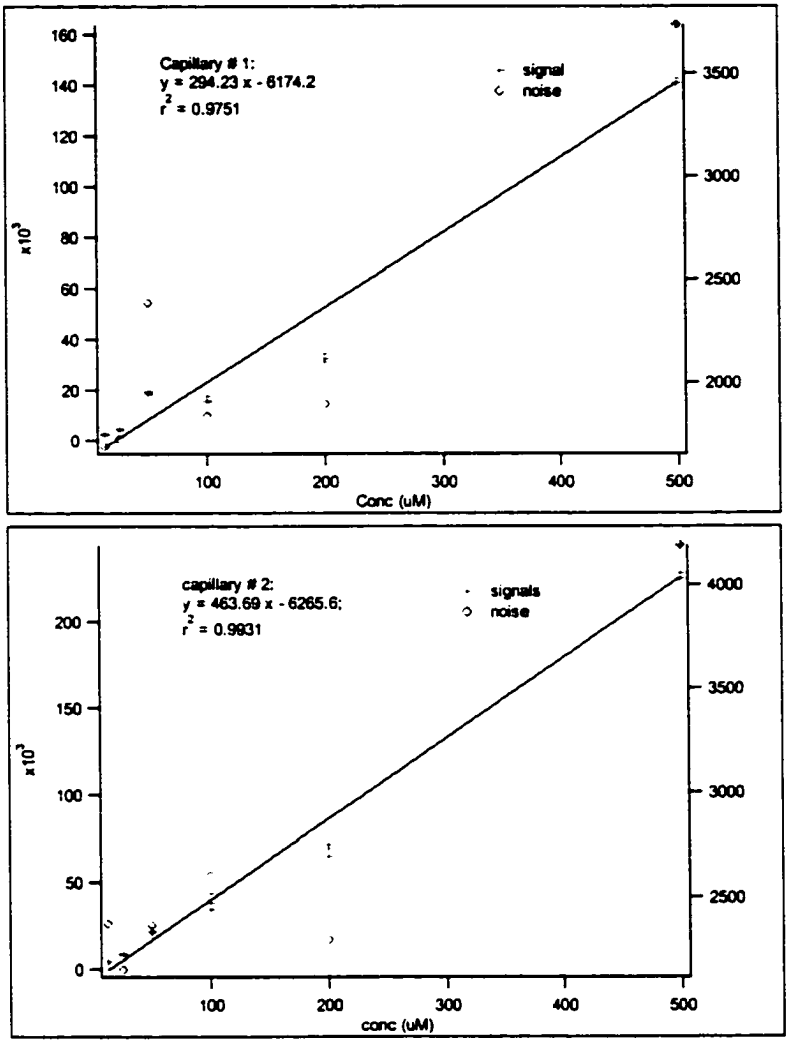

Figure 4.25 (c): Calibration curves for the integrated signals from two capillaries in Figure 4.25a. The right y-axis is for noise. Signal for capillary #1 is the sum of peaks #1, #2 and #3; while the sum of peaks #4, #5 and #6 is for capillary # 2. A series of DABSYL-glycine solution concentrations of 12.5, 25.0, 50.0, 100, 200, 500 μM were used. Other conditions were the same as in Figure 4.25a.

probe beam passes through a sample stream from a single capillary could be predicted as a dominantly Gaussian shape peak with two shoulders on each side.

Figure 4.24 shows the thermo-optical image from multiple capillaries on the photodiode array detector. The intensity was plotted against the position on the photodiode array. As expected, the image of every thermal lens corresponding to an individual capillary was generally shown as three peaks in the graph. The apex of the central peak among the three for one photothermal signal represents the center of each thermal lens. It was also found that normally there was a valley going down to the baseline between the signals from two adjacent capillaries. These regions corresponded the background between the two thermo-optical spots.

4.4.9 Detection of Thermal Lens Signal on PDA

4.4.9.1 Experimental

When the thermo-optical signal was imaged onto the PDA, the thermal lens signal could be expanded by properly changing the position of the optics. A cylindrical lens was placed between the cuvette and the photodiode array to image thermo-lens spots across a much bigger area than the whole PDA detector. The 128 elements of photodiode array were only used to display two thermal lenses from two adjacent capillaries.

In this experiment, a series of DABSYL-glycine solutions in 1:1 water:methanol solvent with concentrations of 12.5, 25.0, 50.0, 100, 200, 500 μM were pumped into capillaries #1 and #2 at the rate of 20 μL/h with a sheath flow height of 13.8 cm and a

waste liquid level of 11.0 cm. The chopper frequency was 8.5 Hz and the pump laser power was 139.7 MW.

4.4.9.2 Results and Discussion

Similar to the results in 4.4.7, Figure 4.25a presents the thermo-optical signals from two capillaries. Peaks #1, #2 and #3 are due to capillary #1 while peaks #4, #5 and #6 belong to capillary #2. The center peaks #2 and #5 are the dominant peaks, and the diodes that represent those peaks can be used as the absorption detectors for the corresponding capillaries.

However, from Figure 4.24, we also observe that the shoulders for the center peak can merge with the center peak or the baseline. From this, it is better to use peak height instead of peak area for quantitative analysis. Two kinds of calibration curves were obtained: 4.25b shows six calibration curves from the corresponding peak heights (#1 - #6) due to two thermo-optical signals, and 4.25c is from the integrated signal (height) of those two capillaries (capillary #1 is the sum of peak #1 - #3, capillary #2 is the sum of # 4 - #6). The good linear relationship between the signal intensity and the concentration indicates the feasibility and reliability of using the center peak as the representative for each thermo-lens signal.

4.4.10 Cross talk (Correlation) between Signals

There are two ways to minimize the cross talk between adjacent capillaries. One is to mount the capillaries spatially separated to reduce the interference between the

signals from adjacent capillaries. Another is to adjust the sheath flow to ensure the image for each individual signal receives minimal influence from its neighbors.

The cuvette used in the multiple capillary thermo-optical experiments has sixteen 150 μm channels for the capillaries and the space between each channel is 150 μm, which is the same as the outer diameter of the capillary. In the following experiments, the capillaries were always placed in every other channel in order to eliminate cross talk.

Using the same protocols as in 4.4.8, the first experiment was done by putting a cylindrical lens in front of the PDA and only imaging two thermo-lens spots across the whole PDA detector. Signals were obtained by lowering the height of sheath flow container.

As shown in Figure 4.26, peaks #1, #2 and #3 are from one capillary, and peaks #4, #5, #6 are for another capillary. During the experiments, it was found that with a decrease of sheath liquid height, the flow inside the cuvette was slower, and the images changed dramatically. Therefore, the flow rate of sheath buffer needs to be monitored carefully in order to obtain the stable signals and avoids cross talk between capillaries.

The second experiment was done to study the correlation of signals when the flow rates of the adjacent capillaries were changed. The signal was obtained on the PDA with the optical system is described in 4.4.7. The 100 mW pump laser was modulated with a chopper frequency of 9.5 Hz and the height difference between the sheath liquid and waste was 2.0 cm. Two capillaries, #4 and #5, were pumped with 200 μM DABSYL-labeled glycine at a flow rate of 3 μL/h and thermal lens signals were acquired 11 times during a 10-minute period. Then 50 μM DABSYL-glycine was introduced onto capillary

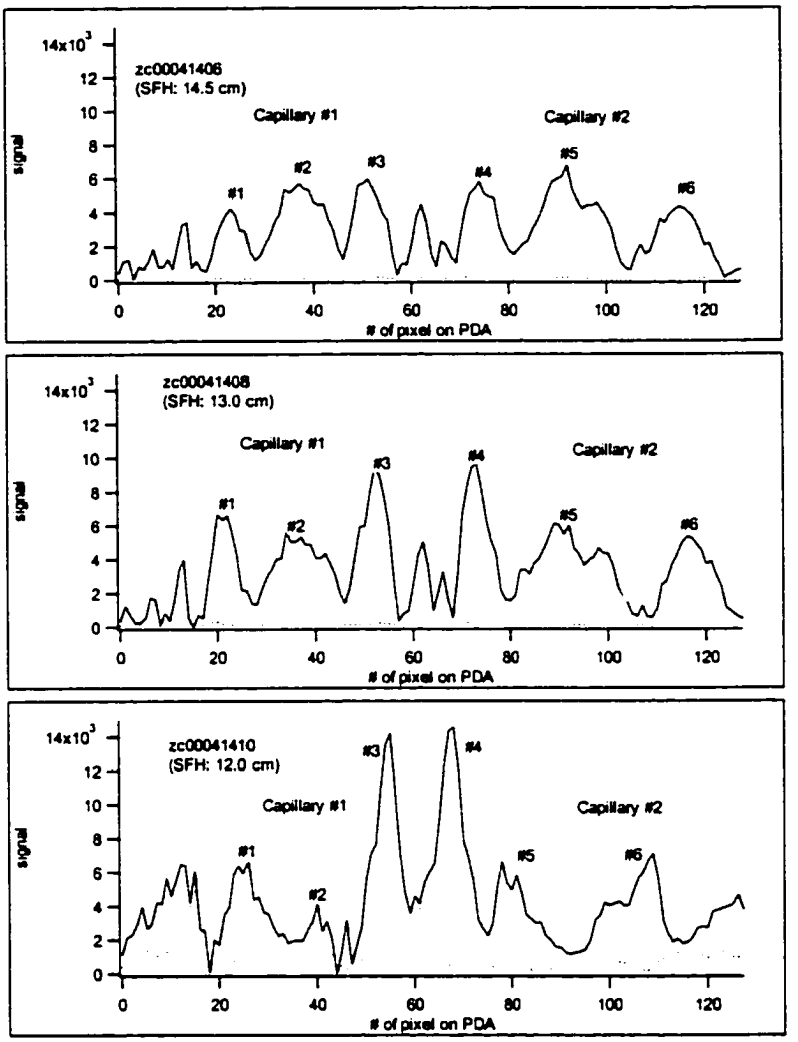

Figure 4.26: Crosstalk between two adjacent capillaries when decreasing the height difference between sheath flow and waste. SFH is the sheath flow height and the waste liquid level was 11.0 cm. Other conditions were the same as Figure 4.25a.

#2 with flow rate in a range of 0-96 μL/h while the infusion rate and concentration of sample in capillary #4 and #5 were unchanged.

Figure 4.27a shows the reproducibility of thermal lens signals on the PDA when the flow rates in the capillaries were fixed. The relative standard deviations (RSD) for photothermal signals with regard to position and intensity are 1.9%, and 7.6% for capillary #4 and 1.8%, and 16% for capillary # 5, respectively. Moreover, Figure 4.27b demonstrates the images of the thermal lens when the flow rate in the adjacent capillary #2 changed. From the signal in Figure 4.27c and the linearity in Figure 4.27d, it is concluded that there are no significant changes in the position and intensity of thermal optical signals from capillary #4 and #5 when the flow rate in capillary #2 was increased linearly.

4.4.11 Signal-to-Noise Considerations

A clear understanding of the noise sources for the signals is important because the noise level will determine the baseline level, the accuracy and the detection limit. As with any instrumental methods, both chemical and instrumental noise are encountered. Because the chemical components in the multiplex capillary system are exactly the same as the single capillary experiments, this section deals exclusively with noise that is generated in the various instrument components. Some noise from the PDA can be attributed to dark current noise, diode reset noise, and circuit noise, which are not dependent on the input light intensity. However, in real thermo-optical absorbance

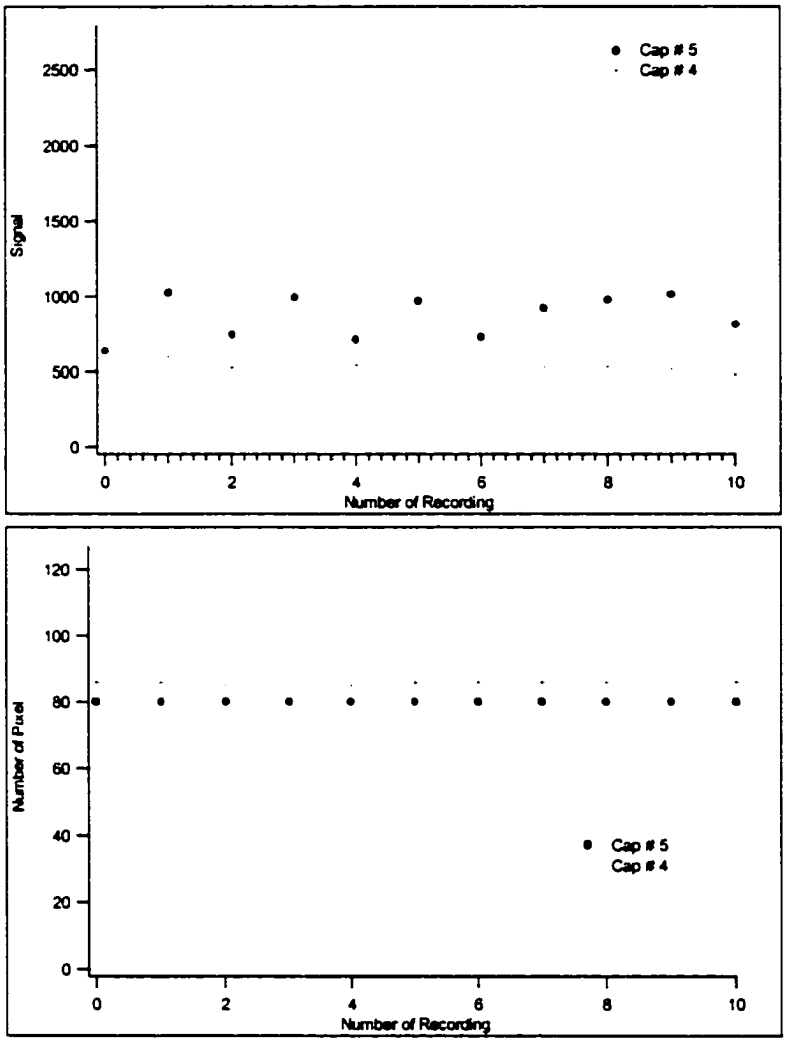

Figure 4.27 (a): The reproducibility of signals when the flow rates in capillaries are fixed. Capillaries #4 and #5 were pumped with 200 μM DABSYL labeled glycine at flow rate of 3 μL/h and thermal lens signal were acquired 11 times during 10 minutes. The power for the pump laser was 139 mW and the chopper frequency was 9.5 Hz.

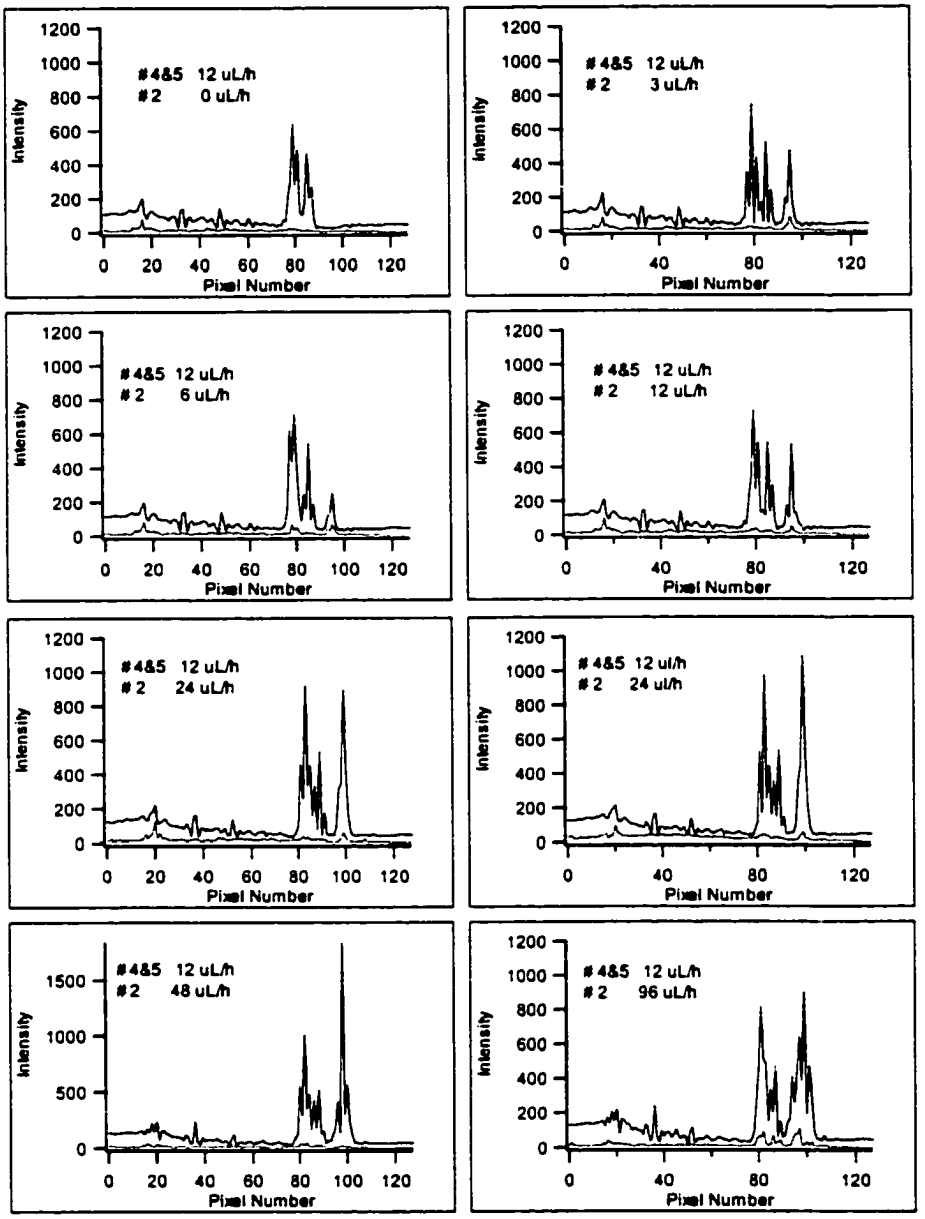

Figure 4.27 (b): The change of signal when increasing the flow rate in the adjacent capillaries. 50 μM DABSYL-glycine was introduced onto capillary #2 with a flow rate in the range of 0-96 μL/h while the infusion rate of the same concentration sample in capillary #4 and #5 was kept as 12 μL/h. The power for the pump laser was 139 mW and the chopper frequency was 9.5 Hz.

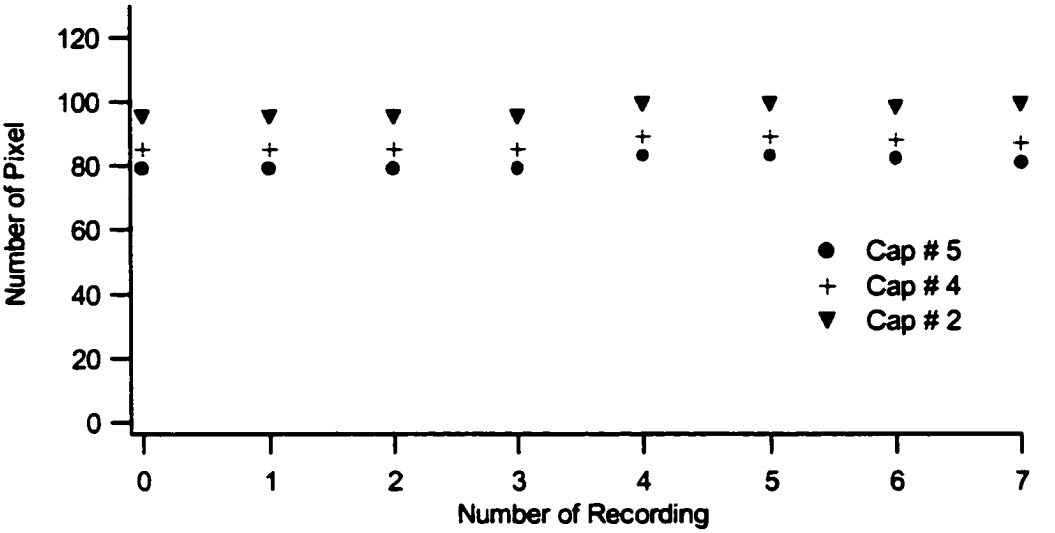

Figure 4.27 (c): The corresponding thermal lens position in Figure 4.27b when increasing the flow rate in capillaries # 2.

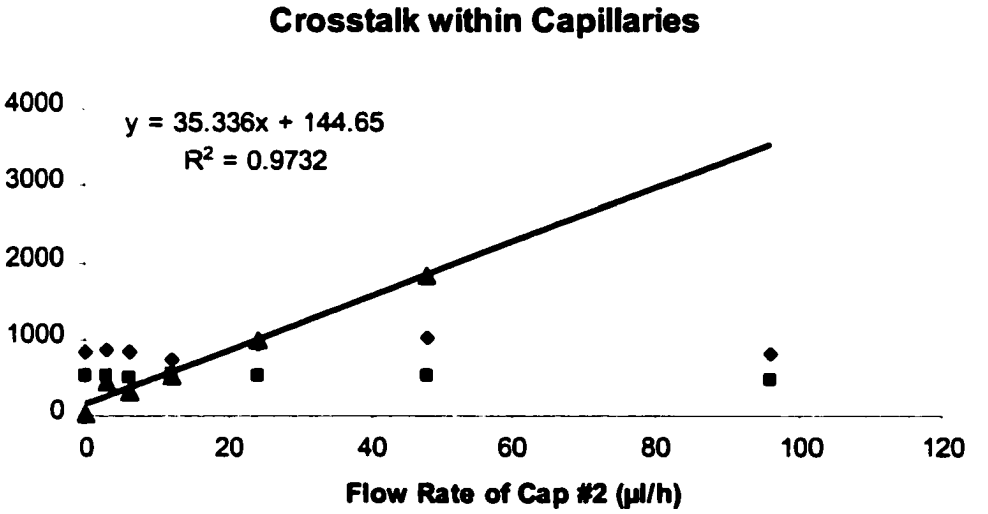

Figure 4.27 (d): The corresponding thermal lens signal intensity in Figure 4.27b when increasing the flow rate in capillary # 2.

detection, the baseline can drift due to some uncontrollable reasons, such as extra brightness of the image fringe, variation of pump laser intensity, fluctuation of the room light and also the uniformity of the probe laser beam. In order to enhance the signal from this type of noise, Fourier processing was performed to obtain the differential signal between the signals when the pump laser was on and blocked by the chopper blade. It is also noteworthy that the power lines cause noise at low frequencies; therefore the frequency of 60 Hz should be always avoided to reduce environmental noise.

4.5 Evaluation of Multi-capillary Thermal-optical Absorbance Detector

4.5.1 Detection Limit

The detection limits (LOD) for the multiple capillary thermal lens absorbance detector were determined for continuous injection and for CE. The results from continuous injection experiments provide information about the performance of the sheath flow cuvette and the PDA optical system; the one from the CE run evaluates the performance of the overall detection system, which contains both the separation conditions and optical system. The LOD of the CE system will be discussed later in Chapter 4.5.2.3.

In the design process, three optical systems were investigated with DABSYL-glycine continuously infused under an electric field of 300 V/cm, Figure 4.28. In the first optical system, a set of lenses was employed to expand the probe laser beam through the sheath flow cuvette. This probe beam illuminated the entire cuvette and a mirror

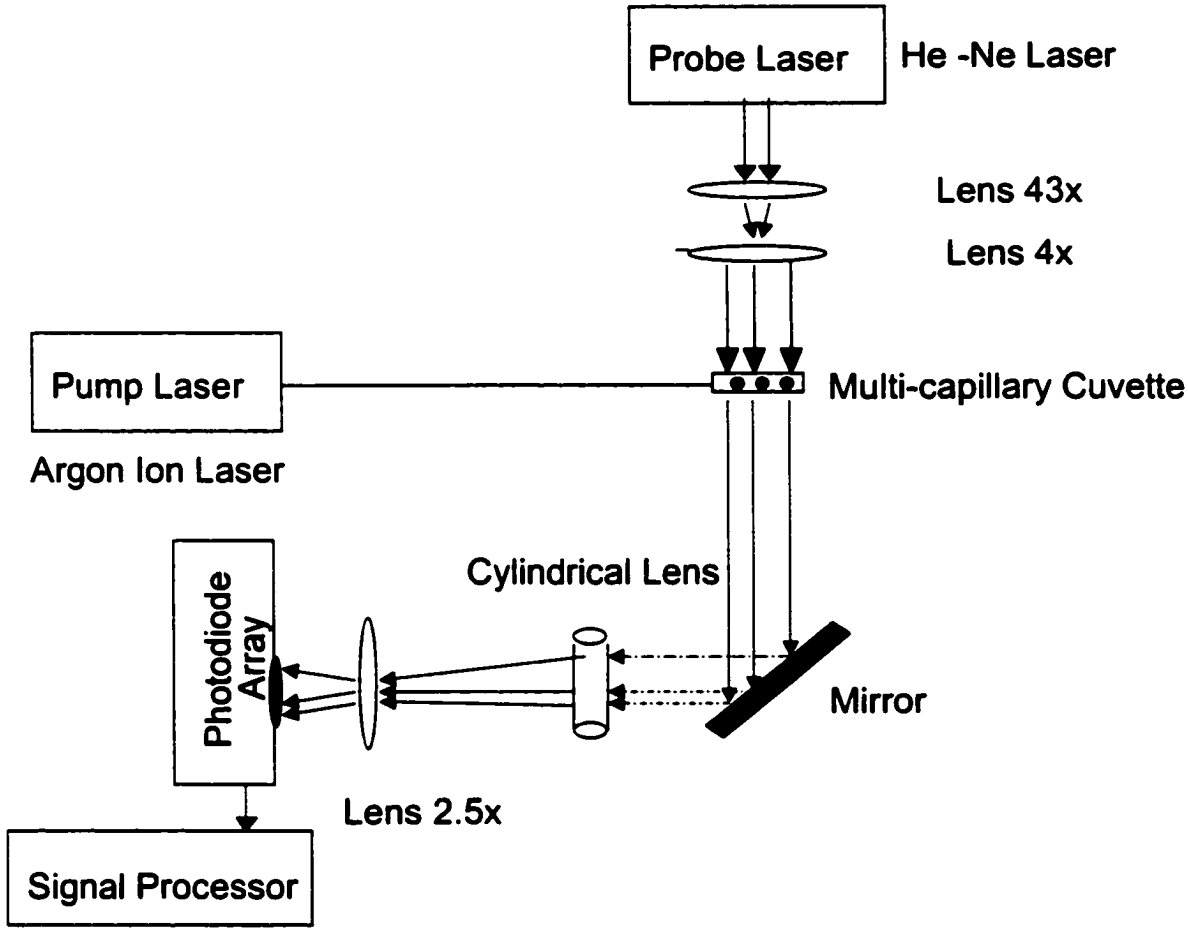

Figure 4.28 (a): A block diagram for the first optics arrangements.

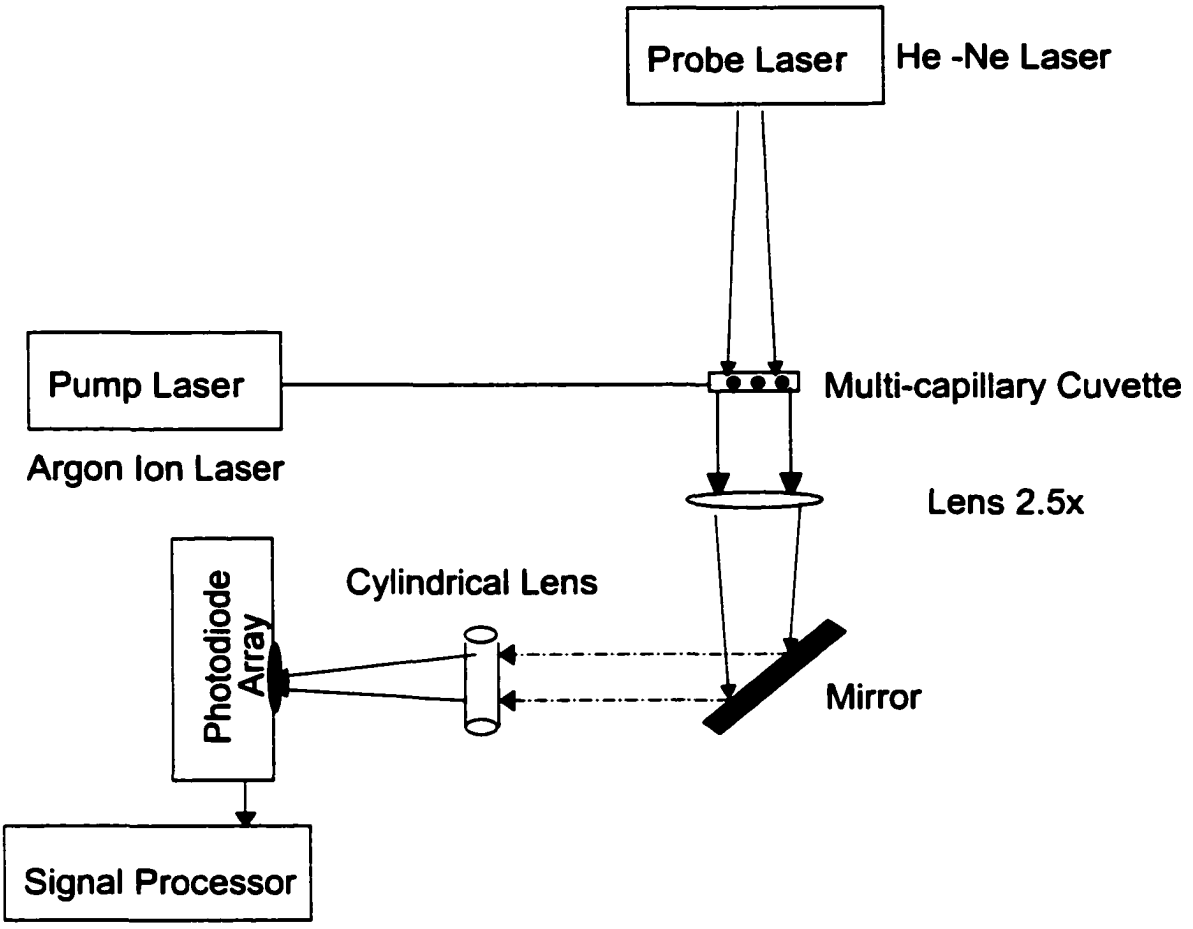

Figure 4.28 (b): A block diagram for the second optics arrangements.

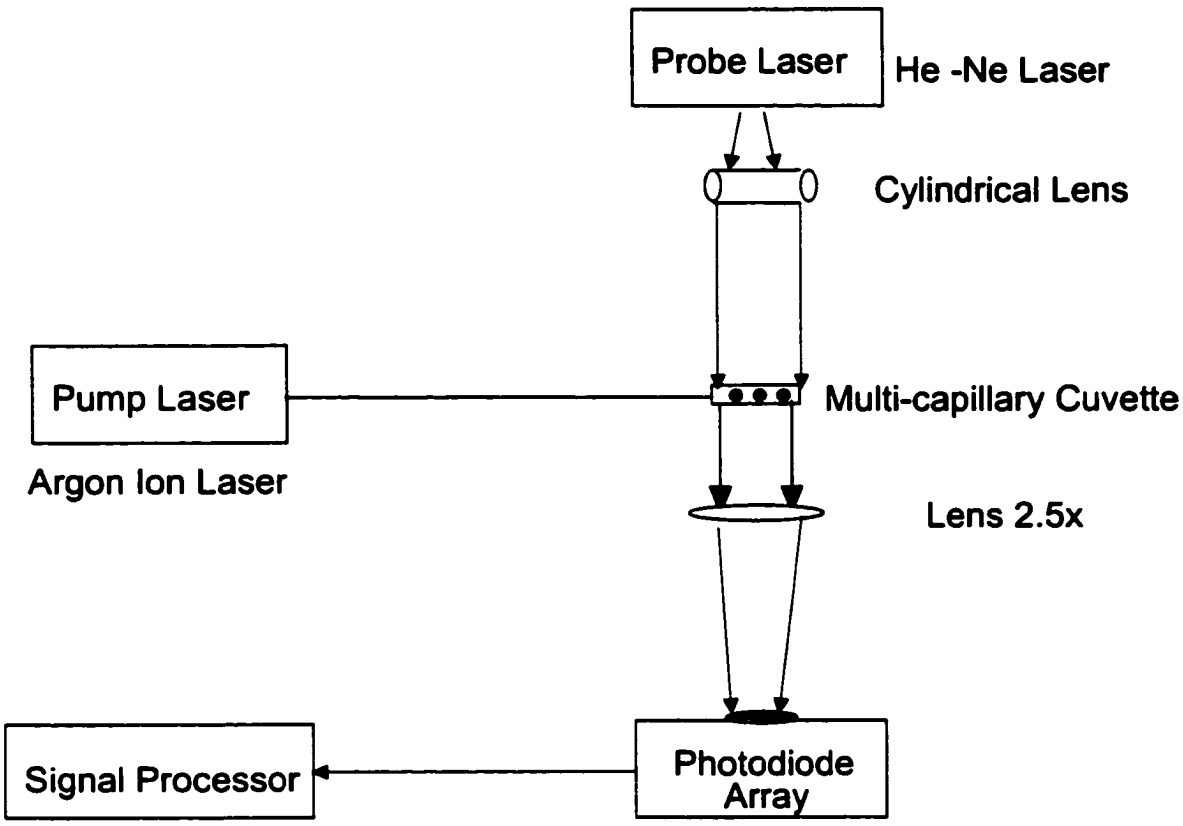

Figure 4.28 (c): A block diagram for the third optics arrangements.

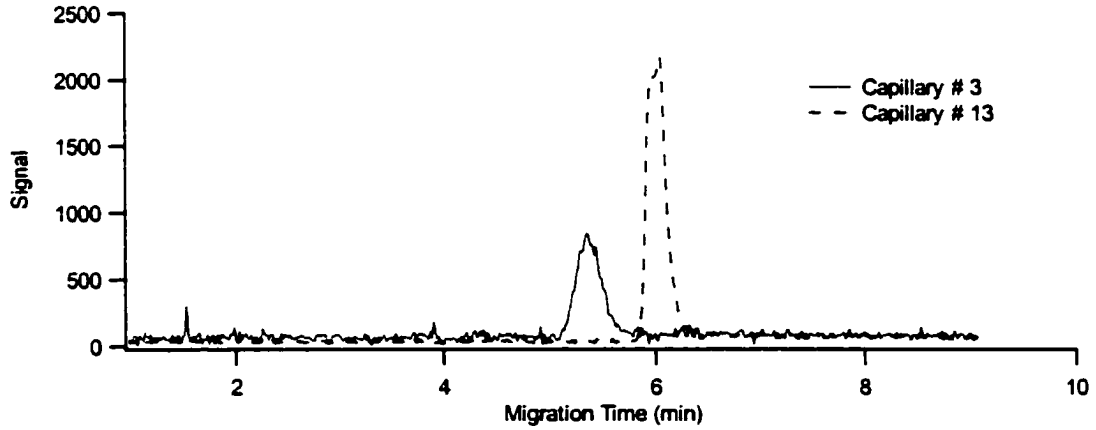

Figure 4.29 (a): An electropherogram of a multi-capillary thermal lens absorbance system. Length of capillary # 3 is 50.0 cm and capillary # 13 is 48.0 cm.

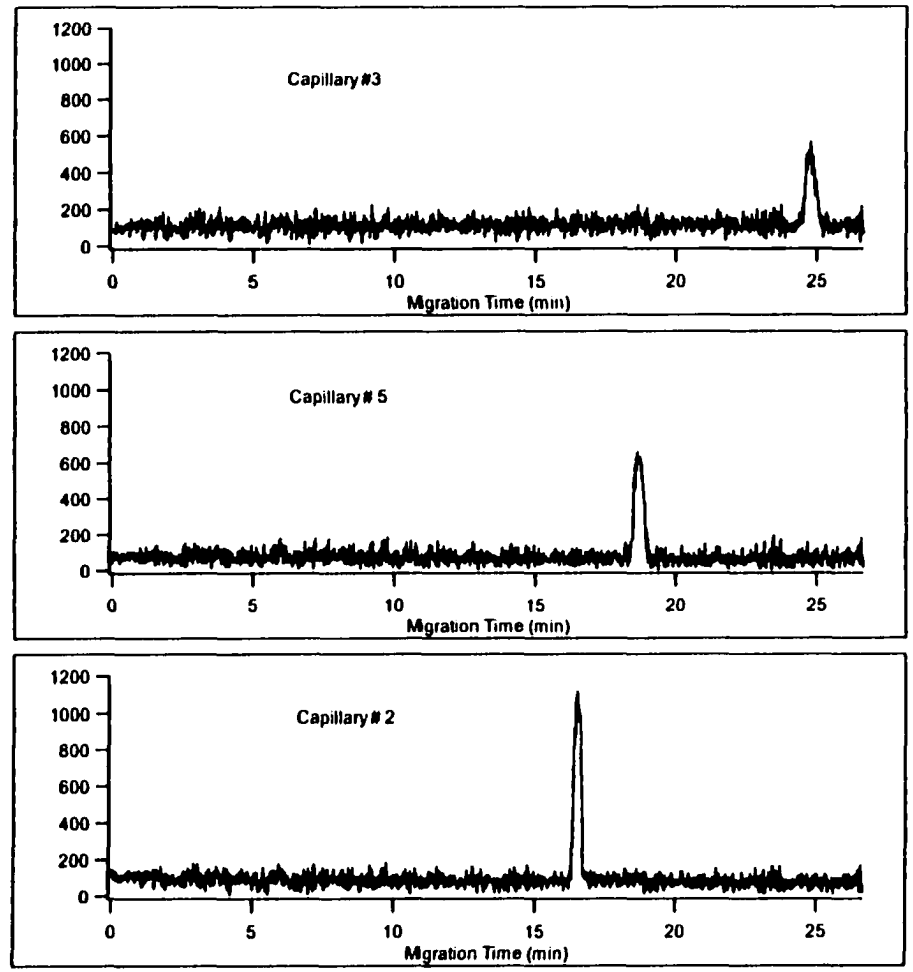

Figure 4.29 (b): The signals of multi-capillary thermal lens absorbance system corresponding to the PDA.

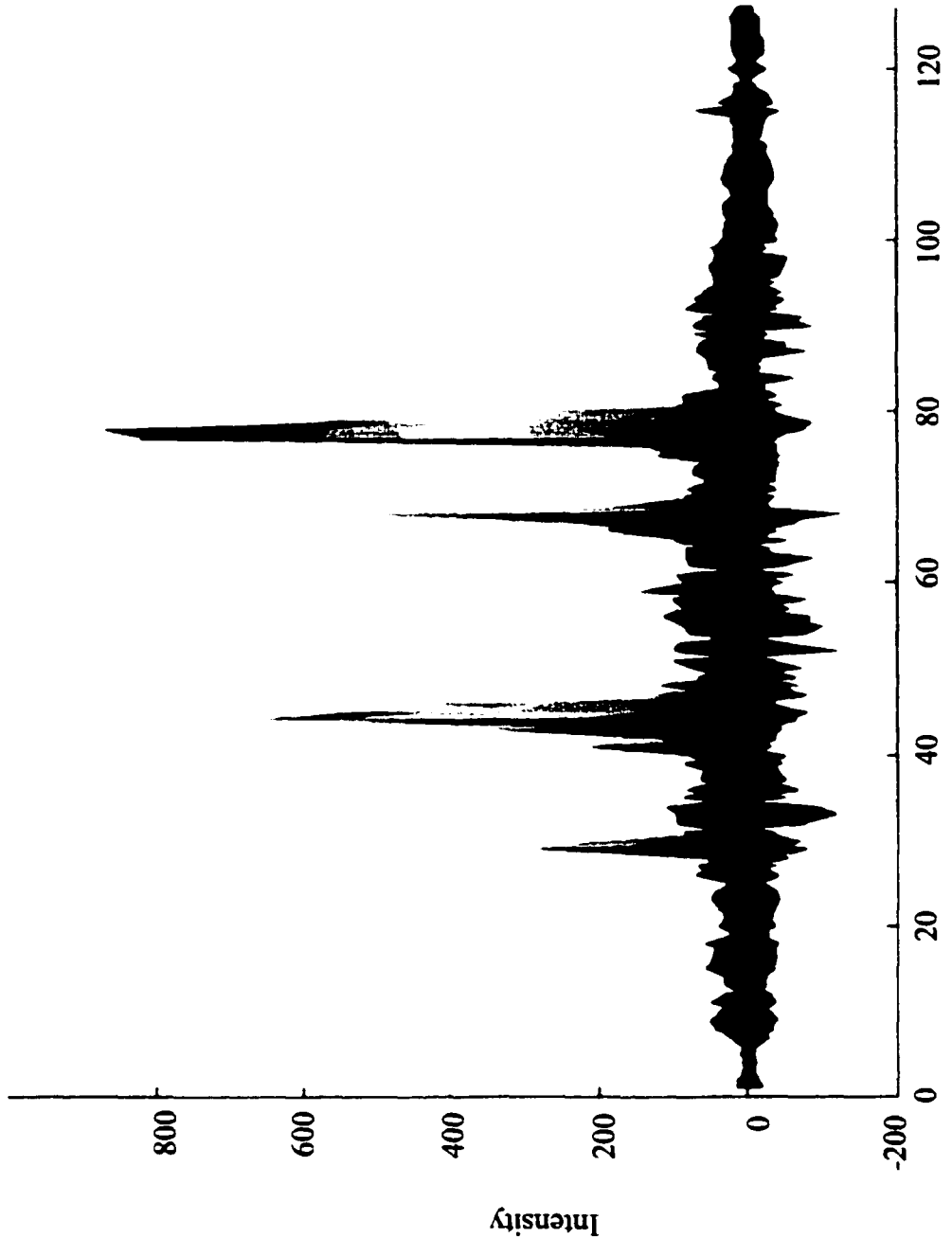

Figure 4.29 (c): Two dimension signals (viewed down time axis) of multi-capillary thermal lens absorbance system.

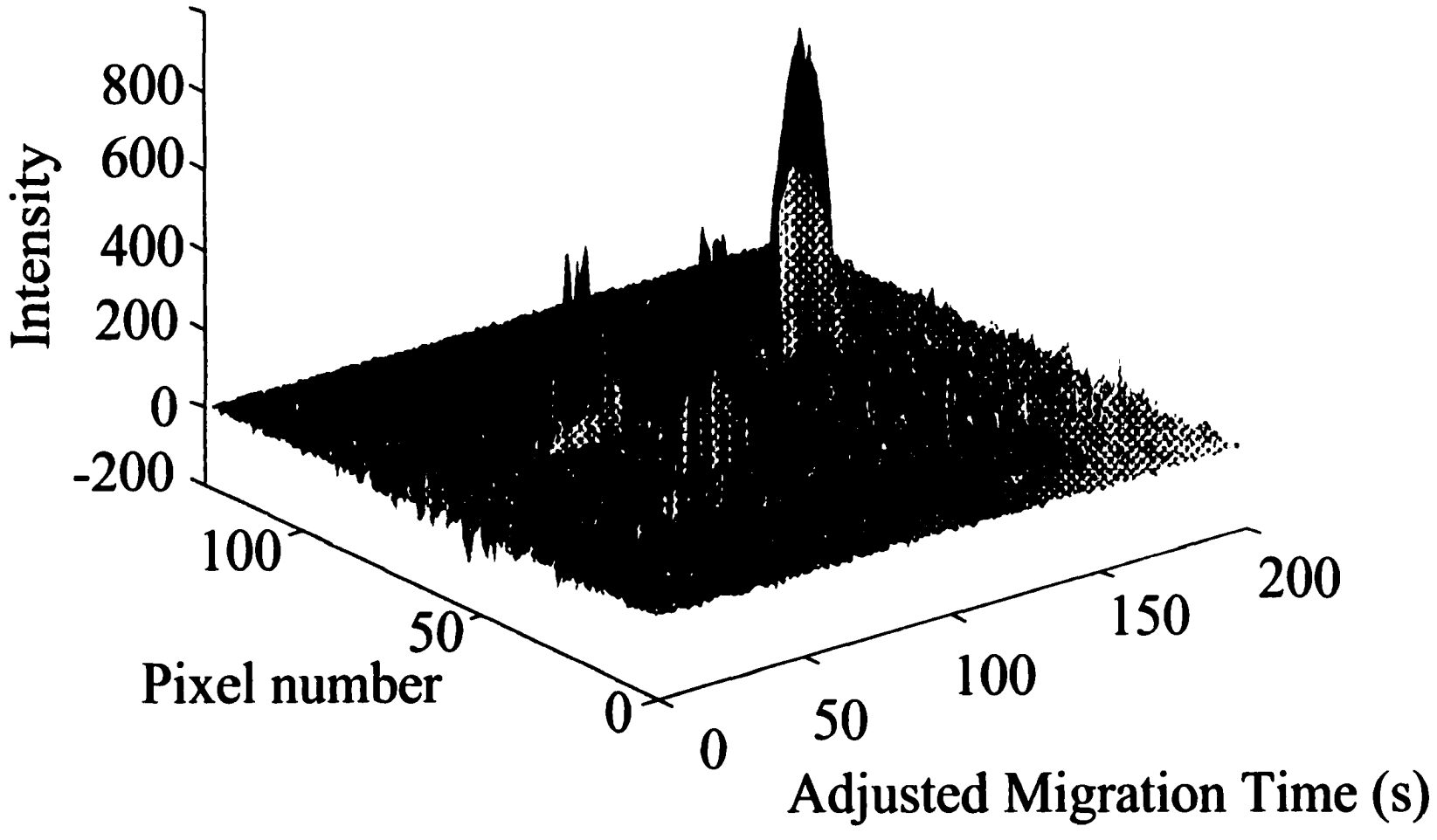

Figure 4.29 (d): Three dimension signals of multi-capillary thermal lens absorbance system.

reflected the light to the PDA through a pair of lenses. In the second design, the probe beam was directed on the sheath flow cuvette, and a pair of lenses (one cylindrical) focused the transmitted beam on the PDA. In the third design, the cylindrical lens defocused the probe beam to pass through the entire cuvette and then another lens focused the light to the PDA.

It is interesting to compare the data shown in Table 4.1. The best LOD (S/N = 3) can be generated from the third design, and the value after adjusting the optical elements improved to 65 times that of the original design.

	# 1	# 2	# 3
LOD (μM)	622	195	9.53

Table 4.1: The LODs of DABSYL-glycine in 2 mM borate buffer (50 % methanol) with different optic designs. The 145 mW pump laser was modulated by 8.5 Hz chopper frequency.

4.5.2 CE Performance of DABSYL-labeled Amino Acids

4.5.2.1 Electropherograms

Free zone electrophoresis was first used on this multiple capillary system to characterize its performance. Figure 4.29 presents the electropherograms of a 500 μM solution of DABSYL-glycine (16 pL injected) with different capillaries. The peaks generated in the multiplex capillary thermal-optical absorbance system should have a Gaussian shape. The separation efficiency in terms of theoretical plates, N, is given as $N = 5.54 (t_r / w_{1/2})^2$,

where t_r is the migration time of a component in the sample solution and $w_{1/2}$ is the full peak width at half peak height in time units. Calculation shows that N reaches as high as 16000 (ranges from 12000 to 16000 for calibration curves) per meter for a typical run when DABSYL-glycine migrated through the capillaries, which were 37.5 cm long and filled with 10 mM borate buffer (50% ethanol, pH 9.2), under an electric field of 25 kV.

4.5.2.2 Reproducibility between Capillary Electrophoresis Runs

Figure 4.30 demonstrates the reproducibility of the CE experiments. First 200 μM DABSYL-labeled glycine was introduced electrokinetically into the capillaries from a sample vial at 10 or 25 kV for 3, 5, 8, 10 seconds respectively, and then a 25 kV electrical potential was applied to the capillaries. The relative standard deviations (RSDs) of signal position on the photodiade array were 1.2 and 1.1 %, and the RSDs for migration times were 1.1 % and 0.8 % with capillaries 3 and 13.

The use of discrete capillaries results in a compromise in order to achieve uniform signal levels with different capillaries. Even though the source was the same, there were differences in signal levels due to the position of capillary tips. Alignment was performed to generate similar sensitivity for each detection channel, and the pump laser was focused at the center of the cuvette, which sacrificed the sensitivity of some capillaries.

4.5.2.3 Linear relationship and LOD

The 50-μm ID, 145-μm OD capillaries were filled with a 5 mM borate and 50% ethanol buffer, pH 9.2. Separation was at 20 kV across the 42 cm long capillaries; 19 nL

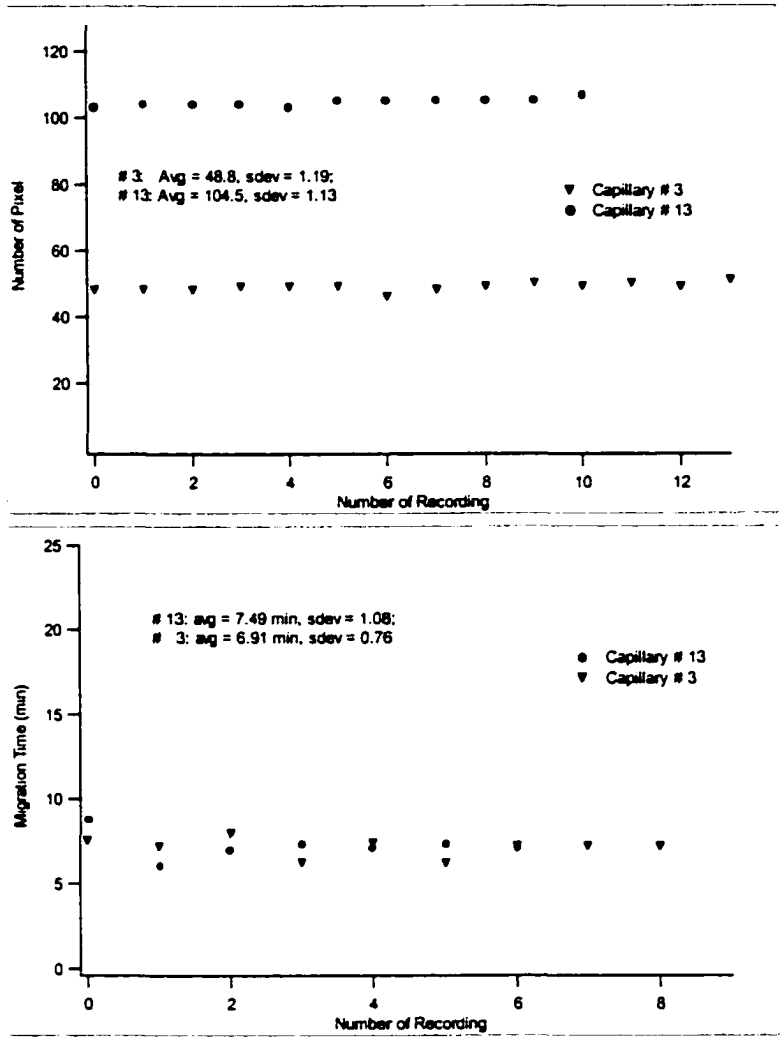

Figure 4.30: The reproducibility of capillary electrophoresis. Length of capillary # 3 is 50.0 cm and capillary # 13 is 48.0 cm.

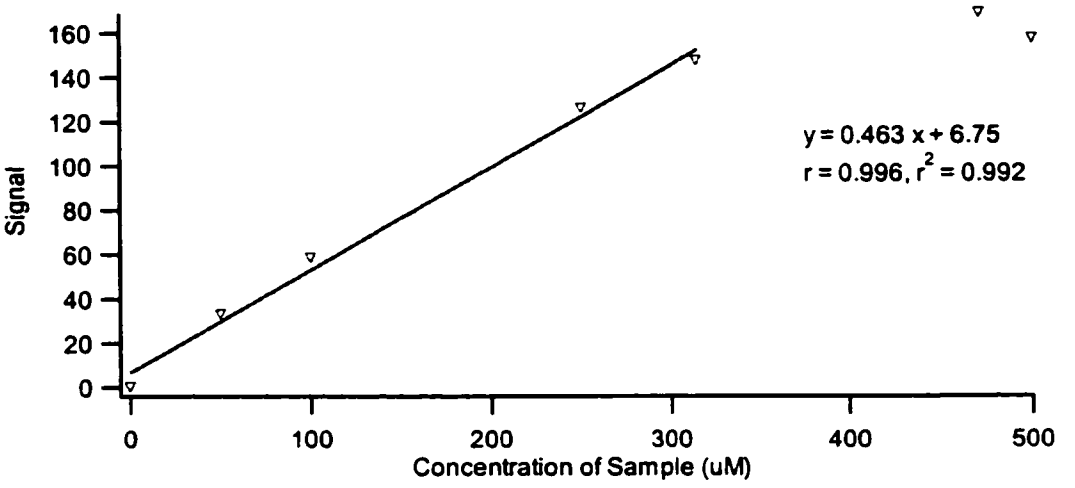

Fig 4.31: Linear relationship of multiple capillary thermal lens absorbance system.

sample were injected electrokinetically (20 kV, 5 sec). A series of six DABSYL-glycine solutions were prepared, whose concentrations were 50, 100, 250, 315, 471, and 500 μM. When the sample migrated from the capillary, DABSYL-glycine absorbed the energy from a 139-mW argon ion laser beam at 488 nm. Blank injection was performed by dipping the capillary into the buffer with the same potential and time interval as used for the sample solution; no peaks were detected from the blank. A linear calibration curve was obtained from the blank to 300 μM with a correlation coefficient of 0.992 and is shown in Figure 4.31. The detection limit (3σ) was 0.3 pmol (15 μM) injected onto the capillary. The performance reflects the high sensitivity of the thermal-optical absorbance system.

The data were similar to the detector LOD presented in section 4.5.1, but did not improve compared to the one generated in section 4.3.3, where the concentration and absorbance detection limits with single capillary system were achieved as 5.7×10^{-7} M and 2.1×10^{-5} respectively. There are several reasons for this. First, the use of multiple capillaries resulted in a higher background level in the sheath flow cuvette. Second, the lock-in amplifier used in 4.3 has superior noise rejection capability to that of the software used here.

It needs to be pointed out that the system should provide an even better detection limit if the excitation is shifted to a shorter wavelength. From the spectrum of glycine, the maximum absorbance is at 466 nm; only eighty percent of the maximum absorbance signal is observed at 488 nm.

There is also a compromise between pump laser power and the dynamic linear range. As can be seen in Figure 4.31, beyond the concentration level of 300 μM, the

calibration curve begins to bend. The practical analysis range is only one order of magnitude.

4.5.2.4 Practical Limitations

The sample buffer, running buffer, and sheath flow fluid should be kept the same to achieve the most sensitive thermal lens signal. No stacking was introduced because the difference between sample buffer and sheath liquid will complicate the detection of the thermal-optical signals. Though usually pure organic solvent provides the best thermal lens signal-to-noise ratio, conductive ions besides organic compound need to be added to the running buffer to maintain stable current during the CE experiments. Thus in free zone CE, a compromise between obtaining shorter migration time and achieving higher sensitivity has to be made. Equal volumes of ethanol and borate solution were mixed as running buffer and proved to be a suitable environment for separations.

The CE experiments also generated very high current, which is 10 μA per capillary and approximately 0.16 mA for the 16 capillary array. Thus a large amount of Joule heating was produced. Bubbles were often observed during the experiments. Some approaches needed to be employed to dissipate the heat. In most experiments, only 8 capillaries were placed in the sheath flow cuvette in order to reduce the current and give more space to help with heat dissipation. However, the increased space between the capillaries changes the flow rate of sheath buffer dramatically, which makes the alignment of the thermal lens experiment very critical and which decreases the sensitivity to some extent.

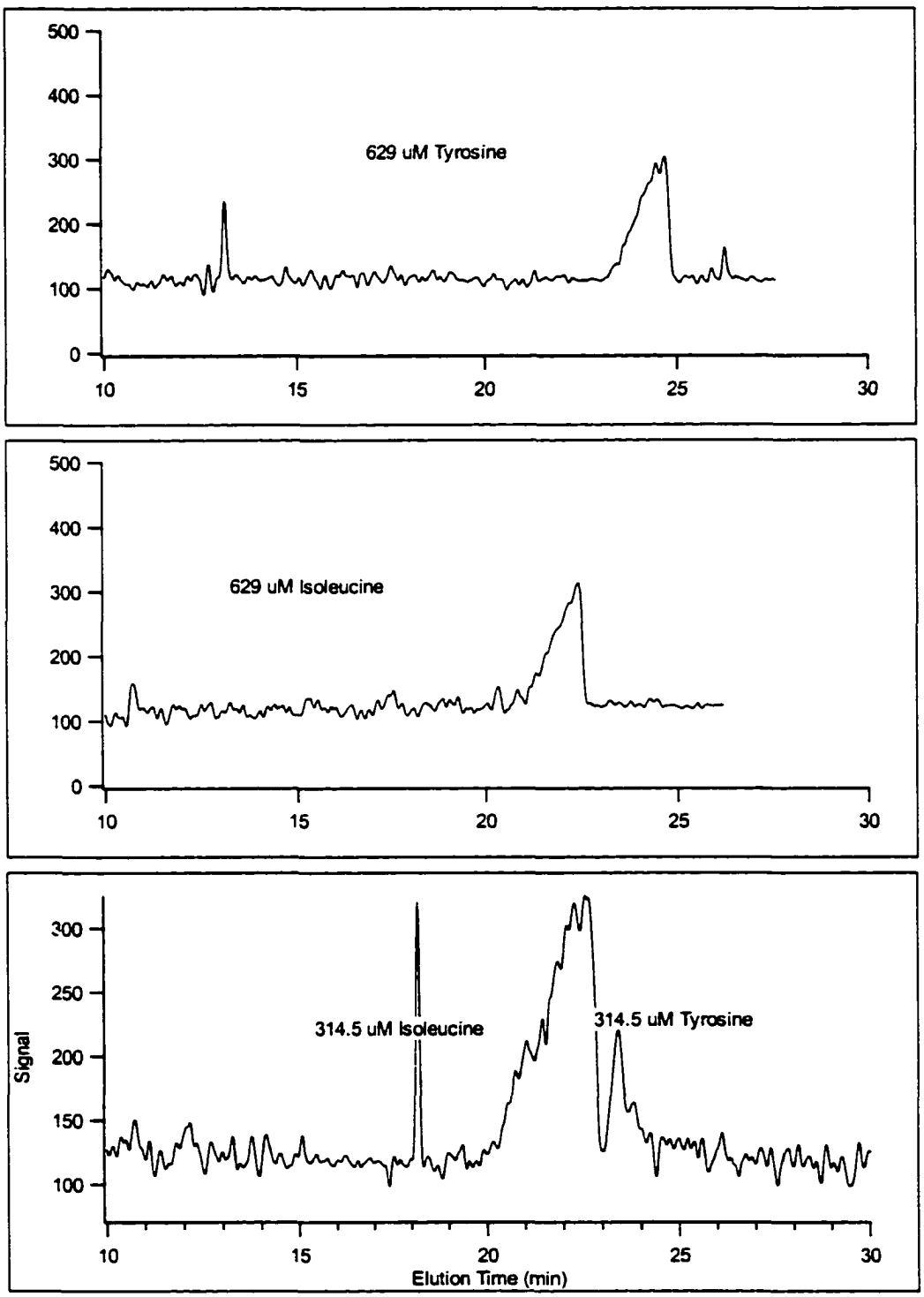

Fig 4.32: Separation of DABSYL-labeled amino acids using a multiple capillary thermal lens absorbance system. Running buffer was 5.0 mM borate and 50 % ethanol (pH 9.2).

4.5.2.5 Separations of Dabsyl Amino Acids

Figure 4.32 illustrates the separation and detection of DABSYL-labeled amino acids. There were two DABSYL amino acids: tyrosine, and isoleucine. The injection ends were inserted into the mixture of labeled amino acids or running buffer. The separation buffer and sheath flow fluid were 5.0 mM borate and 50 % ethanol, pH = 9.2. Samples were loaded by manual electrokinetic injection at 20 kV for 10 seconds, and the separation proceeded at 20 kV. Not as sensitive as the determination of DABSYL-glycine, the electropherogram had two fronting peaks. This serious fronting problem indicates that regions of the sample zone toward the front moved faster than regions of the zone nearer the center. This probably happens because the sample buffer has higher conductivity (10 mM borate) than the running buffer (5 mM borate). More work is needed to improve the separations.

Another running buffer system, 7.5 mM or 10.0 mM borate with 50 % ethanol was tried to improve separation but was not successful because the current was too high and generated too many bubbles during the experiment.

4.6 Conclusion and Future Work

So far two major problems for the first generation thermal lens absorbance on a multiple capillary electrophoresis system have been solved: a multiple capillary instrument with thermal-optical absorption detection has been constructed. The LOD

achievable from this system is an order of magnitude poorer than the single capillary thermal-optical instrument. Since the similar sampling and separation techniques for multiplexed capillaries in fluorescence determination have been developed commercially, it should be possible to fully automate the multi-capillary thermal lens absorbance system and eventually obtain a high throughput.

Much work remains. In terms of further separations of DABSYL amino acids, the running buffer still appears as a problem. Micellar electrokinetic capillary chromatography (MEKC) has already become the most popular CE tool to separate ionic and neutral molecules, but the introduction of most common surfactant ions into the running buffer could make the current even higher and produce more bubbles. Presumably, it should be possible to find other surfactants to achieve better thermal lens signals.

The separation buffer contains salt ions, which give discrimination for different sample molecules during the injection. Employing hydrodynamic sampling, instead of electrokinetic injection, may be a good choice for separation applications.
During the experiments, it was found the flow rate of sheath buffer is quite critical for obtaining the signals. With the faster flow rate, no thermal lens signals can be observed; and it cannot be too slow, otherwise a serious cross talk problem will be generated. A mechanical pump instead of simple siphoning force is recommended for stabilizing the signal and achieving better reproducibility of elution time. On the other hand, changing the space between the capillary channels in a modified cuvette is another option to reduce the interference between adjacent capillaries. Furthermore, using capillaries with different diameters also can be helpful.

The S/N issue is still an important aspect for this project. Using a blank signal from one capillary as a reference instead of chopper wheel to remove the largest moving part of the set-up is another method to be considered to improve the S/N. Another option is to change the optical setup by mounting the pump laser at a 45° angle to the plane of 16 capillaries because the distortion of light due to one capillary can affect the following capillaries if the blue laser is passed through the same plane as the capillaries.

Finally, the further performance of the instrument needs to be evaluated by using small molecules in drug samples. A possible application of this instrument may be found in the study of combinatorial chemistry. In the meantime, matrix effects need to be considered due to the background absorbance.

References

1. J.M. Harris and N.J. Dovichi, *Analytical Chemistry,* 1980, 52, 695A.
2. N.J. Dovichi, *Progress in Analytical Spectroscopy*, 1988, 11, 179.
3. T.G. Nolan, B.K. Hart and N.J. Dovichi, *Analytical Chemistry,* 1985, 57, 2703.
4. Y.F. Cheng and N.J. Dovichi, *Mikrochimica Acta,* 1986, III, 351.
5. W.A. Weimer and N.J. Dovichi, *Journal of Applied Physics,* 1986, 59, 225.
6. W.A. Weimer and N.J. Dovichi, *Analytical Chemistry,* 1988, 60, 662.
7. K.C. Waldron and N.J. Dovichi, *Analytical Chemistry,* 1992, 64, 1396.
8. M. Chen, K.C. Waldron, Y. Zhao and N.J. Dovichi, *Electrophoresis,* 1994, 15, 1290.
9. X-F. Li, C-S. Liu, P. Roos, E.B. Hansen, C.E. Cerniglia and N.J. Dovichi, *Electrophoresis,* 1998, 19, 3178.
10. R.C.C. Leite, R.S. Moore and J.R. Whinney, *Applied Physical Letter,* 1964, 5, 141.
11. D.J. Bornhop and N.J. Dovichi, *Analytical Chemistry,* 1986, 58,504.
12. M. Yu and N.J. Dovichi, *Mikrochimica Acta,* 1988, 111, 27.
13. M. Yu and N.J. Dovichi, *Analytical Chemistry,* 1989, 61(1), 37.
14. M. Yu and N.J. Dovichi, *Applied Spectroscopy,* 1989, 43(2), 196.
15. B. Krattiger, A.E. Bruno, H.M. Widmer and R. Dandliker, *Analytical Chemistry,* 1995, 67(1), 124.
16. Y.F. Cheng and N.J. Dovichi, *Science,* 1988, 242, 562.
17. J. Zhang, K. Voss, D. Shaw, D. Lewis and N.J. Dovichi, *Nucleic Acids Research,* 1999, 27, 24.
18. N.J. Dovichi, *CRC Critical Reviews in Analytical Chemistry,* 1987, 17(4), 357.

19. D.Y. Chen and N.J. Dovichi, *Analytical Chemistry,* 1996, 68, 690.

20. T. Hunkapiller, R.J. Kaiser, B.F. Koop and L. Hood, *Science,* 1991, 254, 59.

21. C.T. Culbertson and J.W. Jorgenson, *Analytical Chemistry,* 1998, 70, 2629.

22. J-K. Lin and J-Y Chang, *Analytical Chemistry,* 1975, 47, 1634.

23. J-K. Lin and C-C Lai, *Analytical Chemistry,* 1980, 52, 630.

24. T.G. Nolan, W.A. Weimer and N.J. Dovichi, *Analytical Chemistry,* 1984, 56, 1704.

25. T.G. Nolan and N.J. Dovichi, *Analytical Chemistry,* 1987, 59, 2803.

Chapter 5

Conclusions and Future Work

5.1 Conclusions

Capillary electrophoresis has been and, for the foreseeable future, will continue to be, one of the major analytical techniques for analysis of small molecules in biological samples. This thesis has demonstrated the applications of CE coupled with various detection methods, such as mass spectrometry, laser-induced fluorescence and thermal lens absorbance.

On-line electrospray mass spectroscopy has been successfully applied to CE with the assistance of a makeup liquid. A rapid and sensitive CE-ESI-MS method has been developed to determine eight amines normally present in food. In addition to the advantages associated with CE, such as high resolving power and low sample requirement, this universal method also has been used to determine amines which are undetectable with UV or LIF. The dynamic range is from 5 μM to 350 μM and the detection limits are from 1.2 μM to 0.02 μM.

The Laser-induced fluorescence detector is the most sensitive detector currently available for CE. Fluorescence detection based on a sheath flow cuvette has been successfully applied for the simultaneous determination of 16 neurotransmitters in a single capillary system. The separation methodologies based on micelle electrokinetic chromatography have been developed for the analysis of neurotransmitters in brain

microdialysates and homogenate samples by CE-LIF, with minimum sample pretreatment and small sample requirement.

The design, construction and performance of a multi-capillary detector based on thermal optical absorbance have been demonstrated. The design of the sheath flow cuvette makes the thermo-lens system applicable for multiple capillaries. The first generation of multi-capillary thermal absorbance detector has been developed with theoretical plate number of 10^4.

5.2 Future Work

The methodology developed for biogenic amine analysis using CE-ESI-MS could be applied to other food samples, such as soy sauce, wine, cheese and fish, etc. In principle, the method also can be scaled to work with a single cell. The determination of those amines in yeast, cell extracts or a single cell itself could be done with proper experimental facilities. So far, the CE-ESI-MS can be performed only at relatively high analyte concentrations and the components for the separation buffer are quite limited. Future research will be focused on sensitivity enhancement and the introduction of more buffer compounds.

The future work regarding CE-LIF application in neurotransmitter determination will focus on those transmitters which are playing important roles in message transmission between neurons, but present in very low concentrations, including neuropeptides, some other amines and proteins. Pharmacokinetic and neurochemical studies on other drugs also could be studied. Some instrumental modifications, such as

the interface coupled CE with microdialysis on-line or on-column labeling protocols, could be useful for monitoring real-time analysis.

To enhance the performance of the thermal absorbance multiple capillary system, suitable separation buffers must be found. The ideal running buffer should have a low thermal optical background and low thermal conductivity. In addition, the application of the developed multiple capillary absorbance instruments to small drug targets or metabolites in pharmaceutical samples needs to be investigated. Finally, full automation of the multiple capillary absorbance system and then high throughput instrumentation should be accomplished in the near future.

Appendix

DAQ Program for Multicapillary Thermo-optical Absorbance Detector

```
/*+++++++++++++++++++++++++++++++++++++++++++++++++++++++++++++++++++++++++++++
++++++++++++++++++*/
/*                MULTI-CAPILLARY TOAD DAQ PROGRAM                    */
/*   Program Functionality: Program to acquire data from Multi-Capillary      */
/*                    Thermo Optical Absorbance Detector                */
/*   Programming Software:  Lab Windows CVI V5.0 on Windows NT 4.0 Workstation
*/
/*   Start Date:    February 01, 2000                                    */
/*   Last Revised:  June 05, 2000                                        */
/*   Version:       2.00                                                 */
/*                                                                       */
/*   Changes:                                                            */
/*   V2.00                                                               */
/*   - Change buffer and save values from double precision to floating point.   */
/*   - Current reading is saved as the 129th point.                      */
/*   - Line active status check box indicators are updated as status is changed  */
/*     in Align Panel.                                                   */
/*                                                                       */
/*+++++++++++++++++++++++++++++++++++++++++++++++++++++++++++++++++++++++++++++
++++++++++++++++++*/
#include <ansi_c.h>
#include <cvirte.h>   /*Need if linking in external compiler; harmless otherwise */
#include <userint.h>
#include <utility.h>
#include <formatio.h>
#include <string.h>
#include "Panel.h"
#include "nidaqex.h"
/*+++++++++++++++++++++++++++++++++++++++++++++++++++++++++++++++++++++++++++++
++++++++++++++++++*/
/*   Define and initialize variables   def=dafault                      */
/*
                                                                        */
/*                                                                       */
/*+++++++++++++++++++++++++++++++++++++++++++++++++++++++++++++++++++++++++++++
++++++++++++++++++*/
#define enable 0       /* used to enable buttons in user interface */
#define disable 1              /* used to disable buttons in user interface */
#define active 1               /* used to define active status of check box */
#define inactive 0             /* used to define inactive status of check box */
```

```
/*++++++++++++++++++++++++++++++++++++++++++++++++++++++++++++++++++++++++++++
++++++++++++++++++*/
/*   Initialize variables   def=dafault                                    */
/*
                                                                          */
/*                                                                        */
/*++++++++++++++++++++++++++++++++++++++++++++++++++++++++++++++++++++++++++++
++++++++++++++++++*/
static int mainPanelHandle,   /* Handle to main panel  */
        setupPanelHandle,                   /* Handle to setup panel */
        alignPanelHandle,                   /* Handle to Align panel */
        saveFileHandle,                      /* Handle to saving file */
        iRunCE=0,                           /* 1=run CE, 0=do not run (stop) */
        piChartLineCtrlID[16], /* Control ID #s for stripchart lines in main panel */
        piLineToPixelCtrlID[16],/* Control ID #s for pixel number controller */
        piAPanelLineStatCtrlID[16],  /* Control ID #s for line active status check boxes
in align panel */
        piMPanelLineStatCtrlID[16],  /* Control ID #s for line active status check boxes
in main panel */
   iLineWidthInPix=3,               /* Width of a line in pixels */
   iNumLinesToDraw=16,              /* Number of lines to be drawn in strip chart */
        piAlignBarCtrlID[16],       /* A gray bar showing the selected pixels for a
given line in Align panel */
        iDAQTimerCtrlID,      /* Control ID generated for DAQ Timer */
        buf1PlotHandle,
        buf2PlotHandle,
        bufDPlotHandle,
        iPlottedOnce=0;
double  dDAQTimerFreq;



struct prefStruct {
        int iInjectTime;                    /* injection time in seconds */
        int iInjectVolts;                   /* injection voltage in volts 30,000 max */
        int iCEVolts;                       /* High voltage for the test in volts 30,000
max */
        double dCapLength;                  /* Length of capillaries in cm */
        int iDAQTimerInterval;              /* How often DAQ Timer is called in mili
sec. */
        double dChopSpeed;                  /* Speed of the chopper motor rev/sec */
        int iNumStripChartPoints;  /* number of points per strip chart -1 */
   int piChartDraw[16];        /* 1=draw in strip chart 0=do not draw in strip chart*/
   int piLineActive[16];       /* 1=line is active, 0=line is not active */
   int piLineMidPixel[16];     /* Middle pixel num (out of 1 to 128) for a given line */
        char sDataFileName[MAX_PATHNAME_LEN]; /* File name for saving data */
```

```
        } pref;

short   piBuf1[12800] = {0}, /* Values from first scan */
                piBuf2[12800] = {0}, /* Values from second scan */
                piDiffBuf[12800],       /* abs(piBuf1-piBuf2) */
        iStatus = 0,    /* DAQ function return value */
                iRetVal = 0,    /* for Error Handler */
                iDevice = 1,    /* Device number */
                iChan = 0,              /* First AI channel */
                iStartTrig = 1, /* type of triggering to use.1-external */
                iExtConv = 1, /* How A/D conversion pulses generated, 1-externally */
                iGain = 1,              /* gain of 1/2 given by -1 */
                iSaveBuff=1, /* which buffer is used for saving acquired data at the
moment */
                piCurrent[3]; /* buffer to save reading of current (min three points
needed to use Daq_Start)*/

float   pfBuf[129] = {0.0},             /* 128 data points, 129 th point is current */
        pfChartPoint[16]={0.0}; /* latest intensity value for line n */

double
        dInjectField,                   /* Injection field V/cm */
        dCEField,                               /* Field during CE in V/cm */
  dGainAdjust = 1.0,
  dOffset = 0.0;



unsigned int uiCount = 12800; /*the number of data points to be acquired */
  i16 iSampTB = 0; /*unit of resolution to be used in determining the sampling rate
                                0-external clock used as timebase (PFI8 pin for E
Series boards) */
  u16 uSampInt = 1; /*number of timebase units that will elapse between A/D
conversions. */
  i16 iDAQstopped = 0;
  u32 ulRetrieved = 0;
  i16 iIgnoreWarning = 0;
  i16 iYieldON = 1;
  int i;
        i16 piSaveArray[32];
```

```
/*+++++++++++++++++++++++++++++++++++++++++++++++++++++++++++++++++++++++++++
++++++++++++++++++*/
/*   Function Definitions                                                   */
/*                                                                          */
/*                                                                          */
/*                                                                          */
/*++++++++++++++++++++++++++++++++++++++++++++++++++++++++++++++++++++++++++
++++++++++++++++++*/
void Initialize (void);
void InitializeDAQ (void);
void ClearDAQ (void);
void DrawAlignPanelBars(void);
int CVICALLBACK DAQTimerCallback (int panel, int control, int event,
                void *callbackData, int eventData1, int eventData2);
int CVICALLBACK TestTimerCallback (int panel, int control, int event,
                void *callbackData, int eventData1, int eventData2);


/*++++++++++++++++++++++++++++++++++++ MAIN
++++++++++++++++++++++++++++++++++++++++++*/

/*+++++++++++++++++++++++++++++++++++++++++++++++++++++++++++++++++++++++++++
++++++++++++++++++*/
/*  Function:  main                                                         */
/*       Descript:  Display main screen.                                    */
/*                                                                          */
/*++++++++++++++++++++++++++++++++++++++++++++++++++++++++++++++++++++++++++
++++++++++++++++++*/
int main (int argc, char *argv[])
{
        if (InitCVIRTE (0, argv, 0) == 0)      /* Needed if linking in external compiler;
harmless otherwise */
                return -1;      /* out of memory */
        if ((mainPanelHandle = LoadPanel (0, "Panel.uir", MAINPANEL)) < 0)
                return -1;
        if ((setupPanelHandle = LoadPanel (0, "Panel.uir", SETUPPANEL)) < 0)
                return -1;
        if ((alignPanelHandle = LoadPanel (0, "Panel.uir", ALIGNPANEL)) < 0)
                return -1;
   Initialize();
        DisplayPanel (mainPanelHandle);
        RunUserInterface ();
        return 0;
}
```

```
/*++++++++++++++++++++++++++++++++++++++++++++++++++++++++++++++++++++++++
++++++++++++++++++*/
/* Function: Initialize                                          */
/* Called by: main                                               */
/*       Descript: Initialize parameters.                                  */
/*                                                        */
/*++++++++++++++++++++++++++++++++++++++++++++++++++++++++++++++++++++++++
++++++++++++++++++*/
void Initialize (void)
{
        int fsize;
        FILE *filePointer;

        piChartLineCtrlID[0]=MAINPANEL_LINEPLOT_1;  /* Get automatically
assigned */
        piChartLineCtrlID[1]=MAINPANEL_LINEPLOT_2;  /* control ID values for */
        piChartLineCtrlID[2]=MAINPANEL_LINEPLOT_3;  /* strip chart lines */
        piChartLineCtrlID[3]=MAINPANEL_LINEPLOT_4;
        piChartLineCtrlID[4]=MAINPANEL_LINEPLOT_5;
        piChartLineCtrlID[5]=MAINPANEL_LINEPLOT_6;
        piChartLineCtrlID[6]=MAINPANEL_LINEPLOT_7;
        piChartLineCtrlID[7]=MAINPANEL_LINEPLOT_8;
        piChartLineCtrlID[8]=MAINPANEL_LINEPLOT_9;
        piChartLineCtrlID[9]=MAINPANEL_LINEPLOT_10;
        piChartLineCtrlID[10]=MAINPANEL_LINEPLOT_11;
        piChartLineCtrlID[11]=MAINPANEL_LINEPLOT_12;
        piChartLineCtrlID[12]=MAINPANEL_LINEPLOT_13;
        piChartLineCtrlID[13]=MAINPANEL_LINEPLOT_14;
        piChartLineCtrlID[14]=MAINPANEL_LINEPLOT_15;
        piChartLineCtrlID[15]=MAINPANEL_LINEPLOT_16;

        piLineToPixelCtrlID[0]=ALIGNPANEL_LINE1PIXEL;  /* Get automatically
assigned */
        piLineToPixelCtrlID[1]=ALIGNPANEL_LINE2PIXEL;  /* control ID values for
*/
        piLineToPixelCtrlID[2]=ALIGNPANEL_LINE3PIXEL;  /* mid pixel value of
each line */
        piLineToPixelCtrlID[3]=ALIGNPANEL_LINE4PIXEL;
        piLineToPixelCtrlID[4]=ALIGNPANEL_LINE5PIXEL;
        piLineToPixelCtrlID[5]=ALIGNPANEL_LINE6PIXEL;
        piLineToPixelCtrlID[6]=ALIGNPANEL_LINE7PIXEL;
        piLineToPixelCtrlID[7]=ALIGNPANEL_LINE8PIXEL;
        piLineToPixelCtrlID[8]=ALIGNPANEL_LINE9PIXEL;
        piLineToPixelCtrlID[9]=ALIGNPANEL_LINE10PIXEL;
        piLineToPixelCtrlID[10]=ALIGNPANEL_LINE11PIXEL;
        piLineToPixelCtrlID[11]=ALIGNPANEL_LINE12PIXEL;
```

```
        piLineToPixelCtrlID[12]=ALIGNPANEL_LINE13PIXEL;
        piLineToPixelCtrlID[13]=ALIGNPANEL_LINE14PIXEL;
        piLineToPixelCtrlID[14]=ALIGNPANEL_LINE15PIXEL;
        piLineToPixelCtrlID[15]=ALIGNPANEL_LINE16PIXEL;

        piAPanelLineStatCtrlID[0]= ALIGNPANEL_LINESTAT_1;  /* Get
automatically assigned */
        piAPanelLineStatCtrlID[1]= ALIGNPANEL_LINESTAT_2;  /* control ID
values for     */
        piAPanelLineStatCtrlID[2]= ALIGNPANEL_LINESTAT_3;  /* line active
status control */
        piAPanelLineStatCtrlID[3]= ALIGNPANEL_LINESTAT_4;  /* check boxes in
align panel */
        piAPanelLineStatCtrlID[4]= ALIGNPANEL_LINESTAT_5;
        piAPanelLineStatCtrlID[5]= ALIGNPANEL_LINESTAT_6;
        piAPanelLineStatCtrlID[6]= ALIGNPANEL_LINESTAT_7;
        piAPanelLineStatCtrlID[7]= ALIGNPANEL_LINESTAT_8;
        piAPanelLineStatCtrlID[8]= ALIGNPANEL_LINESTAT_9;
        piAPanelLineStatCtrlID[9]= ALIGNPANEL_LINESTAT_10;
        piAPanelLineStatCtrlID[10]= ALIGNPANEL_LINESTAT_11;
        piAPanelLineStatCtrlID[11]= ALIGNPANEL_LINESTAT_12;
        piAPanelLineStatCtrlID[12]= ALIGNPANEL_LINESTAT_13;
        piAPanelLineStatCtrlID[13]= ALIGNPANEL_LINESTAT_14;
        piAPanelLineStatCtrlID[14]= ALIGNPANEL_LINESTAT_15;
        piAPanelLineStatCtrlID[15]= ALIGNPANEL_LINESTAT_16;

        piMPanelLineStatCtrlID[0]= MAINPANEL_LINESTAT_1;  /* Get
automatically assigned */
        piMPanelLineStatCtrlID[1]= MAINPANEL_LINESTAT_2;  /* control ID
values for     */
        piMPanelLineStatCtrlID[2]= MAINPANEL_LINESTAT_3;  /* line active status
control */
        piMPanelLineStatCtrlID[3]= MAINPANEL_LINESTAT_4;  /* check boxes in
align panel */
        piMPanelLineStatCtrlID[4]= MAINPANEL_LINESTAT_5;
        piMPanelLineStatCtrlID[5]= MAINPANEL_LINESTAT_6;
        piMPanelLineStatCtrlID[6]= MAINPANEL_LINESTAT_7;
        piMPanelLineStatCtrlID[7]= MAINPANEL_LINESTAT_8;
        piMPanelLineStatCtrlID[8]= MAINPANEL_LINESTAT_9;
        piMPanelLineStatCtrlID[9]= MAINPANEL_LINESTAT_10;
        piMPanelLineStatCtrlID[10]= MAINPANEL_LINESTAT_11;
        piMPanelLineStatCtrlID[11]= MAINPANEL_LINESTAT_12;
        piMPanelLineStatCtrlID[12]= MAINPANEL_LINESTAT_13;
        piMPanelLineStatCtrlID[13]= MAINPANEL_LINESTAT_14;
        piMPanelLineStatCtrlID[14]= MAINPANEL_LINESTAT_15;
        piMPanelLineStatCtrlID[15]= MAINPANEL_LINESTAT_16;
```

```
        GetFileInfo ("Preferences.daq",&fsize ); /* get file size */
        if ((filePointer=fopen("Preferences.daq","r"))!= NULL && fsize==fsize){
/*change one fsize to the real value */
                fread (&pref, sizeof(struct prefStruct), 1, filePointer); /* read values from
the file */
                fclose(filePointer);
                for (i=0;i<16;i++){  /* set line active status in align panel*/
                        SetCtrlVal (alignPanelHandle, piAPanelLineStatCtrlID[i],
pref.piLineActive[i]);
                }
                for (i=0;i<16;i++){   /* get mid pixel value for each line */
                        SetCtrlVal (alignPanelHandle, piLineToPixelCtrlID[i],
pref.piLineMidPixel[i]);
                }
                for (i=0;i<16;i++){  /* set which lines to be drawn in strip chart*/
                        SetCtrlVal (mainPanelHandle, piChartLineCtrlID[i],
pref.piChartDraw[i]);
                }
                for (i=0;i<16;i++){  /* set line active status in main panel*/
                        SetCtrlVal (mainPanelHandle, piMPanelLineStatCtrlID[i],
pref.piLineActive[i]);
                }
                SetCtrlVal (setupPanelHandle, SETUPPANEL_INJECTTIME,
pref.iInjectTime);
                SetCtrlVal (setupPanelHandle, SETUPPANEL_INJECTVOLTS,
pref.iInjectVolts);
                SetCtrlVal (setupPanelHandle, SETUPPANEL_CEVOLTS,
pref.iCEVolts);
                SetCtrlVal (setupPanelHandle, SETUPPANEL_CAPLENGTH,
pref.dCapLength);
                SetCtrlVal (setupPanelHandle,
SETUPPANEL_DAQTIMERINTERVAL,pref.iDAQTimerInterval);
                SetCtrlVal (setupPanelHandle, SETUPPANEL_CHOPSPEED,
pref.dChopSpeed);
                SetCtrlVal (mainPanelHandle, MAINPANEL_CHARTPOINTSSLIDE,
pref.iNumStripChartPoints);
                SetCtrlAttribute (mainPanelHandle, MAINPANEL_CHART,
ATTR_POINTS_PER_SCREEN,pref.iNumStripChartPoints+1 );
                SetCtrlAttribute (mainPanelHandle, MAINPANEL_CURRENTCHART,
ATTR_POINTS_PER_SCREEN,pref.iNumStripChartPoints+1 );
                ResetTextBox (setupPanelHandle,
SETUPPANEL_DATAFILENAME,pref.sDataFileName);
        }
        else {  /* if preferences file not found, use settings in panels as default */
```

```
                for (i=0;i<16;i++){  /* get line active status from align panel*/
                        GetCtrlVal (alignPanelHandle, piAPanelLineStatCtrlID[i],
&pref.piLineActive[i]);
                }
                for (i=0;i<16;i++){  /* set line active status in main panel same as in align
panel*/
                        SetCtrlVal (mainPanelHandle, piMPanelLineStatCtrlID[i],
pref.piLineActive[i]);
                }
                for (i=0;i<16;i++){ /* get which lines to be drawn in strip chart*/
                        GetCtrlVal (mainPanelHandle, piChartLineCtrlID[i],
&pref.piChartDraw[i]);
                }
                for (i=0;i<16;i++){   /* get mid pixel value for each line */
                        GetCtrlVal (alignPanelHandle, piLineToPixelCtrlID[i],
&pref.piLineMidPixel[i]);
                }
                GetCtrlVal (setupPanelHandle, SETUPPANEL_INJECTTIME,
&pref.iInjectTime);
                GetCtrlVal (setupPanelHandle, SETUPPANEL_INJECTVOLTS,
&pref.iInjectVolts);
                GetCtrlVal (setupPanelHandle, SETUPPANEL_CEVOLTS,
&pref.iCEVolts);
                GetCtrlVal (setupPanelHandle, SETUPPANEL_CAPLENGTH,
&pref.dCapLength);
                GetCtrlVal (setupPanelHandle,
SETUPPANEL_DAQTIMERINTERVAL,&pref.iDAQTimerInterval);
                GetCtrlVal (setupPanelHandle, SETUPPANEL_CHOPSPEED,
&pref.dChopSpeed);
                GetCtrlVal (setupPanelHandle, SETUPPANEL_DATAFILENAME,
pref.sDataFileName);
                GetCtrlVal (mainPanelHandle, MAINPANEL_CHARTPOINTSSLIDE,
&pref.iNumStripChartPoints);
                SetCtrlAttribute (mainPanelHandle, MAINPANEL_CHART,
ATTR_POINTS_PER_SCREEN,pref.iNumStripChartPoints+1 );
                SetCtrlAttribute (mainPanelHandle, MAINPANEL_CURRENTCHART,
ATTR_POINTS_PER_SCREEN,pref.iNumStripChartPoints+1 );
        }
        /* Set calculated field values */
        dInjectField=pref.iInjectVolts/pref.dCapLength;
        dCEField=pref.iCEVolts/pref.dCapLength;
        dDAQTimerFreq=1000/pref.iDAQTimerInterval;
        SetCtrlVal (setupPanelHandle, SETUPPANEL_INJECTFIELD, dInjectField);
        SetCtrlVal (setupPanelHandle, SETUPPANEL_CEFIELD, dCEField);
        SetCtrlVal (setupPanelHandle, SETUPPANEL_DAQTIMERFREQ,
dDAQTimerFreq);
```

```
}

/*+++++++++++++++++++++++++++++++++++++++++++++++++++++++++++++++++++++++++
++++++++++++++++++*/
/* Function: InitializeDAQ                                          */
/* Called by: StartExpCallback                                      */
/*       Descript: Initialize DAQ board to acquire data.            */
/*                                                                  */
/*+++++++++++++++++++++++++++++++++++++++++++++++++++++++++++++++++++++++++
++++++++++++++++++*/
void InitializeDAQ (void)
{
        /* General initialization */
        Timeout_Config (1, 100);  /* timeout in 100 x 55 ms */
        /* Calibration necessary? - Have to disconnect cable */
        /* Setup for external start trigger into PFI0 with iStartTrig=1 */
        iStatus = Select_Signal (iDevice, ND_IN_START_TRIGGER, ND_PFI_0,
ND_LOW_TO_HIGH);
   /* Setup for external conversions into PFI2 with iExtConv = 1. */
        iStatus = Select_Signal (iDevice, ND_IN_CONVERT, ND_PFI_2,
ND_LOW_TO_HIGH);
        iStatus = DAQ_Config(iDevice, iStartTrig, iExtConv);

}

/*+++++++++++++++++++++++++++++++++++++++++++++++++++++++++++++++++++++++++
++++++++++++++++++*/
/* Function: AlignCapsPanelCallback                                 */
/* Called by:                                                       */
/*       Descript:                                                  */
/*                                                                  */
/*+++++++++++++++++++++++++++++++++++++++++++++++++++++++++++++++++++++++++
++++++++++++++++++*/
int CVICALLBACK AlignCapsPanelCallback (int panel, int control, int event,
                void *callbackData, int eventData1, int eventData2)
{
        switch (event)
                {
                case EVENT_COMMIT:
                        DrawAlignPanelBars();
                        HidePanel (mainPanelHandle);
                        DisplayPanel (alignPanelHandle);
                        SetCtrlAttribute (alignPanelHandle,
ALIGNPANEL_STOPTESTCEBTN,ATTR_DIMMED, disable);
```

```
                        break;
                }
        return 0;
}

/*+++++++++++++++++++++++++++++++++++++++++++++++++++++++++++++++++++++++++
++++++++++++++++++*/
/* Function: SetupExpCallback                                          */
/* Called by:                                                          */
/*      Descript:                                                      */
/*                                                                     */
/*+++++++++++++++++++++++++++++++++++++++++++++++++++++++++++++++++++++++++
++++++++++++++++++*/
int CVICALLBACK SetupExpCallback (int panel, int control, int event,
                void *callbackData, int eventData1, int eventData2)
{
        switch (event)
                {
                case EVENT_COMMIT:
                        HidePanel (mainPanelHandle);
                        DisplayPanel (setupPanelHandle);
                        break;
                }
        return 0;
}

/*+++++++++++++++++++++++++++++++++++++++++++++++++++++++++++++++++++++++++
++++++++++++++++++*/
/* Function: InjectCallback                                            */
/* Called by:                                                          */
/*      Descript:                                                      */
/*                                                                     */
/*+++++++++++++++++++++++++++++++++++++++++++++++++++++++++++++++++++++++++
++++++++++++++++++*/
int CVICALLBACK InjectCallback (int panel, int control, int event,
                void *callbackData, int eventData1, int eventData2)
{
        switch (event)
                {
                case EVENT_COMMIT:

                        break;
                }
        return 0;
}
```

```
/*+++++++++++++++++++++++++++++++++++++++++++++++++++++++++++++++++++++++++++++
++++++++++++++++++*/
/* Function: StartExpCallback                                          */
/* Called by: Main Panel - Start Experiment button                     */
/*      Descript: Initiate start sequence.                             */
/*                                                                     */
/*+++++++++++++++++++++++++++++++++++++++++++++++++++++++++++++++++++++++++++++
++++++++++++++++++*/
int CVICALLBACK StartExpCallback (int panel, int control, int event,
            void *callbackData, int eventData1, int eventData2)
{
        int iFileStat, iConfirm;
        int iFileStatOK; /* 1=file status is ok: 0=file status is not ok */
        long iFileSize;
        double timer_tick;
        switch (event)
                {
                case EVENT_COMMIT:
                        /* check if save file name already exist */
                        /* 0-file does not exist;  1 - file exists; -1 - an error occurred  */
                        iFileStat = GetFileInfo (pref.sDataFileName, &iFileSize);
                        switch (iFileStat)  /* status of file */
                                {
                                case 1: /* 1 - file exists */
                                        iConfirm = ConfirmPopup ("Overwrite
Confirmation!",
                                                "The file you specified already exist. Do you
want to overwrite this file?");
                                        /* iConfirm=1 if Yes selected, iConfirm=0 if No
selected */
                                        if (iConfirm==1) iFileStatOK = 1;
                                        else iFileStatOK = 0;
                                        break;
                                case 0: /* 0-file does not exist */
                                        iFileStatOK = 1;
                                        break;
                                default:        /* -1 - an error occurred */
                                        iFileStatOK = 0;
                                        MessagePopup ("Error!", "Data acquisition was not
initiated due to file access problems!");
                                        break;
                        }
                        if (iFileStatOK==1){
                                iRunCE=1;
                                iPlottedOnce=0;
```

```
                        InitializeDAQ ();
                        ClearStripChart (mainPanelHandle,
MAINPANEL_CHART);
                        /* Set Stepper motor speed and start it */
                        /* Set high voltage output */
                        iSaveBuff=1;
                        SetCtrlAttribute (mainPanelHandle,
MAINPANEL_ALIGNBTN,ATTR_DIMMED, disable); /*disable buttons */
                        SetCtrlAttribute (mainPanelHandle,
MAINPANEL_STARTEXPBTN,ATTR_DIMMED, disable);
                        SetCtrlAttribute (mainPanelHandle,
MAINPANEL_INJECTBTN,ATTR_DIMMED, disable);
                        SetCtrlAttribute (mainPanelHandle,
MAINPANEL_SETUPEXPBTN,ATTR_DIMMED, disable);
                        SetCtrlAttribute (mainPanelHandle,
MAINPANEL_SHUTDOWNBTN,ATTR_DIMMED, disable);

        ResetTextBox(mainPanelHandle,MAINPANEL_STARTTIME,TimeStr ());

        ResetTextBox(mainPanelHandle,MAINPANEL_CURTIME,TimeStr ());/*main
panel:current time indicator */
                        iStatus = DAQ_Start (iDevice, iChan, iGain, piBuf1,
uiCount, iSampTB, uSampInt);
                        timer_tick=pref.iDAQTimerInterval/1000;
                        iDAQTimerCtrlID = NewCtrl (mainPanelHandle,
CTRL_TIMER, "",10,10);
                        SetCtrlAttribute (mainPanelHandle, iDAQTimerCtrlID,
ATTR_INTERVAL, timer_tick);
                        InstallCtrlCallback (mainPanelHandle, iDAQTimerCtrlID,
DAQTimerCallback,&iDAQTimerCtrlID);
                        }
                    break;
                }
        return 0;
}

/*++++++++++++++++++++++++++++++++++++++++++++++++++++++++++++++++++++
++++++++++++++++++*/
/* Function: DAQTimerCallback                                    */
/* Called by:                                                    */
/*      Descript:                                                */
/*                                                               */
/*++++++++++++++++++++++++++++++++++++++++++++++++++++++++++++++++++++
++++++++++++++++++*/
int CVICALLBACK DAQTimerCallback (int panel, int control, int event,
            void *callbackData, int eventData1, int eventData2)
```

```
{
        int iVal1,iVal2,j, in;


        double iTrigFactor, dA,dB;

        in = floor (0.5 + pref.dChopSpeed * 0.320);  /*data for each pixel comes at 3.2 ms
intervals */
        iTrigFactor = 2 * 3.14159265359 * in / 100;   /*data for each pixel comes at 3.2
ms intervals */

        switch (event){
                case EVENT_TIMER_TICK:
                        iDAQstopped=0;  /* get data */
                        while ((iDAQstopped != 1) && (iStatus == 0)) { /* Loop until all
acquisition is complete - 12800 points */
                                iStatus = DAQ_Check(iDevice, &iDAQstopped,
&ulRetrieved);
                        }
                        /* get current reading from channel 1, gain 1 */
                        iStatus = DAQ_Start (iDevice, 1, 1, piCurrent, 3,iSampTB,
uSampInt);  /*acquire 1 data pt, 10 micro sec */
                        iDAQstopped=0;  /* get data */
                        while ((iDAQstopped != 1) && (iStatus == 0)) { /* Loop until all
acquisition is complete - 12800 points */
                                iStatus = DAQ_Check(iDevice, &iDAQstopped,
&ulRetrieved);
                        }
                        if (iSaveBuff==1){
                                iSaveBuff=2;   /* start daq to buf2 while working on buf1
data */
                                iStatus = DAQ_Start (iDevice, iChan, iGain, piBuf2,
uiCount, iSampTB, uSampInt);
                                for (j=0; j<128; j++){
                                        dA=0;
                                        dB=0;
                                        for (i=0; i<100; i++){
                                                dA=dA+(piBuf1[i*128+j] * sin
(iTrigFactor*i));
                                                dB=dB+(piBuf1[i*128+j] * cos
(iTrigFactor*i));
                                        }
                                        pfBuf[j]=sqrt(dA * dA + dB * dB);
                                }
                        }
                        else {
```

```
                        iSaveBuff=1;   /* start daq to buf1 while working on buf2
data */
                        iStatus = DAQ_Start (iDevice, iChan, iGain, piBuf1,
uiCount, iSampTB, uSampInt);
                        for (j=0; j<128; j++){
                                dA=0;
                                dB=0;
                                for (i=0; i<100; i++){
                                        dA=dA+(piBuf2[i*128+j] * sin
(iTrigFactor*i));
                                        dB=dB+(piBuf2[i*128+j] * cos
(iTrigFactor*i));
                                }
                                pfBuf[j]=sqrt(pow (dA,2) + pow (dB,2));
                        }
                }
                pfBuf[128]=piCurrent[0]; /* 129 th point is the current */

        ResetTextBox(mainPanelHandle,MAINPANEL_CURTIME,TimeStr ());/*main
panel:current time indicator */
                DeleteGraphPlot (mainPanelHandle, MAINPANEL_GRAPH, -1,
1); /* clear graph */
                PlotY (mainPanelHandle, MAINPANEL_GRAPH, pfBuf, 128,
VAL_FLOAT,
                        VAL_THIN_STEP, VAL_EMPTY_SQUARE,
VAL_SOLID, 1, VAL_RED);  /* plot line  */
                /*plot strip chart points */
                for (i=0; i<16; i++){
                        if ( pref.piLineActive[i]==1){
                                /* assumed iLineWidthInPix=3 - change this if it's
changed */
                                if ( pref.piChartDraw[i]==1){
                                        pfChartPoint[i] = (
pfBuf[(pref.piLineMidPixel[i])-2]
                                                                        +
pfBuf[(pref.piLineMidPixel[i])-1]
                                                                        +
pfBuf[(pref.piLineMidPixel[i])  ] )/3; /* Nth point is given by piBuf1[N-1] */
                                }
                                else{
                                        pfChartPoint[i]=0;
                                }
                        }
                        else{
                                pfChartPoint[i]=0;
                        }
```

```
                    }
                    PlotStripChartPoint (mainPanelHandle,
MAINPANEL_CURRENTCHART, piCurrent[0]);
                    PlotStripChart (mainPanelHandle, MAINPANEL_CHART,
pfChartPoint, 16, 0,
                                                    0, VAL_FLOAT);
                    if (iPlottedOnce==1){
                        ArrayToFile (pref.sDataFileName, pfBuf, VAL_FLOAT,
129, 1,
                                                    VAL_GROUPS_TOGETHER,
VAL_GROUPS_AS_COLUMNS,
                                                    VAL_CONST_WIDTH, 10,
VAL_BINARY, VAL_APPEND);
                    }
                    else {
                        ArrayToFile (pref.sDataFileName, pfBuf, VAL_FLOAT,
129, 1,
                                                    VAL_GROUPS_TOGETHER,
VAL_GROUPS_AS_COLUMNS,
                                                    VAL_CONST_WIDTH, 10,
VAL_BINARY, VAL_TRUNCATE);
                    }
                    iPlottedOnce=1;
                    break;
                }
        return 0;
}



/*+++++++++++++++++++++++++++++++++++++++++++++++++++++++++++++++++++++++
++++++++++++++++++*/
/* Function: StopExpCallback                                    */
/* Called by:                                                   */
/*      Descript:                                               */
/*                                                              */
/*+++++++++++++++++++++++++++++++++++++++++++++++++++++++++++++++++++++++
++++++++++++++++++*/
int CVICALLBACK StopExpCallback (int panel, int control, int event,
                void *callbackData, int eventData1, int eventData2)
{
        switch (event)
                {
                case EVENT_COMMIT:
                    if(iRunCE==1){
```

```
                        iRunCE=0;
                        SetCtrlAttribute (mainPanelHandle, iDAQTimerCtrlID,
ATTR_ENABLED, 0);  /*disable timer */
                        SetCtrlAttribute (mainPanelHandle,
MAINPANEL_ALIGNBTN,ATTR_DIMMED, enable); /*disable buttons */
                        SetCtrlAttribute (mainPanelHandle,
MAINPANEL_STARTEXPBTN,ATTR_DIMMED, enable);
                        SetCtrlAttribute (mainPanelHandle,
MAINPANEL_INJECTBTN,ATTR_DIMMED, enable);
                        SetCtrlAttribute (mainPanelHandle,
MAINPANEL_SETUPEXPBTN,ATTR_DIMMED, enable);
                        SetCtrlAttribute (mainPanelHandle,
MAINPANEL_SHUTDOWNBTN,ATTR_DIMMED, enable);
                        ClearDAQ ();
                    }
                    break;
            }
    return 0;
}


/*++++++++++++++++++++++++++++++++++++++++++++++++++++++++++++++++++++++++
++++++++++++++++++*/
/* Function: ShutdownCallback                                    */
/* Called by:                                                 */
/*      Descript:                                                */
/*                                                          */
/*++++++++++++++++++++++++++++++++++++++++++++++++++++++++++++++++++++++++
++++++++++++++++++*/
int CVICALLBACK ShutdownCallback (int panel, int control, int event,
            void *callbackData, int eventData1, int eventData2)
{
    FILE *filePointer;
    int fileHandle;
    switch (event)
            {
            case EVENT_COMMIT:
                    iRunCE=0;
                    QuitUserInterface (0);
                    if ((filePointer=fopen("Preferences.daq","w"))!= NULL){
                            fwrite (&pref, sizeof(struct prefStruct), 1, filePointer); /*
write struct to file */
                            fclose(filePointer);
                    }
                    else printf("Could not save preferences.\n");
```

```
                        break;
                }
        return 0;
}

/*+++++++++++++++++++++++++++++++++++++++++++++++++++++++++++++++++++++++++
++++++++++++++++++*/
/* Function: ChangeStripChartScaleCallback                              */
/* Called by: Main Panel                                                */
/*      Descript: This function will update the horizontal scale of the strip charts */
/*         according to the value selected in the slide control.        */
/*                                                                      */
/*+++++++++++++++++++++++++++++++++++++++++++++++++++++++++++++++++++++++++
++++++++++++++++++*/
int CVICALLBACK ChangeStripChartScaleCallback (int panel, int control, int event,
                void *callbackData, int eventData1, int eventData2)
{
        switch (event)
                {
                case EVENT_COMMIT:
                        GetCtrlVal (mainPanelHandle,
MAINPANEL_CHARTPOINTSSLIDE, &pref.iNumStripChartPoints);
                        SetCtrlAttribute (mainPanelHandle, MAINPANEL_CHART,
ATTR_POINTS_PER_SCREEN,pref.iNumStripChartPoints+1 );
                        SetCtrlAttribute (mainPanelHandle,
MAINPANEL_CURRENTCHART,
ATTR_POINTS_PER_SCREEN,pref.iNumStripChartPoints+1 );
                        break;
                }
        return 0;
}


/*+++++++++++++++++++++++++++++++++++++++++++++++++++++++++++++++++++++++++
++++++++++++++++++*/
/* Function: LineDrawStatusCallback                                     */
/* Called by: Main Panel                                                */
/*      Descript: If a check box for plot graph is clicked, this function will  */
/*         change the relevant parameter.                               */
/*                                                                      */
/*+++++++++++++++++++++++++++++++++++++++++++++++++++++++++++++++++++++++++
++++++++++++++++++*/
int CVICALLBACK LineDrawStatusCallback (int panel, int control, int event,
                void *callbackData, int eventData1, int eventData2)
{
        switch (event)
```

```
                {
                case EVENT_COMMIT:
                        i=0;
                        while (i<16){
                                if (control==piChartLineCtrlID[i]){
                                        if (pref.piChartDraw[i]==0) pref.piChartDraw[i]=1;
                                        else pref.piChartDraw[i]=0;
                                        i=16;                                   /* exit loop */
                                }
                                i=i+1;
                        }

                        break;
                }
        return 0;
}


/*++++++++++++++++++++++++++++++++ Setup Panel
++++++++++++++++++++++++++++++++++*/

/*++++++++++++++++++++++++++++++++++++++++++++++++++++++++++++++++++++++++++++
++++++++++++++++++*/
/* Function: UpdateFieldsCallback                                   */
/* Called by:                                                  */
/*      Descript:                                                  */
/*                                                          */
/*++++++++++++++++++++++++++++++++++++++++++++++++++++++++++++++++++++++++++++
++++++++++++++++++*/
int CVICALLBACK UpdateFieldsCallback (int panel, int control, int event,
                void *callbackData, int eventData1, int eventData2)
{
        double injectField, cEField;
        switch (event)
                {
                case EVENT_COMMIT:
                        GetCtrlVal (setupPanelHandle, SETUPPANEL_INJECTVOLTS,
&pref.iInjectVolts);
                        GetCtrlVal (setupPanelHandle, SETUPPANEL_CEVOLTS,
&pref.iCEVolts);
                        GetCtrlVal (setupPanelHandle, SETUPPANEL_CAPLENGTH,
&pref.dCapLength);
                        injectField =pref.iInjectVolts/pref.dCapLength;
                        cEField    = pref.iCEVolts / pref.dCapLength;
                        SetCtrlVal (setupPanelHandle, SETUPPANEL_INJECTFIELD,
injectField);
```

```
                        SetCtrlVal (setupPanelHandle, SETUPPANEL_CEFIELD,
cEField);
                        break;
                }
        return 0;
}

/*+++++++++++++++++++++++++++++++++++++++++++++++++++++++++++++++++++++++++
++++++++++++++++++*/
/* Function: ChangeFileNameCallback                                        */
/* Called by:                                                  */
/*      Descript:                                                  */
/*                                                          */
/*+++++++++++++++++++++++++++++++++++++++++++++++++++++++++++++++++++++++++
++++++++++++++++++*/
int CVICALLBACK ChangeFileNameCallback (int panel, int control, int event,
                void *callbackData, int eventData1, int eventData2)
{
        char fileName[MAX_PATHNAME_LEN];
        switch (event)
                {
                case EVENT_COMMIT:
                        GetCtrlVal (setupPanelHandle,
SETUPPANEL_DATAFILENAME,fileName);

                        if (FileSelectPopup ("", fileName, "*.dat", "Name of File to Save",
                                                        VAL_OK_BUTTON, 0, 1,
1, 1, fileName) > 0) {
                        ResetTextBox (setupPanelHandle,
SETUPPANEL_DATAFILENAME,fileName);
                        }
                        break;
                }
        return 0;
}

/*+++++++++++++++++++++++++++++++++++++++++++++++++++++++++++++++++++++++++
++++++++++++++++++*/
/* Function: UpdateDAQTimerFrequencyCallback                               */
/* Called by:                                                  */
/*      Descript:                                                  */
/*                                                          */
/*+++++++++++++++++++++++++++++++++++++++++++++++++++++++++++++++++++++++++
++++++++++++++++++*/
int CVICALLBACK UpdateDAQTimerFrequencyCallback (int panel, int control, int
event,
```

```
                void *callbackData, int eventData1, int eventData2)
{
        int timerInterval;
        double frequency;
        switch (event)
                {
                case EVENT_COMMIT:

                        GetCtrlVal (setupPanelHandle,
SETUPPANEL_DAQTIMERINTERVAL,&timerInterval);
                        frequency = 1000.0/timerInterval;
                        SetCtrlVal (setupPanelHandle,
SETUPPANEL_DAQTIMERFREQ, frequency);


                        break;
                }
        return 0;
}


/*++++++++++++++++++++++++++++++++++++++++++++++++++++++++++++++++++++++++
++++++++++++++++++*/
/* Function: SetupOkCallback                                        */
/* Called by:                                                  */
/*      Descript:                                                  */
/*                                                          */
/*++++++++++++++++++++++++++++++++++++++++++++++++++++++++++++++++++++++++
++++++++++++++++++*/
int CVICALLBACK SetupOkCallback (int panel, int control, int event,
                void *callbackData, int eventData1, int eventData2)
{
        switch (event)
                {
                case EVENT_COMMIT:

                        GetCtrlVal (setupPanelHandle, SETUPPANEL_INJECTTIME,
&pref.iInjectTime);
                        GetCtrlVal (setupPanelHandle, SETUPPANEL_INJECTVOLTS,
&pref.iInjectVolts);
                        GetCtrlVal (setupPanelHandle, SETUPPANEL_CEVOLTS,
&pref.iCEVolts);
                        GetCtrlVal (setupPanelHandle, SETUPPANEL_CAPLENGTH,
&pref.dCapLength);
                        GetCtrlVal (setupPanelHandle, SETUPPANEL_INJECTFIELD,
&dInjectField);
```

```
                    GetCtrlVal (setupPanelHandle, SETUPPANEL_CEFIELD,
&dCEField);
                    GetCtrlVal (setupPanelHandle,
SETUPPANEL_DATAFILENAME, pref.sDataFileName);
                    GetCtrlVal (setupPanelHandle, SETUPPANEL_CHOPSPEED,
&pref.dChopSpeed);
                    GetCtrlVal (setupPanelHandle,
SETUPPANEL_DAQTIMERINTERVAL,&pref.iDAQTimerInterval);
                    GetCtrlVal (setupPanelHandle,
SETUPPANEL_DAQTIMERFREQ, &dDAQTimerFreq);

                    HidePanel (setupPanelHandle);
                    DisplayPanel (mainPanelHandle);
                    break;
            }
    return 0;
}

/*++++++++++++++++++++++++++++++++++++++++++++++++++++++++++++++++++++++
++++++++++++++++++*/
/* Function: SetupCancelCallback                                    */
/* Called by:                                                       */
/*      Descript:                                                   */
/*                                                                  */
/*++++++++++++++++++++++++++++++++++++++++++++++++++++++++++++++++++++++
++++++++++++++++++*/
int CVICALLBACK SetupCancelCallback (int panel, int control, int event,
            void *callbackData, int eventData1, int eventData2)
{
    switch (event)
            {
            case EVENT_COMMIT:
                    /* Reset parameters to old values */
                    SetCtrlVal (setupPanelHandle, SETUPPANEL_INJECTTIME,
pref.iInjectTime);
                    SetCtrlVal (setupPanelHandle, SETUPPANEL_INJECTVOLTS,
pref.iInjectVolts);
                    SetCtrlVal (setupPanelHandle, SETUPPANEL_CEVOLTS,
pref.iCEVolts);
                    SetCtrlVal (setupPanelHandle, SETUPPANEL_CAPLENGTH,
pref.dCapLength);
                    SetCtrlVal (setupPanelHandle, SETUPPANEL_INJECTFIELD,
dInjectField);
                    SetCtrlVal (setupPanelHandle, SETUPPANEL_CEFIELD,
dCEField);
```

```
                        ResetTextBox (setupPanelHandle,
SETUPPANEL_DATAFILENAME,pref.sDataFileName);
                        SetCtrlVal (setupPanelHandle, SETUPPANEL_CHOPSPEED,
pref.dChopSpeed);
                        SetCtrlVal (setupPanelHandle,
SETUPPANEL_DAQTIMERINTERVAL,pref.iDAQTimerInterval);
                        SetCtrlVal (setupPanelHandle,
SETUPPANEL_DAQTIMERFREQ, dDAQTimerFreq);
                        HidePanel (setupPanelHandle);
                        DisplayPanel (mainPanelHandle);
                        break;
                }
        return 0;
}



/*++++++++++++++++++++++++++++++++ Align Panel
++++++++++++++++++++++++++++++++*/

/*++++++++++++++++++++++++++++++++++++++++++++++++++++++++++++++++++++++++++++
++++++++++++++++++*/
/* Function: AlignOkCallback                                        */
/* Called by:                                                  */
/*      Descript:                                                   */
/*                                                          */
/*++++++++++++++++++++++++++++++++++++++++++++++++++++++++++++++++++++++++++++
++++++++++++++++++*/
int CVICALLBACK AlignOkCallback (int panel, int control, int event,
                void *callbackData, int eventData1, int eventData2)
{
        switch (event)
                {
                case EVENT_COMMIT:
                        for (i=0;i<16;i++){   /* update mid pixel values */
                                GetCtrlVal (alignPanelHandle, piLineToPixelCtrlID[i],
&pref.piLineMidPixel[i]);
                        }
                        for (i=0;i<16;i++){   /* update line active status */
                                GetCtrlVal (alignPanelHandle, piAPanelLineStatCtrlID[i],
&pref.piLineActive[i]);
                        }
                        for (i=0;i<16;i++){   /* set line active status in main panel same as
in align panel*/
                                SetCtrlVal (mainPanelHandle, piMPanelLineStatCtrlID[i],
pref.piLineActive[i]);
```

```
                    }
                    HidePanel (alignPanelHandle);
                    DisplayPanel (mainPanelHandle);
                    break;
                }
        return 0;
}

/*++++++++++++++++++++++++++++++++++++++++++++++++++++++++++++++++++++++++++++
++++++++++++++++++*/
/* Function: AlignCancelCallback                                        */
/* Called by:                                                   */
/*      Descript:                                                       */
/*                                                              */
/*++++++++++++++++++++++++++++++++++++++++++++++++++++++++++++++++++++++++++++
++++++++++++++++++*/
int CVICALLBACK AlignCancelCallback (int panel, int control, int event,
                void *callbackData, int eventData1, int eventData2)
{
        switch (event)
                {
                case EVENT_COMMIT:
                        for (i=0;i<16;i++){  /*Reset to old values */
                                SetCtrlVal (alignPanelHandle, piLineToPixelCtrlID[i],
pref.piLineMidPixel[i]);
                        }
                        for (i=0;i<16;i++){   /* get line active status */
                                SetCtrlVal (alignPanelHandle, piAPanelLineStatCtrlID[i],
pref.piLineActive[i]);
                        }
                        HidePanel (alignPanelHandle);
                        DisplayPanel (mainPanelHandle);
                        break;
                }
        return 0;
}

/*++++++++++++++++++++++++++++++++++++++++++++++++++++++++++++++++++++++++++++
++++++++++++++++++*/
/* Function: DrawAlignPanelBars                                         */
/* Called by:                                                   */
/*      Descript:                                                       */
/*                                                              */
/*++++++++++++++++++++++++++++++++++++++++++++++++++++++++++++++++++++++++++++
++++++++++++++++++*/
void DrawAlignPanelBars(void)
```

```
{
        double dX1,dY1,dX2,dY2;
        for (i=0;i<16;i++){
                dX1=pref.piLineMidPixel[i]-1;
                dY1=0.0;
                dX2=pref.piLineMidPixel[i]+1+1; /*extra one added 'cause of the way
rect drawn */
                dY2=2500;
                piAlignBarCtrlID[i]=PlotRectangle (alignPanelHandle,
ALIGNPANEL_ALIGNGRAPH,
                                                        dX1, dY1, dX2, dY2,
VAL_GRAY, VAL_GRAY);
        }
}


/*++++++++++++++++++++++++++++++++++++++++++++++++++++++++++++++++++++++++
++++++++++++++++++*/
/* Function: RunTestCECallback                                          */
/* Called by:                                                   */
/*      Descript:                                                       */
/*                                                              */
/*++++++++++++++++++++++++++++++++++++++++++++++++++++++++++++++++++++++++
++++++++++++++++++*/
int CVICALLBACK RunTestCECallback (int panel, int control, int event,
                void *callbackData, int eventData1, int eventData2)
{
        double timer_tick;
        switch (event)
                {
                case EVENT_COMMIT:
                        iRunCE=1;
                        iPlottedOnce=0;
                        InitializeDAQ ();
                        /* Set Stepper motor speed and start it */
                        /* Set high voltage output */
                        SetCtrlAttribute (alignPanelHandle,
ALIGNPANEL_ALIGNOK,ATTR_DIMMED, disable); /*disable OK and Cancel
buttons */
                        SetCtrlAttribute (alignPanelHandle,
ALIGNPANEL_ALIGNCANCEL,ATTR_DIMMED, disable);
                        SetCtrlAttribute (alignPanelHandle,
ALIGNPANEL_RUNTESTCEBTN,ATTR_DIMMED, disable);
                        SetCtrlAttribute (alignPanelHandle,
ALIGNPANEL_STOPTESTCEBTN,ATTR_DIMMED, enable);
```

```
                        DeleteGraphPlot (alignPanelHandle,
ALIGNPANEL_ALIGNGRAPH, -1, 1); /*clear graph */
                        DrawAlignPanelBars();
                        timer_tick=.1;          /* update every .1 seconds */
                        iDAQTimerCtrlID = NewCtrl (mainPanelHandle, CTRL_TIMER,
"",10,10);
                        SetCtrlAttribute (mainPanelHandle, iDAQTimerCtrlID,
ATTR_INTERVAL, timer_tick);
                        InstallCtrlCallback (mainPanelHandle, iDAQTimerCtrlID,
TestTimerCallback,&iDAQTimerCtrlID);


                        break;
                }
        return 0;
}



/*++++++++++++++++++++++++++++++++++++++++++++++++++++++++++++++++++++++++++++
++++++++++++++++++*/
/* Function: TestTimerCallback                                          */
/* Called by:                                                  */
/*      Descript:                                                  */
/*                                                          */
/*++++++++++++++++++++++++++++++++++++++++++++++++++++++++++++++++++++++++++++
++++++++++++++++++*/
int CVICALLBACK TestTimerCallback (int panel, int control, int event,
                void *callbackData, int eventData1, int eventData2)
{
        switch (event){
                case EVENT_TIMER_TICK:
                        iStatus = DAQ_Start (iDevice, iChan, iGain, piBuf1, 128,
iSampTB, uSampInt);
                        iDAQstopped=0;  /* get the first set of data */
                        while ((iDAQstopped != 1) && (iStatus == 0)) { /* Loop until all
acquisition is complete - 128 points */
                                iStatus = DAQ_Check(iDevice, &iDAQstopped,
&ulRetrieved);
                        }
                        iStatus = DAQ_Start (iDevice, iChan, iGain, piBuf2, 128,
iSampTB, uSampInt); /*set board for next DAQ */
                        iDAQstopped=0; /* get the second set of data */
                        while ((iDAQstopped != 1) && (iStatus == 0)) { /* Loop until all
acquisition is complete - 128 points */
```

```
                        iStatus = DAQ_Check(iDevice, &iDAQstopped,
&ulRetrieved);
                }

                for (i=0; i<128; i++){
                        piDiffBuf[i] = 0.667 * piDiffBuf[i] + 0.333 * 50 *
fabs(piBuf1[i]-piBuf2[i]);
                }
                if (iPlottedOnce>0){
                        DeleteGraphPlot (alignPanelHandle,
ALIGNPANEL_ALIGNGRAPH, buf1PlotHandle, 1); /*clear graph */
                        DeleteGraphPlot (alignPanelHandle,
ALIGNPANEL_ALIGNGRAPH, buf2PlotHandle, 1); /*clear graph */
                        DeleteGraphPlot (alignPanelHandle,
ALIGNPANEL_ALIGNGRAPH, bufDPlotHandle, 1); /*clear graph */
                }
                buf1PlotHandle = PlotY (alignPanelHandle,
ALIGNPANEL_ALIGNGRAPH,
                                                piBuf1, 128,
VAL_SHORT_INTEGER,
                                                VAL_THIN_STEP,
VAL_EMPTY_SQUARE, VAL_SOLID, 1,
                                                VAL_RED); /* plot
line 1 */
                buf2PlotHandle = PlotY (alignPanelHandle,
ALIGNPANEL_ALIGNGRAPH,
                                                piBuf2, 128,
VAL_SHORT_INTEGER,
                                                VAL_THIN_STEP,
VAL_EMPTY_SQUARE, VAL_SOLID, 1,
                                                VAL_BLUE); /* plot
line 2 */
                bufDPlotHandle = PlotY (alignPanelHandle,
ALIGNPANEL_ALIGNGRAPH,
                                                piDiffBuf, 128,
VAL_SHORT_INTEGER,
                                                VAL_THIN_STEP,
VAL_EMPTY_SQUARE, VAL_SOLID, 1,
                                                VAL_YELLOW); /*
plot the difference */
                iPlottedOnce=1;
                break;
        }
    return 0;
}
```

```
/*+++++++++++++++++++++++++++++++++++++++++++++++++++++++++++++++++++++++++
++++++++++++++++++*/
/* Function: StopTestCECallback                                          */
/* Called by:                                                            */
/*      Descript:                                                        */
/*                                                                       */
/*+++++++++++++++++++++++++++++++++++++++++++++++++++++++++++++++++++++++++
++++++++++++++++++*/
int CVICALLBACK StopTestCECallback (int panel, int control, int event,
            void *callbackData, int eventData1, int eventData2)
{
      switch (event)
            {
            case EVENT_COMMIT:
                  if(iRunCE==1){
                        iRunCE=0;
                        SetCtrlAttribute (mainPanelHandle, iDAQTimerCtrlID,
ATTR_ENABLED, 0);  /*disable timer*/
                        iStatus = DAQ_Start (iDevice, iChan, iGain, piBuf1, 128,
iSampTB, uSampInt); /*set board for next DAQ */
                        Delay(.5);
                        iStatus = DAQ_Config(iDevice, 0, 0);
                        /* Set PFI line back to initial state. */
                        iStatus = Select_Signal(iDevice, ND_IN_CONVERT,
ND_INTERNAL_TIMER, ND_LOW_TO_HIGH);
                        DAQ_Clear(iDevice);
                        SetCtrlAttribute (alignPanelHandle,
ALIGNPANEL_ALIGNOK,ATTR_DIMMED, enable);
                        SetCtrlAttribute (alignPanelHandle,
ALIGNPANEL_ALIGNCANCEL,ATTR_DIMMED, enable);
                        SetCtrlAttribute (alignPanelHandle,
ALIGNPANEL_RUNTESTCEBTN,ATTR_DIMMED, enable);
                        SetCtrlAttribute (alignPanelHandle,
ALIGNPANEL_STOPTESTCEBTN,ATTR_DIMMED, disable);

                        if(iPlottedOnce==1){
                              buf1PlotHandle = PlotY (alignPanelHandle,
ALIGNPANEL_ALIGNGRAPH,
                                                piBuf1, 128,
VAL_SHORT_INTEGER,
                                                VAL_THIN_STEP,
VAL_EMPTY_SQUARE, VAL_SOLID, 1,
                                                VAL_RED);  /* plot
line 1 */
```

```
                                        buf2PlotHandle = PlotY (alignPanelHandle,
ALIGNPANEL_ALIGNGRAPH,
                                                                piBuf2, 128,
VAL_SHORT_INTEGER,
                                                                VAL_THIN_STEP,
VAL_EMPTY_SQUARE, VAL_SOLID, 1,
                                                                VAL_BLUE); /* plot
line 2 */
                                        bufDPlotHandle = PlotY (alignPanelHandle,
ALIGNPANEL_ALIGNGRAPH,
                                                                piDiffBuf, 128,
VAL_SHORT_INTEGER,
                                                                VAL_THIN_STEP,
VAL_EMPTY_SQUARE, VAL_SOLID, 1,
                                                                VAL_YELLOW); /*
plot the difference */
                                }

                        }
                        break;
                }
        return 0;
}
/*++++++++++++++++++++++++++++++++++++++++++++++++++++++++++++++++++++++
++++++++++++++++++*/
/* Function: AdjustPixelBarCallback                                    */
/* Called by:                                                  */
/*       Descript:                                                 */
/*                                                       */
/*++++++++++++++++++++++++++++++++++++++++++++++++++++++++++++++++++++++
++++++++++++++++++*/
int CVICALLBACK AdjustPixelBarCallback (int panel, int control, int event,
                void *callbackData, int eventData1, int eventData2)
{
        double dX1,dY1,dX2,dY2;
        switch (event)
                {
                case EVENT_COMMIT:
                        i=0;
                        while (i<16){
                                if (control==piLineToPixelCtrlID[i]){
                                        GetCtrlVal (alignPanelHandle,
piLineToPixelCtrlID[i], &pref.piLineMidPixel[i]);
                                        dX1=pref.piLineMidPixel[i]-1;
                                        dY1=0.0;
```

```
                                        dX2=pref.piLineMidPixel[i]+1+1; /*extra one
added 'cause of the way rect drawn */
                                        dY2=2500;
                                        DeleteGraphPlot (alignPanelHandle,
ALIGNPANEL_ALIGNGRAPH,
                                                                piAlignBarCtrlID[i],
VAL_IMMEDIATE_DRAW); /*clear bar */
                                        piAlignBarCtrlID[i]=PlotRectangle
(alignPanelHandle, ALIGNPANEL_ALIGNGRAPH,
                                                                dX1, dY1,
dX2, dY2, VAL_GRAY, VAL_GRAY);
                                        i=16;  /* exit loop */
                                }
                                i=i+1;
                        }
                        break;
                }
        return 0;
}

/*++++++++++++++++++++++++++++++++++++++++++++++++++++++++++++++++++++++++++++
++++++++++++++++++*/

/*++++++++++++++++++++++++++++++++++++++++++++++++++++++++++++++++++++++++++++
++++++++++++++++++*/
/*  Function:  ClearDAQ                                         */
/*  Called by:                                                  */
/*        Descript:                                             */
/*                                                              */
/*++++++++++++++++++++++++++++++++++++++++++++++++++++++++++++++++++++++++++++
++++++++++++++++++*/
void ClearDAQ (void)
{
        /* CLEANUP - Don't check for errors on purpose. */
        /* Set sample timing back to initial state. */
        Delay(2.0);
        iStatus = DAQ_Config(iDevice, 0, 0);
        /* Set PFI line back to initial state. */
        iStatus = Select_Signal(iDevice, ND_IN_CONVERT, ND_INTERNAL_TIMER,
ND_LOW_TO_HIGH);
        DAQ_Clear(iDevice);

}
```